

Flexibility for large-scale deployment of PV systems in low-voltage grids

Présentée le 12 juillet 2021

Faculté des sciences et techniques de l'ingénieur
Laboratoire de photovoltaïque et couches minces électroniques
Programme doctoral en énergie

pour l'obtention du grade de Docteur ès Sciences

par

Jordan HOLWEGER

Acceptée sur proposition du jury

Prof. J. A. Schiffmann, président du jury
Prof. C. Ballif, Dr N. Würsch, directeurs de thèse
Prof. M. Patel, rapporteur
Dr P. Cuony, rapporteur
Prof. F. Maréchal, rapporteur

Remerciements

Ce manuscrit résume quatre années de travaux scientifiques au PVLAB, mais il ne dit rien sur cette formidable aventure humaine. Les collaborations et les échanges ont été riches et ont permis de réaliser ce travail. Les moments partagés, les discussions et les souvenirs m'ont permis de vivre une expérience inoubliable.

Pour commencer, j'aimerais remercier, Prof. Christophe Ballif qui m'a transmis sa passion pour le photovoltaïque et guidé sur le sinueux chemin de la recherche. Un grand merci à Nicolas Wyrsh, mon codirecteur pour ses conseils avisés et son immense soutien tout au long de ces quatre années. Un merci tout particulier à Lionel Bloch, compagnon de route, infatigable, coach de ski et de grimpe sur glace, sans qui ces dernières années auraient été bien compliquées. Merci également à Aïcha Hessler-Wyser pour son soutien et sa disponibilité. C'est entre autres grâce à vous tous que j'ai pu mener une thèse et construire ma vie de famille.

Je voudrais aussi remercier tous les collègues du PVLAB, la team technique, Aymeric, Cédric, Nicolas, Nathan, l'équipe admin., Karine et Marie-Claude, et tous les collègues doctorants-es, postdoc et ingénieurs, Ana, Andrew, Eleonora, Federica, Florent, Frank, Franz, Jan, Janina, Jérémie, Jonathan, Julie, Laurie-Lou, les deux Luca, Matthias, Marina, Marine, Mario, Marion, Philippe, les Quentin, Raphaël, Samira, Vincent, et les solides collègues de bureau Sylvain et Xavier pour toutes ces discussions engagées. Special thanks to Peter for his precious help on the title.

Un grand merci aussi aux civilistes, étudiants-es, et stagiaires avec qui j'ai beaucoup appris : Alessandro, Marokh, Loïc, Emma, Cédric, Nicolas Jo., Diane, Antoine, Justine, Julie et Nacer. Je remercie aussi mes parents, mes frères et ma belle-famille, pour leur soutien.

Audrey, Mya et Chloé, merci pour votre patience, votre soutien et d'avoir été à mes côtés dans ce projet.

Enfin merci à toi, cher-e lecteur-riche, qui a lu jusqu'ici, qui continuera (je l'espère) et qui donne un sens à ce travail.

Genève, le 16 juin 2021

J. H.

Abstract

To meet the net-zero emission target by 2050, Switzerland must install between 34 and 50 GW of distributed photovoltaic (PV). The inherent challenge with such an extensive integration of stochastic generation is to provide the flexibility for balancing supply and demand. Otherwise, grid reinforcements or PV generation curtailment are required. Both have a cost that can be reduced by using flexibility. Most of the PV capacity will be installed on rooftops. As the need for flexibility will mainly come from districts, this thesis investigates how to promote flexibility of PV systems for their large-scale deployment in low-voltage grids.

First, we investigated how the citizens' and consumers' behavior can balance supply and demand. Our findings from a field trial highlight that the households' reaction to remunerative incentives is low but still observable. In contrast, new PV adopters, under an inherent moral and remunerative incentive, show a significant consumption behavior change. We evaluated that the households' potential for shiftable energy is around 18%. A 20% increase in the PV penetration can be achieved using this flexibility. Second, technical measures such as batteries, heat pumps, electric heaters, and PV power curtailment can effectively contribute to the systems' flexibility and mitigate network impact. We proposed strategies to promote flexibility and mitigate grid impact. In particular, we showed that variable volumetric tariffs promote large storage used for trading energy and increase the grid stress. In contrast, capacity and block rate tariffs reduce heat pumps' capacity, increase storage capacity to lower consumption peak, and increase PV curtailment to reduce injection peak. The consequence is an overall grid stress reduction. We also showed that aggregating individual systems to form energy communities negatively impacts the grid but increases their profitability. Finally, flexible PV systems can be harvested by distribution network operators to keep the network in a safe state. We investigated the cost of exploiting distributed flexibility compared to grid reinforcement cost. The former is profitable for moderate PV penetration until a break-even point where the latter becomes the most economical option.

Along with answering the central question of promoting PV systems flexibility, we provided an analytical tool to disaggregate households' smart meter measurements into appliance categories. We also provided two approaches to use smart meter data in the context of network impact studies while coping with privacy-preserving regulation.

Keywords: photovoltaic, flexibility, electricity tariffs, electrical network, demand-side management, battery, heat pump, grid impact

Résumé

Pour atteindre l'objectif de neutralité carbone d'ici 2050, la Suisse doit installer entre 34 et 50 GW de capacité photovoltaïque (PV). Le défi inhérent à un tel taux de pénétration d'énergie intermittente est de fournir la flexibilité pour équilibrer la demande et la production. Autrement, il est nécessaire de procéder à des renforcements du réseau ou à la réduction volontaire de la production PV. Ces actions sont coûteuses et doivent être évitées autant que possible. La majeure partie de la capacité PV devra être installée sur les toits. Puisque les besoins en flexibilité viendront essentiellement des quartiers, cette thèse étudie comment promouvoir la flexibilité des systèmes PV pour atteindre leur déploiement à grande échelle dans les réseaux basses-tensions.

Premièrement, nous avons évalué comment le comportement des citoyens et consommateurs peut équilibrer la production et la consommation. Notre essai sur le terrain montre que la réaction des ménages à une incitation financière est faible, mais observable. A l'opposé, les nouveaux propriétaires d'installation PV montrent un changement significatif de leur comportement de consommation grâce à la double incitation financière et morale. Nous avons évalué que le potentiel d'énergie déplaçable est d'environ 18%. Une augmentation de 20% du taux de pénétration PV peut être atteinte en utilisant cette flexibilité. Deuxièmement, des mesures techniques, comme des batteries, des pompes à chaleur, des chauffages électriques et la réduction de la production PV peuvent contribuer à la flexibilité du système et limiter l'impact sur le réseau. Nous avons présenté des stratégies pour encourager la flexibilité et limiter celui-ci. En particulier, nous avons démontré que des tarifs variables encouragent les propriétaires à installer de plus grandes batteries. Cependant, avec ces tarifs, celles-ci augmentent la pression sur le réseau. A l'inverse, des tarifs capacitifs ou progressifs réduisent la taille des pompes à chaleur, augmentent la capacité de stockage pour réduire les pics de consommation et réduisent davantage la production PV pour limiter les pics d'injection. Il en résulte une réduction globale de la pression sur le réseau. Nous avons également montré que l'agrégation de systèmes individuels pour former des communautés énergétiques a un léger impact négatif sur le réseau, mais augmente la rentabilité de celles-ci. Pour finir, les systèmes PV flexibles peuvent être exploités par les gérants de réseaux de distribution pour les aider à exploiter le réseau dans un état acceptable. Nous avons évalué le coût d'exploitation de la flexibilité distribuée comparée aux coûts de renforcements réseau. Celle-ci peut être rentable pour des pénétrations PV modérées jusqu'à un certain point où le renforcement réseau devient plus économique.

En répondant à la question centrale sur l'encouragement de la flexibilité des systèmes PV,

Résumé

nous avons également proposé un outil d'analyse. Cet outil permet de désagréger les mesures fournies par des compteurs intelligents en des catégories d'appareils électriques. Nous avons aussi présenté deux approches pour exploiter les données des compteurs intelligents dans le contexte d'étude d'impact sur le réseau tout en respectant la réglementation sur la protection des données.

Mots-clés : photovoltaïque, flexibilité, tarif d'électricité, réseau électrique, gestion de la demande, batterie, pompe à chaleur, impact réseau

Contents

Remerciements	iii
Abstract (English/Français)	v
Acronyms	xiii
Introduction	1
1 A disaggregation method for household's smart meter analytics	21
1.1 Introduction	21
1.2 Algorithm	26
1.2.1 Activity chain modeling	26
1.2.2 Algorithm's main steps	28
1.3 Validation methodology	48
1.3.1 Selected state-of-the-art algorithms	49
1.3.2 Test datasets	51
1.3.3 Metrics	53
1.4 Results and discussion	56
1.5 Conclusion	62
2 Experimental determination of the households demand flexibility	65
2.1 Introduction	65
2.2 Available data	68
2.2.1 Smart meter measurements	68
2.2.2 Surveys	72
2.3 Methodology	76
2.3.1 Interventions	76
2.3.2 Analysis	79
2.4 Results	83
2.4.1 Time-of-use treatments	83
2.4.2 Comparing the experimental and theoretical household flexibility	89
2.4.3 Results of the PV owners analysis	93
2.5 Conclusion	96
3 Technical flexibility at the building level	99

Contents

3.1	Introduction	99
3.2	Modeling technical flexibility	102
3.3	Comparing technical flexibility and behavioral flexibility	111
3.4	A heuristic heat pump control algorithm	115
3.4.1	Description of the algorithm	116
3.4.2	Reference design and optimal control definition	120
3.4.3	Benchmark	120
3.4.4	Case study	124
3.4.5	Results	128
3.5	Impact of regulations on components size and profitability	135
3.6	Conclusion	141
4	Using electricity tariffs to trigger flexibility	145
4.1	Introduction	145
4.2	Impact of tariffs on the design of a flexible PV system	149
4.2.1	Methodology	149
4.2.2	Results	154
4.2.3	Discussion	158
4.3	Methodologies for creating realistic test cases for energy planners	159
4.3.1	Load profiles allocation	160
4.3.2	Smart meter anonymization	164
4.3.3	Benchmark methodology	172
4.3.4	Results	178
4.3.5	Discussion	182
4.4	Mitigating the impact of distributed PV using electricity tariffs	183
4.4.1	Methodology	184
4.4.2	Results	189
4.5	Conclusion	197
5	Harvesting flexibility from a DSO perspective	201
5.1	Introduction	201
5.2	Using energy community and spatial aggregation to enhance flexibility	203
5.2.1	Methodology	203
5.2.2	Case study	209
5.2.3	Results	212
5.2.4	Discussion	219
5.3	Potential of ideal behavioral flexibility to increase the PV penetration in a low-voltage grid	220
5.3.1	Methodology	221
5.3.2	Case study and available shiftable power	223
5.3.3	Results	223
5.3.4	Discussion	226
5.4	Harvesting the flexibility of PV systems	227

5.4.1	Methodology	228
5.4.2	Case study	235
5.4.3	Results	239
5.4.4	Discussion	246
5.5	Conclusion	248
6	Conclusion	251
6.1	Policy recommendations for the promotion of distributed PV in Switzerland . .	255
6.1.1	Citizen involvement in the energy transition	255
6.1.2	Comments on the current Swiss framework	256
6.1.3	Toward 50 GW PV capacity in Switzerland	256
6.2	Conclusions and perspectives	258
6.3	Summary for distribution system operators and policymakers	260
A	FLEXI 2 survey	261
B	FLEXI 2 PV owner survey	277
C	Rolle buildings parameters	281
	Bibliography	283
	Curriculum Vitae	301

Acronyms

AC	alternative current	HP	heat pump
API	application programming inter- face	ICT	information and communica- tion technology
CAPEX	capital cost	IEA	international energy agency
CIGRE	conférence internationale des grands réseaux Electriques	IEEE	institute of electrical and elec- tronics engineer
CO	combinatorial optimization	IP	integer programming
COP	coefficient of performance	IRENA	international renewable energy agency
DDSC	discriminative disaggregation via sparse coding	LCOE	levelized cost of energy
DHI	diffused horizontal irradiance	LMO	lithium manganese oxide
DHW	domestic hot water	NPV	net present value
DPP	discounted payback time	OPEX	operating cost
DSO	distribution system operator	OPF	optimal power flow
DUE	device usage estimaion	PCA	principal component analysis
EH	electric heater	PV	photovoltaic
EPEX	European power exchange	RMS	root mean square
ER	energy retailer	RSGP	recursive spectral graph parti- tioning
FHMM	factorial hidden Markov model	SGP	spectral graph partitioning
GHG	greenhouse gas	SMS	short message system
GHI	global horizontal irradiance	TOTEX	total cost of ownership
GSP	graph signal processing	TSO	transmission system operator
HCA	heuristic control algorithm		
HMM	hidden Markov model		

Introduction

“Our house is on fire. I am here to say, our house is on fire.” said Greta Thunberg at the 2019 World Economic Forum in Davos. Nevertheless, we have not yet failed. This thesis aims to add a little stone to the most crucial challenge humanity has ever faced: climate change.

Motivation

The Swiss Federal Council decided on 28 August 2019 that Switzerland should not emit more greenhouse gas (GHG) than it can absorb naturally or with technical means by 2050. This carbon neutrality target should limit the global temperature increase by 1.5 °C. By doing so, Switzerland joins a growing list of states with net-zero emission targets, including France, Germany, Sweden, Denmark, and the United Kingdom. All sectors of our fossil-fuel addict society emit GHG. In 2019, the largest sources were buildings (heating, and appliances, with 11 MtCO₂eq), transport (15 MtCO₂eq), and industry (heat and process, 12 MtCO₂eq)). The GHG emissions per sector from 1990 to 2019 are reported in Figure 1. The emission reduction in these sectors can be achieved by, amongst other solutions, electrification [Sugiyama, 2012]. For instance, in the buildings sector, a growing share of the heat demand could be covered by efficient power-to-heat technologies such as heat pumps. Such technologies essentially improve the energy efficiency of heat production. Similarly, electric engines instead of internal combustion in the transport sector allow a significant decrease in primary energy needs. For electrification to result in real GHG emission reduction, the decarbonization of the power sector is required. In other words, zero-carbon electricity must be produced to power our lights, electric vehicles, heat pumps, machines, or any other appliances.

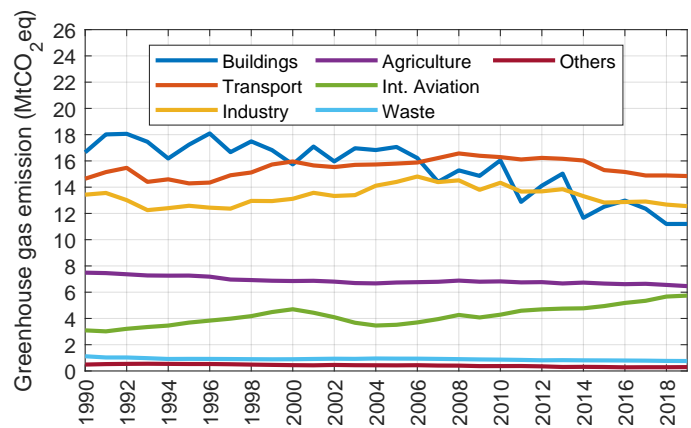


Figure 1 – Greenhouse gas emission by sector, adapted from [FOEN, 2021]

The massive integration of renewable energy sources is the pillar of the power sector decarbonization [Child et al., 2019]. Recent reports from the International Energy Agency show a growing share of renewable energy in the global electricity generation mix [IEA, 2019]. This growth is driven by a constant drop in the cost of these technologies, as highlighted in Figure 2. Solar and wind energy have the most rapidly decreasing cost between 2010 and 2019. In particular, solar photovoltaic (PV) cost has been divided by five in less than ten years to reach an average generation cost at 6.8 cts/kWh (USD) in 2019. The PV generation can be even lower than 2 cts/kWh for large plants in sunny countries¹.

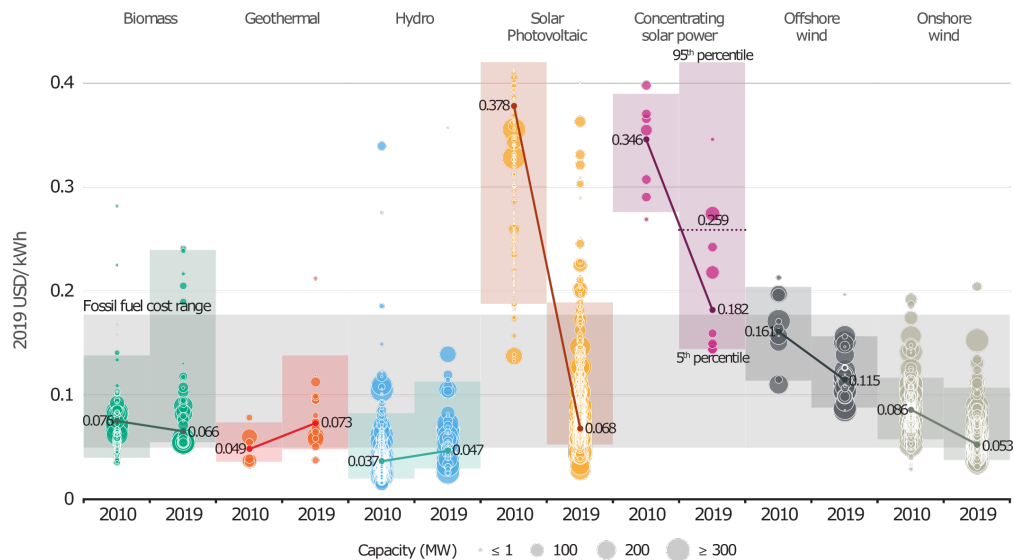


Figure 2 – Levelized cost of energy for utility-scale renewable generation technologies adapted from [IRENA, 2020]

¹In 2021, Saudi Arabia draw a world record low bid of 1 cts/kWh <https://www.pv-magazine.com/2021/04/08/saudi-arabias-second-pv-tender-draws-world-record-low-bid-of-0104-kwh/>

Solar energy is available everywhere. On average, between 800 and 2700 kWh/m² of solar energy can be harvested yearly. In Switzerland, this value lies typically between 1000 and 1300 kWh/m², i.e., equivalent to the energy content of one barrel of oil per year and square meter. Hence, there is a high potential for cheap, clean, and widely available solar energy. Distributed renewable energy sources are given by multiplying small (kW range) to medium scale (MW range) renewable energy-based generation plants. Their penetration, defined as their energy production compared with the energy demand at any specified scale, is critical for the transition toward a zero-carbon power sector.

In this work, we will primarily focus on photovoltaic energy, although some of the concepts and modeling approaches could also apply to other distributed renewable energy sources.

The main issue with the massive integration of renewable energy is its intermittent and stochastic nature. Figure 3 illustrates the global horizontal irradiance (GHI) for a particular autumn day in Neuchâtel. The irradiance can drop from 630 to 160 W/m² in just 5 minutes, then rise again by 500 W/m² in 5 minutes. These variations are difficult to predict and can cause numerous energy infrastructure challenges. In particular, according to [Viral and Khatod, 2012], the main limitations of PV integration (but could also apply for any distributed intermittent generation) in the current electrical network are:

reverse power flow If the generation becomes locally higher than the load, the power will flow from the network end-nodes to the local district transformer. It becomes a significant issue if the reverse power exceeds the transformer limits.

voltage levels Again, if the generation becomes locally higher than the load, the voltage can rise and even over-pass the voltage limits imposed by voltage disturbance standards [Markiewicz and Klajn, 2004].

frequency control With the increasing penetration of distributed generation, the amount of inertia available on the network gets lower as fewer conventional rotating generators (with heavy turbines and alternators) are used simultaneously. The inertia can be seen as the network's ability to damp frequency fluctuations by absorbing or injecting kinetic energy [Tielens and Van Hertem, 2016].

harmonics and power quality For grid-connected PV installation, an alternative current converter is a mandatory component. To generate a sinusoidal output current, converters use pulse-width modulation through MOSFETs transistor [Enslin and Heskes, 2004]. To limit harmonics, some low-pass filters are used at the output. However, studies [Enslin and Heskes, 2004, Poosri and Charoenlarnopparut, 2016] have shown that when reaching a high PV penetration level (above 50%), the total harmonic distortion can approach the 5% limits of the IEEE standard [Blooming and Carnovale, 2006].

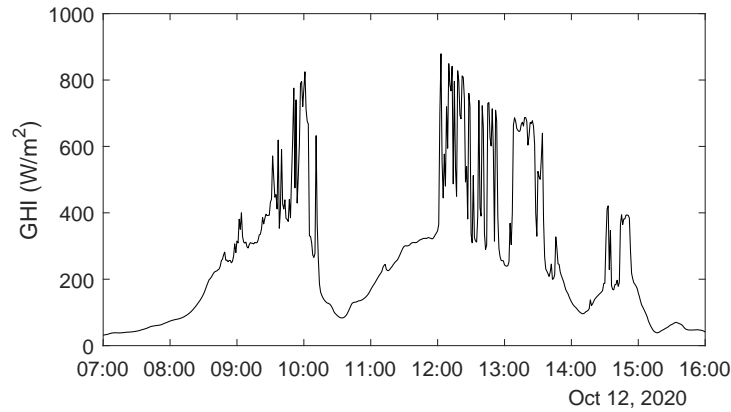


Figure 3 – Measure of the global horizontal irradiance on an autumn day

To overcome these issues, three approaches can be undertaken. The first is to prevent or restrict distributed renewable generation penetration and stick with conventional generation. This is not compatible with GHG emission reduction targets. The second approach is to undertake grid reinforcement, i.e., replacing grid components (transformer and lines) with larger and stronger ones to sustain the duty. This is feasible but with a particular cost that we will consider avoidable. Finally, the remaining option, and the one we will investigate in this work, is to increase the distributed generation's flexibility.

In this work, we consider that *flexibility* is the ability to change the amount of power a given energy system consumes or produces. A PV plant, if not supplemented by any complementary technologies, is not flexible as the instantaneous weather condition determines its production. A PV inverter with the ability to curtail the PV generation and reducing the production is already a source of flexibility.

Flexibility is sometimes also referred to as the ability to balance generation and demand [Cruz et al., 2018, Eid et al., 2019, Olivella-Rosell et al., 2018, IRENA, 2018]. In contrast, others define flexibility as the ability to provide a quick response to the renewable energy source unpredictability [Goutte and Vassilopoulos, 2019, Kondziella and Bruckner, 2016] or to time-shift some events [Zhang et al., 2020]. Network flexibility sometimes refers to the network's ability to adapt and reconfigure (topologically) to answer unexpected events [Cruz et al., 2018]. These considerations are outside the scope of this thesis. This work's primary focus is on flexibility as adding controllability at a fraction of hour-scale.

This thesis aims to provide insights and critical contributions for promoting flexibility of PV systems and their integration in the electrical network.

The remaining part of this introduction will present the current Swiss framework, in light of a transition toward net zero-emission by 2050, some basic concepts about PV systems, and the

scientific contributions to the field. To understand how far this goal is from the current status, we must also understand the current Swiss energy needs, production means, and distribution infrastructures.

The Swiss energy context

The primary energy consumption of Switzerland lies around 800 PJ (230 TWh). About 2/3 of our needs are covered by fossil fuel, while 25% is covered by electricity, the rest comes from biomass and waste incineration. We use energy for three primary services. The first and larger one (45%) is heat production, i.e., the heating of buildings, hot water, and hot process in the industry. The second is transportation (38%), i.e., the movement of humans or goods. The rest of our energy needs is for our daily activities and manufacturing (besides heat demand). Figure 4 summarized our energy needs and how they are supplied.

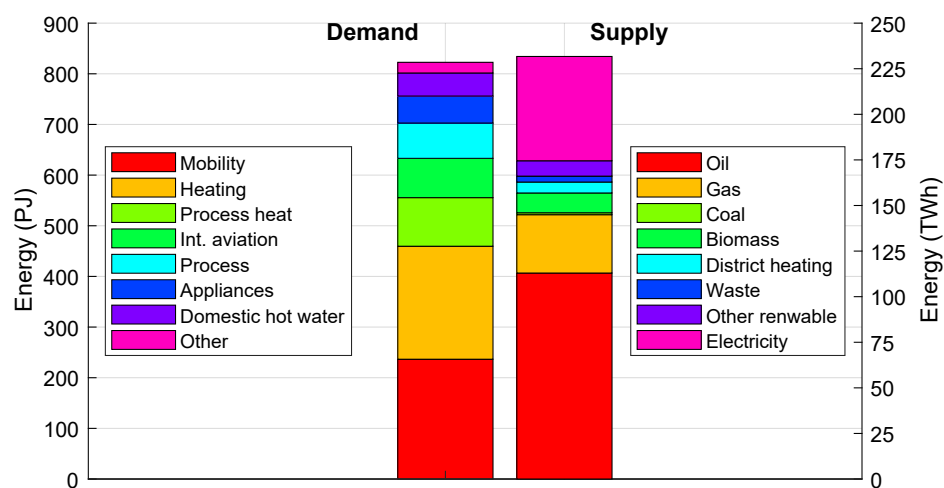


Figure 4 – Energy demand (primary, from [Infras et al., 2020] supply (final consumption, from [SFOE, 2019a])

The electricity share is strongly expected to rise in the coming years, despite energy efficiency measures. In the 2050 energy perspective of the Swiss Federal Office for Energy [SFOE, 2021], the total electricity demand is expected to reach 71 TWh. To cover this demand, hydropower plants are expected to produce 45 TWh, and PV production should reach 34 TWh using mostly distributed PV. Additionally, 8 TWh are generated by wind, biomass, and geothermal. About 3 TWh of renewable energy are curtailed. The difference between production and consumption is the loss in transmission lines (5 TWh) and pumped-hydro storage (8 TWh).

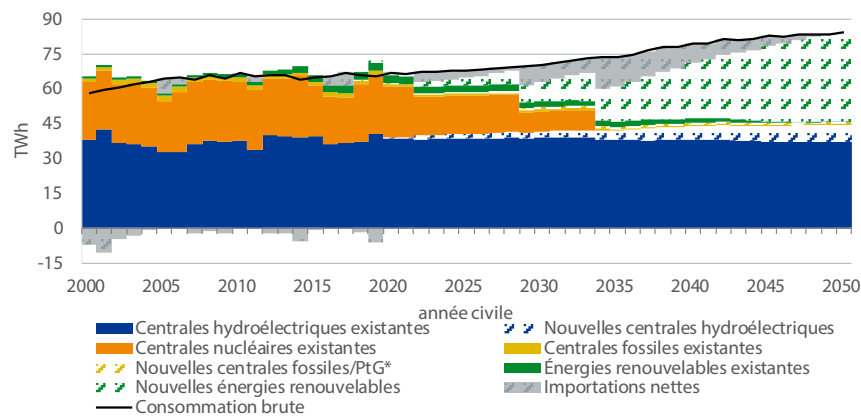


Figure 5 – Electricity production forecast to 2050. Source: [SFOE, 2021]

There are political propositions to produce 50 TWh of electricity using PV [Nordmann, 2019]. Such a high PV penetration cannot be achieved without flexibility. The authors of [SFOE, 2021] foresee that Switzerland should account for 16 GW of flexible capacity (hydro, pumped-storage, biomass feed combined cycle power plant) to cover a maximum of 11 GW peak demand. They also claim that demand flexibility is also essential and can be achieved using distributed storage, power-to-heat, and power-to-gas technologies.

Looking at the renewable energy generation trend from 2009 to 2019 [SFOE, 2019b] and the activated energy for control purposes [Swissgrid, 2021] reported in Figure 6, these claims seem reasonable. Indeed the need to control energy to cope with unexpected events in the generation or consumption side decreases both in absolute value and relative to the total energy consumption. Simultaneously, the variable renewable energy has known a drastic increase since 2009 to reach 4% of the electricity demand.

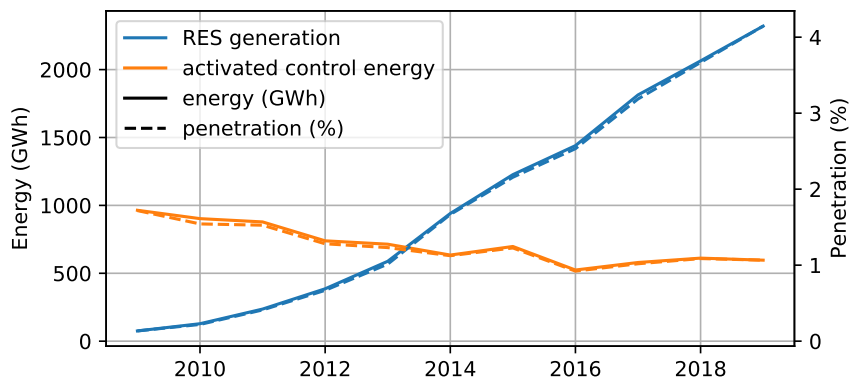


Figure 6 – Generation from variable renewable energy (PV and Wind) and activated control energy

The challenge with a large PV penetration might not be at the large scale but rather at a local scale. To bring the energy from the producer to the customer, several levels of infrastructure are needed. The electrical network can be decomposed into the transmission lines and the distribution lines. A very high voltage is required to minimize losses to transport energy. Typically the transmission lines are composed of very high voltage (220-380 kV) lines. They are operated by the transmission system operator (TSO) to ensure that the energy supply and demand are balanced at all times. It activates, when needed, some control reserve capacity (namely large power capacity) to adjust in case of an unexpected event. The TSO is responsible for keeping the voltage and frequency of the electrical network within a given tolerance. Figure 7 illustrates the different network levels. The distribution system operator (DSO) is responsible for the infrastructure to distribute energy to the end customers. Typically, the low-voltage grids (level 7) are maintained by the DSO. The DSO can also operate medium to high voltage lines up to level 3. His role is to provide reliable access to the energy infrastructure. As such, the DSO is responsible for planning grid maintenance, expansion, and reinforcement when needed. According to the Swiss electricity provision act, the DSO charges the end customers for the network operation, maintenance, balancing, and investment cost in a given area². The so-called grid tariff must be uniform for a given customer segment and voltage level.

In this framework, this thesis focuses on the consequences of a large-scale deployment of PV systems in low-voltage grids. It aims at mitigating any resulting increase in the grid maintenance, investment, and operating cost. Distributed PV (as opposed to large centralized PV power plants) will mostly be integrated into low-voltage networks. Thus, all inherent challenges, over-voltage, line ampacity breaking, reverse-power flow, are potentially concentrated at this network level.

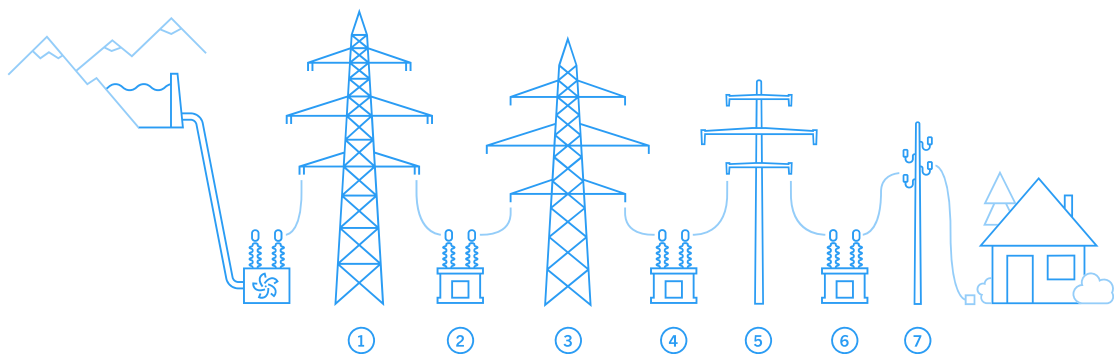


Figure 7 – The seven grid level, from the transmission system (level 1, 220-380 kV) to the distribution system (level 7 < 1 kV)

The energy production and distribution infrastructure maintenance are separated from the retail energy business. In other words, one company is responsible for the distribution infrastructure, the DSO. Another company is responsible for generating electricity, and a third

²art 5,6,14 and 15 LApEl <https://www.fedlex.admin.ch/eli/cc/2007/418/fr>

Introduction

company is buying energy from the producer to sell it to the end customers. This is the energy retailer (ER). In a fully liberalized energy market, any customer should contract any ER to ensure its supply. This is currently not the case in Switzerland for small customers (if their consumption is below 100 MWh/year). A new regulation should come soon, but a complete liberalization of the energy market is still under debate. Under the current regulation, the DSO has to buy renewable energy from the producer. In this framework, self-consumption is allowed, i.e., the direct consumption of a generation's share. For PV systems, this is currently the primary business model. The PV energy generated is first consumed locally to avoid withdrawing energy from the grid, the remaining energy being sold to the DSO, and providing extra revenue.

This thesis primarily focuses on the residential sector and assumes that the customers are tied to the DSO and ER, which form, in most cases, a single entity.

To illustrate the electricity tariff structure, Table 2 reports examples of electricity tariff extracted from the Federal Electricity Commission (Elcom)³ for *Romande Energy* as ER and DSO. The local tax applies to the Rolle district (as an example).

Table 2 – Example of electricity tariffs, network tariffs, taxes, and feed-in tariffs for three customers categories

	Unit	H4 ¹		H6 ²		C7 ³	
Network		9.68	(46%)	5.62	(36%)	3.95	(27%)
Energy	cts/kWh	7.73	(37%)	6.21	(40%)	6.99	(48%)
Local tax		1.32	(6%)	1.32	(9%)	1.32	(9%)
Federal tax		2.30	(11%)	2.3	(15%)	2.3	(16%)
Total	cts/kWh	21.03	(100%)	14.56	(100%)	18.28	(100%)
Feed-in	cts/kWh	8.16 ⁴		7.2 ⁵			

¹ H4: small residential customers with annual consumption < 4'500 kWh/year

² H6: small residential customers with annual consumption < 25'000 kWh/year

³ C7: large commercial customers with annual consumption of 500'000 kWh/year, a fixed fee also applies

⁴ assuming a PV capacity < 30 kW

⁵ assuming a PV capacity < 3'000 kW

This section presented the Swiss context and some basic definitions of the structure of the Swiss energy system. The following will now presents some fundamental principles about PV systems.

³<https://www.strompreis.elcom.admin.ch/>

Photovoltaic technology

The photovoltaic effect is the generation of an electric current or voltage when a particular material is illuminated. The phenomenon, extensively described in [Shah, 2020], occurs when the incoming light's energy is high enough to drive the separation of an electron-hole pair, as illustrated in Figure 8. Without going too much into the details, the power extracted from a solar cell is proportional to the irradiance (instantaneous power of the incoming light normal to the solar cell plane) and the illuminated area. This section aims to provide the basic model of a PV system.

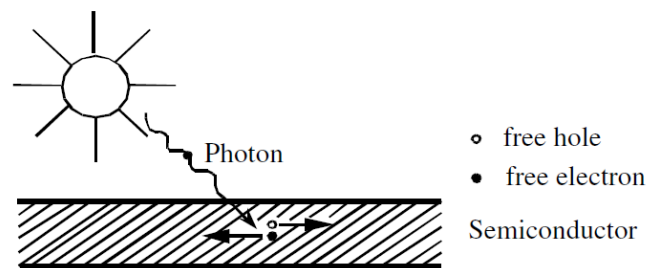


Figure 8 – The photovoltaic effect: generation of an electron-hole pair by absorption of an incoming photon

A PV module is the assembly of a collection of solar cells, with essentially two relevant characteristics: the nominal power and the power temperature coefficient. The nominal power is defined as the maximum power extracted from a module under standard test conditions, i.e., 1000 W/m^2 , 25°C , and a normalized light spectrum (AM1.5G for completeness). We will denote the nominal power of a module by P^{mod} . The power temperature coefficient η models the variation of the maximum power as a function of the cell's temperature. For crystalline solar cells, the maximum power decrease when the cell temperature increase. Thus, this coefficient is negative.

Outside the Earth's atmosphere, the solar irradiance is around 1300 W/m^2 (measured in the horizontal plane, it is called horizontal extra-terrestrial irradiance, EHI). Due to absorption in the atmosphere, only a fraction of this energy reaches the ground. It is usually decomposed between a direct component (DNI , direct normal to the sun irradiance) and diffused component (DHI , diffused horizontal irradiance). Weather stations measure the combination of DHI and DNI projected on a horizontal plane. It is called the global horizontal irradiance (GHI). The instantaneous generation of a PV module depends on the solar irradiance coming in the plane of the modules (denoted GTI for global tilted irradiance), which is the sum of a direct and diffused component (BTI and DTI , respectively). The basic principle is to translate the global and diffused horizontal irradiance into the module tilted plane. The power output

Introduction

is calculated using the following set of equations derived from [King et al., 2004]:

$$\text{Modules output power} \quad P^{\text{PV}} = P^{\text{mod}} \cdot \frac{GTI}{1000} \cdot \left(1 + \eta * (T^{\text{cell}} - T^{\text{ref}})\right) \quad (1a)$$

$$\text{Cell temperature} \quad T_{\text{cell}} = T_{\text{mod}} + GTI/1000 * \Delta T \quad 4 \quad (1b)$$

$$\text{Module temperature} \quad T^{\text{mod}} = GTI \cdot \exp(a + b \cdot WS) + T^{\text{amb}} \quad 4 \quad (1c)$$

$$\text{Global Tilted Irradiance} \quad GTI = BTI + DTI \quad (1d)$$

$$\text{Diffused tilted irradiance} \quad DTI = DHI * \left(A * R_b + (1 - A) * \frac{(1 + \cos(\beta))}{2} \right) \quad 5 \quad (1e)$$

$$\text{with} \quad (1f)$$

$$A = \frac{DNI}{EHI} \quad 5 \quad (1g)$$

$$R_b = \frac{\cos(\theta)}{\cos(\delta)} \quad 5 \quad (1h)$$

$$\text{Beam tilted irradiance} \quad BTI = DNI \cdot \cos(\theta) \quad (1i)$$

$$\text{Direct normal irradiance} \quad DNI = \frac{GHI - DHI}{\cos(\delta)} \quad (1j)$$

$$\text{Angle of incidence} \quad \cos(\theta) = \cos(\beta) \cos(\delta) + \sin(\beta) \sin(\delta) \cos(\phi - \gamma) \quad (1k)$$

where T^{ref} is the standard condition temperature (25 °C). ΔT is the temperature difference between the cells and modules at 1000 W/m² and typically depends on the mounting (open-rack or insulated back). WS is the wind speed, a, b empirical coefficients. T^{amb} is the ambient temperature. Angles β and γ are the tilt and azimuth of the modules, and the angles δ and ϕ are the solar zenith and azimuth angle as illustrated in Figure 9.

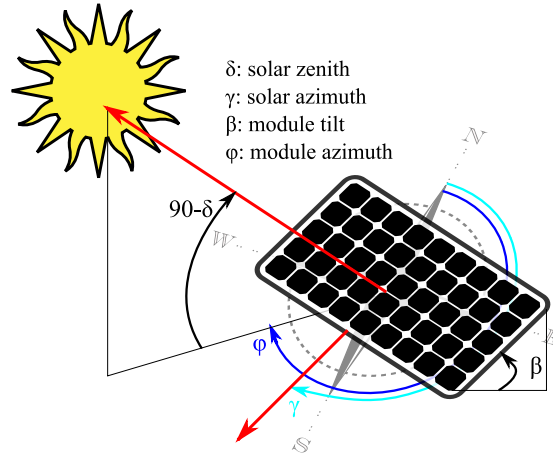


Figure 9 – Illustration of the solar and modules angle

⁴Cell and module temperature model from [King et al., 2004]

⁵Diffuse irradiance transposition model from [Hay and Davis, 1978]

The sun position can be calculated as a function of time using the algorithm proposed by [Reda and Andreas, 2004]. In contrast, the diffuse and global horizontal irradiance (DHI , GHI) are obtained from weather station measurements. A slightly more advanced model is implemented in the PVLIB toolbox from the Sandia National Laboratory [Stein et al., 2016] and will be used all along with this thesis for PV generation simulation.

Using Equations 1a to 1k allows simulating the PV generation of a single module with given orientations along time. These equations can apply to any set of modules having any orientations. The simulation of a complete PV system can be achieved by summing the individual modules' generation. PVLIB integrates advanced models for inverters and module properties mismatch.

The current business model of distributed PV is to reduce the energy bill by covering a given share of its consumption with its PV generation. This action is referred to as self-consumption. Denoting P^{load} the uncontrollable electric load of a PV system, P^{imp} the net power withdrawn from the grid, and P^{exp} the excess of PV generation injected into the grid such that the energy balance of Equation 2 holds. The instantaneous self-consumption ratio sc_t as the share of the PV generation directly consumed by the load:

$$\text{Energy balance} \quad P_t^{\text{imp}} - P_t^{\text{exp}} = P_t^{\text{load}} - P_t^{\text{PV}} \quad (2)$$

$$\text{Power withdrawn from the grid} \quad P_t^{\text{imp}} = P_t^{\text{load}} - sc_t P_t^{\text{PV}} \quad (3)$$

$$\text{Power injected to the grid} \quad P_t^{\text{exp}} = (1 - sc_t) P_t^{\text{PV}} \quad (4)$$

$$\text{Total PV generation} \quad P_t^{\text{PV}} = P_{\text{cap}}^{\text{PV}} \cdot Y_t \quad (5)$$

$$\text{with} \quad Y_t = \frac{GTI_t}{1000} \cdot \left(1 + \eta * \left(T_t^{\text{cell}} - T_t^{\text{ref}}\right)\right)$$

Note that Equation 5 slightly redefines the initial module-based definition from Equation 1a. Both definitions are entirely equivalent, but we prefer using the second one in this case to introduce the notion of PV capacity, which is simply the cumulative power of all installed modules.

The profitability of an energy system can be measured by its *Net present value (NPV)*, which discounts the future saving from the PV system compared with a no investment case. The system is profitable if the *NPV* is positive, as highlighted in Equation 6. In more detail, the original operating cost of an energy system is calculated by integrating the product of load and instantaneous energy tariff as in Equation 7 (to keep the definition as general as possible, let us assume it is time-varying). The new operating cost takes advantage of the self-consumption to reduce the imported energy and increase the revenue from exporting energy to the grid (Equation 8). In this example, we account for an annual maintenance cost proportional to the investment cost by a factor m (Equation 9). The investment cost is simply proportional to the installed PV capacity by a factor C^{PV} which is the PV specific cost in CHF/kW (Equation 10).

Introduction

Net present value of a PV system:
$$NPV = -I + \sum_y^L \frac{-M_y^{PV} - OPEX_y + OPEX_y^0}{(1+r)^y} \geq 0 \quad (6)$$

Original operating cost:
$$OPEX_y^0 = OPEX^0 = \sum_t P_t^{\text{load}} c_t^{\text{imp}} TS \quad (7)$$

New operating cost:
$$OPEX_y = OPEX = \sum_t \left(P_t^{\text{imp}} c_t^{\text{imp}} - P_t^{\text{exp}} c_t^{\text{exp}} \right) TS \quad (8)$$

Annual PV maintenance cost
$$M_y^{PV} = M^{PV} = mI \quad (9)$$

Total investment cost
$$I = C^{PV} \cdot P_{\text{cap}}^{PV} \quad (10)$$

where subscript y denote the cost for a particular year, L is the system lifetime, r the discount rate, and TS is the integration time step.

Integrating Equations 3 to 5 and 7 to 10 into Equation 6 leads to a condition on the profitability of the system as:

$$\begin{aligned} & -P_{\text{cap}}^{PV} \cdot C^{PV} - \sum_{y=1}^N \frac{\gamma P_{\text{cap}}^{PV} \cdot C^{PV}}{(1+r)^y} - \\ & \sum_{y=1}^L \frac{\left(P_t^{\text{load}} - sc_t Y_t \cdot P_{\text{cap}}^{PV} \right) \cdot ts \cdot c_t^{\text{imp}} - \left((1 - sc_t) \cdot Y_t \cdot P_{\text{cap}}^{PV} \right) \cdot ts \cdot c_t^{\text{exp}}}{(1+r)^y} + \\ & \sum_{y=1}^N \frac{P_t^{\text{load}} \cdot ts \cdot c_t^{\text{imp}}}{(1+r)^y} \geq 0 \end{aligned}$$

which can be simplified to derive a strict condition on the maximum PV specific cost for the investment to remain profitable as:

$$C^{PV} \leq \frac{\sum_{y=1}^L \frac{1}{(1+r)^y}}{1 + m \sum_{y=1}^L \frac{1}{(1+r)^y}} \cdot \sum_t Y_t TS \left[c_t^{\text{exp}} + sc_t \cdot (c_t^{\text{imp}} - c_t^{\text{exp}}) \right] \quad (11)$$

From this equation, we can interpret that the maximum PV specific cost is a weighted average of the average energy value lying between the retail and feed-in tariffs (c^{imp} and c^{exp} hereafter referred to as import or export price). The weights are the instantaneous energy yield (in kWh/kW) and the instantaneous self-consumption sc_t . Simplifying further by assuming a constant import and export tariff, we can introduce the definition of the self-consumption as the ratio between the amount of energy self-consumed and the total PV generation:

$$SC = \frac{\sum_t sc_t \cdot P_t^{PV} \cdot TS}{\sum_t P_t^{PV} \cdot TS} = \frac{\sum_t sc_t \cdot Y_t \cdot TS}{\sum_t Y_t \cdot TS} \quad (12)$$

which simplifies even further Equation 11 into:

$$C^{PV} \leq \underbrace{\frac{\sum_{y=1}^L \frac{1}{(1+r)^y}}{1 + \gamma \sum_{y=1}^L \frac{1}{(1+r)^y}}}_{\text{Annuity factor}} \cdot \underbrace{\sum_t Y_t TS}_{\text{Annual energy yield (kWh/kW)}} \cdot \underbrace{\left[c^{exp} + SC \cdot (c^{imp} - c^{exp}) \right]}_{\text{Upper bounds for the cost of PV energy}} \quad (13)$$

In summary, the specific PV cost has an upper bound to ensure the profitability of the investment, which is the product of :

- the **annuity factor** represents the financial conditions. If the interest rate rises or the time horizon decreases (system lifetime L), this annuity factor decreases, tightening the system's profitability constraint.
- the **annual energy yield** represents the local PV performance. It is directly influenced by the local climate (insolation, temperature), and the module's performance. One can also include system performance, degradation, and failures.
- the **upper bound for the cost of PV energy** lies between the grid import and export price. For a pure producer (no self-consumption), this PV energy cost must be lower than the export tariff to be economically viable. Achieving a 100% self-consumption allows having a cost of PV energy just below the import tariff. This quantity is often called the *levelized cost of PV electricity (LCOE)*.

A comparison between the actual specific cost of Swiss PV installation [Planair et al., 2020] and the upper bound calculated using Equation 13 is drawn in Figure 10. Three specific cases are considered. The bold line is the reference condition (1000 kWh/kW, an interest rate of 3%, import tariff of 20 cts/kWh, export tariff at 10 cts/kWh, a maintenance cost of 5% of the investment cost per year, and self-consumption of 40%). The values are reported in Table 3). Two additional lines with + and o markers are pictured, one for optimistic and pessimistic conditions, as defined in Table 3. This figure should be read as follow. For a given time horizon to recover the investment (read on the upper x-axis, can be the system lifetime, let us take 20 years), the maximum acceptable specific cost under the reference price condition is 1940 CHF/kW. The minimum installed capacity in Switzerland to reach such a price are above 10-15 kW (lower x-axis). Second example - a PV installation of 15 kW costs between 1200 and 2400 CHF/kW. In such conditions, the installation is profitable for all self-consumption ratios between 0 and 100% self-consumption ratio under a time horizon of 15 years. Last example - a self-consumption ratio of around 25-30% is accounted for in the residential sector. Under such conditions and a system lifetime of 30 years, a minimum capacity of 5-10 kW is required to guarantee the investment's profitability. The cost data presented in Figure 10 does not include any subsidies (unique retribution or tax reduction). Those are paramount to ensure the profitability of most of the reported PV installations.

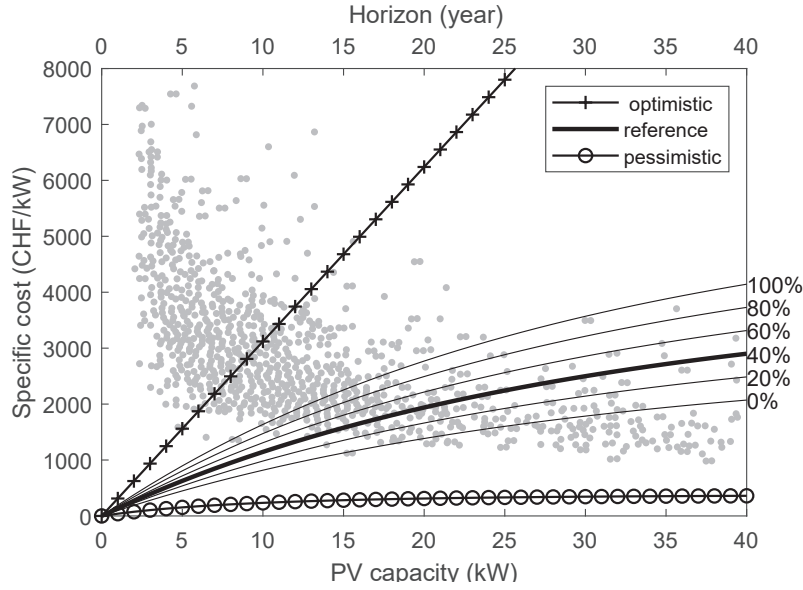


Figure 10 – Dots: PV specific cost as a function of the installed capacity (lower x-axis, source: [Planair et al., 2020]). Lines: maximum PV specific cost as a function of the financial time horizon (upper x-axis) for optimistic, pessimistic, and reference condition and their SC variation, indicated on the right axis.

Table 3 – Reference, optimistic and pessimistic condition values of Figure 10

	Unit	Reference	Optimistic	Pessimistic
Interest rate	%	3	0	7
Energy yield	kWh/kW	1000	1300	900
Import tariff	cts/kWh	20	24	13
Export taiff	cts/kWh	10	13	5
Maintenance cost	%/year	5	0	5
Self-consumption	%	40	100	0

These preliminary results highlight that the current business model of PV systems heavily depends on the tariff and self-consumption. New PV modules can typically reach a lifetime above 25 years which implies that the specific cost of PV should be lower than 3'000 CHF/kW. In light of these results, the challenge of bringing flexibility to PV systems must account for the profitability condition. For instance, any incentives aiming to promote flexibility shall conserve the systems' profitability through a more attractive tariff. Similarly, technical means to increase self-consumption shall increase the system's *NPV*, keeping the other parameters, namely solar insolation, system lifetime, and interest rate constant. In light of these considerations, how can we increase the flexibility of PV systems, ideally in a cost-effective way, to accommodate the network operating constraints and allow a high PV penetration? This brings us to formulate the critical contributions of this thesis and research questions.

Contributions to the field and research questions

This thesis aims to provide critical contributions to increase the integration of PV energy in low-voltage grids. As highlighted in this introduction, the main challenge with the increasing PV penetration at the district scale is that the unbalance between the load and demand can lead to voltage rise, line ampacity breaking, and transformer overloading, which may create damage to the network and the connected loads.

The **main objective** of this work is to reduce the stress on *low-voltage* distribution networks induced by a high penetration of *distributed PV* by promoting *PV systems' flexibility*.

The energy transition implies a significant change in humans' relation to energy. The power sector is shifting from a centralized, dispatchable, and mostly fossil-based generation system to a stochastic, intermittent, and renewable one. In recent decades, the DSOs' role has to ensure that the network has sufficient capacity to meet the demand and uncertainties. With the gradual replacement of conventional generation by renewable energy sources, there is an increasing uncertainty on the supply side. This is where demand-side management (DSM) can play a role. An early definition of DSM was presented by [Gellings, 1985]:

“Demand-side management (DSM) is the planning and implementation of those electric utility activities designed to influence customer uses of electricity in ways that will produce desired changes in the utility's load shape”

Focusing specifically on the residential sector, and the households' consumption behavior, DSM and load shifting have shown promising results to delay investment in additional generation capacity and increasing penetration of renewable energy sources, namely PV [Pina et al., 2012]. This motivates the interest in household flexibility to raise consumption awareness and acceptance of technical flexibility measures. There is still an open question about quantifying the households' flexibility potential and its contribution to the system flexibility. We formulate our first research question as:

Research Question A)

What could be the households' contribution to the PV system flexibility?

This thesis contributes to the field by proposing an analytic tool to quantify this potential from energy measurements. Besides, we attempt to quantify the flexibility by conducting a field experiment to incentivize households to shift their energy and compare this with the estimated potential. This is novel in Switzerland, and such comparison using *in situ* analysis never attempt. A third key contribution to this research question is investigating the consumption pattern change of new PV adopters. While the residential sector's flexibility has

Introduction

been widely discussed, the focus on new PV adopters and their change in consumption habits brings novel insights to the field.

The requirements for flexibility in the power sector [IRENA, 2018] primarily enforce technology coupling roles, such as storage, power-to-heat, and power-to-gas. Such technologies form the second family of flexibility options and will be referred to as technical flexibility. The literature often tackles the combination of these technologies with PV systems from a control point of view [Mulder et al., 2013, Srivastava et al., 2019, Babacan et al., 2017], but there is a lack of research about building up this flexibility.

Research Question B)

How to build cost-effective technical flexibility that reduces the grid impact?

This question implies a definition of the cost-effectiveness that we define as the total cost of ownership of a PV system. Besides, the notion of grid impact should be clarified. First, we contribute to the field by proposing an integrated convex optimization problem to solve simultaneously the design and operation of a PV system with other ancillary technologies (namely electrochemical storage and power-to-heat). Second, we propose design policies to impose (in a coercive way) design rules on PV systems, and investigate their cost-effectiveness. Finally, we contribute to the field by proposing remunerative schemes that enable flexibility by promoting investment in (more) flexible technologies. To contribute to the second part of the research question, namely the grid impact, we investigated how design rules and electricity tariffs potentially modify the grid impact. The interest and focus on tariffs as a lever for enabling flexibility and converting into a positive impact for the grid is, to the best of our knowledge, novel.

The need for flexibility at the district scale is growing with the PV penetration. Nevertheless, it is not clear yet how this flexibility can be harvested. While most studies propose to use centralized flexibility assets to maintain the network in a desirable state [Massucco et al., 2021, Hashemipour et al., 2018], we focus more on how distributed flexibility sources can be used in a coordinated way, with minimum impact on the PV systems owner profitability to achieve the same goal. There is, however, a lack of research about how flexibility can benefit grid operation.

Research Question C)

How can flexible distributed PV systems contribute to mitigating the network expansion cost?

We contribute to this question by evaluating how behavioral and technical flexibility allows to mitigate the grid impact and propose methodologies to assess the economic benefits. We

contribute to the flexibility value definition, which is one of the challenges of the current energy system research field.

Overall this doctoral work resulted in four peer-reviewed publications as main or co-author, two articles in preparation, and several collaborations with the *Industrial Process and Energy Systems Engineering* laboratory of EPFL in the context of the *SCCER-FURIES* project.

Publications

- Holweger, J., Dorokhova, M., Bloch, L., Ballif, C., and Wyrsh, N. (2019). Unsupervised algorithm for disaggregating low-sampling-rate electricity consumption of households. *Sustainable Energy, Grids and Networks*, 19:100244
- Sánchez, C., Bloch, L., Holweger, J., Ballif, C., and Wyrsh, N. (2019). Optimised Heat Pump Management for Increasing Photovoltaic Penetration into the Electricity Grid. *Energies*, 12(8):1571
- Bloch, L., Holweger, J., Ballif, C., and Wyrsh, N. (2019). Impact of advanced electricity tariff structures on the optimal design, operation and profitability of a grid-connected PV system with energy storage. *Energy Informatics*, 2(1):16
- Holweger, J., Bloch, L., Ballif, C., and Wyrsh, N. (2020a). Mitigating the impact of distributed PV in a low-voltage grid using electricity tariffs. *Electric Power Systems Research*, 189:106763
- Holweger, J., Ballif, C., and Wyrsh, N. (2021a). Assessing the cost of distributed flexibility versus grid reinforcement in low-voltage networks. Manuscript in preparation
- Holweger, J., Bloch, L., Ballif, C., and Wyrsh, N. (2021b). Privacy-preserving methods for smart meters based network simulations. Manuscript in preparation

Reports

- Bloch, L., Holweger, J., Wyrsh, N., Tommasi, H., and Girardin, L. (2017). SCCER JA-RED - Description of the multi-energy demonstration system in the RE demo site - Deliverable 1.2.1. Technical report, École Polytechnique Fédérale de Lausanne, EPFL Valais/Neuchâtel
- Holweger, J., Bloch, L., and Wyrsh, N. (2018). SCCER-FURIES - Determination of the flexibilisation potential of the electricity demand. ReEL D114b. Technical report, École Polytechnique Fédérale de Lausanne
- Middelhaue, L., Bloch, L., Girardin, L., Stadler, P. M., Holweger, J., and Tommasi, H. (2018). SCCER-FURIES - Design of Sizes for Buildings Energy Systems as a Function of the Grid Evolution - Deliverable 1.4.1a. Technical report, École Polytechnique Fédérale de Lausanne, EPFL Valais/Neuchâtel

- Perret, L., Chevillat, Y., Wyrsh, N., Bloch, L., Holweger, J., Weber, S., and Péclat, M. (2019). Flexi 2 Déterminer le potentiel de flexibilisation de la demande d'électricité des ménages. Technical report, Fedral office for energy
- Middelhauve, L., Bloch, L., Holweger, J., Stadler, P. M., and Girardin, L. (2019). SCCER JA-RED - Detailed evaluation of the grid operation bottlenecks and load shifting potential for the reference system - Deliverable 1.2.2. Technical report, École Polytechnique Fédérale de Lausanne, EPFL Valais/Neuchâtel
- Holweger, J., Bloch, L., and Wyrsh, N. (2020b). SCCER-FURIES - Definition of optimal control of DHW for self-consumption strategies. Technical report, École Polytechnique Fédérale de Lausanne
- Bloch, L., Girardin, L., Holweger, J., and Middelhauve, L. (2020a). SCCER JA-RED - A list of possible ancillary services for enhanced grid operation and implementation of the most effective ones at the RE demo site - Deliverable 1.2.3. Technical report, École Polytechnique Fédérale de Lausanne, EPFL Valais/Neuchâtel
- Bloch, L., Holweger, J., and Wyrsh, N. (2020b). SCCER-FURIES - Deployment recommendation for large penetration of PV and distributed storage. Technical report, École Polytechnique Fédérale de Lausanne

Outline of the thesis

Chapter 1 contributes to answering Research Question A) by proposing an algorithm to disaggregate the households' electric consumption measurements into categories of appliances and evaluate the shiftable energy potential.

Chapter 2 aims to extend the knowledge about households' flexibility by presenting the results of a field trial and compare them with the potential estimated using the proposed disaggregation method. Besides, the new PV adopters' flexibility is also discussed. This complements Research Question A).

Chapter 3 introduces our fundamental models for technical flexibility. It consists in an integrated optimization problem to solve the design and operation of a PV system with storage and power-to-heat technologies. Contributions to Research Question B) are also presented regarding how design rules can increase technical flexibility in a cost-effective way.

Chapter 4 contributes to Research Question B) by investigating how advanced electricity tariffs impact the design and operation of PV systems, thus, their flexibility. Also, it provides contributions to Research Question C) by investigating the resulting flexibility impact on a low-voltage grid.

Chapter 5 contributes to Research Question C) by investigating how behavioral and technical flexibility allows reaching or increasing the PV penetration in low-voltage grids. A contribution

to the estimation of the flexibility value is also proposed.

Chapter 6 finally proposes critical insight about the decarbonization of Switzerland and the path toward a high distributed PV penetration to reach net-zero emission by 2050.

1 A disaggregation method for household's smart meter analytics

Understanding households' energy consumption composition is critical for proposing customer services such as energy efficiency measures or assessing flexibility potential (ability to adapt its power demand). Non-intrusive load monitoring is a technique to disaggregate households' whole house power measurements and retrieve the original appliances' power. In this chapter, we propose a disaggregation method suited for low-resolution measurements provided by smart meters.

Part of this section has been published in the following work:

Holweger, J., Dorokhova, M., Bloch, L., Ballif, C., and Wyrsh, N. (2019). Unsupervised algorithm for disaggregating low-sampling-rate electricity consumption of households. *Sustainable Energy, Grids and Networks*, 19:100244

1.1 Introduction

To evaluate the households' flexibility potential, one needs to estimate the fraction of their energy consumption that could be shifted in time. This quantity is a valuable flexibility metric for better understanding how to design demand-side management programs and understand how to harvest this flexibility source. For this purpose, non-intrusive load monitoring (NILM) techniques seem promising to measure, potentially *in situ*, the flexibility potential. NILM has been defined by [Hart, 1992] as:

“A non-intrusive load monitoring determines the energy consumption of individual appliances turned on and off in an electric load”

In other words, the problem is to disaggregate, from a whole house load measure, all individual

appliances' consumption curves. In mathematical form, this can be expressed as:

$$\mathbf{P}^t = \sum_m P_m^t + \epsilon_t \quad (1.1)$$

Problem: find an estimate \hat{P}_m^t of P_m^t

where \mathbf{P}^t is the aggregated power signal of a house over time t , P_m^t corresponds to the power signal of the m^{th} appliance, and ϵ_t is the measurement noise.

Regardless of the end goal of such a technique, NILM is a widely addressed topic. The research community has proposed different approaches to disaggregation. Researchers have classified the algorithms into several categories: high and low frequency, supervised and unsupervised, residential and industrial, and others.

One categorization technique is based on the frequency of the aggregated power measurements. As proposed in [Esa et al., 2016], low-frequency measurements correspond to sampling rates of 1 Hz and lower, while high-frequency measurements require data of typically a few kHz to half a MHz. The principle is to measure voltage and current at sufficiently high sampling rates and identify individual appliances' signatures as in [Liang et al., 2010]. These methods are usually based on transient analysis of a power signal, i.e., on extracting a transient waveform's shape and length. Although high-frequency approaches are highly promising, it is currently not cost-effective to implement such sensing capabilities and data transmission requirements in smart meters [Wang et al., 2018].

In contrast, methods requiring a significantly lower sampling frequency are typically based on steady-state features such as measuring the instantaneous power signal at a low sampling rate, as described by [Zoha et al., 2012]. Both active and reactive power can be used as appliances' feature, although active power is the most characteristic feature. Nowadays, most smart meters transmit signals in intervals of 5, 10, or 15 minutes or longer. In an extreme case of divining appliances' consumption with little information, [Birt et al., 2012] attempts to disaggregate the power signal received from smart meters at a one-hour sampling rate. They create a regression model on the external and internal temperatures to separate the consumption of heating and cooling systems from the rest of the load. [Zhao et al., 2018] tackle the disaggregation problem on both 15-min and 1-hour electrical measurements using the supervised K Nearest Neighbours algorithm. [Zhao et al., 2018] extract features from time-of-use profiles of particular appliances and propose a method to select the most valuable features per device. Validation on three publicly available datasets has shown the ability of such an algorithm to disaggregate up to 62% of the daily energy consumption. In [Batra et al., 2016], the proposed methodology uses even less information since only monthly bills are used to disaggregate the end-use energy consumption into categories (e.g., fridge, lights, washing machine, etc.). Batra et al. do this by relating, using carefully selected features, a household equipped with a single smart meter system to a set of K neighboring homes equipped with sub-meters at the appliance level. The consumption of a particular appliance in a test household is predicted by averaging the consumption of the corresponding K sub-metered devices. In

the following, low-frequency measurements refer to sampling rates lower than 1 sample every 5 minutes. Note that this slightly contradicts the notion of [Zoha et al., 2012].

Another way to categorize disaggregation algorithms is to split them into supervised and unsupervised, as suggested in [Faustine et al., 2017]. In a supervised method, the disaggregation of an unknown power signal is preceded by a training phase, where the algorithm "learns" to recognize individual appliances' power signals from the aggregated signal based on available labeled data. An unsupervised method does not require such preliminary treatment as it deals with unlabeled data and can directly perform the disaggregation. In both cases, the approaches were adopted from the field of machine learning.

One of the 'classic' supervised techniques of this field is to build an artificial neural network to train an algorithm to create a non-linear estimator of the disaggregated power measurements [Wang, 2003]. Neural networks have been used successfully in [Ruzzelli et al., 2010, Kelly and Knottenbelt, 2015a, Biansoongnern and Plangklang, 2016]. An event-based method is another approach to disaggregate real-power measurements but requires a relatively high granularity level (typically with a sampling frequency in the range of seconds). A method based on a decision tree was proposed by [Liao et al., 2014] and was used in [Stankovic et al., 2016] to disaggregate 8 s real-power measurements. Similar to computer vision and image processing techniques [Mairal et al., 2009], dictionary learning through sparse coding was proposed by [Kolter et al., 2010] and was tested on a low-sampling-frequency dataset (one-hour time interval). An upgraded version using powerlets as words for dictionary learning was developed in [Elhamifar and Sastry, 2015]. A more recent approach [Singh and Majumdar, 2017] extends the discriminative sparse coding method by decomposing a problem into multiple sub-problems. A similar technique using extended formulation is the Sum-to-k constrained non-negative matrix factorization (S2K-NMF), tested by [Rahimpour et al., 2017]. This method claims the advantage of enabling whole-building disaggregation at a low sampling frequency.

Unsupervised methods, instead, are not concerned with extracting functional dependencies between the data and target variables. Therefore, the preceding training stage of learning from labeled data is absent, and algorithms are directly applied to the dataset of interest. A review of unsupervised methods for load disaggregation can be found in [Bonfigli et al., 2015]. One standard unsupervised method is the factorial hidden Markov model (FHMM) discussed in [Zoha et al., 2013, Kim et al., 2011]. This method can also be applied in a supervised way, as in [Batra et al., 2014, Bonfigli et al., 2017]. The most significant drawback of most unsupervised methods is their requirement of a relatively high sampling frequency (typically higher than 1/60 Hz). This makes it difficult and costly to collect the necessary input data for these algorithms, thus creating obstacles towards implementing such solutions in the real world.

All the methods mentioned above basically perform analysis and transformation of the power signal. An alternative or complementary approach is to investigate the power signal's un-

derlying graph structure [Kumar and Chandra, 2017a]. This is typically described as graph signal processing (GSP). Successful implementation of such algorithms for disaggregation was performed in [Kumar and Chandra, 2017a, He et al., 2016, Kumar et al., 2016, Kumar and Chandra, 2017b]. In [Zhao et al., 2016], a GSP approach was used to perform unsupervised disaggregation.

The drawback of supervised methods is the need for labeled data, which are often not public or generalizable. Therefore unsupervised methods are more appropriate for general study. The unsupervised methods presented above require either high sampling frequency measurements (smaller or equal to 5 minutes) or do not allow to disaggregate several categories of appliances but rather one versus the others such as in [Birt et al., 2012]. Therefore there is a need for an unsupervised disaggregation algorithm designed for a low sampling rate and able to get information on all household's appliances.

In this work, we propose an unsupervised methodology to estimate a household's energy consumption for selected appliance categories based on their characteristics and active power measurements at a low sampling rate (15 min). The method relies only on general information about households and measurements of their energy consumption. Although our proposed methodology does not yet consider space heating or cooling (as the latter is not common in central Europe), it tries to reach a finer level of detail by splitting the load into categories. The categories are formed by grouping appliances together according to their most common usage related to household's activities.

The novelty of this methodology consists in proposing a hybrid approach, which lies between load simulation and load disaggregation. Additionally, we use general household data that were not previously considered for NILM purposes. Table 1.1 summarizes the input features of selected reference algorithms and highlights the original input features required by our algorithm - inhabitants' age groups, employment status, and appliance usage frequency. These features define the household profile. It can be acquired easily through surveys and might be used as well for social science experiments or customer services purposes. Therefore, our methodology can be defined as an unsupervised person-centric load disaggregation algorithm. The proposed methodology is an essential analytical tool to address this thesis' Research Question A) about the households' flexibility potential.

The following section will describe the methodology for disaggregating households' whole house load measurement at a sampling rate of 15min, then compare this algorithm with state-of-the-art disaggregation methods. We use three datasets collected in central Europe to test our proposed algorithm and benchmark it. Additionally, we propose specific performance metrics to compare the algorithms.

Table 1.1 – Summary of the input features for the selected references

Ref.	S/U ^a	Δt	Input features ¹
[Liang et al., 2010]	S ^b	1 s	P , Q , harmonics, instantaneous admittance waveform, current waveform, instantaneous power waveform, eigenvalues, switching transient waveform
[Zhao et al., 2018]	S	1 h	P , Q , appliance list
[Batra et al., 2016]	S	1month ^c	P , house area, #rooms, #occupants, temperature
[Ruzzelli et al., 2010]	S	1 min	P , RMS current, RMS voltage, Peak current, peak voltage, sampling rate, power factor, state
[Kelly and Knottenbelt, 2015a]	S	6 s	P , appliance power time series of pre-defined window length for model training
[Biansoongnern and Plangklang, 2016]	S	1 s	P , Q
[Liao et al., 2014]	S	1 s - 1 min	P
[Kolter et al., 2010]	S	1 h	P
[Elhamifar and Sastry, 2015]	S	1 s	P
[Singh and Majumdar, 2017]	S	10 min	P
[Rahimpour et al., 2017]	S	30 s	P
[Zoha et al., 2013]	S	3 s	P , Q , appliance list
[Bonfigli et al., 2017]	S	1 min	P , Q , individual appliance power signal for model training
[Kumar and Chandra, 2017b]	S	3 s	P
[Birt et al., 2012]	U	1 h	P , temperature, multiple-linear fit ²
[Kim et al., 2011]	U	3 s	P , appliance list ² , states distribution model ² , power distribution model ²
[Zhao et al., 2016]	U	1 min	P , database of appliance signatures ²
Proposed algorithm	U	15 min	P , house heating system type (electric or not), appliance list and usage frequency, inhabitants number and age, nominal power per appliances ² , activity probability ²

^a S: supervised, U: unsupervised

^b the proposed method could also be applied in an unsupervised manner

^c disaggregation done at a one-month resolution and training at 15min

¹ for supervised algorithms, input features are used for both training of the model and disaggregation. All of them require the appliance power time series.

² input parameters of the unsupervised models

1.2 Algorithm

The algorithm introduced in this section is called the *device usage prediction* (DUE) algorithm. The algorithm requires three main inputs:

- a generic time-of-use survey, in order to extract the activity probability
- the characteristics of the household as listed in Table 1.1
- the households whole house load measurements

The following sections will present the methodology's main steps, starting with a refresher on Markov models.

1.2.1 Activity chain modeling

A Markov chain describes a stochastic process in which a system may have multiple states $x \in S$. The probability of switching from state S_i to S_j is described as $a_{i,j} = p(x^t = S_i | x^{t+1} = S_j)$. The resulting matrix $a_{i,j}$ is called the transition matrix. The initial condition for the first element of the chain is described by the initial probability distribution $\pi_i = p(x^0 = S_i)$. A hidden Markov model (HMM) states that the system is observed through a set of external variables y that can have multiple states O_k (the external variable can also be continuous) linked to the system states by the relation $b_{k,i} = p(y^t = O_k | x^t = S_i)$. This matrix is called the emission matrix [Rabiner, 1989].

In the proposed methodology, an activity chain is modeled as a Markov process. The transition matrix and initial probability distribution also depend on two main external features. One is related to the type of day $D \in [\text{weekday, Saturday, or Sunday}]$; the other is related to the household's characteristics, namely, the employment state $E \in [\text{full-time, part-time, student, retired, unemployed}]$ and the age group $G \in [\text{teenager, adult active, senior active, senior inactive}]$ of the inhabitants. Hence the transition matrix and initial probability distribution are functions of D , E , and G .

The 2005 Netherlands time-of-use survey [Sociaal en Cultureel Planbureau, 2005] was chosen as a representative data source to extract the activity probability. Although it is questionable if the behavior of Dutch citizens is representative of the behavior of all central Europeans, it seems like a reasonable assumption, and this limitation could be overcome by the use of similar surveys of other countries such as the 2014-2015 UK time-of-use survey [Gershuny and Sullivan, 2017].

A time-of-use survey provides a diary of activities, in which individuals record what activity was done at each time of the day. In the Dutch time-of-use survey, the reported activities were divided into a set of 14 activity states S , summarized in Table 1.2.

From the diaries, it is possible to extract an activity event table in which each event i is described by an activity $s_i \in S$, that is performed by an individual who belongs to an employment group $e_i \in E$ and age group $g_i \in G$, a start time $t_i^0 \in T$, an end time $t_i^1 \in T$ and a type of day $d_i \in D$. T is the time discretization of a day (here, the day is discretized at a 5-min resolution). For each employment group $e^* \in E$, age group $g^* \in G$, and type of day $d^* \in D$, the computation of the initial state (activity) probability distribution is described by Equation 1.2:

$$\pi_{e^*,g^*,s^*} = \frac{\sum_i (\delta_{e^*,g^*,t^0,i} \cdot \delta_{s^*,i})}{\sum_i (\delta_{e^*,g^*,t^0,i})} \quad \forall s^* \in S$$

where

$$\delta_{e^*,g^*,t^0,i} = \begin{cases} 1, & \text{if } e_i = e^* \cap g_i = g^* \cap t_i^0 = 00:00 \\ 0, & \text{otherwise} \end{cases} \quad (1.2)$$

$$\delta_{s^*,i} = \begin{cases} 1, & \text{if } s_i = s^* \\ 0, & \text{otherwise} \end{cases}$$

To compute the coefficient of the transition matrix, a transition event table is derived from the activity event. Each transition j is defined by two activities $s_j^0, s_j^1 \in S$, at time $t_j \in T$ defined such that for a transition from the activity event k to the activity event l , $t_j = t_k^{end} = t_l^{start}$. As for the activity event table, the employment and age group e_j and g_j is reported. Similar to the initial probability distribution calculation, for each group $e^* \in E$, $g^* \in G$ and for each type of

Table 1.2 – List of possible activity states and related possible appliances used

Activity	Appliances
Cleaning	vacuum, TV, stereo, lights
Using a computer	TV, stereo, PC, laptop, printer, lights
Cooking	stove, oven, microwave, kettle, TV, stereo, lights
Washing dishes	dishwasher, TV, stereo, light
Eating	coffee maker, microwave, kettle, TV, stereo, lights
Do the homework	TV, stereo, PC, printer, laptop, lights
Playing a game	TV, stereo, gaming console, lights
Laundry	washing machine, tumble dryer, TV, stereo, lights
Music	stereo, PC, tablet, laptop, lights
Outdoor	∅
Sleeping	∅
Watching TV	TV, DVD player, PC, tablet, laptop, lights
Showering	hairdryer, TV, stereo, lights
Working	∅

day $d^* \in D$, the coefficient of the transition matrix is computed as described by Equation 1.3:

$$a_{e^*, g^*, s^{1*}, s^{2*}, t^*} = \frac{\sum_j (\delta_{e^*, g^*, t^*, j} \cdot \delta_{s^{1*}, s^{2*}, j})}{\sum_j (\delta_{e^*, g^*, t^*, j} \cdot \delta_{s^{1*}, j})} \quad \forall s^{1*}, s^{2*} \in S \quad \forall t^* \in T \setminus [00:00]$$

where

$$\delta_{e^*, g^*, t^*, j} = \begin{cases} 1, & \text{if } e_j = e^* \cap g_j = g^* \cap t_j = t^* \\ 0, & \text{otherwise} \end{cases}$$

$$\delta_{s^{1*}, s^{2*}, j} = \begin{cases} 1, & \text{if } s_j^1 = s^{1*} \cap s_j^2 = s^{2*} \\ 0, & \text{otherwise} \end{cases}$$

$$\delta_{s^{1*}, j} = \begin{cases} 1, & \text{if } s_j^1 = s^{1*} \\ 0, & \text{otherwise} \end{cases}$$
(1.3)

The generation of an activity chain is performed by generating random integers where each integer value corresponds to the activity state $x^t \in S$. The probability distribution is given either by the transition matrix A or by the initial probability distribution π . Similarly, the activation duration is generated using a discrete probability distribution. The sequence for generating the activity chain is depicted in Figure 1.1.

The algorithm to generate a random integer from a given discrete probability distribution $f(n), n = 1 \dots N$ (corresponding to one column of A) is the following:

$$x_{\text{rand}} = \text{find first } n \text{ such that } \left(\epsilon \leq \frac{F(n)}{\sum_{i=1}^N f(i)} \right)$$
(1.4)

with $F(n)$ being the cumulative probability distribution, i.e., $F(n) = \sum_{i=1}^n f(i)$, and ϵ a pseudo uniformly distributed random number ($\epsilon \in]0, 1[$) from the MATLAB `rand()` command.

The following will describe how the input parameters π and a are used to break down the house's power measurement into eight categories. Each category consists of a group of appliances, as presented in Table 1.3.

1.2.2 Algorithm's main steps

As presented previously, the basic idea is to find an estimate \hat{P}_m^t of P_m^t from the total power signal P^t as stated in Equation 1.1. The approach chosen here is to link the observed power signal P^t with each household inhabitant's activity chain. The main workflow is presented in Figure 1.2 and can be described as the following. For a given household, knowing its characteristics and a given measured power signal $L(t)$, the algorithm takes each day separately and performs a sequence of actions:

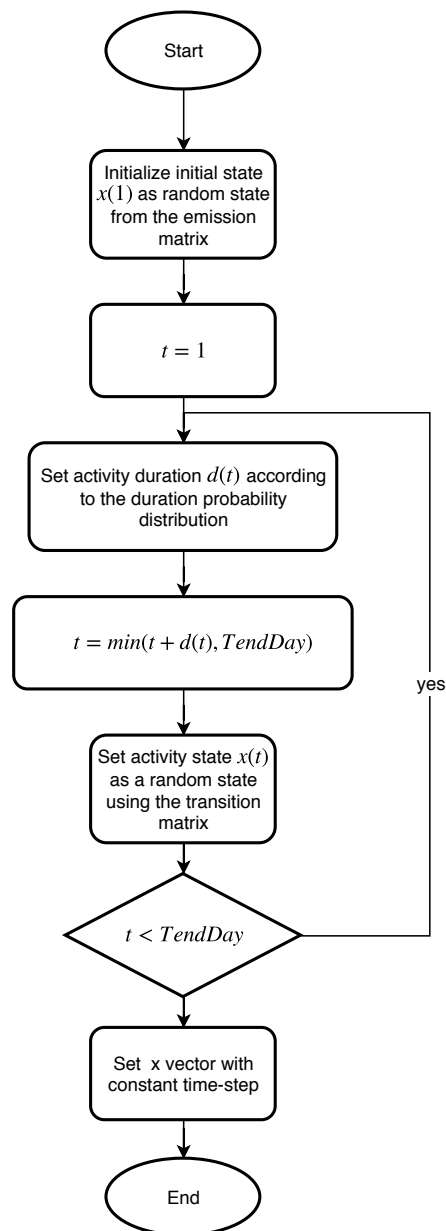


Figure 1.1 – Generation of random activity

1. Filter out the standby consumption by identifying the minimum power over the considered day. $\hat{P}_{standby}^t = \min_t(P^t) \forall t \in T$ where T is the time domain of the considered day. This definition of standby results in a constant part of the fridge consumption to standby. Thus, the fridge consumption recognition steps only deal with the variable part of the fridge consumption.
2. Filter out the fridge. The typical periodic signal (considered over all nights of the load curve) is extracted for the first day. This is assumed to be the fridge's consumption pattern. Then, each subsequent day, the fridge signal is synchronized with the measured power signal before filtering out. The seasonal variations of the fridge consumption are taken into account by daily capture of the signal pattern. The fridge consumption pattern is removed from the power signal for the following steps.
3. Detect the peaks using the method from [Billauer, 2012]¹. A peak in a vector v can be seen as the highest point between two valleys. In other words, a peak and valley are defined by a thresholds $\delta = v^{\text{peak}} - v^{\text{valley}}$. The method goes through v and records moving maximum. When the difference between the previous maximum and the current element is greater than the thresholds, this means that the previous maximum is a local peak. The inverse method applies to local valleys. After each local peak/valley is found, the moving maximum/minimum is reset to the current value.
4. If any peak indicates that someone is at home for this day, infer the power signal (including lights) generated by each person. This procedure is described in the next paragraph.

The methodology to infer the power signal generated by each person in the household can be summarized as follows. An activity chain is generated for each person in the household, then a corresponding power signal is estimated. The procedure is repeated until the difference between the measured and simulated load curves is smaller than a given tolerance. The workflow of this process is depicted in Figure 1.3.

¹<http://www.billauer.co.il/peakdet.html>

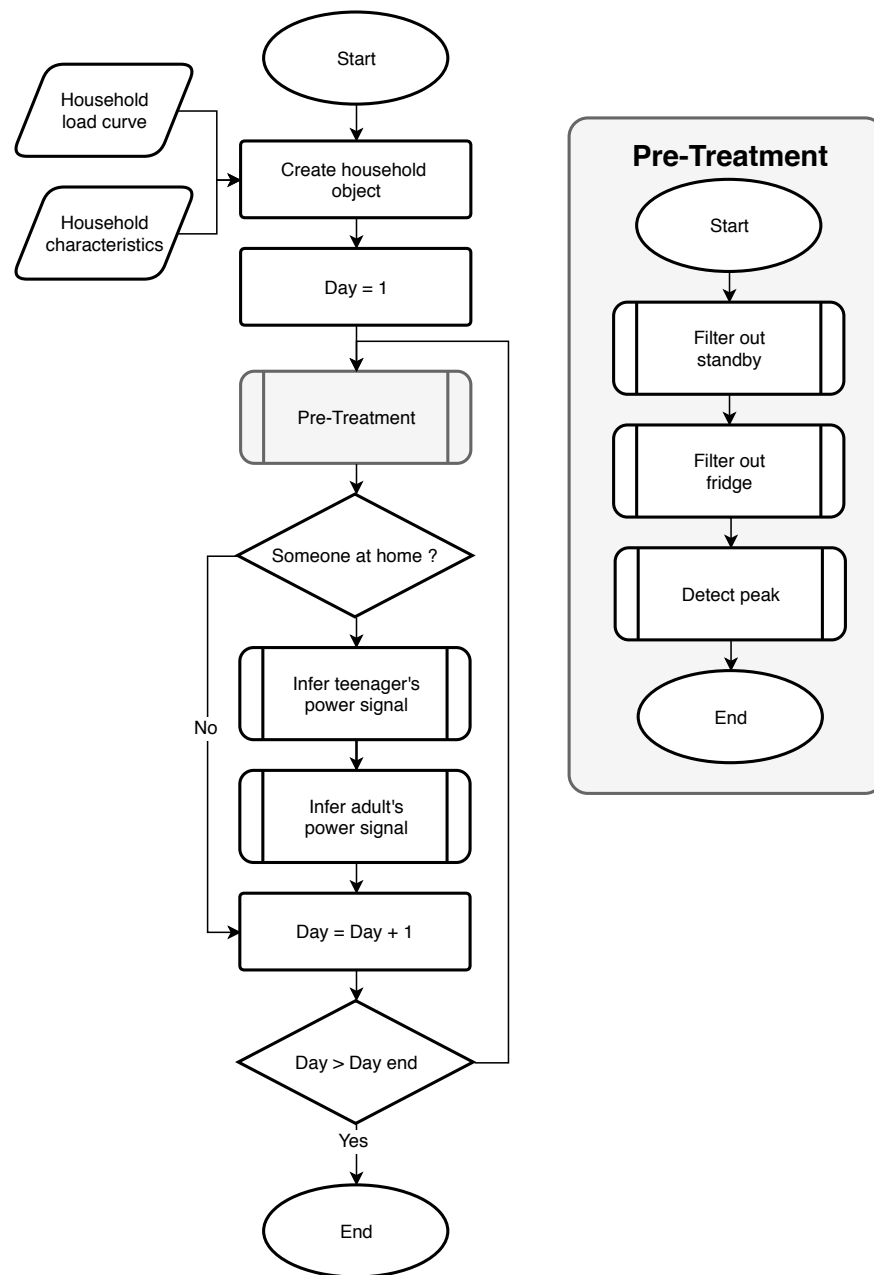


Figure 1.2 – General workflow of the proposed methodology

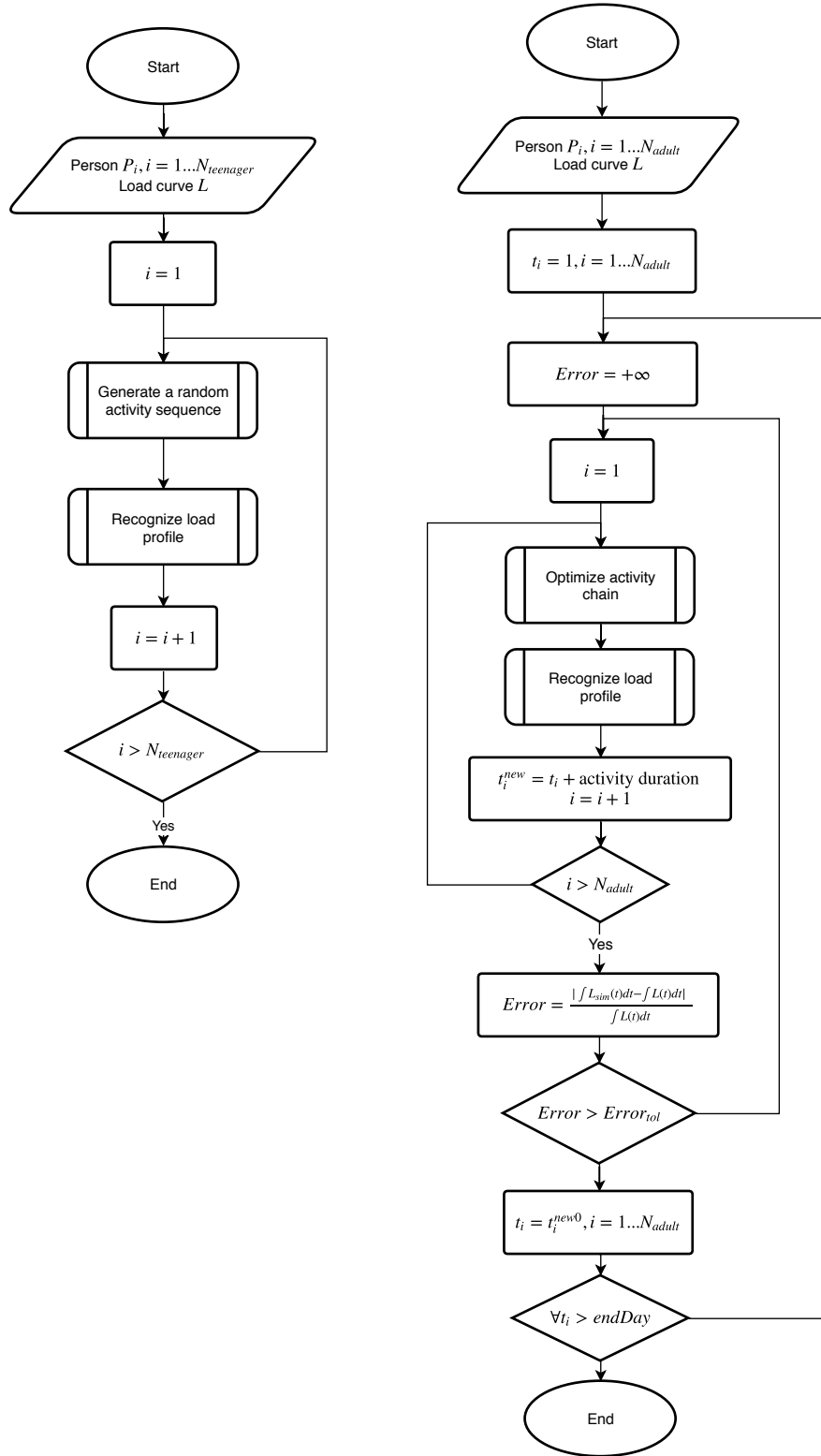


Figure 1.3 – Methodology to infer the individual power signal of a teenager (left) and adult (right)

The inhabitants of the household are treated separately in this step. Teenagers (10 to 18 years old) are considered to have unpredictable activity chains and are treated independently, as depicted in Figure 1.3. Adults, the main energy consumers of the households, are considered together in the optimization step. If any power peaks are detected in the considered daily load curve, all inhabitants are assumed to be at home. No partial occupancy is considered here, although this could be an option for further improvements.

The following sections will detail the sub-processes mentioned in Figures 1.2 and 1.3, namely, the "pre-treatment", procedure from Figure 1.2, and the standby and fridge consumption recognition. Then the optimize activity chain and the recognize load profile process from Figure 1.3 will also be presented.

A "Pre-treatment" process

The pre-treatment process consists in filtering out the standby consumption and fridge consumption (as shown in Figure 1.2). Retrieving the standby power from the aggregated load curve is straightforward. The minimum value of the current day's load is considered the standby consumption. This value is then subtracted from the aggregated power signal, as shown in Figure 1.4.

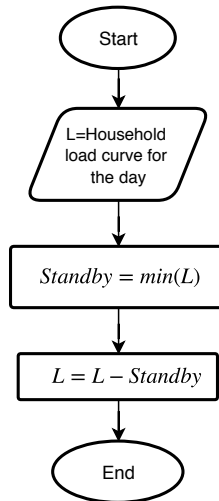


Figure 1.4 – Standby filtering

Filtering out the fridge consumption pattern involves a few more steps. The main workflow is represented in Figure 1.5. On the first call (i.e., for the first considered day), a filter is applied to extract all nights of the dataset. The night starts at 02h30 and ends at 05h00. The resulting samples are further clustered based on the mean power consumption (using simply the MATLAB `hist` command). The mean power of the largest cluster is then considered to be the mean power consumption of the fridge during the night. At the end of this procedure, the actual fridge nominal power is estimated and saved in the household inventory according to

the following expression:

$$P_{\text{fridge New}} = P_{\text{fridge Old}} \cdot \frac{\text{fridge mean power}}{P_{\text{fridge Old}} \cdot \beta_2} \quad (1.5)$$

where $P_{\text{fridge Old}}$ is the default nominal fridge power, and β_2 is the fridge's duty cycle during the night. Both are reported in Table 1.3.

Finally, the fridge cycle is adjusted by minimizing, for the cycle start time and the cycle length, the sum of the squared error between the measured power signal at night (L_{night}) and the simulated power signal (L_{fridge}).

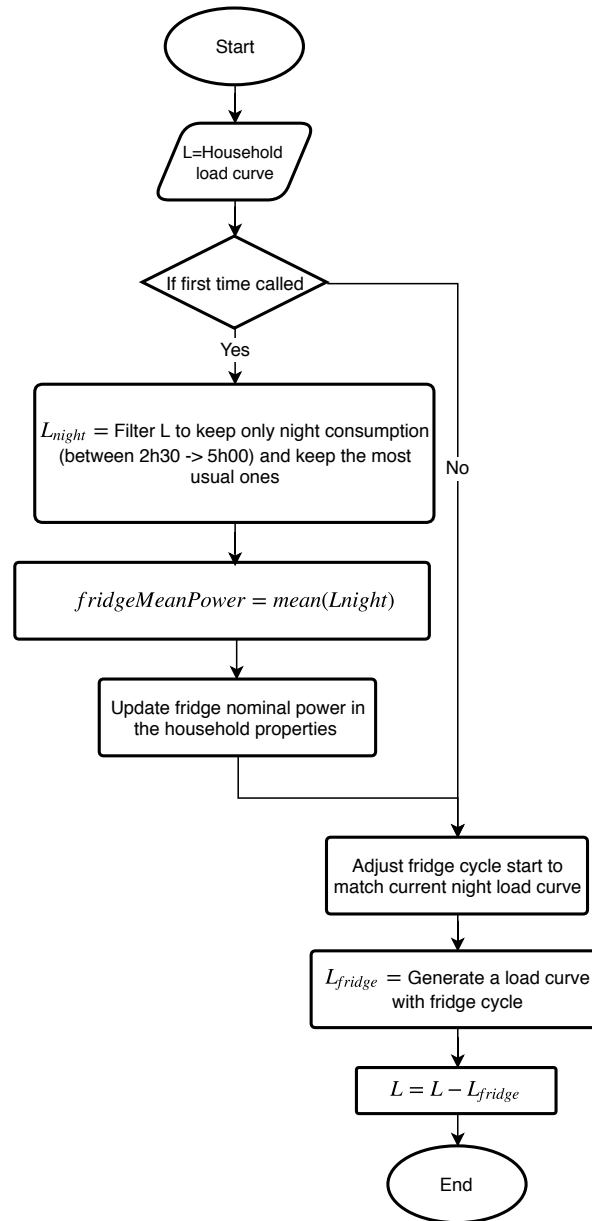


Figure 1.5 – Fridge filtering flow chart

B The "Optimize activity chain" process

This process aims at identifying a possible activity for a given household inhabitant, considering the available energy budget for the respective time frame and the characteristics of this person. This process is divided into three steps:

1. First, a list of possible activities and their corresponding probability of occurrence are defined. In other words, this step selects transition matrix a (or initial probability

distribution π , if it corresponds to the first element in the chain) according to the type of day d , the employment state of the person e and the person's age group g . The whole list of possible activities is summarized in Table 1.2.

2. Secondly, an activity is selected based on the probability of this activity occurring (i.e., the transition matrix or the initial probability distribution), as well as the duration of this activity based on the duration probability distribution corresponding to this activity.
3. Finally, the compatibility between the chosen activity and the measured load curve is evaluated. If the measured load power is low (relative to the mean power level of the inventory of household appliances), the selected activity cannot be an activity that requires high-power appliances and vice versa. This step applies only to adults. For teenagers, it is assumed that the activity chain is random.

Our method relates the energy usage to the activities within it by assuming the appliance usage probability per activity and the power demand per device. The activity chain could be used as an additional output of the algorithm, but this is not the central scope here and would require a particular caution for the analysis. This is an opposite approach from the one used by [Stankovic et al., 2016], who employed a supervised NILM method and individual appliance monitoring to actually correlate the activity chain from the disaggregated energy consumption.

C The "Recognize load profile" process

At this stage, an assumption on a single inhabitant's activity and the duration of that activity has been formulated. Based on this hypothesis, this process aims to infer the possible power signal of each appliance category sequentially. As shown in Figure 1.6, the appliance category recognition sequence is organized so that the most energy-consuming activities are treated first. The Light category is an exception, as it is treated after the Heating category. This is because lighting has a weak correlation with the type of activity but a strong correlation with the occupancy.

The standard procedure for each of these steps is the following:

1. Identify the period in which the activities that correspond to the category were detected.
2. For each appliance that belongs to this activity and exists in the household inventory, check if the energy budget and time budget are sufficient to run the appliance. Note that at every iteration of this step, the order of devices is set randomly to not always start with the same appliance. The list of appliances that belong to each activity is presented in Table 1.2.
3. If the energy budget and time budget are sufficient, set the device as used and simulate the corresponding power signal. If the house has several appliances of the same type,

a power signal is generated for each appliance. Based on the NILM wiki² and field experience, the nominal power, probability, and duration usage for each appliance have been reported in Table 1.3. These reference values should be updated with the appliances' market evolution and the introduction of more efficient devices.

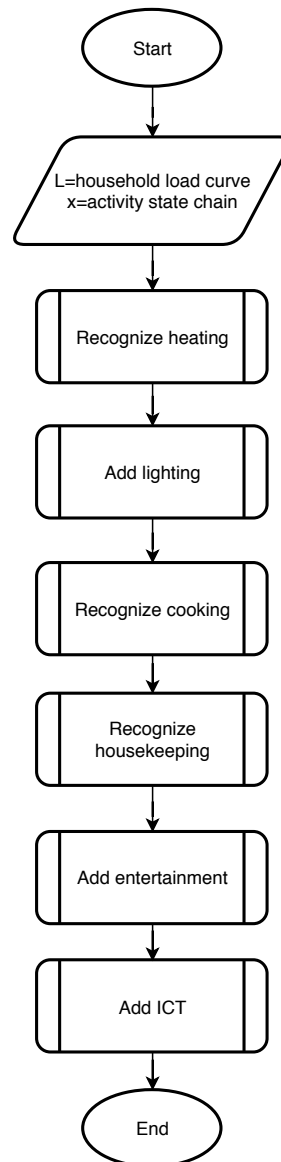


Figure 1.6 – Workflow to infer each category of appliance in the aggregated power signal

The following provides more details about each sub-process of Figure 1.6. At the start of the process, the aggregated load curve and activity chain for the considered person are the two main input arguments. Each sub-process also includes a device state vector that is not always

²<http://wiki.nilme.eu/appliance.html>

explicitly mentioned for clarity. This state vector prevents the use of the same appliance by two people simultaneously and hence an overestimation of the consumption of this category. Additionally, when several of the same appliances are in the house, the state vector helps to consider that a similar appliance might be already in use when simulating a new device power signal.

"Recognize Heating". The current version does not consider yet central electric heating. Only a hairdryer is explicitly extracted.

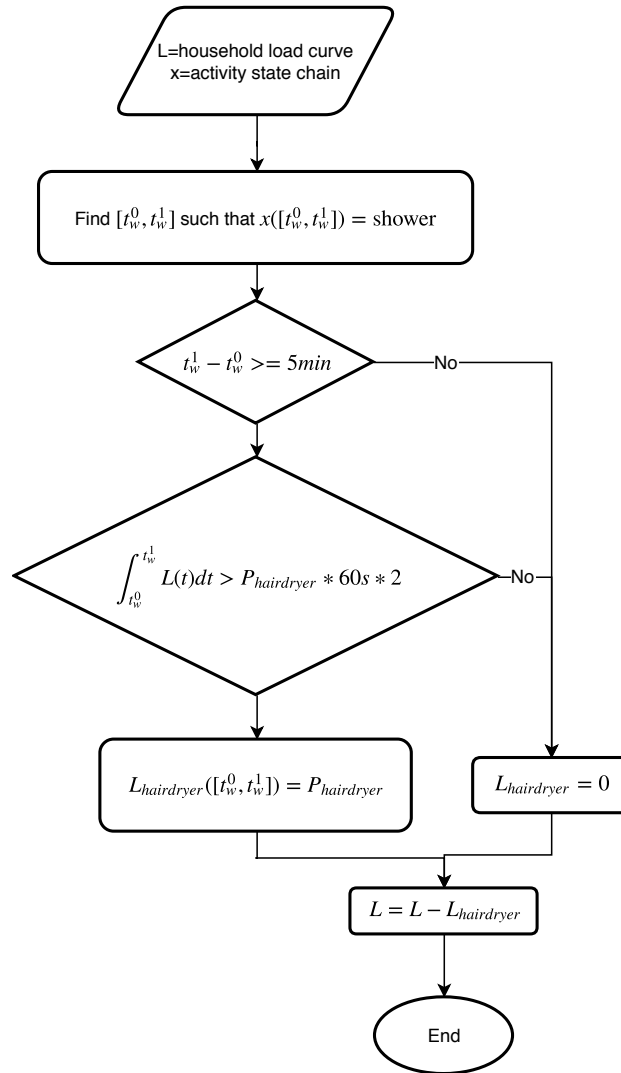


Figure 1.7 – Recognize Heating sub-process

The first step consists in detecting a period $[t_w^0, t_w^1]$ where the activity corresponds to *Shower*, then check that the duration of this activity is at least 5 min. The core of this process, depicted in Figure 1.7, is to check that enough energy is consumed between t_w^0 and t_w^1 for the hairdryer to run. Finally, the corresponding power signal $L_{\text{hairdryer}}$ is generated and subtracted from the

aggregated load curve L .

"Add Lighting". As light is not strictly related to activity but rather to occupancy, this sub-process occurs at the beginning of the "recognize load profile" process.

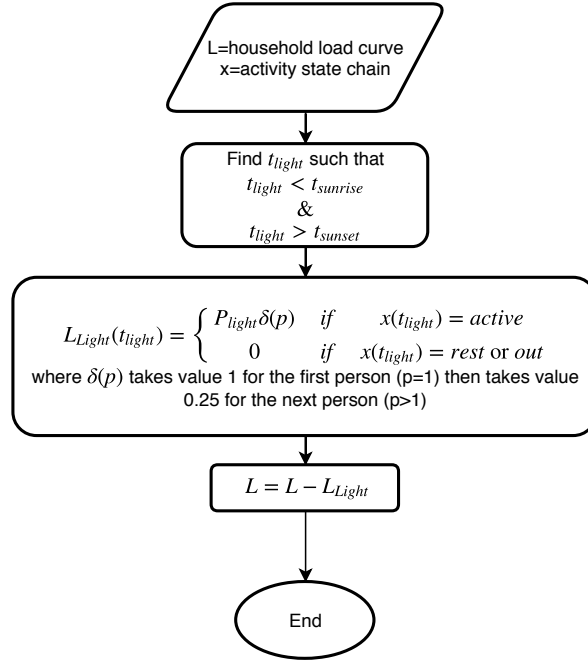


Figure 1.8 – Add Lighting sub-process

As the first condition (in Figure 1.8), lighting is assumed to be on only before sunrise and after sunset. t_{sunrise} and t_{sunset} are calculated for each day using an approximate equation of time. Lighting is assumed to be on only for active people. When people are resting or out of the house, the lighting is off. These "no-light" activities are (with respect to Table 1.2), *Sleep*, *Outdoor*, and *Work*. To avoid overestimating light consumption, a damping variable $\delta(p)$ is introduced. It takes the value of 1 if $p = 1$ (first person) then 0.25 for each additional person.

"Recognize Cooking". As shown in Figure 1.9, the first step is to detect periods corresponding to this category's possible activities. The cooking-related activities are: *Cook* and *Eat*. Then, a loop on all possible appliances (see Table 1.2) is performed. At each iteration, a random appliance usage duration D is selected according to the mean appliance usage duration (reported in Table 1.3). If the length of the activity period is long enough and the power budget is satisfied (condition $\max(L([t^0, t^0 + D(d)])) \leq P(d)$, with $P(d)$ the nominal power of the appliance d), the power signal for the selected appliance is generated. A Boolean value $\gamma \in [0, 1]$ sets the power signal to 0 with probability $1 - \beta_i$, $i = 1..3$ according to three different conditions. These conditions correspond to the actual probability of usage of each particular appliance. In this case, it is the probability of usage during breakfast, lunch, and dinner time.

This is also reported in Table 1.3 under footnote 1.

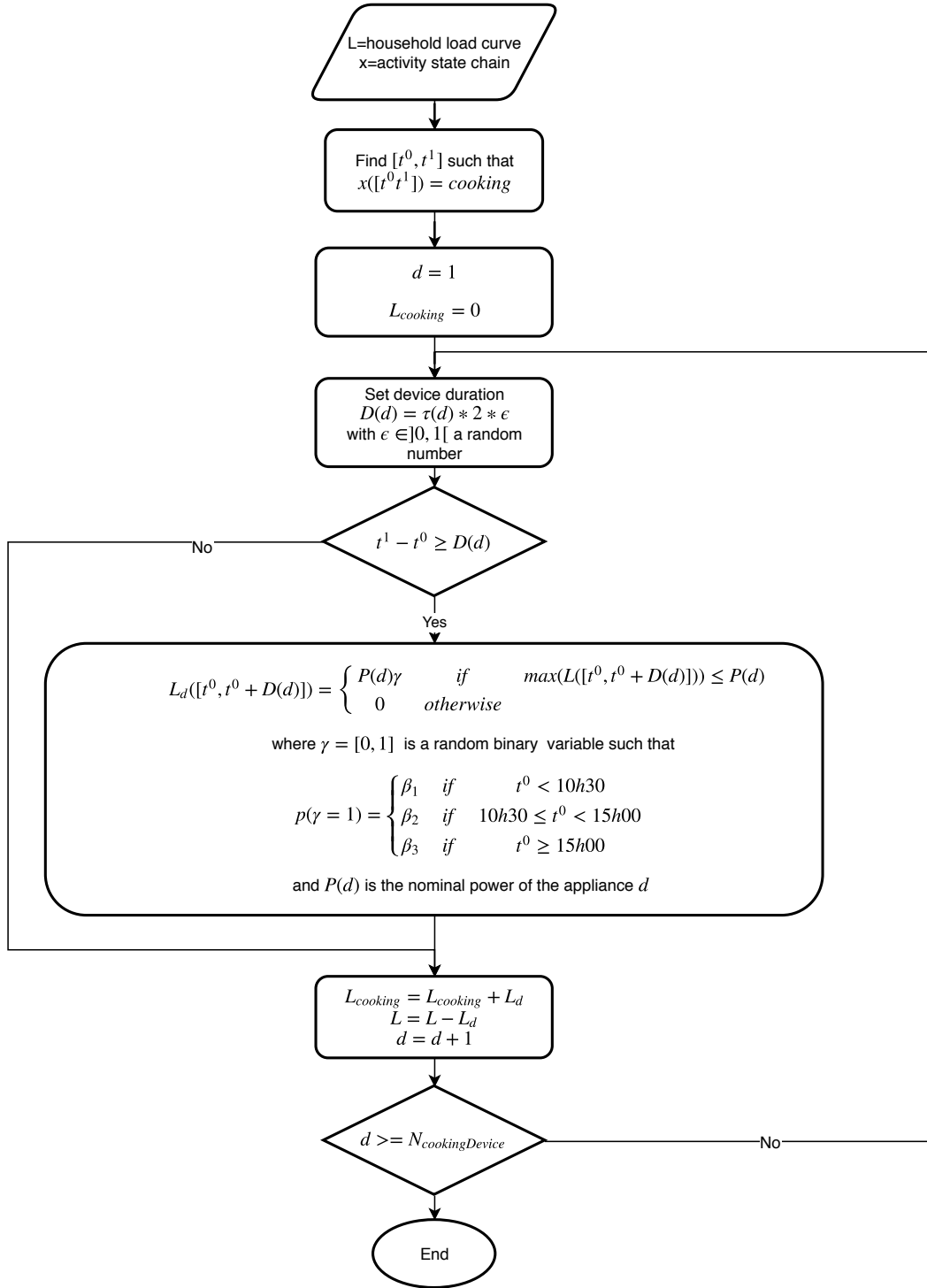


Figure 1.9 – Recognize Cooking sub-process

The final step consists in subtracting the generated appliance power signal L_d from the

aggregated load curve L .

"Recognize Housekeeping". First, the activity period is extracted as previously, and a loop on all appliances that might be used by the *Housekeeping* activities is performed. These activities are (according to Table 1.2) *Clean*, *Wash dishes*, and *Laundry*. The compatibility between the activity duration and the appliance duration is checked before generating the appliance power signal L_d . Here again, the power budget is checked by comparing the nominal appliance power $P(d)$ with the maximum power of the load L . The activation Boolean variable γ is used to consider the probability of usage of each individual appliance. In the general case, probability β_1 and β_2 correspond to the likelihood of using the appliance if it is the first time the appliance is used or if it was already used during the current day. In the tumble dryer case, it can be used only right after the washing machine with probability β_1 and only once a day ($\beta_2=0$). The corresponding conditions are given in footnote 9 of Table 1.3.

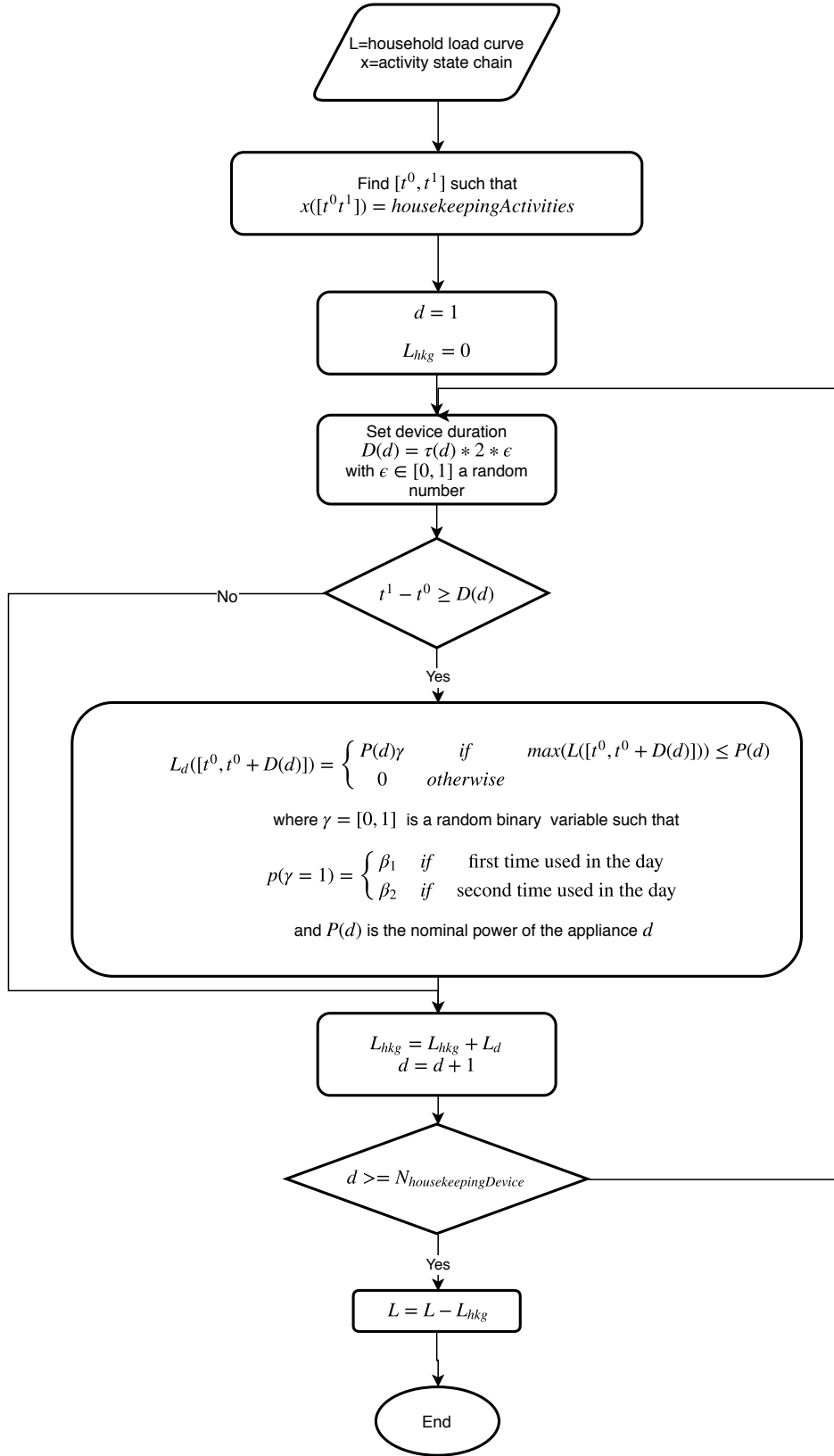


Figure 1.10 – Recognize Housekeeping subprocess

"Add Entertainment". As entertainment appliances, which are defined in Table 1.2, can be used simultaneously with almost any other activity, some specific adaptation has been made in this sub-process (see Figure 1.11). The probability of using a particular appliance is defined according to whether the activity is specifically to use this appliance. For instance, considering TV, if the activity is explicitly *Watch TV*, the usage probability β_1 is equal to 0.9. This probability is not 1 because this activity could be achieved on other appliances such as a laptop or smartphone. However, if the current activity is *Clean*, the TV can be on in the background with probability $\beta_2 = 0.1$. Moreover, a state vector Γ tracks the on/off state of each appliance. If more than one item of the same appliance are in the household inventory and the first item is already on ($\Gamma([t^0, t^0 + D(d)], d) = 1$), the probability of usage of the next item is β_3 . Finally, a particular condition is formulated for households that do not own a TV. The activity *Watch TV* can still occur, but the TV can be replaced by a PC or laptop with a specific probability of usage (see Table 1.3, footnote 4). At the end of the iteration, the state vector Γ is updated with the activation variable γ .

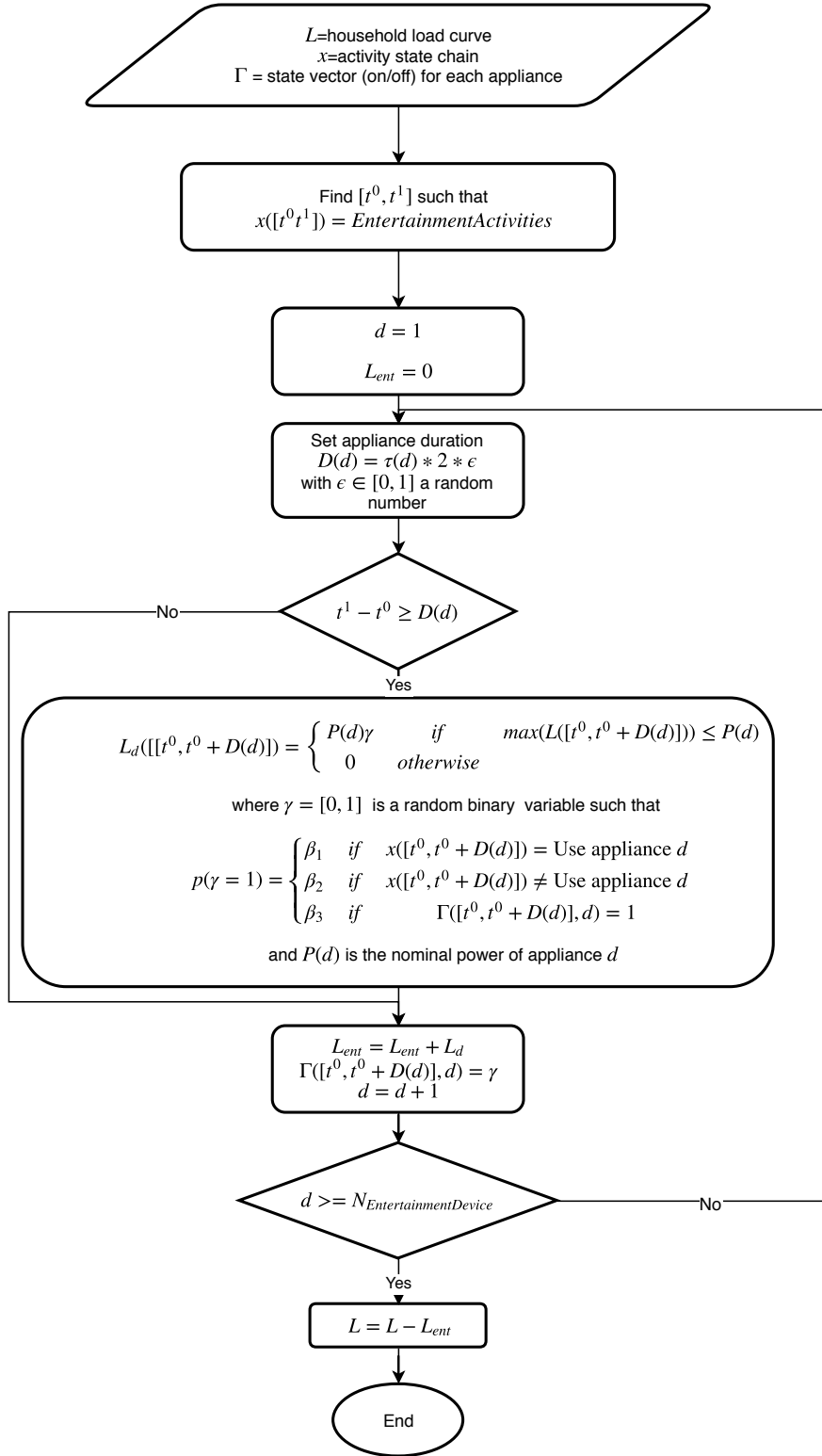


Figure 1.11 – Add Entertainment subprocess

"Add ICT". Figure 1.12 is similar to the previous one, with one major exception. The probability of usage depends on either the state Γ of the computer appliances (PC and laptop) or whether the activity is *Work* or *Homework*.

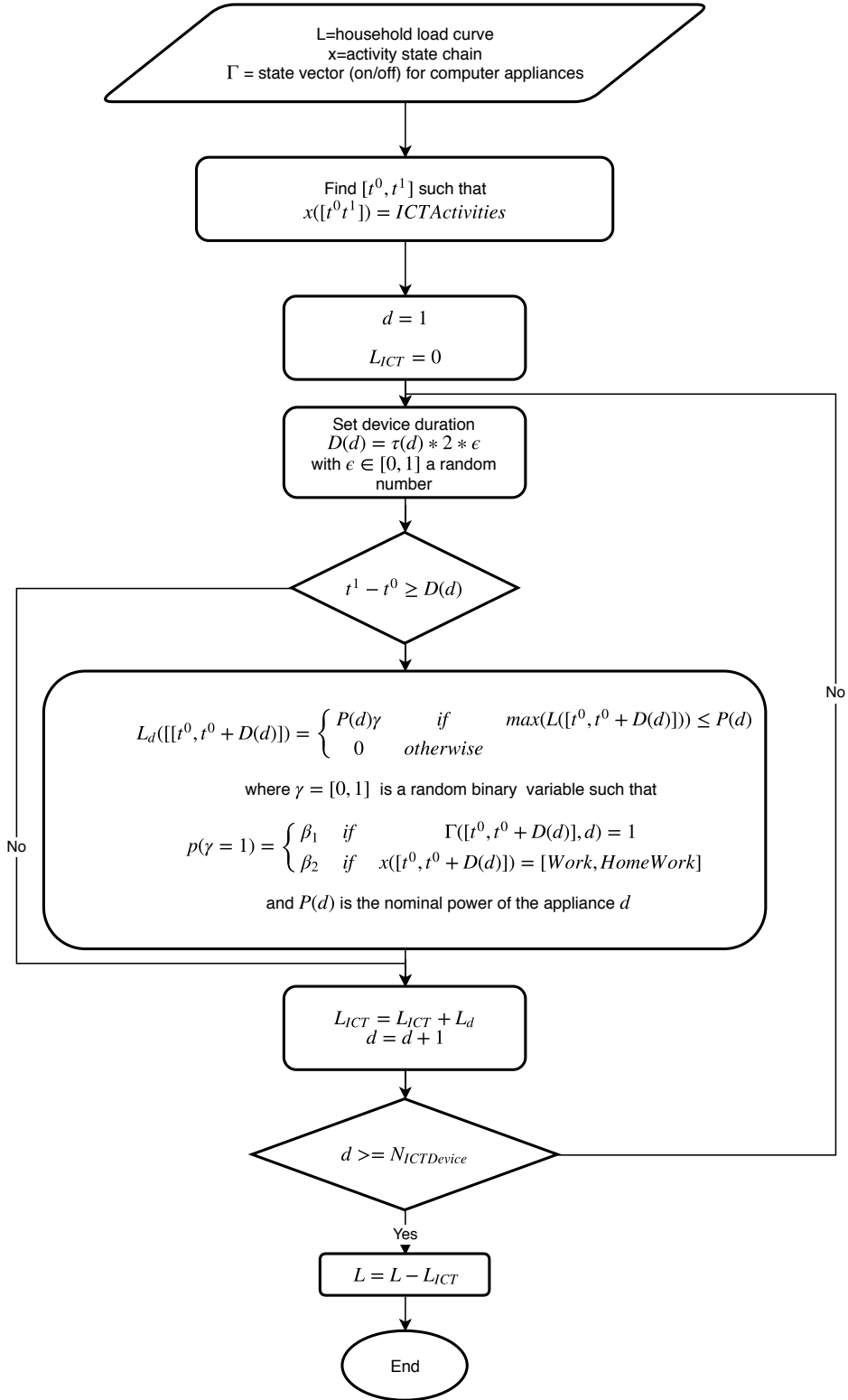


Figure 1.12 – Add ICT subprocess

Table 1.3 – Appliance per category and nominal power, parameters of usage, and duration

Category	Appliance	P_{Nominal} (W)	β_1	β_2	β_3	τ (min)	Note
Cooking	coffee maker	800	0.8	0.7	0.5	3	1
	microwave	1250	0.3	0.5	0.4	5	1
	kettle	1800	0.3	0.5	0.8	2	1
	oven	2400	0.1	0.3	0.4	50	1
	stove	500	0.5	1.0	1.0	30	1
Entertainment	TV	124	0.9	0.1	0.5	20	2
	TV box	20	1.0				2
	DVD player	80	0.1	0.0	0.0	0	2
	PC	110	0.5	0.1	0.2	30	3 4
	laptop	55	0.5	0.2	0.4	20	3 4
	tablet	7			0.4		3
	stereo	100	0.9	0.2	0.5	20	2
	gaming console	180	0.3	0.0	0.1	80	2
Fridge	fridge (with a freezer)	94	0.3	0.3		25	5
	fridge (without a freezer)	66	0.3	0.3		25	5
	freezer alone	62	0.5	0.5		63	5
Heating	hairdryer	600	0.2				
	boiler	2000					8
	heat pump	1000					8
Housekeeping	washing machine	406	0.5	0.4		60	6
	tumble dryer	2500	0.5	0.0		60	9
	dishwasher	1131	0.4	0.0		34	6
	vacuum	2000	0.5	0.2		10	6
ICT	printer	23	0.1	0.1		5	4
Light	lighting	137	0.25				7
Standby	modem (and similar)	8	8.0				10

Table 1.4 – Note of Table 1.3

Note	Comment
1	$\beta_{1,2,3}$ probability of usage for respectively breakfast, lunch, dinner. These values can be set to 0 according to the households habits (namely number of lunch and dinner at home), if provided, as presented in Table 1.5.
2	β_1 probability of usage when the activity is <i>Watching TV</i> , β_2 probability of usage for other activities, β_3 probability of use if one is already used (for an additional person).
3	β_3 probability of usage when it is used as a replacement for TV. This is used if no TV is reported in the appliance ownership table, as presented in Table 1.6.
4	β_1 probability of usage when the activity is <i>Using computer</i> , β_2 probability of usage when the activity is <i>Working</i> or <i>Do the homework</i>
5	β_1 duty cycle during the day, β_2 duty cycle at night, τ is the duration of the active cooling phase.
6	β_1 probability of usage once during the day, β_2 probability of usage additional times. This probability can be set to 0 according to the households habits (namely usage of the washing machine per week), as provided in Table 1.5.
7	$\beta_1 P_{Nominal}$ is used for the first person in the house, $P_{Nominal} * \beta_1$ is used for each additional person.
8	Presently our algorithm only accounts for hairdryers.
9	β_1 probability of usage right after washing machine. This probability can be set to 0 according to the household habits if provided, as reported in Table 1.5.
10	The modem (or internet router) is in the Standby category for the obvious reason that it is always on. Its power consumption is assumed to be independent of occupancy and the inhabitants' activities.

The presented unsupervised algorithm needs to be validated against state-of-the-art algorithm to assess the performance and validity. The following will present the validation methodology.

1.3 Validation methodology

To assess the validity and performance of our DUE algorithm with respect to other methods of the field, this section will present a selection of NILM algorithms and representative performance metrics. To obtain a confidence interval on the selected metrics, the tests were performed successively on different datasets.

The following set of algorithms was chosen to benchmark the performance of the DUE algorithm:

- Combinatorial optimization (CO) [Hart, 1992]

- Factorial hidden Markov model (FHMM) [Kim et al., 2011]
- Graph signal processing (GSP) [Kumar and Chandra, 2017a, He et al., 2016]
- Discriminative disaggregation via sparse coding (DDSC) [Kolter et al., 2010]

1.3.1 Selected state-of-the-art algorithms

A Combinatorial optimization

Combinatorial optimization (CO) is a well-studied benchmark algorithm presented by Hart [Hart, 1992]. Assuming a linear model for each appliance $i = 1 \dots M$, a Boolean switch process $a(t) = a_i(t), i = 1 \dots M$ identifies which of the appliances are "on" and "off" at time t . Therefore, the aggregated power load at time t is the sum of all the individual power loads of the appliances that are "on" at that time. Naturally, a combinatorial optimization problem emerges in order to minimize the difference between the predicted and observed power: $\hat{a}(t) = \min_{a_i} |P^t - \sum_{i=1}^n a_i P_i|$, where $\hat{a}(t) = \hat{a}_i(t)$ is a matrix representing the estimated "on" or "off" state of an appliance in time and P_i represents the nominal power of appliance i . The learning phase will construct a power basis P_i from the disaggregated signal. The disaggregation phase will solve the problem for all $a_i(t)$ at every time step. This approach is computationally intractable, as the algorithm's complexity grows exponentially with the number of appliances. Thus one cannot solve the problem exactly. Additional difficulties of this method include detecting simultaneous appliance state changes and a lack of complete information about the individual power loads. Therefore, a switch continuity principle was adopted that supposes that only a small number of appliances can change state simultaneously.

For this study, the CO algorithm was implemented through the Non-Intrusive-Load-Monitoring-Toolkit (NILMTK)³ [Batra et al., 2014].

B The factorial hidden Markov model

The factorial hidden Markov model (FHMM) is another benchmark algorithm provided in the NILMTK [Batra et al., 2014]. Considering that the only observable value is the aggregated power measurement P^t , each appliance's individual power load is modeled separately as HMM with hidden states $x_i(t)$ representing the status of the appliance. The use of a FHMM over HMM reduces the parametric complexity when modeling time series generated by the interaction of several independent processes — in our case, several appliances [Kim et al., 2011, Kolter and Johnson, 2011]. In order to build the model, four main components need to be defined:

- Finite set of hidden states

³<http://github.com/nilmtn/nilmtn>

- Transition matrix a , which represents the probability of changing a state
- Emission matrix b , which indicates the probability of emitting an observation
- Initial distribution of probabilities among the states π

The learning phase consists in building both matrices a and b , and the disaggregation phase aims at finding hidden states such that the probability of observing the signal \mathbf{P}^t is maximized. In other words: $\hat{x}_i^t = \max_x p(\mathbf{P}^t | x_i^t)$ The DUE algorithm is not a derivation of the FHMM since it relies on a try-and-fail method rather than an optimization problem.

C Graph signal processing

Graph signal processing (GSP) is a novel supervised concept for load disaggregation, which is neither state- nor event-based. The methodology's success for applications such as filtering, clustering, classification, convolution, and modulation [Kumar and Chandra, 2017a, Kumar et al., 2016] inspired researchers to develop a solution to the NILM problem. The approach relies on the regularization of graph signals, assuming that if the signal is piecewise smooth, then the total graph variation is generally small. [He et al., 2016, Stankovic et al., 2014] The proposed GSP methodology has several advantages over conventionally used algorithms: short training periods [He et al., 2016], reliable performance in the presence of noise, unknown or uncommon appliances [Zhao et al., 2016], the ability to handle different sampling rates, including every 15 minutes [Kumar and Chandra, 2017a, Kumar et al., 2016] and the use of active power alone [Kumar and Chandra, 2017b].

The algorithm's basis lies in constructing an undirected graph G using aggregated power measurements, where each vertex V corresponds to a load sample. The weights W of the edges connecting the vertices reflect the degree of similarity between nodes [Stankovic et al., 2014]. The overall sequence of the algorithm's main steps can be summarized as follows under the formulation proposed in [Kumar and Chandra, 2017a, Kumar et al., 2016]:

- Learn the weights W from aggregated power data using a Gaussian kernel weighting function.
- Construct the graph G using W and compute the respective graph Laplacian L .
- Define graph signals s , where s equals the appliances' ground truth (GT) during the training period and equals zeros during the testing period.
- State an optimization problem of minimizing the smoothness term $\|s^T L s\|_2^2$.
- Evaluate signal s^* as a solution to the optimization problem.
- Subtract the disaggregated signal s^* from the aggregated power measurements.

The procedure described above has to be repeated sequentially for each appliance, starting from the highest-consuming one. The GSP approach for this study was implemented in MATLAB using the Graph Signal Processing Toolbox [Perraudin et al., 2014].

D Discriminative disaggregation via sparse coding

Discriminative disaggregation via sparse coding (DDSC) is the application of the source separation problem to the NILM problem. The algorithm's idea is to train models separately to find approximate representations for each appliance in the form of $X = BA$, where B is the set of basis functions, also called a dictionary, and A is a sparse activations matrix. Therefore, the objective function of the method is $\min_A \frac{1}{2} \|X - BA\|_F^2 + \lambda \|A\|_1$ subject to $A, B \geq 0$. The training phase will learn the dictionary B_i for each appliance ($i = 1 \dots n$) from the individual appliance signal X_i by solving the equation $\min_{A_i} \frac{1}{2} \|X_i - B_i A_i\|_F^2 + \lambda \|A_i\|_1$ for A_i and B_i sequentially. Then the disaggregation will solve for A using the aggregated signal X [Kolter et al., 2010, Elhamifar and Sastry, 2015, Leijonmarck, 2015, Yu et al., 2016].

One method to decompose the aggregated signal into a sparse combination of dictionary elements is non-negative sparse coding [Hoyer, 2012]. When this approach was utilized for solving the NILM problem, many improvements to the method emerged. [Kolter et al., 2010] proposed to discriminatively optimize basis functions in order to minimize disaggregation error. [Elhamifar and Sastry, 2015] incorporated additional priors such as device sparsity, knowledge of cooperating devices, and temporal smoothness, and [Singh and Majumdar, 2017] extended the approach to multiple layers of dictionary learning for each device.

This method is potentially suited for low-sampling rate datasets, as demonstrated in [Kolter et al., 2010], in an attempt to disaggregate meter readings at 1h intervals. For the current study, the DDSC algorithm was implemented in PYTHON based on the representation in [Kolter et al., 2010, Leijonmarck, 2015].

1.3.2 Test datasets

Instead of testing on a single dataset as it is usually done in the literature, we propose a broader experiment by testing on several datasets. The underlying objective is to get a confidence interval on each of the selected performance metrics. Our requirements for the datasets are the following:

- Each dataset must consist of households with information about consumption at the appliance level
- Each household must be located in Europe as the time-of-use survey [Sociaal en Cultureel Planbureau, 2005] was collected in Europe
- There must be a sufficient description of the characteristics of each inhabitant

To emulate data acquired from smart meters (considered here as average power over a particular time interval), all datasets were down-sampled to a 15-min sampling rate, keeping the real power only. The resulting power signal is hence the average real power over each 15-min time interval. To be consistent for the disaggregation, the appliances' power signals were aggregated according to the categories presented above to create the reference ground truth. The reference whole-house power measurement is defined as the sum of the sub-measurements to ensure energy conservation. This implies that the noise is not considered since averaging the power measurement on a 15-min time window should minimize its influence. Additionally, as the DUE algorithm disaggregates the whole house energy consumption, the noise should be included in one of the categories, most likely, the standby. Moreover, the datasets' meta-data was used to complete the household information requirements as briefly described in Table 1.1.

Three publicly available datasets were selected: ECO[Beckel et al., 2014a], SMARTENERGY.KOM [Alhamoud et al., 2014] and UK-DALE[Kelly and Knottenbelt, 2015b]. The following section will briefly present these datasets.

A The ECO dataset

The dataset was made by ETH Zurich [Beckel et al., 2014a, Beckel et al., 2014b] and collected during eight months (from the beginning of July 2012 to the end of January 2013) from six households in Switzerland. Registered measurements represent a new level of detail, comprising the voltage, current, and phase shift between voltage and current readings for each of the three phases. This makes the dataset useful for algorithms that require both active and reactive power. The sampling rate of 1 Hz distinguishes this dataset from others in the field, together with the information provided about the households' occupancy. For this study, we used House n°2 from June 1st to October 30th, 2012.

B SMARTENERGY.KOM dataset

Initially, this dataset was developed to propose energy-savings recommendations based on detecting the users' activities [Alhamoud et al., 2015]. The collection of energy consumption data by the appliances is complemented by the measurement of motion (i.e., occupancy), temperature, and brightness in the environment. The dataset accounts for more than 42 million data points for two households, and it is the first dataset to combine power and environmental sensors' measurements with user feedback [Alhamoud et al., 2014].

The data from Apartment n°1 were collected for 82 days, while Apartment n° 2 participated in the experiment for 60 days. For both of the deployments, there are nine respective activities that should be recognized, such as sleeping, watching TV, eating, ironing, reading, etc. For the following, we used the Apartment n°1 from March 5th to June 25th, 2013.

C UK-DALE,

This open-access dataset for NILM research is the first out of the UK with a high temporal resolution. To the best of our knowledge, this public dataset covers the longest period in Europe, from December 2012 to April 2017, for the latest release [Kelly, 2017].

The dataset records the active power demand from appliances and the whole-house apparent power for the five households that participated in the data collection. The sampling rate for both the main power and for the power of individual appliances is six seconds. Distinct from other public datasets for load disaggregation, UK-DALE contains metadata as well. These additional data files include the type of ownership, the number of inhabitants, inhabitants' characteristics, the heating type, and any energy improvements made to the house. This information was fed into the proposed algorithm to complete the households' characteristics. UK-DALE is included in the NILMTK [Kelly, 2017, Batra et al., 2014] framework. For testing, we used the House n°1 during the period from April 2014 to April 2015. We chose this house because it was the most documented one because a large share of appliances' consumption data is available.

For each dataset, the metadata is used to complete the household characteristics as provided in Table 1.5. The appliance list is provided in Table 1.6.

1.3.3 Metrics

To evaluate the performance of the proposed algorithm, it is necessary to define appropriate metrics that are consistent with the ultimate goal of this work. Typical performance metrics are based on event detection and come from classification algorithms literature [Faustine et al., 2017]. The accuracy is defined as the algorithm's ability to detect whether an appliance is on or off (see Equation 1.6).

$$\text{ACC} = \frac{\text{Correct matches}}{\text{Total possible matches}} \quad (1.6)$$

However, this metric is not appropriate for appliances that are in one state most of the time (like a TV is mostly off). To correct this, researchers often use the F measure [Faustine et al., 2017] defined in Equation 1.9.

$$\text{Precision} = \frac{\text{TP}}{\text{TP} + \text{FP}} \quad (1.7)$$

$$\text{Recall} = \frac{\text{TP}}{\text{TP} + \text{FN}} \quad (1.8)$$

$$F = \frac{2 \times \text{Precision} \times \text{Recall}}{\text{Precision} + \text{Recall}} \quad (1.9)$$

where TP = True Positive, FP = False Positive and FN = False Negative.

Table 1.5 – Household information, assumed or retrieved from dataset metadata

	ECO	SMARTENERGY.KOM	UK-DALE
Household composition			
Total number of people	2	1	4
Number of children (<10 y.o)	0	0	0
Number of teenagers	0	0	2
Employment state			
Person 1	full-time	full-time	full-time
Person 2	full-time		full-time
Person 3			student
Person 4			student
Age			
Person 1	senior active	senior active	senior active
Person 2	senior active		senior active
Person 3			teenager
Person 4			teenager
Household habits			
Usage of the washing machine per week	0	1	1
Usage of the tumble dryer per week	0	0	0
Usage of the dishwasher per week	0	0	4
Usage of the computer	normal	normal	occasional
Usage of the TV	occasional	occasional	occasional
Usage of the stereo	high	normal	high
Usage of gaming console	high	normal	high
# lunch at home per week	7	7	7
# dinner at home per week	7	7	7
House information			
Electric heating	No	No	No

Beckel [Beckel et al., 2014a] used the root mean square error of the m^{th} appliance signal as defined in Equation 1.10.

$$\text{RMSE}_m = \sqrt{\frac{1}{T} \sum_t (\hat{P}_m^t - P_m^t)^2} \quad (1.10)$$

With this last metric, the comparison between appliances having a high difference in power

Table 1.6 – Number of appliances owned for each household

	ECO	SMARTENERGY.KOM	UK-DALE
Coffee maker	1	1	1
Microwave	0	0	1
Kettle	1	1	1
Oven	1	1	1
Stove	1	1	1
TV	1	1	1
PC	1	1	1
Tablet	0	0	0
Stereo	1	1	1
DVD	0	1	1
Gaming console	1	1	0
TV box	0	0	1
Laptop	0	0	0
Fridge (with Freezer)	1	0	1
Freezer	0	1	0
Fridge(without freezer)	0	0	0
Hairdryer	0	0	1
Boiler	0	0	0
Heat pump	0	0	0
Washing machine	0	0	1
Tumble dryer	0	0	0
Dishwasher	0	0	1
Vacuum	0	0	1
Printer	1	1	1
Lighting	1	1	1
Modem	1	1	1

consumption (i.e., a stove and an internet box) is problematic. For this reason, a derivation of the root mean squared error called the *Normalized Disaggregation Error* (NDE_m) [Liu et al., 2018, Kolter et al., 2012, Dong et al., 2013] defined in Equation 1.11, normalizes the squared error of a single appliance by the total energy of the signal. Very similarly, [Parson et al., 2012] and [Beckel et al., 2014a] used a *Normalized Error in the total Energy Assigned* ($NEEA_m$) as defined in Equation 1.12.

$$\text{Normalized Disaggregation Error:} \quad NDE_m = \frac{\sum_t (\hat{P}_m^t - P_m^t)^2}{\sum_t (P_m^t)^2} \quad (1.11)$$

$$\text{Normalized Error in the total Energy Assigned:} \quad NEEA_m = \frac{\sum_t |\hat{P}_m^t - P_m^t|}{\sum_t P_m^t} \quad (1.12)$$

[Makonin and Popowich, 2015] used an *Estimation Accuracy* (ESTACC), derived from [Kolter and Johnson, 2011] and [Johnson and Willsky, 2013], of the appliance power signal or across all appliances as in Equations 1.13 and 1.14 respectively.

$$\text{Estimation accuracy per cat.} \quad \text{ESTACC}_m = 1 - \frac{\sum_t |\hat{P}_m^t - P_m^t|}{2 \cdot \sum_t P_m^t} \quad (1.13)$$

$$\text{Estimation accuracy} \quad \text{ESTACC} = 1 - \frac{\sum_t \sum_m |\hat{P}_m^t - P_m^t|}{2 \cdot \sum_t \sum_m P_m^t} \quad (1.14)$$

In this thesis, we choose the *Estimation Accuracy* as a reference metric to compare the disaggregation performance since it is a popular metric in recent literature. The root mean squared error would not be appropriate because it is impossible to use it for multiple appliance comparisons for the reason explained above. Finally, the original benchmark performed with the normalized disaggregation error has shown similar trends as what will be discussed in the following section. So this metric was given away for clarity reason. Also, because our methodology aims to infer the energy share by category of appliances as defined in Equation 1.15, the *Energy Share Error* per category is defined in Equation 1.16.

$$\text{Energy share per category} \quad \hat{S}_m = \frac{\sum_t \hat{P}_m^t}{\sum_t \sum_m \hat{P}_m^t} \quad (1.15)$$

$$\text{Energy Share Error:} \quad \text{ESE}_m = \frac{\sum_t \hat{P}_m^t}{\sum_t \sum_m \hat{P}_m^t} - \frac{\sum_t P_m^t}{\sum_t \sum_m P_m^t} \quad (1.16)$$

Note that in the following, the index m corresponds to an appliance category as defined in Table 1.3.

1.4 Results and discussion

We compared our proposed method's performance to the four standard algorithms of the NILM literature presented above. Testing was performed using the three datasets (presented in Section 1.3.2) to evaluate all algorithms' performance. As described in Section 1.3.3, relevant metrics in the context of flexibility estimation are the *Energy Share Error* per category and the *Estimation Accuracy*. Additionally, the execution times for training and testing were also compared.

Each test was conducted by dividing the dataset into a training period and a testing period. The length of the training period is approximately two times the length of the testing period. As our proposed algorithm does not require any training, it was tested on the testing period

only. The duration of the training and testing periods for different datasets is reported in the following table:

Table 1.7 – Testing and training periods for the three datasets

	Training period			Testing period		
	from	to	days	from	to	days
ECO	2012-06-01	2012-09-30	121	2012-10-01	2012-10-30	29
SMARTENERGY.KOM	2013-03-05	2013-05-19	75	2013-05-19	2013-06-25	37
UK-DALE	2014-04-01	2015-04-01	365	2015-04-01	2015-07-01	91

The *Energy Share Errors* for each category, as defined in Equation 1.16, are reported in Table 1.8. "NA" means that this category was not measured in the respective dataset. In the GSP columns, all values corresponding to the UK-DALE dataset are NAs because this algorithm was not run on this dataset. Indeed, the complexity of the GSP algorithm increases non-linearly with the length of training and testing periods. Therefore it is more appropriate for short training periods, as shown in [He et al., 2016]. Although various strategies have been tested, we have not been able to find a satisfying implementation of the GSP algorithm that would allow performing disaggregation on a large dataset. A comparison of the performance for each dataset for this metric is shown in Figure 1.13. A positive error means an overestimation of the energy share. The *Energy Share Error* is highly dependent on both the dataset and the observed categories. Surprisingly, the *Energy Share Error* is especially high for the ICT category in the SMARTENERGY.KOM dataset. This may be due to the unusually high share of energy consumed by this category (about 40%, whereas it is below 20 % in the other two datasets). The estimation of light consumption is too high for the DUE algorithm for the ECO and SMARTENERGY.KOM datasets. One has to consider that the datasets are often incomplete, i.e., they do not represent the whole and real power consumption of a house. Authors of such datasets choose the appliances to be monitored depending on their capabilities while neglecting the appliances that were too difficult or impossible to monitor. This is also why no Housekeeping is present in the SMARTENERGY.KOM dataset. As the DUE algorithm is based on surveys and statistics, it always assumes that all categories are present in the house, thus explaining these differences.

Table 1.8 – *Energy Share Error* per category (in %) (ECO, SMARTENERGY.KOM, UK-DALE)

	CO	FHMM	DUE	DDSC	GSP
Cooking	(17, 7, 7)	(1, -2, 0)	(2, 6, -1)	(2, -5, -6)	(1, -2, NA)
Entertainment	(-25, -4, 2)	(-15, 6, 2)	(-20, 11, 17)	(-12, -2, 4)	(9, -6, NA)
Fridge	(-9, -9, -1)	(-4, -8, 0)	(2, 12, 2)	(3, -8, 3)	(-1, 2, NA)
Heating	(NA, 7, -5)	(NA, 2, 1)	(NA, -2, -12)	(NA, 27, 4)	(NA, -2, NA)
Housekeeping	(4, NA, -2)	(1, NA, 1)	(-12, NA, -17)	(-9, NA, -17)	(-5, NA, NA)
ICT	(6, -19, -4)	(5, -2, -2)	(6, -35, -5)	(19, -29, 1)	(-4, 0, NA)
Light	(7, 14, -3)	(13, 3, -7)	(22, 6, -4)	(-3, 4, -2)	(-4, 0, NA)
Standby	(NA, 3, 6)	(NA, 0, 40)	(NA, 1, 20)	(NA, 13, 12)	(NA, -1, NA)

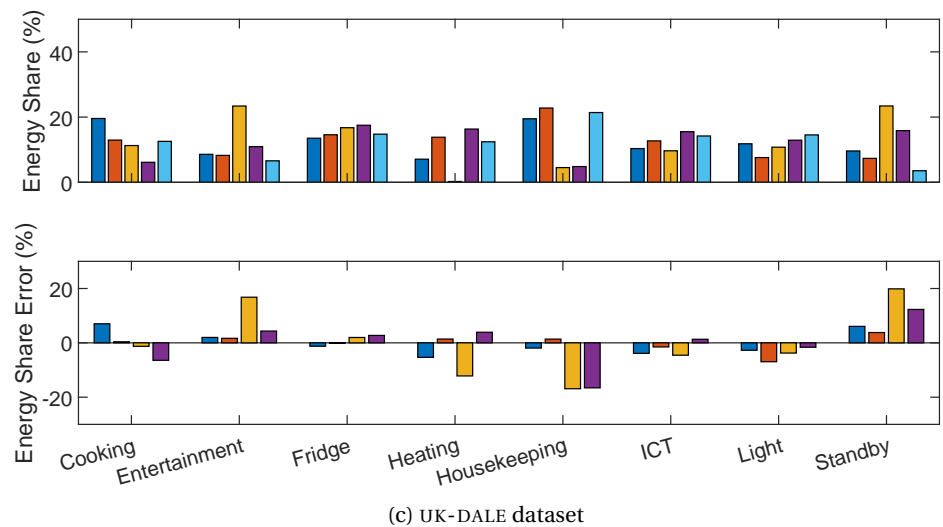
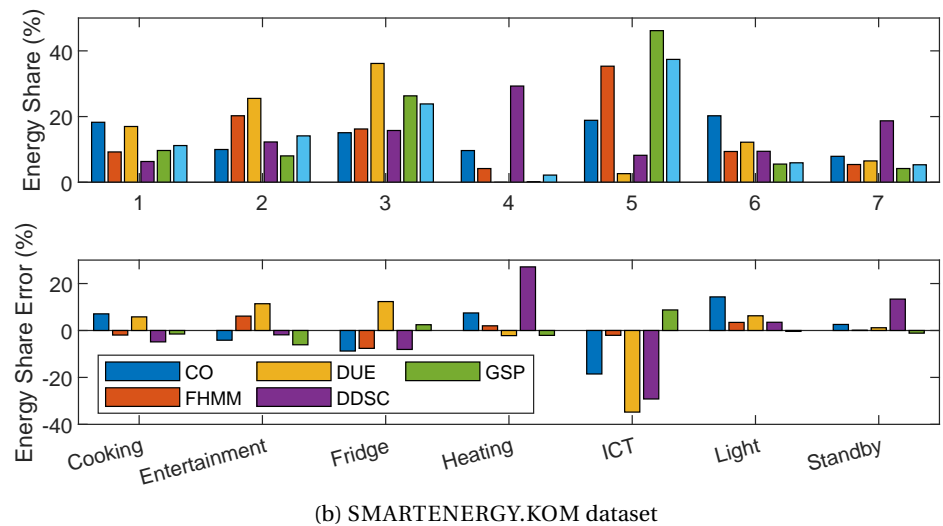
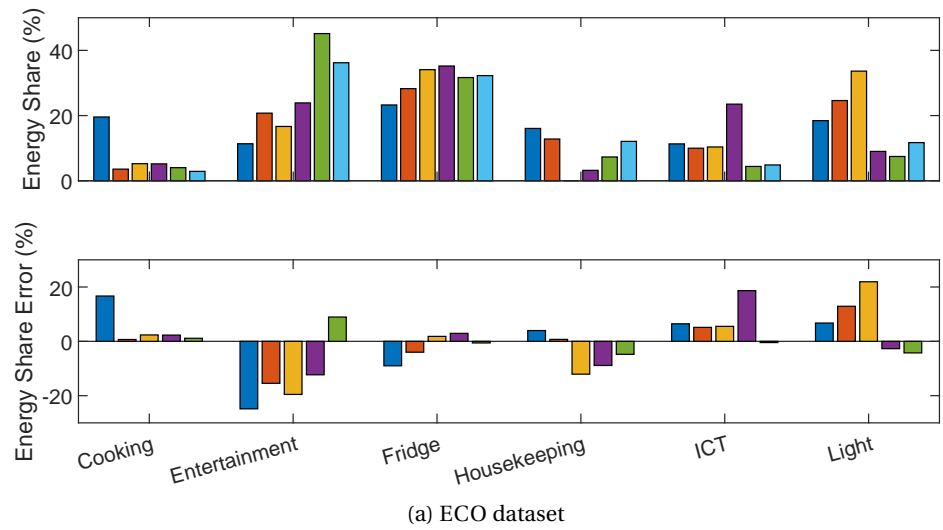


Figure 1.13 – Energy share and error

The global uncertainty (here defined as the error on the energy share) is in the range of 20% for all algorithms except the DUE as depicted in Figure 1.14. The uncertainty is lower on average for the supervised algorithms, especially for the FHMM. The excellent performance of the GSP algorithm has to be counter-balanced because this algorithm has not been tested on the UK-DALE dataset. Considering that not all categories were present in each of the two other datasets, only a few data points were extracted to present these metrics.

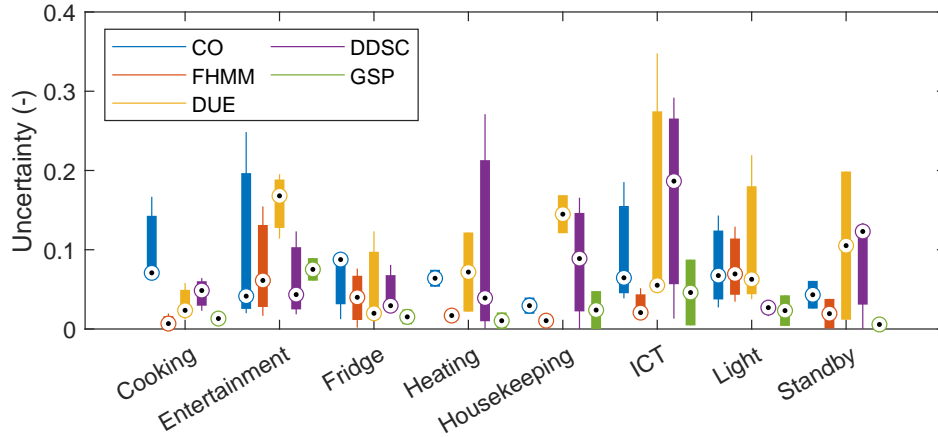


Figure 1.14 – Energy share uncertainties across all datasets

The *Energy Share Error* per category is a global metric that does not consider temporal accuracy. To focus on this aspect, the *Estimation Accuracy* is more appropriate. The *Normalized Disaggregation Error* could serve as an equivalent metric. However, the *Estimation Accuracy* metric is more commonly seen in the recent literature, explaining its usage in the present benchmark. Moreover, the following outcomes would have been similar if the *Normalized Disaggregation Error* had been used.

The *Estimation Accuracies* for each category are reported in Figure 1.15. Negative values indicate a poor disaggregation result, occurring when the sum of the absolute errors is larger than two times the signal's energy. The y-axis has been intentionally cropped between -2 and 1 for the sake of comparison across datasets. All algorithms experienced negative values for this metric but not always on the same categories. Looking specifically at categories that seem easier to disaggregate (all *Estimation Accuracy* are larger than zero), the DUE algorithm performs similarly compare to the other algorithms. Considering that the DUE algorithm relies only on statistical information to infer the power signal of each category, the temporal accuracy, especially for categories linked to short-duration activities like ICT and Entertainment, is challenging to catch in an unsupervised way. Some extreme negative values are difficult to explain (for instance, the disaggregation of cooking in the ECO by the CO algorithm). As regards with the Standby category, the poor performance of the DUE algorithm can be explained by the fact that DUE considers standby as a constant load, while in the ground truth, it is not constant and considered as any other appliance by the other algorithms.

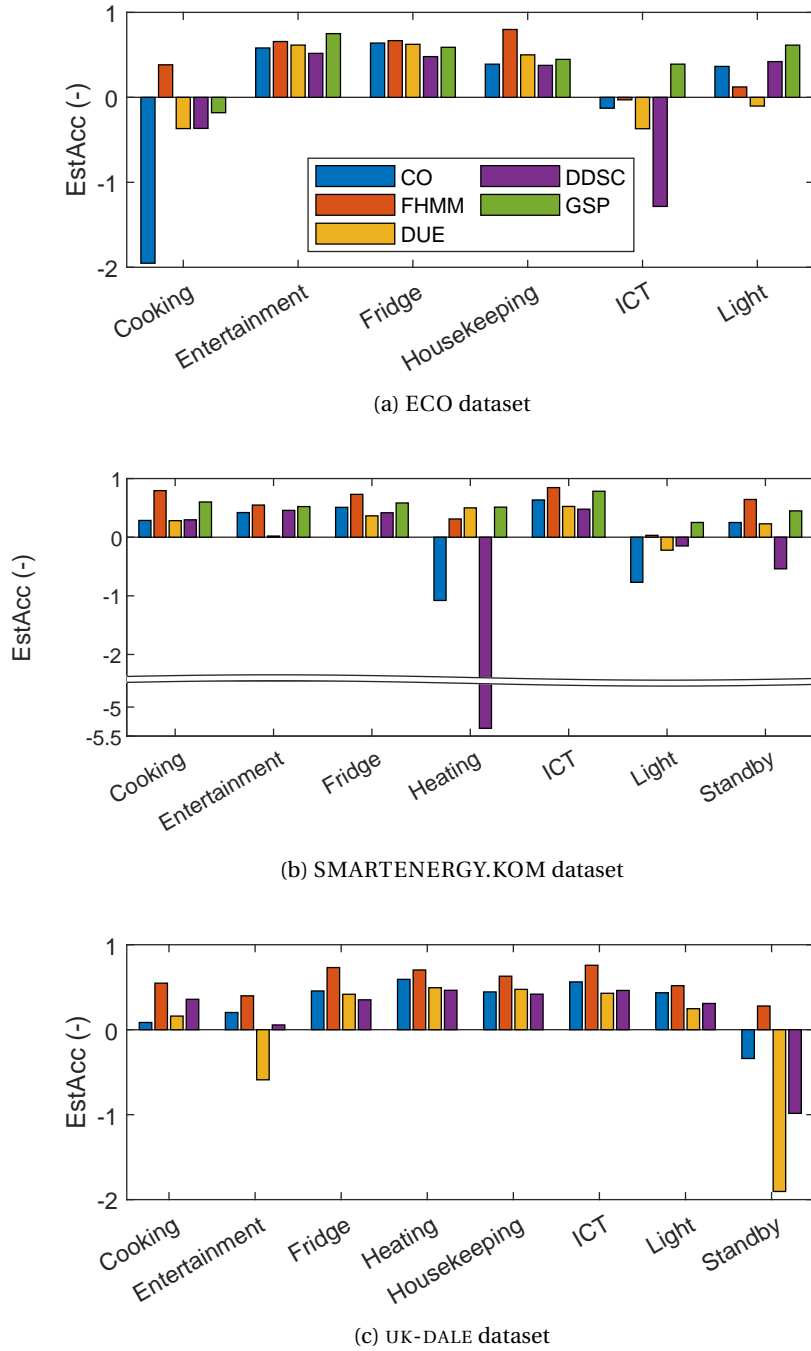


Figure 1.15 – Estimation Accuracy

One has to remember that forecasting a constant zero power signal leads to an *Estimation Accuracy* of 0.5. This is typically achieved by the DUE algorithm for the Heating category on the SMARTENERGY.KOM. This is the drawback of this metric. It is easy to interpret a value close to one as a good performance, but it is hard to interpret the quality of an algorithm that

produces an *Estimation Accuracy* close to zero or even negative.

To summarize, careful analysis of the *Energy Share Error* and the *Estimation Accuracy* shows that the DUE algorithm performs similarly to other algorithms, although its temporal accuracy suffers from the statistical approach. As this algorithm's goal is to be used by a utility on a large number of households, it must have an acceptable computational cost in addition to a reasonable accuracy. The following section aims at comparing the algorithms taking into account these considerations.

The execution time is reported in Table 1.9. As expected, execution time scales with the dataset's length (in terms of both training and testing periods). The CO algorithm, which has the lowest complexity, is always the fastest to execute, as also reported by [Manivannan et al., 2017]. One should keep in mind that the GSP algorithm was not tested on the UK-DALE dataset due to the algorithm's characteristics. Namely, GSP performs training and disaggregation in a single step (for each category of appliances) by constructing a graph and solving the optimization problem. This step requires much computational effort. Hence the execution time becomes too long compared with other algorithms. For short datasets, the DUE algorithm has an execution time comparable to those from FHMM and DDSC. However, these algorithms scale poorly with the dataset's length (or require advanced parallelization techniques, which were not implemented here). Due to its sequential nature, the DUE algorithm's execution time increases linearly with the length of the dataset.

Table 1.9 – Execution time

	ECO		SMARTENERGY.KOM		UK-DALE	
	training 121 days	testing 29 days	training 75 days	testing 37 days	training 365 days	testing 91 days
CO	2s	<1s	<1s	<1s	<1s	9s
FHMM	17s	7s	13s	88s	58s	1h
DUE		59s		45s		6min
DDSC	42s	<1s	19s	<1s	5min	6s
GSP	9h		4h		NA	

Figure 1.16 depicts the global *Estimation Accuracy* (defined in Equation 1.14 as a function of the total execution time, i.e., the sum of the testing time and training time, if any). FHMM is the best compromise as the gain in accuracy according to this metric is significant, although the execution time is one order of magnitude greater than the DUE for the longest dataset (UK-DALE).

These results confirm the fact that supervised algorithms perform better than unsupervised algorithms. Although the disaggregation uncertainty is generally higher for the DUE than for the best supervised algorithm, it falls within the same range. The *Estimation Accuracy* is used to assess both the magnitude and temporal accuracy of the algorithm on the dataset and shows that DUE performs averagely with respect to other algorithms. For large-scale disaggregation

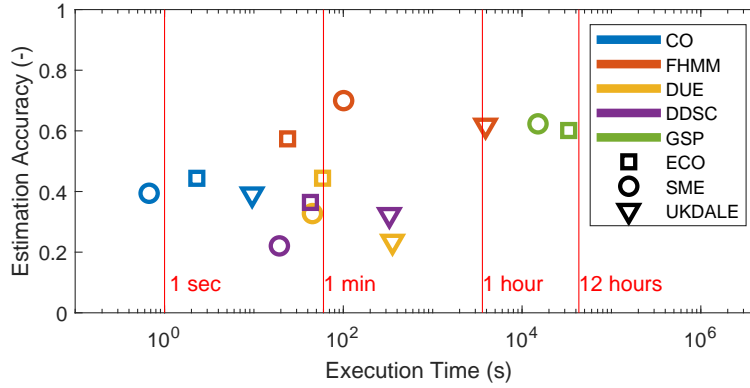


Figure 1.16 – *Estimation Accuracy* versus execution time

of households' energy consumption, it is not always possible to monitor all households at the appliance level as it was done in [Hakell et al., 2015]. Similarly, there is not always a set of reference houses with power consumption data at the appliance level (as in [Batra et al., 2016]), on which training can be achieved before performing disaggregation of whole-house power consumption. In the case where the only available information is the households' characteristics and smart meter measurements, the DUE algorithm can disaggregate the energy consumption with an uncertainty range comparable to supervised NILM algorithms and does not suffer from computational limitations.

As the whole-house power signal is assumed to be the sum of each category's sub-signal, the resulting synthetic power measurement does not correspond precisely to the actual whole-house power measurement. Each dataset covers a certain number of individual appliances, which were grouped to form the categories. For UK-DALE, about 20 appliances were monitored, while for two other datasets, this number is approximately 10. In all cases, this is not representative of complete coverage of the electric power consumption of a house. As a result, this might lead to some errors in the DUE. By design, it assumes that the input power measurement, as the whole-house power consumption, represents the complete household energy activities. Hence, providing partial electric power information of the household activities might significantly impact the performance of the algorithm. However, it is challenging to evaluate this claim, as to our knowledge, no dataset has a complete coverage of all appliances used by a household over several weeks.

1.5 Conclusion

This chapter presented a non-intrusive appliance load monitoring method for low-resolution smart meter data. The *device usage algorithm* (DUE) split the whole house energy measurement into eight categories of appliances. The method is based on generating an activity chain using a Markov model while adapting the transition probability by restricting possible activities according to the power budget for the next time step. The algorithm is a hybrid

between a load simulator and a non-intrusive load monitoring algorithm that disaggregates whole-house power measurement at a very low sampling rate.

A benchmark of this method highlights that its performance is comparable to the four selected state-of-the-art algorithms: the factorial hidden Markov model, combinatorial optimization, discriminative disaggregation via sparse coding, and graph signal processing. The results show better performance on average for the state-of-the-art algorithms as all of them are supervised and were trained on each dataset before being tested. Emphasizing that our *device usage estimation* method is unsupervised, its prediction uncertainties typically remain under 20%. The DUE can sustain large datasets without suffering from computation burden. The time to disaggregate increases linearly with the dataset size. The main advantage of the proposed algorithm is the absence of a training requirement.

A potential application of this method is to propose disaggregation as a service to end customers. The only requirements are an appropriate smart-metering infrastructure and household information that can easily be obtained from a customer survey. Utilities and energy retailers easily reach those requirements. A more research-oriented application is the evaluation of the customers' potential for shiftable energy. Using distribution system operator's smart meter data and their ability to reach end customers to send them a survey, the determination of the household flexibility potential is one of the goals of the FLEXI 2 project that will be described later on.

The following chapter will present how this method has been used in the framework of the FLEXI 2 project.

2 Experimental determination of the households demand flexibility

This chapter presents the results of a field trial aiming to assess the households' flexibility potential. First, we submitted a panel of households to time of use tariffs and evaluated their reaction using a dedicated flexibility score. Second, we compare their response with their potential by applying our disaggregation algorithm to determine this flexibility potential. Finally, we analyzed the consumption pattern change of new PV adopters.

Part of this section has been published in the following work:

Perret, L., Chevillat, Y., Wyrsh, N., Bloch, L., Holweger, J., Weber, S., and Péclat, M. (2019). Flexi 2 Déterminer le potentiel de flexibilisation de la demande d'électricité des ménages. Technical report, Federal office for energy

2.1 Introduction

The increasing PV and renewable energy penetration emphasize the need for flexibility in order to balance energy demand and supply. Demand-side management (DSM) and load shifting are potential solutions to delay investment in additional generation capacities [Pina et al., 2012]. [Denholm and Margolis, 2007] evaluate the requirements for reaching 50% of PV penetration and highlights the role of DSM and load shifting to avoid storage capacity investment. [Boogen et al., 2017] investigate the impact of demand-response (DR) on Switzerland's electricity demand, showing that DSM programs mainly reduce household consumption by about 5%. [Srivastava et al., 2019] highlight how DR programs' implementation helps increase the customers' awareness and raise attractiveness in smart-appliance. Similarly, [Yilmaz et al., 2020] highlight that households that would accept to have some of their appliances controlled remotely by their distribution system operator (DSO) are the ones that have the most attention to their energy supply (not only the electricity tariff but also the energy origin, for instance). Hence, there is a correlation between promoting behavioral change and the residential sector's acceptance of technical measures that would technically increase their

flexibility. This motivates the interest in behavioral flexibility as it significantly raises the attractiveness and acceptance of flexibility measures.

Many attempts to quantify experimentally potential for household flexibility and demand-response have been conducted recently. A pilot study in Norway where 40 households were equipped with remote load control for heating devices and peak hour reminders was presented by [Saele and Grande, 2011]. They showed a response of about 1kW average power thanks to the concurrent effect of the remotely controllable load and the real-time information provided to the households. The work of [Filippini, 2011] aims to quantify the price elasticity of Swiss households. A real-time pricing study conducted by [Allcott, 2011] shows that households reduce their energy consumption during peak hours but do not necessarily increase their consumption during off-peak hours. On the opposite, the findings of [Torriti, 2012] show that the introduction of time-of-use tariffs increases global energy consumption by 13% and specifically during the evening peak hour. The authors point out the low awareness of the customers to explain this counter-intuitive result. Another study specifically focused on wet appliances (such as dishwashers, tumble-dryer, etc.) has been conducted in [Staats et al., 2017], showing a limited impact of DSM on the overall energy consumption. Similarly, a study on the potential of flexibility coming from the heating needs has been conducted in [Kepplinger et al., 2016] and [Darby, 2018]. The latter highlights some interesting research questions related to the policy condition to enable households to benefit from this flexibility. Obviously, practical experiments rely mostly on the current status of the regulation, market, and technology and are often limited by these factors. The work of [Hinterstocker et al., 2017] evaluates the households' potential for load shifting under a two-rate electricity tariff and questions the efficiency of this tariff model compared with a capacity-based tariff. From a theoretical point of view, understanding how and when energy could be potentially shifted is essential. This knowledge allows for better policy, energy pricing, and technological bottleneck assessment. This kind of research is performed using a model-based approach.

From a technical point of view, [Paetz et al., 2013] modeled the household electric system, including electric mobility and storage capability. The model was also validated using an experiment in a smart-home laboratory. The study highlights the complex task of providing comprehensive information to households so that their acceptance and understanding of a DSM program enable a good response. It highlights the difficulties of forecasting flexibility. A data-driven attempt to forecast the flexibility using neural networks is presented in [Ponocko and Milanovic, 2018]. However, data-driven approaches do not provide any gain of understanding of the underlying phenomenon that enables flexibility. Alternatively, the methodology proposed in [Roje et al., 2017] tries to model flexibility by employing a Markov model. This method allowed authors to simulate the behavior of a household equipped or not equipped with a DSM interface. The specificity of this study is that the validation experiment was conducted on an isolated network relying on both renewable energy sources and fossil fuel. They highlight how a well-adjusted DSM program can enable savings of fuel consumption.

So far, only remunerative incentives are considered. From the classification of [Callahan, 2004, Koenig, 2011], there are two other types of incentives. Coercive incentives result from a physical force used if the desired behavior is not achieved and moral incentives. The latter is of interest for behavioral flexibility. The household's behavior change after installing a PV system is not widely studied. A survey in Texas from 2011 [Rai and McAndrews, 2012] investigates the decision-making and behavior change of PV adopters. The authors report an increase in electricity consumption awareness while not being able to measure the behavior change. [Hondo and Baba, 2010] reports that new PV owners generally change their behavioral behavior and tend to push others to do so after installing a PV system. Differences exist between early PV adopters (before grid parity) and new PV adopters (after grid parity), as reported by [Wittenberg and Matthies, 2018]. Their study primarily focuses on energy saving that is explained for the early adopter by increasing energy consumption awareness, while for new adopters, it is the load shifting activities that drive energy saving. The work of [Sekitou et al., 2018] confirms this finding. However, none of the mentioned studies evaluated the households' intraday load-shifting effort.

The purpose of the FLEXI 2 experiment is to quantify the household energy demand flexibility potential. This chapter presents this thesis' essential contribution to Research Question A). For this purpose, two specific time-of-use (TOU) tariffs were used. The first tariff leveraged on the first FLEXI project [Perret et al., 2015] and consisted in lowering the price of electricity lower (bonus) between 11:00 and 15:00. To compensate, the electricity price was slightly increased (malus) during the rest of the day. Although the time window for the low rate could be chosen arbitrarily, it corresponds to the hour of higher PV production in Switzerland. The second TOU tariff was based on the weather forecast. The sunshine hour forecast for the next day was used to determine whether a low rate or a high rate should apply during three different periods of the day (10:00 to 13:00, 13:00-16:00, and 16:00-19:00). In other words, for a given period, if the solar irradiation was high enough, the electricity price was lowered (by the same bonus as for the first tariff). As for the first tariff, the electricity rate was increased during the rest of the day by the same malus. The households subject to this treatment were informed by SMS (short message system) every day at 17:00 of the next day's low rate periods. The households' reaction to these two treatments is measured by analyzing the intraday consumption patterns. This is possible because the local energy retailer *La Goule* has been an early adopter of smart-metering technology. Combining those consumption measurements with detailed surveys is one of the outstanding achievements of this project, making such a dataset quite rare in Switzerland.

A dedicated analysis on new PV adopters was conducted, which adds relevant information to answer the Research Question A). Using the smart meter data, the consumption behavior change of new PV owners was observed. This allows studying the effect of moral and remunerative incentives on the households flexibility.

Section 2.2 presents the data treatment and some statistical analysis. One outcome of this experiment is the treatment of these data that happens to be not so trivial. The details of the pre-treatment of the smart meter data are given in Section 2.2.1. To build up the experiment

and select the households, the survey collects various socio-demographic information about the households. Besides, the phone numbers were requested to contact the households (mandatory for the second tariff). The survey and some statistical information about the household structure are given in Section 2.2.2. The complete methodology to design the experiment and analyze the results is provided in Section 2.3. In particular, the design of the treatments (Section 2.3.1) and analysis method (Section 2.3.2) are detailed. The results of the project are summarized in Section 2.4.

2.2 Available data

2.2.1 Smart meter measurements

The smart meter data from 630 households between August 2013 and March 2018 were provided by the energy retailer and DSO *La Goule*. As *La Goule* was one of the pioneers to deploy smart metering technology, the reliability of the data acquisition and transmission system was a great challenge (keeping in mind that for their entire network, the number of data points to transmit is around 350'000 per day). The first step of this work consists in pre-processing these data to make them plausible and reliable for research purposes. The early installed smart meters sample the electric consumption at a 1-hour resolution while the more recent ones have a resolution of 15 min.

Each data point contains four essential information:

- The installation number, a number identifying the electric installation being metered (a house or a flat)
- The date and time of the measure
- The quantity of energy consumed between the last measure and the current one
- The value of the "index" at the last measure and the current measure. The difference between these two indexes should be equal to the quantity of energy consumed

In the following, $E_{i,t}$ denotes the quantity of energy consumed by the i^{th} household between time $t - 1$ and t . These time series are often not continuous as missing data points, measurement errors, and inconsistencies happen. An example of such a time series is pictured in Figure 2.1.

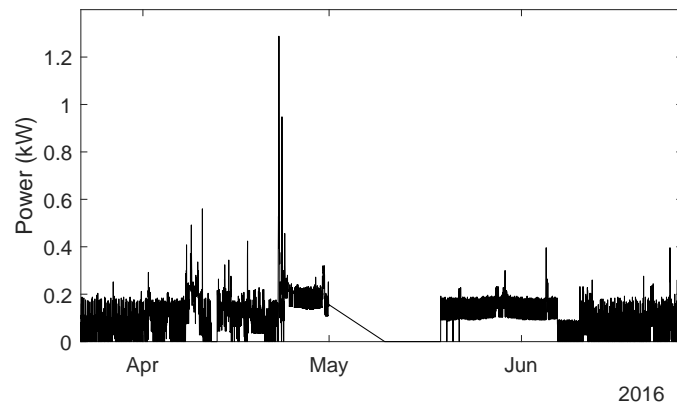


Figure 2.1 – An example of a smart meter measurement with missing data, suspected measurement error, and inconsistent data

As Figure 2.1 shows, significant periods without data can happen for unknown reasons. Figure 2.2 pictures the availability of the data. A black dot represents each missing data point. The first task is to clean up the dataset to remove incorrect or implausible data and then fill the missing data before performing further analysis. The exact procedure for cleaning and filling up missing data is described in the following.

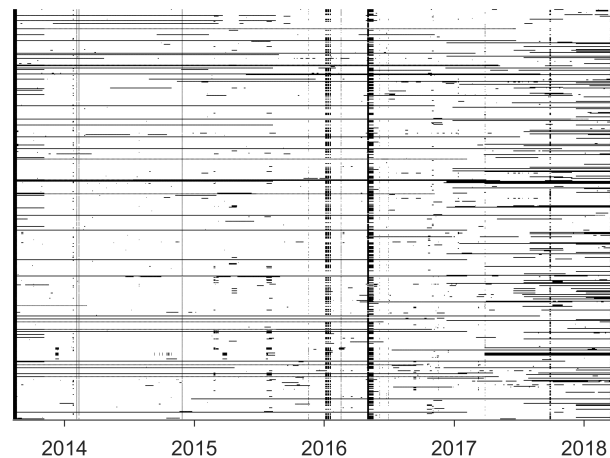


Figure 2.2 – Original data availability map. The time series are stacked vertically (time-synchronized). A data point is represented by a black pixel, if it is missing, a white one otherwise.

For all households except the PV owner, a data point is considered valid if it fulfills the following condition:

Chapter 2. Experimental determination of the households demand flexibility

- $E_{i,t} > 0$, it is very unlikely that the consumption is exactly 0 even at 15min resolution.
- $P_{i,t} = \frac{E_{i,t}}{\Delta T} < \begin{cases} 10 \text{ kW} & \text{if } \Delta T = 0.25 \text{ h} \\ 8 \text{ kW} & \text{if } \Delta T = 1 \text{ h} \end{cases}$ as none of the households are equipped with heavy electric appliance such as electric boiler or heat pump (this is a mandatory condition see Section 2.2.2).

The maximum admissible power depends on the sampling rate as a longer integration interval flatten high power peak. The thresholds of 10 and 8 kW have been defined by studying the power histogram of the dataset.

To fill the missing data point, a dedicated procedure is defined. Each household load measurement is considered separately. We consider the valid data ratio as the ratio between the number of valid data points in the time series and the number of time steps between the beginning and the end of the time series. For instance, at 15 min resolution, a one-day time series has 96 time steps. If the time series has only 94 data points, the valid data ratio is 98%.

A household load measurement is assumed to be valid if the valid data ratio is at least 50%. If this ratio is below the threshold, it is discarded.

The basic principle to fill the missing data is to select three neighboring portions of the time series that correspond to the desired portion of missing data (a portion can be a sequence of data points of length ≥ 1). Each portion should correspond in time (hour of the day) and the day of the week to the missing portion. The selected portions are then averaged to fill the missing data portion. Two additional criteria play a role in the selection of the portion. The first aims to keep the occupancy state. If the household's occupants are assumed to be at home just before the missing data period, the three selected portions must also correspond to the periods where people are assumed to be at home. The second criterion matches the electricity rate. If the electricity rate for the current households corresponds to the low rate (bonus) during the missing data period, the three selected portions should also correspond to the time of low electricity rate. For instance, let us assume no data are available for a particular household from Monday 13 march between 13:00 and 14:30, that the occupants are assumed to be at home during this time, and that the electricity rate is low during these hours. We look for three time series portions, corresponding to a Monday between 13:00 and 14:30 when people are at home with a low electricity rate to fill the target missing data period.

As it is often impossible to fulfill all the criteria (day of the week and time, occupancy state, electricity rate), the algorithm will first ignore the occupancy state, then the electricity rate criterion to fill the missing portion. The filling algorithm is graphically represented in Figure 2.3. To determine the households' occupancy state, the considered day's maximum power is compared to the mean daily maximum power. If the considered daily maximum is above 1/3 of the mean daily maximum, the households' occupants are assumed to be at home. This is, again, graphically represented in Figure 2.4.

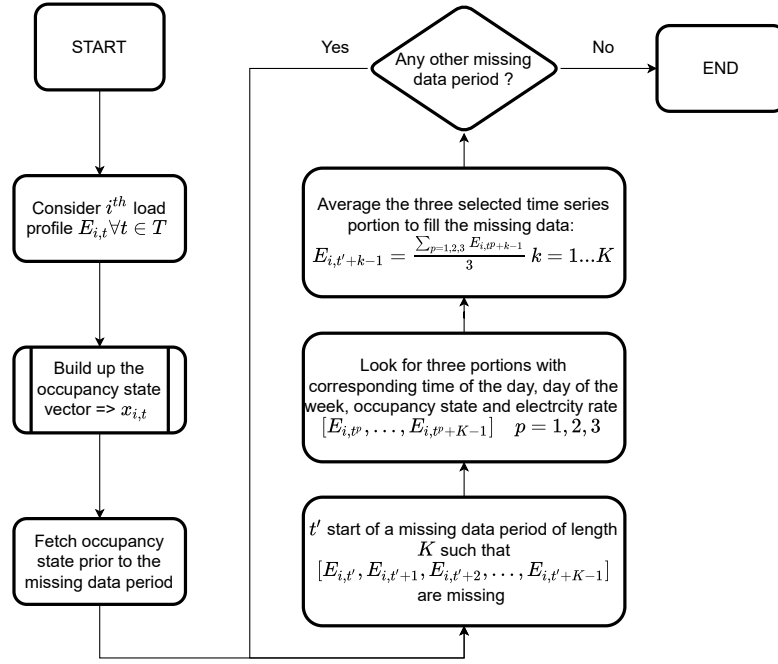


Figure 2.3 – Missing data filling algorithm

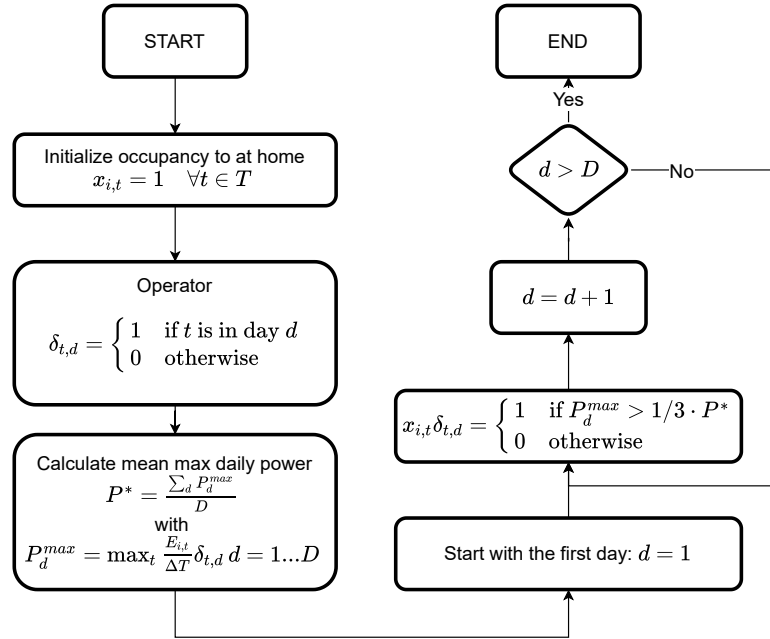
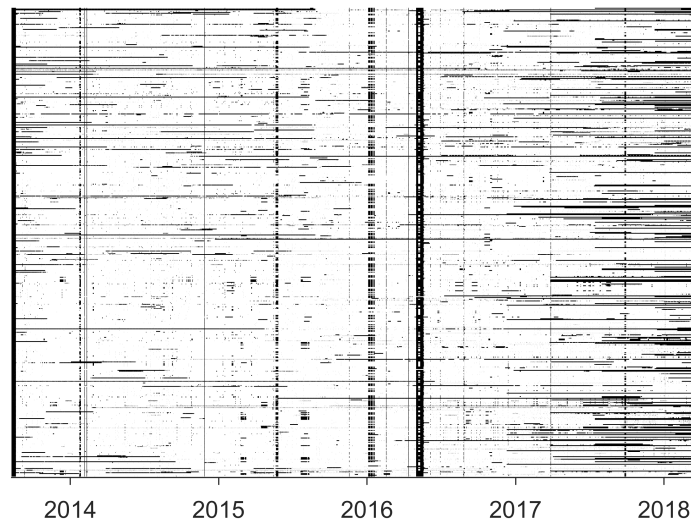
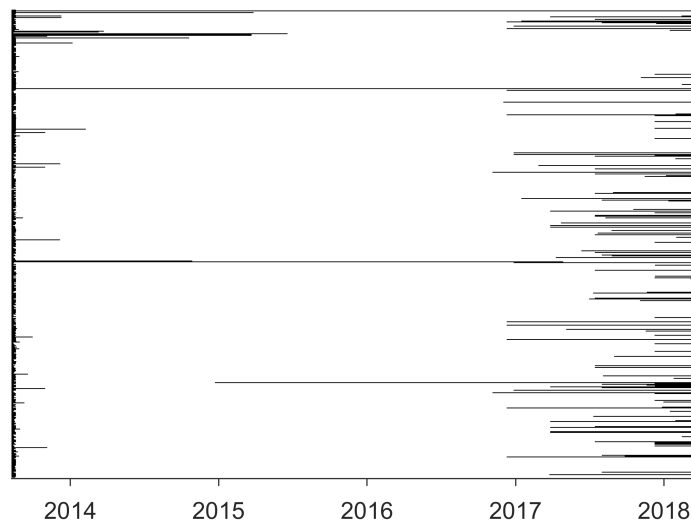


Figure 2.4 – Household's occupancy state estimation

Figure 2.5 qualitatively compares the number of missing data points at the end of the cleaning and the filling process. Unfortunately, some technical issues arose starting from 2017, which caused the large unavailability of valuable data.



(a) Right after cleaning



(b) After cleaning and filling

Figure 2.5 – Data availability map

2.2.2 Surveys

To build up the control and treatment groups, a survey was performed among *La Goule's* customers on a dedicated website <http://www.flexi-goule.ch>. The original survey is available in Appendix A. The questions in the survey allow us to acquire the following information:

- Dwelling type (single-family house, or apartment)
- Type of ownership (owner or tenant)
- Number of rooms, bathrooms, or other (numerical)
- Housing footage
- Number of people in the household and their age
- Employment status (full-time worker, part-time worker jobless, etc.)
- Household type (family or couple, single-parent family, apartment-sharing, single)
- Education level
- Income
- Heat source for space heating (direct electric, fuel, gas, heat pump ...)
- Heat source for domestic hot water (same as above)
- List of appliances. The users tick what they own from a list of appliances. For some of them, they can mention how many they own.
- Consumption habit (for instance, number of dishwasher per week)
- Fraction of low consumption light bulb
- Degree of environmental concern. The users were asked how they are concerned with particular statements about the environment, climate, and economy.

Figure 2.6 pictures the variety of households and dwelling types. Significant differences can be observed between single-family houses with footage of around 200 m² for annual consumption of 3000 kWh and apartments that are smaller (100 m² typically) and consumption just below 2000 kWh. In this dataset, the number of inhabitants seems to have a negligible effect on energy consumption. As highlighted by Figure 2.7, most single-family houses are owned by the households, while most apartments are rented. The age is the one of the person who filled the survey. As pictured in Figure 2.8, most of the participants are above 50 years old. Finally, Figure 2.9 highlights that an average household holds two people with a monthly income of around 6000 CHF/month, which is close to the Swiss median salary[FSO, 2020].

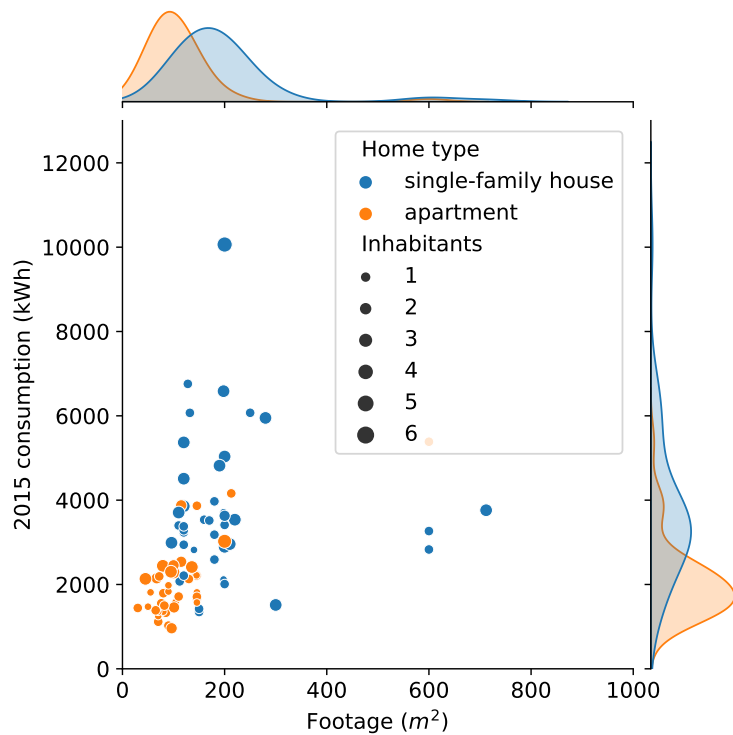


Figure 2.6 – Annual consumption (2015) vs. house footage. The size of the point indicates the number of inhabitants and the color is the dwelling type.

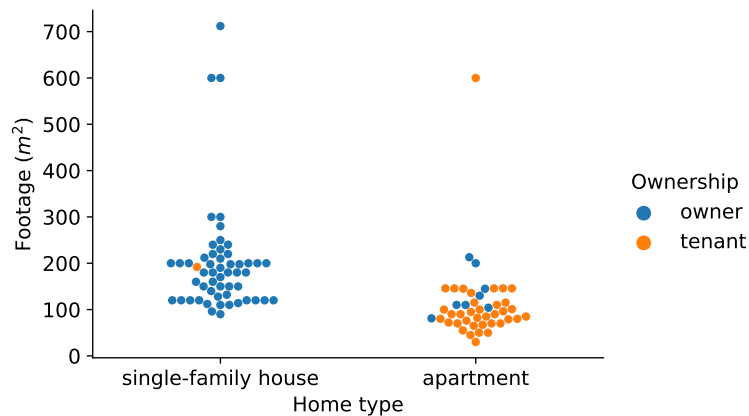


Figure 2.7 – Distribution of the housing size as a function of the dwelling type and ownership

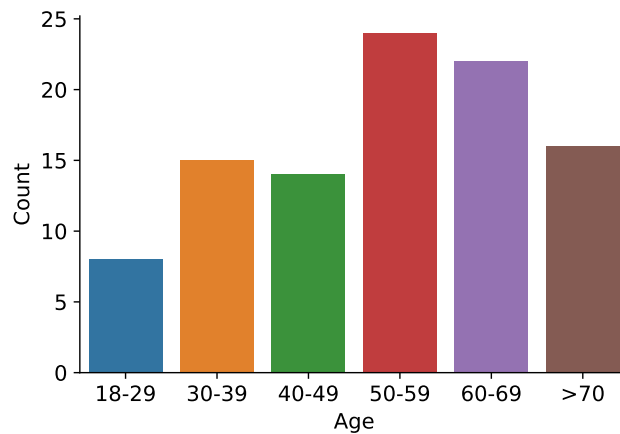


Figure 2.8 – Age group distribution

>14000	0	1	0	1	0	0
12000-13999	0	3	0	1	0	0
10000-11999	0	6	2	4	0	1
8000-9999	0	5	0	7	1	0
6000-7999	2	18	4	7	1	0
4000-5999	6	12	0	1	0	0
2000-3999	7	3	2	0	0	0
<2000	1	2	0	1	0	0
	1	2	3	4	5	6

Figure 2.9 – Number of households per income group and household size

A dedicated survey was sent to the PV owners to acquire some information about their PV system: The nominal PV capacity, roof orientation, and availability of any production measurement were requested. The original survey is reproduced in Appendix B. This group of households is referred to as the PV group.

For all households except the PV owner, dedicated interventions were designed. The following section provides some details about the design of these treatments.

2.3 Methodology

2.3.1 Interventions

Two interventions (or tariffs) were used in this experiment. For both of them, the electricity rate was changing along the day. The main difference between the two interventions is that in the first tariff, the high and low rate hours are the same every day, as for the second intervention, the low rate hours change every day depending on the weather forecast. The two tariffs were based on the standard single electricity rate of *La Goule* at the time of the experiment (2017-2018). For the standard rate, the price of a kWh is 27.45 cts/kWh. The low rate corresponds to a reduction (bonus) of 15 cts/kWh, while the high rate is an increase (malus) of 4 cts/kWh. For the first treatment, hereafter referred to as T1, the low rate hours are determined according to the mean daily irradiance pattern as pictured in Figure 2.10a. Between 11:00 and 15:00, 50% of the global daily irradiance is received. For this reason, this time window was chosen as the low rate period (see Figure 2.10b).

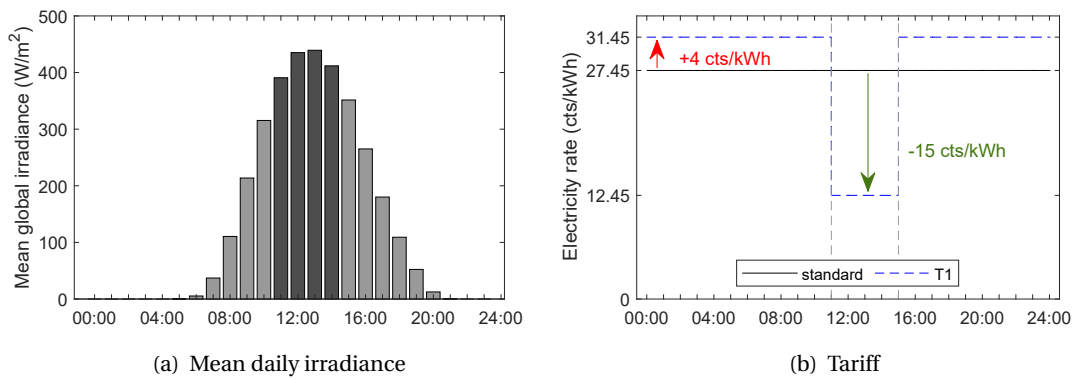


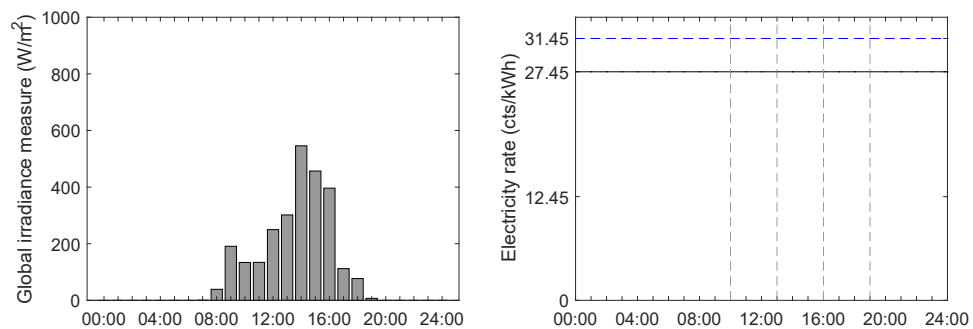
Figure 2.10 – Treatment T1

The bonus and malus were calibrated so that an average household, if it did not change its consumption pattern, did not make any gain or lose. This treatment has the advantages of being repetitive. Hence it is expected that it would be easier for the households to adopt new habits. In the real world, it would also be easier for the DSO to implement it.

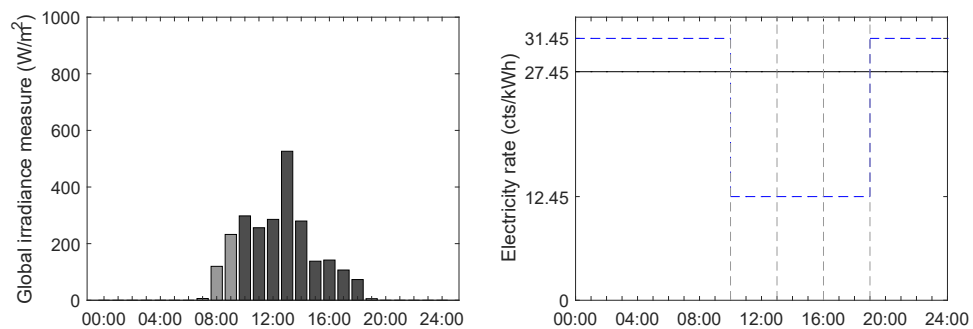
The second treatment, hereafter referred to as T2, consists in a variable tariff that was communicated to the participants one day in advance by SMS, and that depends on the weather forecast of the considered day. Depending on the sunshine forecast (provided by <https://www.meteoblue.com>), the low rate hours were activated or not. This approach is more realistic than the first treatment because the low rate period actually corresponds to the period of high irradiance (and potentially PV generation). In more detail, three activation periods were possible, 10:00 - 13:00, 13:00 - 16:00, or 16:00 - 19:00 (only possible during the summertime).

For each possible period, if the sunshine was "good enough" a low rate period was activated.

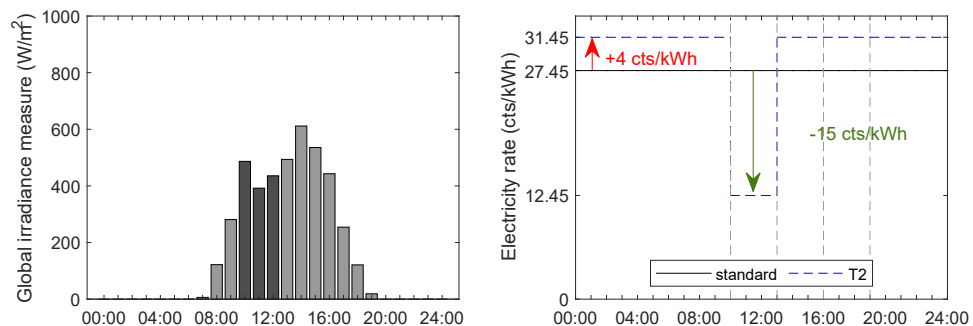
This statement was translated into a specific criterion that was compatible with the *meteo blue* API. As an example, Figure 2.11 pictures the actual global irradiance and corresponding tariff for three consecutive days. The bonus and malus were kept the same as for treatment 1. The limitation of this approach is obviously linked with the accuracy of the weather forecast. As highlighted by Figure 2.11a or 2.11c, the weather forecast could lead to the activation of only one low rate period or even no period at all, while the irradiance was actually still fairly high. The households were advised of the next day's low rate periods at 17:00 by SMS.



(a) 20th September 2016



(b) 21st September 2016



(c) 22nd September 2016

Figure 2.11 – Treatment T2

Chapter 2. Experimental determination of the households demand flexibility

The households were split into three distinct groups:

- A control group, which received no information about the experiment except, and subject to the standard electricity tariff.
- A group receiving treatment 1, referred to as group 1, will follow the tariff T1.
- A group receiving treatment 2, referred to as group 2, will follow the tariff T2.

Each group should be statistically similar. Hence, the age of the people who filled the survey and the annual consumption were used to split the households into the three groups, making sure that the distributions of the two mention features are the same in each group. The survey was carried out from April 2016. Between this date and July 2016, only 44 people answered the survey. Those were split into three groups and are referred to as the first wave, which started the experiment on the 1st July 2016. After more intensive communication, 48 additional households were recruited at the beginning of September 2016. These households are the second wave that started the experiment on the 1st October 2016. Because the number of participants was still too low, it was decided to recruit, just by informing them by mail, 500 new participants who did not complete any survey. Those are referred to as wave 3. It is important to note that participating in the experiment was risk-free for the participant. Indeed, if the energy bill under the new tariff (T1 or T2) was higher than the bill with the standard tariff, the household was required to pay the standard bill. The participants from this 3rd wave were not recruited in treatment 2 because the latter required a mobile phone number which was not available. The experiment starting date for each wave and the number of households in each treatment group are indicated in Table 2.1.

Table 2.1 – Distribution of the households into the groups and waves

Wave	Experiment start	Group				Total
		C	T1	T2	PV	
1	01.07.2016	14 (9)	15 (10)	15 (10)	-	44 (29)
2	01.10.2016	16 (14)	16 (12)	16 (4)		48 (30)
3	01.01.2017	253 (192)	252 (197)	-	-	505 (389)
Total		283 (215)	283 (217)	31 (14)	38 (31)	635 (477)

Following the exposure of the framework of the FLEXI 2 experiment, the following section presents the methodology to evaluate the behavior change according to the different treatments.

2.3.2 Analysis

Two main metrics are used in this analysis. The first metric consists in the daily energy consumption (see Equation 2.1). The second is the "Flexi score". The score is defined as the ratio between the mean power during a low-rate period and the mean power during the corresponding day (see Equation 2.2). Both metrics are evaluated daily. Recalling the notation of Section 2.3.1, those metrics are given as follow:

$$\text{Daily energy consumption:} \quad E_{i,d}^{day} = \sum_t E_{i,t} \delta_{t,d} \quad (2.1)$$

$$\text{Flexi score:} \quad S_{i,d} = \frac{\frac{\sum_t E_{i,t} \delta_{i,t,d}^{flexi}}{\sum_t \delta_{i,t,d}^{flexi} \Delta T}}{\frac{E_d^{day}}{24}} = \frac{\overline{P}_{i,d}^{flexi}}{\overline{P}_{i,d}^{day}} \quad (2.2)$$

where $\delta_{t,d}$ is one if time step t fall during day d , and $\delta_{i,t,d}^{flexi}$, if time step t fall during a low-rate period of the day d ¹. As a reminder, $E_{i,t}$ is the consumption (in kWh) of the i^{th} households during the interval $[t-1, t)$ and ΔT is 0.25 h.

The flexibility score and the daily energy consumption can be calculated for any household and any day in the pre-treatment and treatment periods. The difference between these metrics during those two periods somehow defines the behavior change. By comparing this behavior change with the control group (that did not receive any treatment), we can evaluate the treatment's effect. The treatment and pre-treatment periods are given in Table 2.2. All recruitment waves did not start the experiment simultaneously, so their corresponding pre-treatment and treatment periods are not the same.

Table 2.2 – Treatment and pre-treatment periods

wave	pre-treatment		treatment	
	start	end	start	end
1	01.07.2015	30.06.2016	01.07.2016	30.06.2016
2	01.10.2015	30.09.2016	01.10.2016	30.09.2017
3	01.01.2016	31.12.2016	01.01.2017	31.12.2017

To evaluate the theoretical potential for households' flexibility, we applied the *device usage estimation* (DUE) algorithm (presented in the previous chapter) to disaggregate the load measurements into the eight appliance categories defined in Table 1.3. We define three flexibility levels, not shiftable, hardly shiftable, or easily shiftable, and link them with the appliance category in Table 2.3.

¹ the subscript i just remind that the low-rate periods depend on the treatment. It does not strictly depend on the household

Table 2.3 – Appliance flexibility degree

Category	Flexibility level
Cooking	not shiftable
Entertainment	hardly shiftable
Fridge	not shiftable
Heating	hardly shiftable
Housekeeping	easily shiftable
ICT	hardly shiftable
Light	not shiftable
Standby	not shiftable

This allows defining a theoretical performance metric, corresponding to a Flexi score where all possible shiftable energy has been moved to the low-rate periods. It is assumed that the easily and hardly shiftable energy is moved (if not already present) into the low-rate period. This translates as:

$$\begin{aligned}
 \text{Shiftable energy outside a low-rate period: } E_{i,d}^{shift} &= \sum_t (E_{i,t}^{easily} + E_{i,t}^{hardly}) \cdot (1 - \delta_{i,t,d}^{flexi}) \\
 \text{Theroretical Flexi score: } S_{i,d}^{theo} &= \frac{\sum_t (E_{i,t} \delta_{i,t,d}^{flexi}) + E_{i,d}^{shift}}{\sum_t \delta_{i,t,d}^{flexi} \Delta T} \quad (2.3) \\
 \text{keeping in mind that } E_{i,t} &= E_{i,t}^{easily} + E_{i,t}^{hardly} + E_{i,t}^{not}
 \end{aligned}$$

with $E_{i,t}^{easily}, E_{i,t}^{hardly}, E_{i,t}^{not}$ the easily, hardly and not shiftable energy, respectively².

For the PV owners' analysis, a different metric is used. Because the households did not face any variable tariff, there is no low-rate period, but instead favorable periods, when their PV system produce energy in which there is an incentive to shift the energy. Thus, it is impossible to define a common period for all households and thus calculate any Flexi score. A possible metric could be to use self-consumption (see definition in Equation 2.4). However, self-consumption depends on the PV capacity compared with the consumption intensity (a small PV capacity coupled with a large consumer will lead to a high self-consumption, for instance). The same applies to self-sufficiency (see definition in Equation 2.5). We defined the normalized self-consumption (Equation 2.6), which normalizes the daily PV generation with the daily consumption to cope with this issue. In other words, the self-consumption of a particular day is calculated assuming that the daily PV generation is equal to the daily consumption. This is illustrated in Figure 2.12.

²The assumption $E_{i,t} = E_{i,t}^{easily} + E_{i,t}^{hardly} + E_{i,t}^{not}$ does not always hold using the DUE algorithm of Chapter 1. Indeed the sum of the disaggregated power is sometimes smaller than whole-house consumption.

Self-consumption:
$$SC_{i,d} = \frac{\sum_t \min(P_{i,t}, G_{i,t}) \delta_{t,d}}{\sum_t G_{i,t} \delta_{t,d}} \quad (2.4)$$

Self-sufficiency:
$$SS_{i,d} = \frac{\sum_t \min(P_{i,t}, G_{i,t}) \delta_{t,d}}{\sum_t P_{i,t} \delta_{t,d}} \quad (2.5)$$

Normalized self-consumption:
$$NSC_{i,d} = \sum_t \min\left(\frac{P_{i,t}}{\sum_t P_{i,t} \delta_{t,d}}, \frac{G_{i,t}}{\sum_t G_{i,t} \delta_{t,d}}\right) \delta_{t,d} \quad (2.6)$$

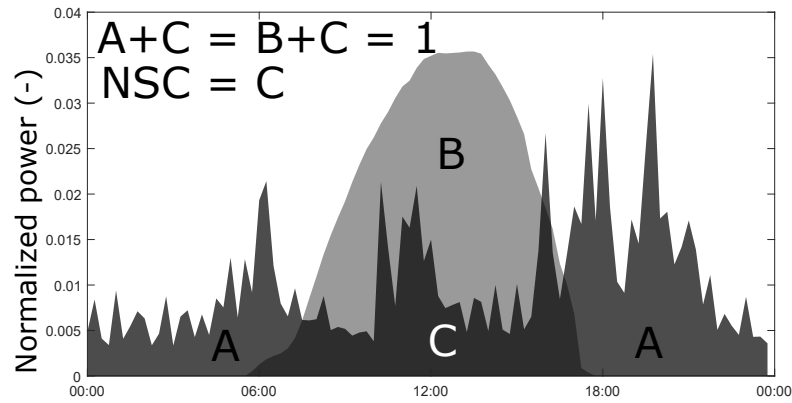


Figure 2.12 – Normalized self-consumption. Area A is the consumption uncovered by the PV generation. Area B is the PV surplus, and area C is the normalized self-consumption.

Thanks to the smart meter data, it is possible to evaluate the PV owners' behavior change by comparing the change in consumption patterns before and after installing the PV system with a control group (without any PV installation). However, a few more preparation are needed to achieve this goal. For PV systems in self-consumption schemes (which is the case for all PV owners of this experiment), the actual consumption and the PV production are not monitored separately. Indeed, smart meters measure the energy flow going both ways in each interval bin. To retrieve the actual consumption, one needs to estimate the PV generation, as illustrated in Figure 2.13.

Using the survey sent to the PV owners (see Appendix B), the installed capacity, roof orientation, and tilt are known for each system. The PV generation $G_{i,t}$ is simulated using the irradiance data from Fahy weather station ³ (this weather station is located in the distribution area of the DSO *La Goule*) using the PVLIB toolbox ⁴. The load or real consumption is retrieved by applying Equation 2.7.

³ data from *idaweb* <https://gate.meteoswiss.ch/idaweb/>

⁴ PVLIB for MATLAB available at https://pvpmc.sandia.gov/applications/pv_lib-toolbox/

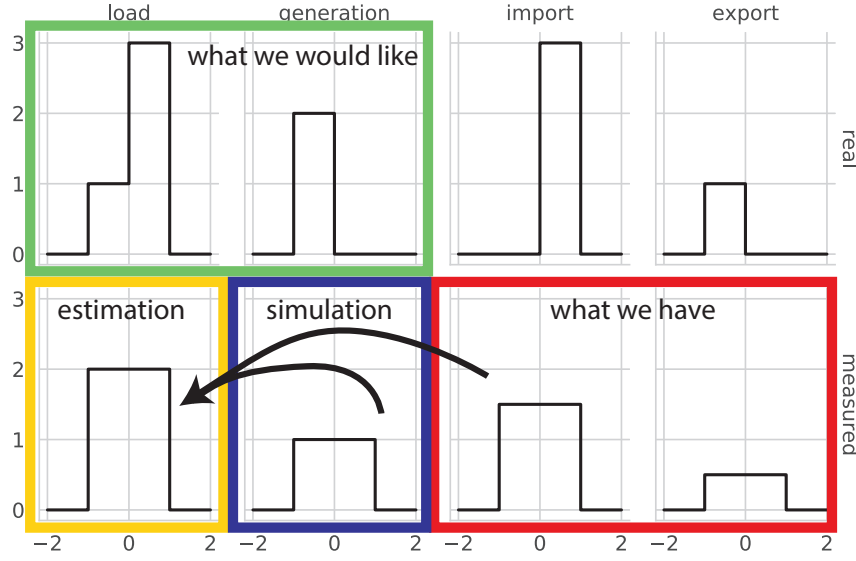


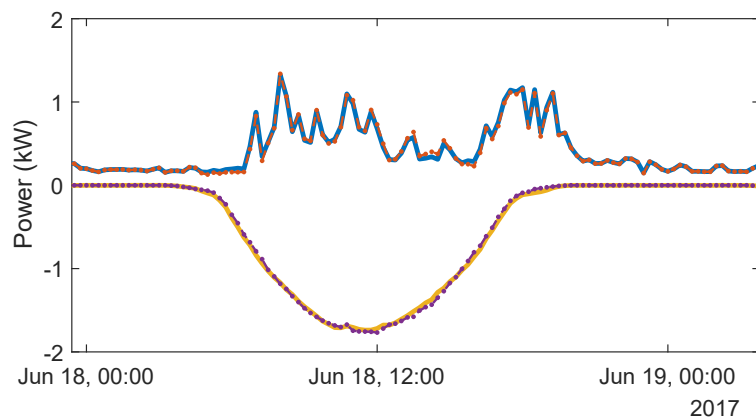
Figure 2.13 – Smart meter measurement illustration. The top row assumes a real power signal of two steps. The smart meter only provides the energy (hence average power) of the last two time steps (15 min in reality) represented by the import and export curve of the bottom row (red square). By simulating the generation (blue square), we can deduce the average consumption (yellow square), which should match the original load and generation (green square).

$$\text{Estimated PV owner's load} \quad P_{i,t} = \max\left(0, P_{i,t}^{imp} + G_{i,t} - P_{i,t}^{exp}\right) \quad (2.7)$$

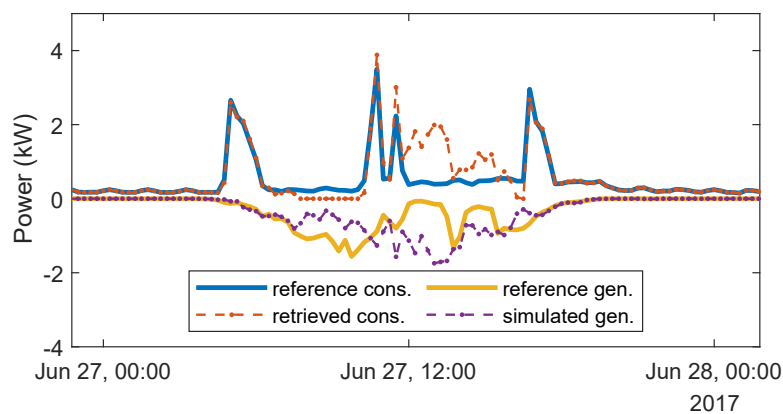
where $P_{i,t}^{imp}$ and $P_{i,t}^{exp}$ are the imported or withdrawn and exported or injected power respectively. Compared to the households without PV system, the notation $P_{i,t} = \frac{E_{i,t}}{\Delta T}$ corresponds to $P_{i,t}^{imp}$ because a consumption means withdrawing power from the grid.

The quality of the actual load estimation heavily depends on the accuracy of the PV generation simulation. Using the provided formulation, an over-estimation of the PV generation will lead to an over-estimation of self-consumption. To illustrate this, Figure 2.14 shows two cases. In the first case, the simulated PV generation is close to a ground truth PV production (both are simulated data, but an error has been introduced using two different weather stations). In the second case, the PV simulation differs from the reference one. From this figure, it is clear that the PV simulation errors lead to an overestimation of the consumption during PV production hours. For this reason, the analysis is restricted to clear sky days.

Using the presented methodology, the following section will describe and discuss the results of this experiment.



(a) Good PV simulation, typically on a clear sky day



(b) Bad PV simulation, typically on a cloudy day

Figure 2.14 – Importance of the PV simulation accuracy on the inferred consumption

2.4 Results

2.4.1 Time-of-use treatments

One qualitative way to visualize the households' reaction to their respective treatments is to look at the mean daily consumption profile. However, using the latter would emphasize high consumption households compared with those with very low consumption. For this reason, we instead have a look at the way the energy is distributed along a day and take the median of these profiles. The normalized power is defined as:

$$P_{i,h}^* = \frac{P_{i,t} \delta_{t,h}}{\frac{\sum_h P_{i,t} \delta_{t,h}}{24}} \quad (2.8)$$

with $\delta_{t,h} = 1$ if time step t falls during hour h .

Chapter 2. Experimental determination of the households demand flexibility

The hourly profiles are reproduced, separately, in Figure 2.15, for the three recruitment waves. As their analysis periods are not the same (recalling Table 2.2), it would not be coherent to cross-compare the pre-treatment, treatment, and control groups on the same graph. This figure highlights a poor reaction from the T1 households, despite a slight increase of the normalized power during the low rate period for the 2nd wave (see Figure 2.15b). All households (including the control group) seem to have lowered their consumption during the evening. This decrease is slightly more pronounced for the T1 group.

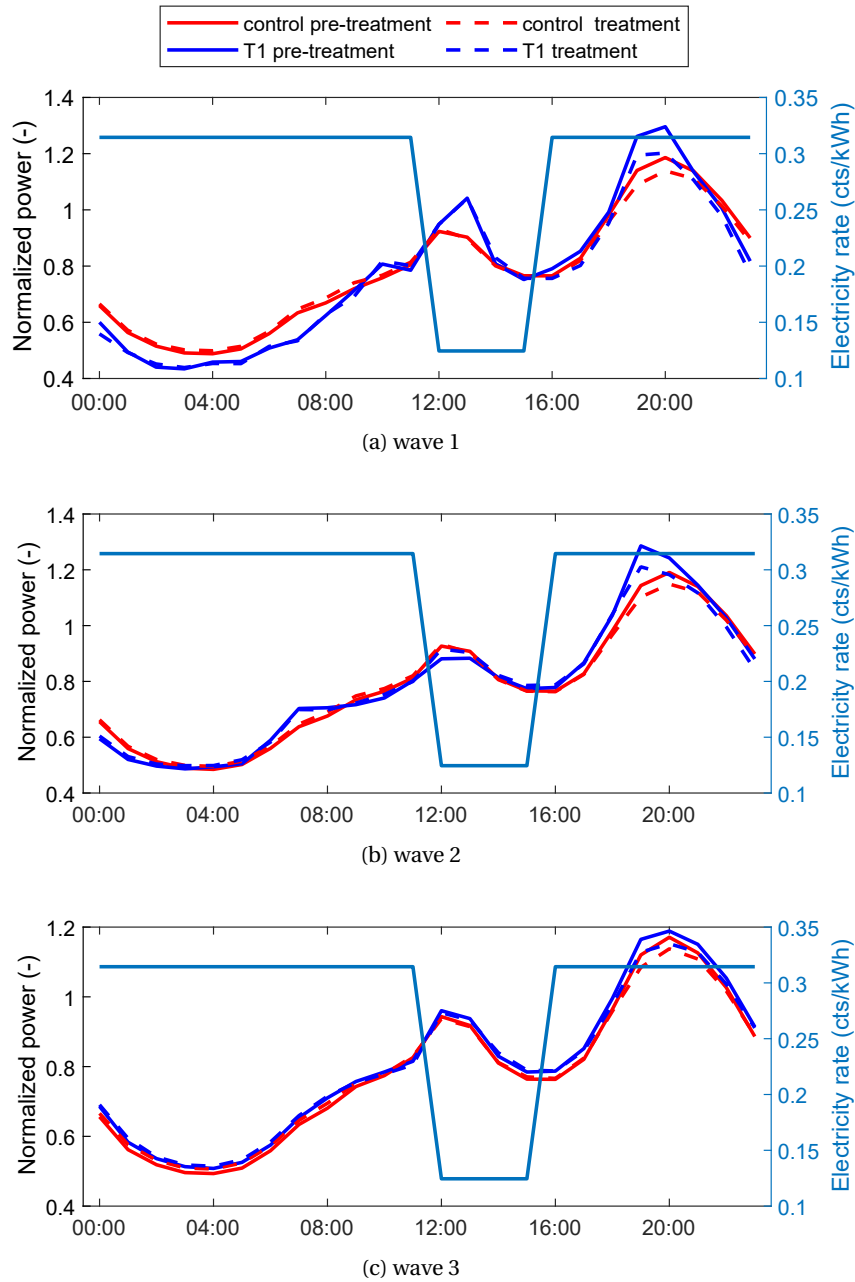


Figure 2.15 – Daily normalized power profile for Treatment 1

The two performance metrics (Flexi score and mean daily consumption) are reported for the first wave of the T1 group in Figure 2.16. Comparing the trajectory of each T1 household on this figure gives an idea of the potential behavior change that the households experienced. It is interesting to note the median metrics' variation (plotted as a large cross for the T1 group and circle for the control group). Indeed, it is the variations of the metric that is relevant to assess the behavior change. The relative variation of the daily consumption and Flexi score are reported in Figure 2.17. For all waves, most T1 households are in the upper part of the graph, indicating an increase in the Flexi score. Some also experienced an increase in the average daily consumption, which is coherent with the findings of [Torriti, 2012]. The control group, which faces the same weather condition, is relatively evenly spread in the four quadrants of the graph. In the 3rd wave's case, most of the control group (54%) decreased their Flexi score while 53% of the T1 group increased their score. Most households of both groups reduced their energy consumption. Despite an apparent low reaction of the households subject to treatment 1, a closer look highlights that the treatment has a small positive effect on the consumption pattern compared with the control group.

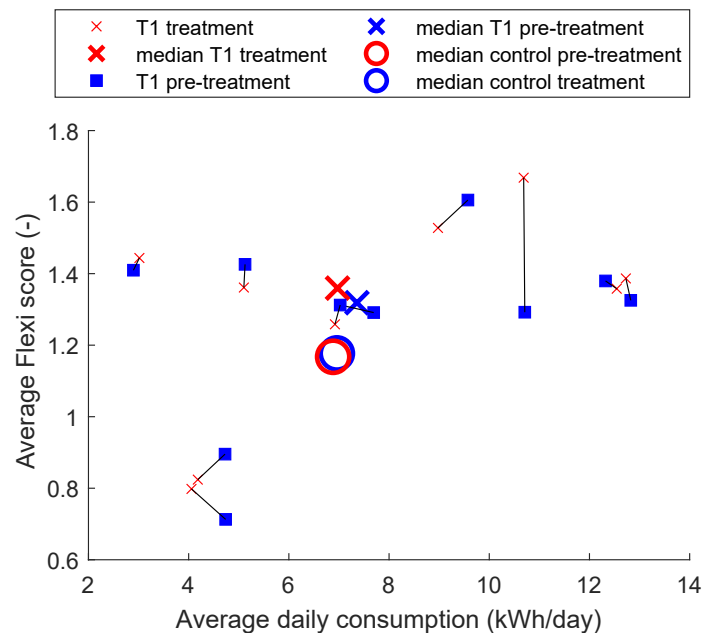


Figure 2.16 – Average Flexi score vs. average daily consumption for T1 wave 1

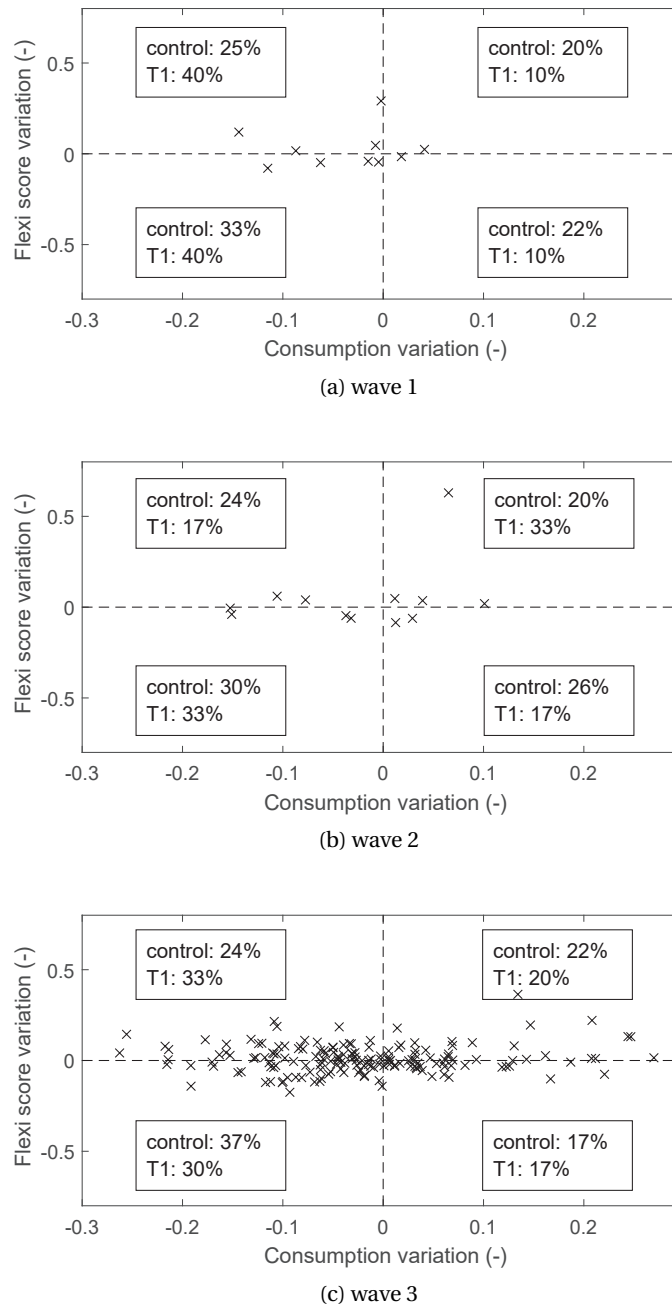


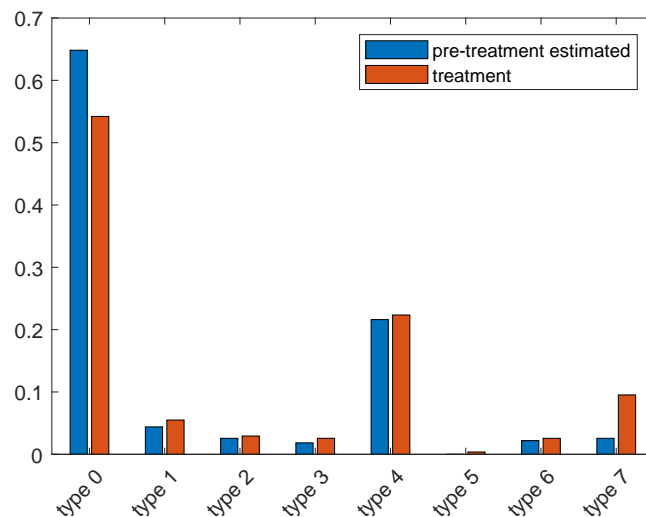
Figure 2.17 – Flexi score relative variation vs. daily consumption relative variation. Only the households of the T1 group are plotted. The fraction of households from the T1 and control groups in each quadrant are indicated in the box.

The second treatment is slightly more tricky to analyze because, contrary to the first one, which is a regular time-of-use (every day the same low rate period), three different low-rate periods can be activated. Table 2.4 represents the eight possible day types according to the activation of the low-rate periods.

Table 2.4 – Treatment 2 day type according to the low (L) and high (H) rate period in the day

	10h-13h	13h-16h	16h-19h
type 0	H	H	H
type 1	L	H	H
type 2	H	L	H
type 3	H	H	L
type 4	L	L	H
type 5	L	H	L
type 6	H	L	L
type 7	L	L	L

The treatment 2 day types distribution is pictured in Figure 2.18. As the number of households for this treatment is small (10 and 4 for the first and second recruitment waves, respectively), it has been decided to use a shorter common analysis period and to treat both waves together. Hence, in the following, the analysis period is restricted to the period from October 1st to June 30th (2015 for the pre-treatment, 2016 for the treatment). As Figure 2.18 shows, for most of the days, no low rate period is activated (type 0). The second more frequent day type is type 4, when the low-rate period occurs from 10:00 to 16:00. The third more frequent case (during the treatment phase) is type 7 with all low-rate periods activated. The daily normalized power profile for those three day types are pictured in Figure 2.19. Again it is difficult to notice a significant change in how the energy is consumed throughout the day.

Figure 2.18 – Distribution of the treatment 2 day type for the period between October 1st and June 30th

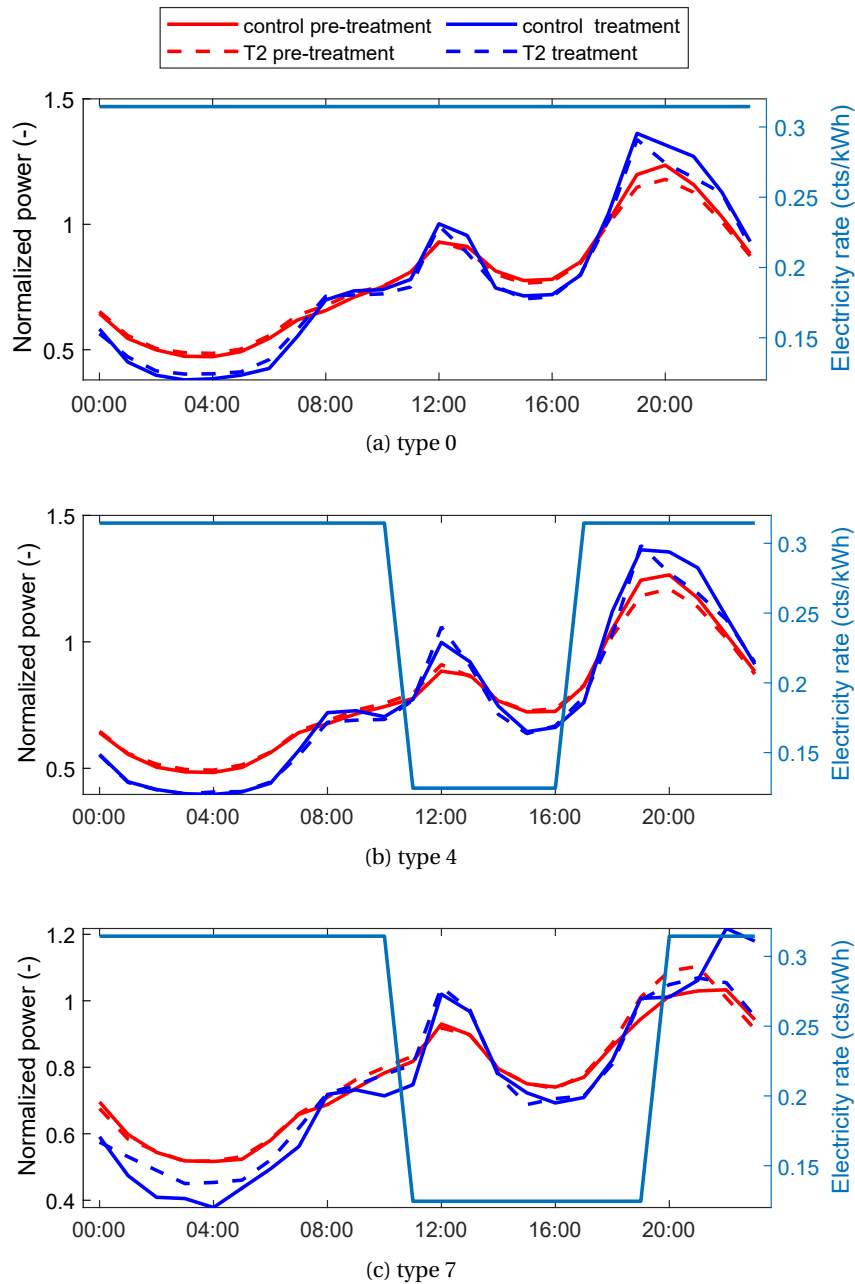


Figure 2.19 – Daily normalized power profile for Treatment 2 (wave 1 & 2 on the period from October 1st to June 30th)

Following a similar approach than the first treatment, the first wave metrics are plotted one against the other in Figure 2.20. Looking at Figure 2.21, again, most T2 households increase the Flexi score and reduce their consumption compared with the control group who is more evenly spread in the four quadrants of the graph. Despite the apparent poor households' reaction, the treatment seems to have a small positive effect in terms of both Flexi score and

consumption awareness. Communication of the tariff information by SMS required that the households of this group agreed to give their phone number. This may imply that the households of this treatment group were the most interested or motivated ones.

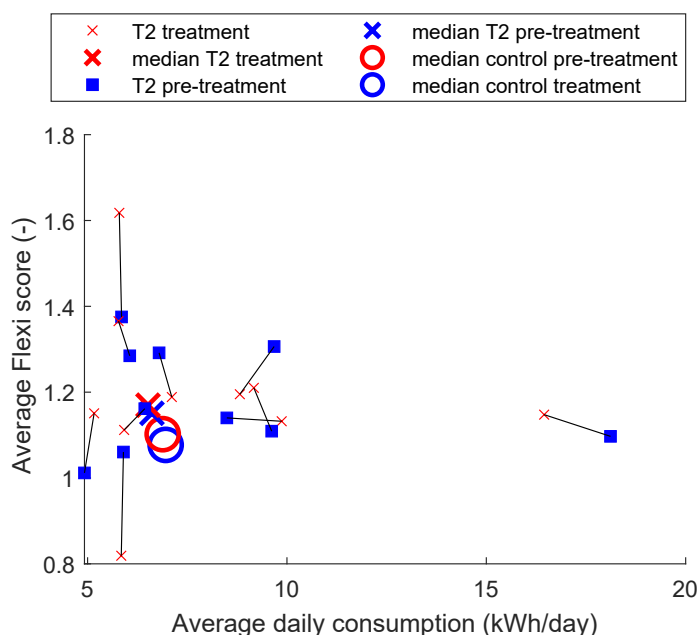


Figure 2.20 – Average Flexi score vs. average daily consumption for T2 wave 1, median per period and group are also indicated

2.4.2 Comparing the experimental and theoretical household flexibility

The DUE algorithm (cf. Chapter 1) is applied to the first and second-wave households (those who fulfilled the survey). The FLEXI 2 datasets of the first and second recruitment waves contain the whole house smart meter measurements and the households characteristics (see Section 1.2). The disaggregation of the energy consumption into the eight appliance categories (stand-by, heating, fridge, light, entertainment, cooking, housekeeping, and ICT) allows extracting the mean fraction of the total energy consumption per category pictured in Figure 2.22. The disaggregation has been performed from July 2015 to the end of the FLEXI 2 project. The analysis in this section only corresponds to the period before starting the experiment, hence from July 2015 to July 2016. One may note that the standby consumption can reach up to 50% of the total energy consumption. This number should be read keeping in mind that in this study, Standby consumption is defined as the daily minimum power consumption. It is not precisely what is commonly defined as the appliances' standby consumption.

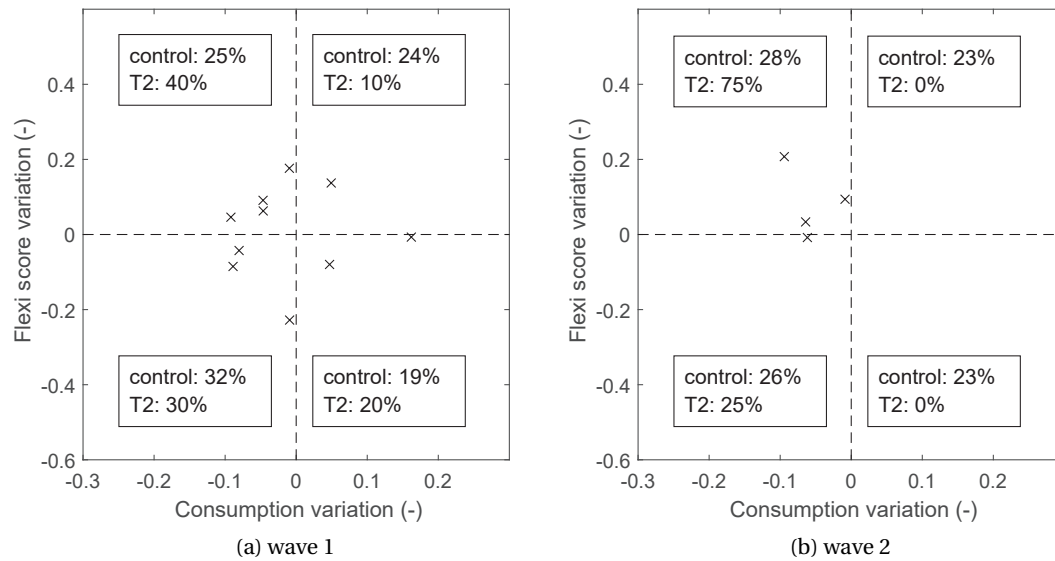


Figure 2.21 – Flexi score relative variation vs. daily consumption relative variation. Only the households of the T2 group are plotted. The fraction of households from the T2 and control groups in each quadrant are indicated in the box.

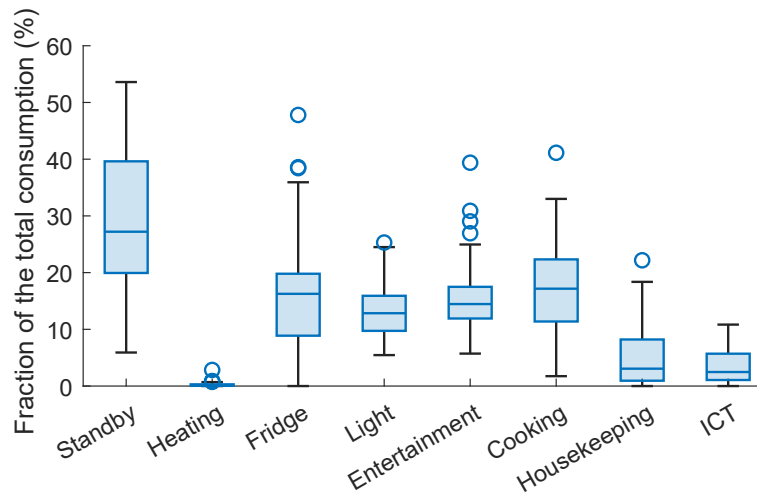


Figure 2.22 – Fraction of the total consumption (59 households) per category

The daily category mean consumption pattern is also pictured in Figure 2.23a. The "cooking" category dominates midday and evening consumption. Housekeeping, which is a flexible category according to Table 2.3, is the most important during the midday hours. Most of the light consumption occurs during the evening, which does not have a high flexibility potential. Recalling the relation between the flexibility level (Table 2.3) and the appliance category, the daily mean power profile by flexibility level is represented in Figure 2.23b.

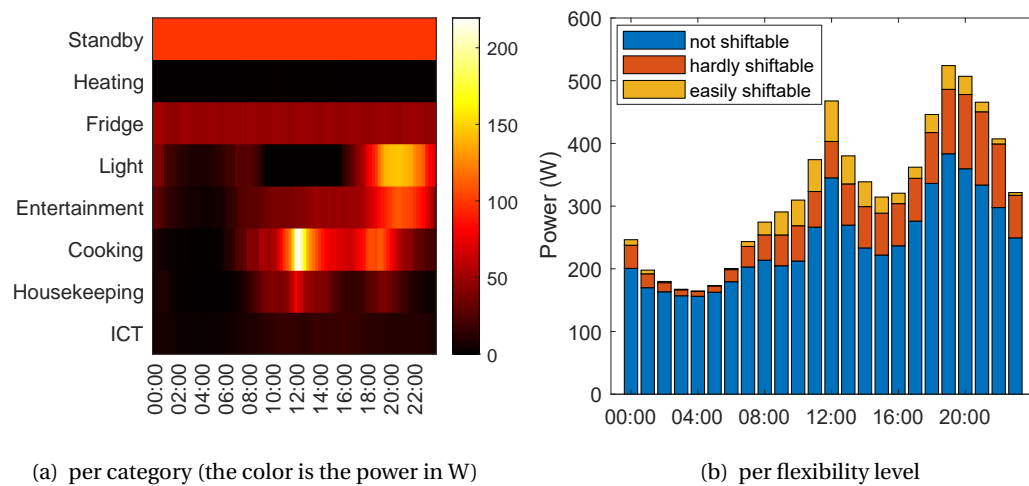


Figure 2.23 – Mean hourly consumption disaggregation

The latter highlights that most of the available flexibility occurs during the midday or evening. Assuming that both the "hardly" and "easily" shiftable power could be shifted in time, the mean flexible power along the day is pictured in Figure 2.24. This picture also represents the 95% confidence interval of the flexible power at each time of the day for all studied households. One may note that the deviation from the mean power can be pretty significant.

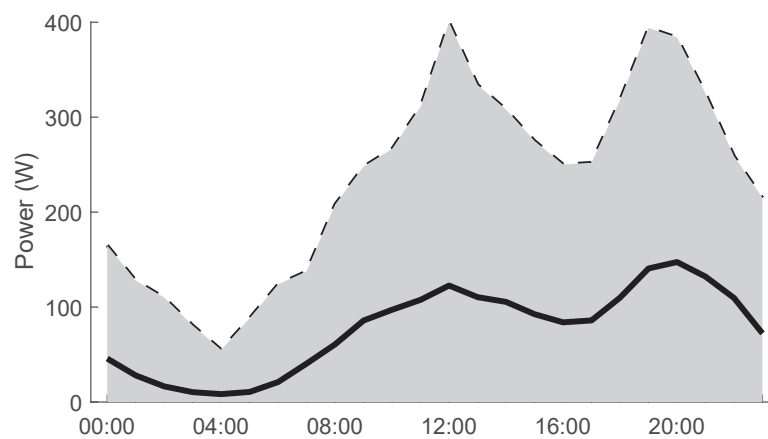


Figure 2.24 – Total shiftable power (hourly). The shaded area represents the 95% confidence interval.

Table 2.5 summarizes the share of the energy consumption according to its shiftability potential. It distinguishes between weekdays and weekends. This highlights that the potential of shiftable energy is slightly higher during the weekend and is between 1% and 18%, depending on the effort that a household can/will make.

Table 2.5 – Shiftable energy fraction potential for all households

Energy fraction	Weekdays	Weekends
Easily shiftable	0.92%	1.05%
Hardly shiftable	15.34%	17.13%
Not shiftable	83.74%	81.82%

To conclude this section and use the results of the potential of shiftable energy, Figure 2.25 shows the achievement level of the two treatment groups (for the control group) and for the first and second waves (keeping in mind that no households of the third wave have filled the survey, hence the disaggregation of their smart meter data into categories could not be achieved). The achievement level is defined as the ratio between the measured Flexi score and the theoretical Flexi score (see Section 2.3.2)⁵. In all cases, the median achievement level increases from the pre-treatment phase to the treatment phase.

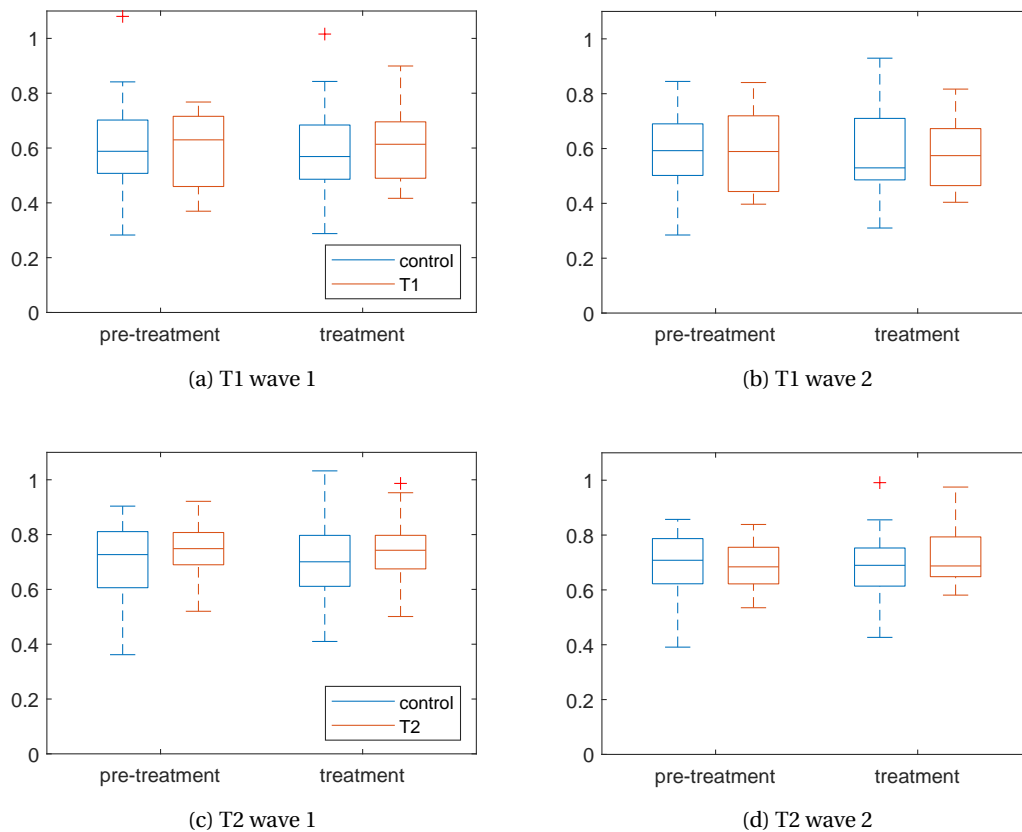
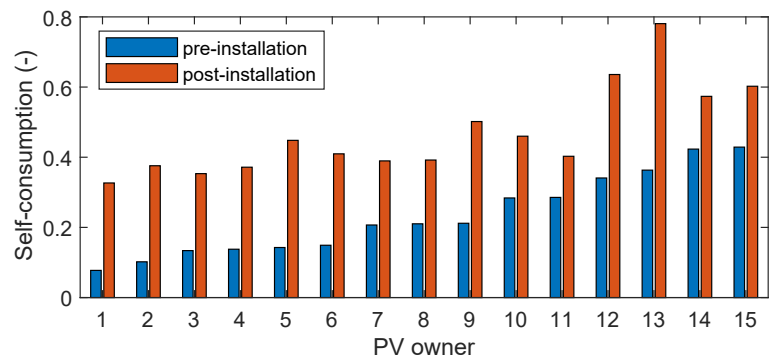


Figure 2.25 – Achievement level

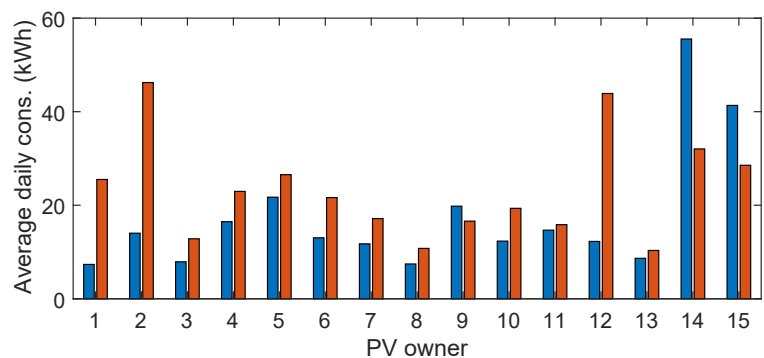
⁵Careful reader may have noticed that the achievement level can be greater than one. In some cases, the disaggregation is not perfect, leading to the total disaggregated energy being smaller than the measured energy (see Section 2.3.2)

2.4.3 Results of the PV owners analysis

The PV owners have a moral and financial incentive to shift their energy. In this section, the claims stating that the PV owners change their consumption behavior after installing PV modules on their roof will be verified. As mention in Section 2.3.2, for each participant, the PV generation has been simulated. A comparison of the self-consumption and mean daily consumption before the installation and after the installation is presented in Figure 2.26. For the period before installing the PV modules, the PV generation is simulated using the same properties (capacity, orientation, and tilt) as for the post-installation period. The self-consumption before the PV installation, reported in Figure 2.26a, ranges from 7% to 40%. These are typical values for single-family houses or farms with quite a large roof. The self-consumption during the post-installation period is larger than during the pre-installation period for all owners. However, most PV owners seem to have increased their consumption (see Figure 2.26). This is linked to the over-estimation of both the self-consumption and total energy consumption introduced by the method to retrieve the load from the smart meter measurements' import and export power. Indeed, any PV generation estimation error results in a load estimation error. As the load is bounded by 0 (the load cannot be negative), it results in an overestimation of the total consumption. See Section 2.3.2 for detailed explanations. A small study to quantify these errors has been performed using a dedicated case study (with known consumption and PV production). In more detail, the PV generation is scaled to emulate a PV capacity estimation error. For each error's magnitude, the resulting self-consumption value is compared with the one of the reference systems. Similarly, the average daily consumption, calculated using the biased PV generation, is compared with the reference value. The results are summarized in Figure 2.27. If the PV capacity is assumed correctly, the self-consumption error ranges from 3% up to 13%. In the most extreme case of a 20% overestimation of the PV capacity, the self-consumption error can reach more than 20%. As this study relies on the exactness of the data from the surveys, it is worth mentioning the range of uncertainty that wrong or inaccurate information can lead to. The mean error on the energy consumption is around 17%.

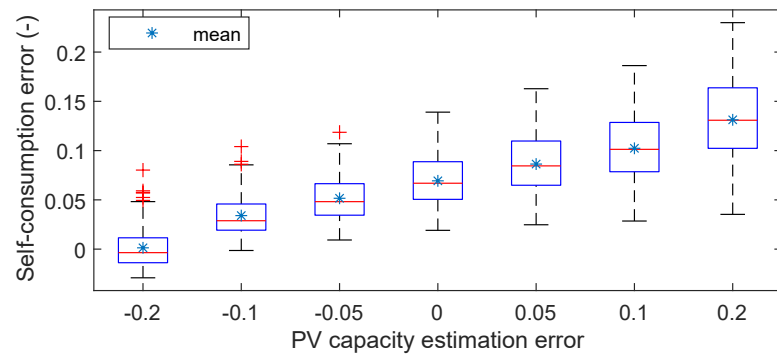


(a) self-consumption

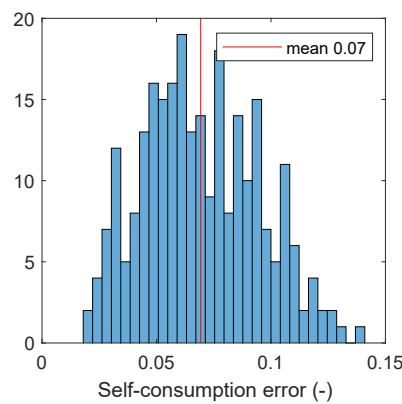


(b) daily consumption

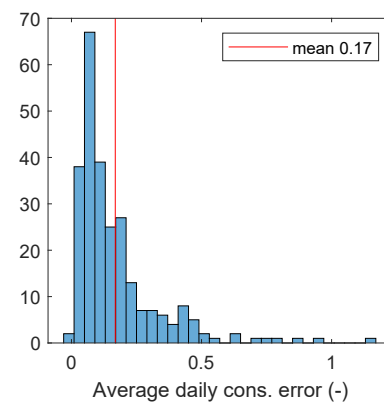
Figure 2.26 – PV owner self-consumption and averaged daily consumption



(a) self-consumption error and PV capacity estimation error



(b) self-consumption error distribution



(c) daily consumption error distribution

Figure 2.27 – Error on self-consumption and daily consumption

Keeping these considerations in mind, the normalized self-consumption (NSC) variation distribution for the PV owner and control households is pictured in Figure 2.28. As discussed in the methodology section and quantified above, the PV generation simulation's inexactness can lead to an overestimation of self-consumption and normalized self-consumption. To put more confidence in the results, the NSC variation distribution is plotted for the clear-sky only days. In both cases, the NSC increases more significantly for the PV owner than for the control group. Despite the impossibility to quantify precisely its magnitude, these results highlight a significant behavior change of the PV owners.

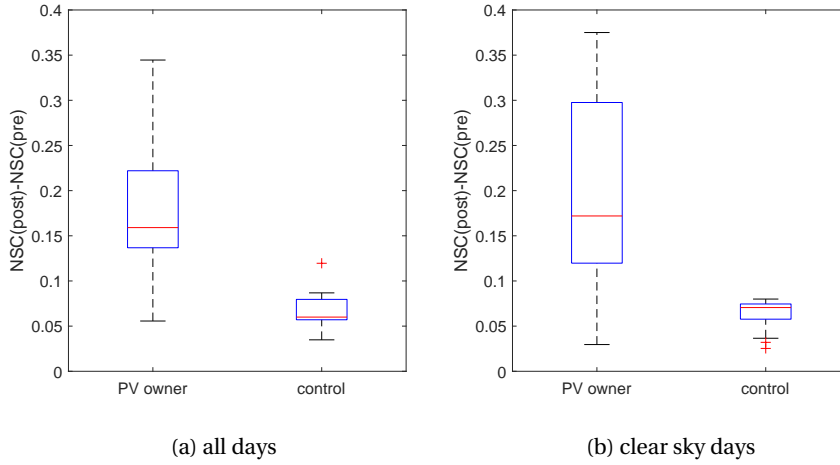


Figure 2.28 – Normalized self-consumption distribution

2.5 Conclusion

The shift from a centralized energy system to decentralized renewable energy production induces a significant change in the way we use and perceive energy. This change in perception is desirable because it can induce behavior changes and increase the acceptance of new technologies. Demand-side management is one possible approach to encourage behavior change and activate the flexibility of the residential sector.

In the first part of this chapter, we presented the FLEXI 2 experiment. This project is typically demand-side management to promote a change in consumption behavior among households by offering remunerative incentives. The incentives were time-of-use tariffs. Two different treatments were attempted. The first was using a constant time-of-use tariff (every day the same), while the second offered a variable one. The opportunity offered by the deployment of smart meters also brings some challenges regarding data quality and availability.

In the second part, we provided a methodology to assess the potential for shiftable energy from households. The methodology consists in using a non-intrusive load monitoring algorithm specially developed for this aim. The algorithm disaggregates the whole-house power measurement (provided by smart meter data at a low resolution of 15 min) into categories of appliances. Those are assigned three flexibility levels ranging from "not shiftable" to "easily shiftable". Using this methodology on the FLEXI 2 smart meter measurements highlights that up to 18% of the total energy consumption could be shifted in time. This represents an average power between 50 and 150 W per household, which is 10 times smaller than what [Saele and Grande, 2011] reported.

The last part of this chapter provided the results of the FLEXI 2 experiment. It showed that the households had a low but still perceptible reaction to the price incentives, whatever the

treatment they received. There are two possible reasons for this poor reactivity. One is the lack of communication between the households and the DSO. The second is the low potential gain compared with the behavioral effort. In a preliminary phase, it was planned that the households could monitor in near-real-time their consumption and their progress regarding their flexibility through a dedicated web app. This was discarded for technical and budget constraints. More active feedback to the households allows for better results regarding the participants' reactivity and awareness[Paetz et al., 2013, Koroleva et al., 2019].

Although all PV owners reported having no interface to track real-time their PV production, their behavior change seems to be more pronounced. The subtle combination of a moral and a financial incentive effectively triggers behavioral flexibility from the residential sector. Table 2.6 summarizes this chapter's essential results.

This paves the way for a global reflection on the accessibility of a more extensive set of households to PV technology. Indeed, the PV owners were all the owners of their homes. As about half of the FLEXI 2 participants, around 60% of the Swiss population are tenants of their home. This raises the question of how to make those people participate in the energy transition. Future research should focus on the effect of the moral and remunerative incentives induced by allowing tenants to invest in a remote PV plant.

Now that the potential and practical households' flexibility has been assessed and quantified, the following chapter will investigate the contribution of large appliances to PV systems' flexibility.

Table 2.6 – Results summary

	Unit	Treatment group	Control group
Fraction of households having increased their Flexi score ...			
... receiving the constant time-of-use tariff (T1) for wave 1,2, and 3	%	50/50/53	45/44/46
... receiving the variable time-of-use tariff (T2) for wave 1, and 2	%	50/75	49/51
Flexibility achievement level for households ...			
... receiving the constant time-of-use tariff (T1) for wave 1, and 2	%	61/57	57/53
... receiving the variable time-of-use tariff (T2) for wave 1, and 2	%	74/69	70/69
Median increase of the normalized self-consumption ratio when installing PV (clear sky day only)	-	0.17	0.07
Share of energy ...			
	unit	weekdays	weekends
... easily shiftable	%	0.92	1.05
... hardly shiftable	%	15.34	17.13
... not shiftable	%	83.74	81.82

3 Technical flexibility at the building level

Technical flexibility is required to integrate a large share of variable renewable energy in the power sector. In this chapter, the basic PV system model is presented. Two ancillary technologies are considered, electrochemical storage and power-to-heat. The technical flexibility is compared with the behavioral one. To dig more into the real deployment of such flexible technologies we propose a heuristic heat pump control algorithm that is compared with optimal control. Finally, we evaluate the effect of design regulation that aims to impose minimum technology size on the flexibility, grid impact, and systems' profitability.

Part of this section has been published in the following work:

Holweger, J., Bloch, L., and Wyrsh, N. (2020b). SCCER-FURIES - Definition of optimal control of DHW for self-consumption strategies. Technical report, École Polytechnique Fédérale de Lausanne

3.1 Introduction

The increasing need for flexibility cannot be fulfilled without technical measures. As shown in the last chapter, behavioral flexibility may provide up to 400 W of reserve capacity in the most optimistic case, which is too low compared with a kW scale domestic PV installation. Technical measures have a much higher potential, as we will see in this chapter. For the residential level, several approaches can be explored to trigger this flexibility. One of them is to use smart appliances as suggested in [Srivastava et al., 2019] and [Yilmaz et al., 2020]. Smart appliances can be any appliances, from the most common one, dishwasher, tumble-dryer, wash-machine, coffee machine, smart plugs, to the biggest and most advanced ones, like electrochemical storage, power-to-heat technologies, or power-to-X. The common denominator, and required criterion to become a "smart" appliance, is to be smart enough to decide or be told what to do and when. A smart steam iron would be smart if it can decide when to heat up according to some criterion concerning any provided information (your wardrobe state?). A smart Hi-Fi would turn on and play your favorite song when you come back from work because your home

manager (being *Alexa*© or something else) told it to. The concept of devices' controllability is key for the technical flexibility to be activated. This chapter aims to investigate the contribution of technical measures to system flexibility compared with behavioral flexibility and how different policies can impose flexibility. It provides some element of answers to Research Question B) and C).

Regarding the notion of cost-effectiveness embedded in Research Question B), it is finally related to the optimization of energy systems. This problem can be solved from two perspectives: The first is the operation of the system, and the second is its design, namely the size of its components. In [Babacan et al., 2017], a convex optimization problem is formulated to provide the optimal scheduling of a battery co-located with an existing residential PV system. The authors proposed a formulation to integrate the monthly capacity charges in the objective function. [Pena-Bello et al., 2017] used a genetic algorithm to optimize the daily operation of a battery to minimize the daily electricity bill. This approach takes advantage of the non-linear solver to analyze different battery usage strategies. The authors showed that in Switzerland, at the current battery price level, such a system is never profitable for self-consumption and load shifting applications. [Zhang and Tang, 2019] recently also used a genetic algorithm to solve the optimal scheduling of a battery and PV system.

[Mulder et al., 2013] implemented a simple rule-based algorithm to solve the operation of a battery combined with PV and optimized the size of the PV and battery capacity using a combinatorial approach (namely evaluating the net present value for a given set of combination). The focus of this study is related to the influence of the (flat) import and export tariff on the optimal size of a PV and battery system. A convex programming approach is used in [Wu et al., 2017] to find the optimal size and daily operation of a battery for a given installed PV capacity under a given feed-in power limit. The above literature does not include a thermal model. This is due to the nature of the control problem, which becomes non-linear due to the principle of power-to-heat technologies such as heat pumps (HP). Indeed, the coefficient of performance (*COP*) depends on the water supply temperature and other factors like the HP part-load efficiency [Salpakari and Lund, 2016, Verhelst et al., 2010, Fischer et al., 2016, Vrettos et al., 2013]. Nonlinear optimal control problems are often addressed using different nonlinear programming solvers, minimizing targets such as energy costs [Anvari-Moghaddam et al., 2015, Zhao et al., 2015], HP power consumption [Verhelst et al., 2010], and user discomfort [Anvari-Moghaddam et al., 2015]. However, studies conducted in [Verhelst et al., 2010, Anvari-Moghaddam et al., 2015, Zhao et al., 2015] presented results only over one-day periods, restricted by the time-consuming mathematical background of these solvers. This gives a motivation to simplify the original control problem into a linear model since linear programming solvers can guarantee global convergence and require lower computational efforts. Investigations conducted in [Girardin, 2012, Stadler et al., 2016] performed linear programming and mixed-integer linear programming (MILP) techniques using linear *COP* expressions with correction factors based on the theoretical Carnot cycle efficiency. Performance maps given by manufacturers were also used in [Verhelst et al., 2010, Vrettos et al., 2013, Fischer et al., 2014, Verhelst et al., 2012]. In [Verhelst et al., 2012, Bianchi, 2006, Halv-

gaard et al., 2012, Wimmer, 2004], a linear *COP* was also assumed by considering the water supply temperature constant to find the optimal operation of HPs coupled with underfloor heating systems. Likewise, [Beck et al., 2017] employed a MILP strategy with a constant *COP*, assuming that heat source and sink temperatures are constant. These considerations can be supported by long HP operation cycles and smooth water supply temperature changes induced by underfloor heating or building large thermal inertia.

The integrated optimization of the PV and battery sizing and energy management can be solved following two kinds of formulations: either non-linear programming techniques or convex (linear or quadratic) programming. A non-linear approach is used in [Ansari et al., 2016] to include the formulation of the voltage support to the grid. Using a similar method, [O'Shaughnessy et al., 2018] includes (among others) a non-linear model of the air conditioning. A linear model is used in [Lauinger et al., 2016] to provide a general decision-making tool for large energy systems. In [Deetjen et al., 2018], the authors included a linear model of a chiller, thermal energy storage, and micro-turbine generator to study the optimal component sizing with different time-of-use electricity rate structures. Similarly, a two-stage formulation is proposed by Talent et al. [Talent and Du, 2018] to solve first the optimal design according to the estimated net present value of the system, and second the energy management to minimize the electricity bills.

The papers mentioned above present a broad overview of the current state-of-the-art on operational research. This chapter will combine a few of the mentioned concepts to provide a complete model of a PV energy system with essentially two ancillary technologies, electro-chemical energy storage, and power-to-heat to fulfill the space heating (SH) and domestic hot water (DHW) demand. This model will be used in the framework of a MILP formulation to obtain the optimal size and operation of the system. We contribute to the research field by proposing a new combined design and operation optimization of PV, battery, and power-to-heat technology. Besides, we propose a novel view on the comparison between behavior and technical flexibility. Second, we investigate how to design policies that can impact the systems' financial profitability and their operation. Finally, we contribute to the energy management control field by proposing a novel heuristic HP control algorithm.

This chapter is organized as follows. In Section 3.3, we will provide key results to compare the obtained technical flexibility with the behavioral flexibility discussed in Chapter 2. We will provide in Section 3.5 key findings on the imposition of design rules forcing to deviate from this optimal design and their economic and operational impacts. Finally, Section 3.4 will propose a novel, simple, efficient heuristic control algorithm for PV and HP systems.

3.2 Modeling technical flexibility

In this work, a generic PV system, pictured in Figure 3.1, is composed of:

- PV modules spread on one or more roofs
- An electrochemical energy storage element referred to as the battery (batt)
- An air-water heat pump (HP)
- An auxiliary direct electric heater (EH)

The PV provide energy to the system is uncontrollable and can be curtailed. The battery acts as the main energy storage technology. The HP and EH are dedicated to both the SH and DHW heating (which can act as storage, as we'll see later on). When needed, the system can exchange power with the electrical grid (including charging and discharging the battery).

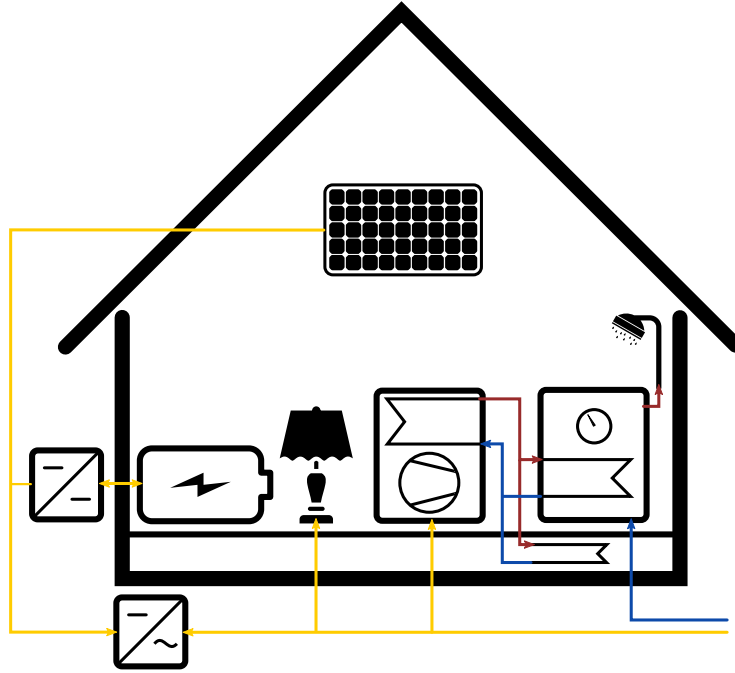


Figure 3.1 – A basic sketch of the system under study

The system's power balance is described in Equation 3.1 and must be satisfied for all time steps.

$$\underbrace{P_t^{\text{load}}}_{\text{uncontrollable load}} - \underbrace{P_t^{\text{PV}} + P_t^{\text{cur}}}_{\text{PV gen.}} + \underbrace{P_t^{\text{cha}} - P_t^{\text{dis}}}_{\text{battery}} + \underbrace{P_t^{\text{hp}} + P_t^{\text{el}}}_{\text{power-to-heat}} = \underbrace{P_t^{\text{imp}} - P_t^{\text{exp}}}_{\text{grid exchange}} \quad \forall t \in T \quad (3.1)$$

where P^{load} is the uncontrollable load, P^{PV} is the total PV generation, P^{cur} is the curtailed PV generation, $P^{\text{char,dis}}$ are the battery charging and discharging power, $P^{\text{hp,el}}$ are the power drawn by the HP and EH, and $P^{\text{imp,exp}}$ are the power imported from and exported to the grid.

The PV system's modeling equations are described in Equations 3.2a to 3.2c. Several PV configurations can be considered, represented by different roofs or technologies, for instance. For each technology, the power generation of one module is pre-calculated and stored in the matrix P^{mod} of size $[T \times N]$. The resulting sum is the total PV production (Equation 3.2a). The system can curtail up to the total PV generation (Equation 3.2c).

$$\text{PV generation at time } t \quad P_t^{\text{PV}} = \sum_{i=1}^N P_{t,i}^{\text{mod}} \cdot n_i^{\text{mod}} \quad (3.2a)$$

$$\text{Area constraints for all roofs } j \in J \quad \sum_{i=1}^{N_j} n_i^{\text{mod}} \cdot A_i^{\text{mod}} < A_j^{\text{roof}} \quad \forall j \in J \quad (3.2b)$$

$$\text{Curtailment constraint} \quad P_t^{\text{cur}} < P_t^{\text{PV}} \quad (3.2c)$$

where N is the number of PV configuration, $P_{t,i}^{\text{mod}}$ is the power output of one module of the i^{th} configuration, n_i^{mod} is the number of installed modules of the i^{th} configuration, J is the number of roofs, N_j is the number of configuration for the j^{th} roof, A_i^{mod} is the module area, and A_j^{roof} is the roof area.

The battery model is derived from [Heussen et al., 2010] and [Stadler et al., 2016]. Although the model could be valid for any electricity storage system technology, we consider a lithium manganese oxide (LMO) battery. Even though LMO batteries are mostly used for mobility purposes, we use them to exemplify the calendar aging and cycle degradation impact in a post-processing step, using a model from [Xu et al., 2018]. The battery is modeled as a non-ideal storage in Equations 3.3a to 3.3f. The initial and final state of charge constraints to be equal in Equation 3.3c and introduce a cyclic condition. The charging and discharging power abounded by the C-rate $\text{CR}^{\text{dis,cha}}$ in Equations 3.3e and 3.3f. It should be operated within the given bounds of the state of charge SOC_{min} and SOC_{max} , according to Equation 3.3d.

$$\text{Battery energy balance} \quad E_{t+1}^{\text{bat}} = (1 - \alpha) \cdot E_t^{\text{bat}} + \eta^{\text{cha}} P_{t+1}^{\text{cha}} \cdot TS_t - \frac{1}{\eta^{\text{dis}}} P_{t+1}^{\text{dis}} \cdot TS_t \quad (3.3a)$$

$$\text{Initial state} \quad E_0^{\text{bat}} = \text{SOC}_{\text{init}} \cdot E_{\text{cap}}^{\text{bat}} \quad (3.3b)$$

$$\text{Final state} \quad E_T^{\text{bat}} = E_0^{\text{bat}} \quad (3.3c)$$

$$\text{State of charge limit} \quad \text{SOC}_{\text{min}} \cdot E_{\text{cap}}^{\text{bat}} \leq E_t^{\text{bat}} \leq \text{SOC}_{\text{max}} \cdot E_{\text{cap}}^{\text{bat}} \quad (3.3d)$$

$$\text{Max charging power} \quad P_t^{\text{cha}} < \text{CR}^{\text{cha}} \cdot E_{\text{cap}}^{\text{bat}} \quad (3.3e)$$

$$\text{Max discharging power} \quad P_t^{\text{dis}} < \text{CR}^{\text{dis}} \cdot E_{\text{cap}}^{\text{bat}} \quad (3.3f)$$

where E_t^{bat} is the energy stored in the battery at time t , $E_{\text{cap}}^{\text{bat}}$ is the battery capacity, TS is the simulation time step, α is the self-discharge coefficient, $\eta^{\text{cha,dis}}$ are the charging and

discharging coefficient, $CR^{\text{cha,dis}}$ are the charge and discharge C-rate, and $SOC_{\text{init,min,max}}$ are the initial, minimum, and maximum state of charge.

The thermal model is based on the electrical-thermal analogy. The reference circuit is pictured in Figure 3.2. The circuit consists of a HP and EH providing heat to a SH circuit, which has its thermal inertia (equivalent capacitance) and transfers its heat (Equation 3.4c) to the building. The latter gains heat from the solar irradiance (through windows, Equation 3.4e) and loses heat in the surrounding environment (Equation 3.4d). This is represented in the heat balance equation of the building (Equation 3.4a). The building temperature is constrained by applying reasonable bounds (Equation 3.4f) to ensure a fair approximation of the occupants' comfort while guaranteeing the optimization feasibility. The initial temperature must also be specified in Equation 3.4h.

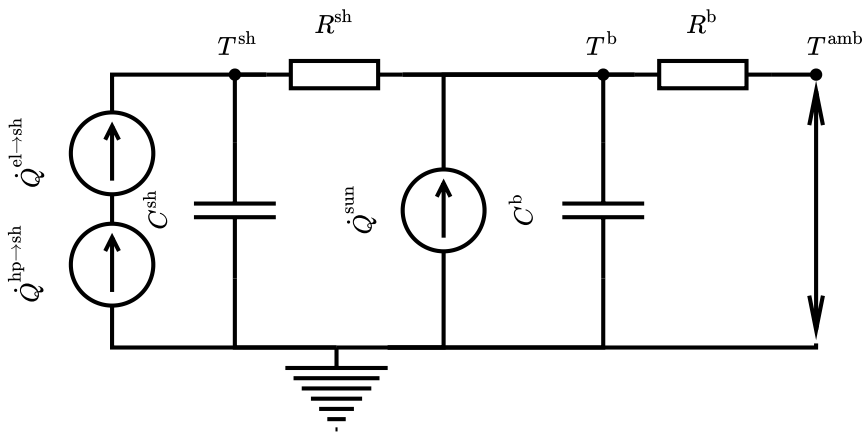


Figure 3.2 – Equivalent electrical circuit of the building and space heating circuit

$$\text{Building thermal balance} \quad C^b \cdot \frac{T_t^b - T_{t-1}^b}{TS_t} = \dot{Q}_t^{\text{sh} \rightarrow b} - \dot{Q}_t^{\text{loss},b} + \dot{Q}_t^{\text{sun}} \quad (3.4a)$$

$$\text{Space heating thermal balance} \quad C^{\text{sh}} \cdot \frac{T_t^{\text{sh}} - T_{t-1}^{\text{sh}}}{TS_t} = -\dot{Q}_t^{\text{sh} \rightarrow b} + \dot{Q}_t^{\text{el} \rightarrow \text{sh}} + \dot{Q}_t^{\text{hp} \rightarrow \text{sh}} \quad (3.4b)$$

$$\text{Heat gain from the space heating circuit} \quad \dot{Q}_t^{\text{sh} \rightarrow b} = \frac{T_t^{\text{sh}} - T_t^b}{R^{\text{sh}}} \quad (3.4c)$$

$$\text{Heat loss in the surrounding environment} \quad \dot{Q}_t^{\text{loss},b} = \frac{T_t^b - T_t^{\text{amb}}}{R^b} \quad (3.4d)$$

$$\text{Heat gain from the sun} \quad \dot{Q}_t^{\text{sun}} = I_{0,t} A_0^{\text{sun}} \quad (3.4e)$$

$$\text{Building temperature constraints} \quad T_{\min}^b \leq T_t^b \leq \max(T_{\max}^b, T_t^{\text{amb}}) \quad (3.4f)$$

$$\text{Space heating temperature constraint} \quad T_{\min}^{\text{sh}} \leq T_t^{\text{sh}} \leq T_{\max}^{\text{sh}} \quad (3.4g)$$

$$\text{Initial building temperature constraint} \quad T_0^b = T_{\text{init}}^b \quad (3.4h)$$

$$\text{Initial space heating temperature constraint} \quad T_0^{\text{sh}} = T_{\text{init}}^{\text{sh}} \quad (3.4i)$$

where, C^b, C^{sh} are the building and SH circuit thermal equivalent capacitance, T_t^b and T_t^{sh} are the building and SH temperature at time t , R^b and R^{sh} are the building and SH thermal equivalent resistance, $I_{0,t}$ is the global horizontal irradiance, A_0^{sun} is this horizontal equivalent building window area, $T_{\min, \max}^b$ and T_{\min}^{sh} are the temperature lower and upper bounds, $T_{\text{init}}^b, T_{\text{init}}^{\text{sh}}$ are the initial temperatures, T^{amb} the ambient temperature, and $\dot{Q}^{\text{hp}, \text{el} \rightarrow \text{sh}}$ are the heat provided by the HP and EH to the SH circuit.

To fulfill the DHW demand (\dot{Q}_t^{DHW}), the hot water tank acts as a thermal reservoir supplied by the HP and EH (see the thermal balance in Equation 3.5a). The tank heat loss depends on the tank temperature (Equation 3.5b), and the surrounding temperature, T_t^{room} , which is assumed as constant à 20 °C. This assumption allows reducing the building model complexity as it does not require modeling the tank's room interaction with the surrounding environment and the rest of the building. The temperature in the tank is bounded (Equation 3.5c). The tank heat loss is not considered as heat gain for the building. Hence, the tank is a non-ideal storage

Chapter 3. Technical flexibility at the building level

which improves the convexity of the problem.

$$\text{Tank heat balance} \quad C^{\text{tank}} \cdot \frac{(T_t^{\text{tank}} - T_{t-1}^{\text{tank}})}{TS} = \dot{Q}_t^{\text{el} \rightarrow \text{tank}} + \dot{Q}_t^{\text{hp} \rightarrow \text{tank}} - \dot{Q}_t^{\text{loss},t} - \dot{Q}_t^{\text{DHW}} \quad (3.5a)$$

$$\text{Heat loss from the tank} \quad \dot{Q}_t^{\text{loss},t} = \frac{T_t^{\text{tank}} - T_t^{\text{room}}}{R^{\text{tank}}} \quad (3.5b)$$

$$\text{Initial tank temperature constraint} \quad T_0^{\text{tank}} = T_{\text{init}}^{\text{tank}} \quad (3.5c)$$

$$\text{Tank temp. constraint} \quad T_{\min}^{\text{tank}} \leq T_t^{\text{tank}} \leq T_{\max}^{\text{tank}} \quad (3.5d)$$

where \dot{Q}^{DHW} is the DHW load at time t , T_t^{tank} , C^{tank} and R^{tank} are the tank temperature (at time t), capacitance and resistance, T^{room} is the room temperature in which the tank is located, $T_{\text{init},\min,\max}^{\text{tank}}$ are the initial, minimum and maximum tank temperature, and $\dot{Q}^{\text{hp,el} \rightarrow \text{tank}}$ are the heat provided by the HP and SH to the tank.

To provide the required heat in both the SH circuit and the DHW tank circuit, the HP and EH consume electric power as described in Equations 3.6a and 3.6b. The coefficient of performance (COP) is derived from the Carnot definition and assumes constant hot and cold source temperature (both for the SH and tank side, Equations 3.6c and 3.6d). The maximum input power demand defines the unit's capacity for both the HP and the EH (Equations 3.6e and 3.6f).

$$\text{Electric power for the HP} \quad P_t^{\text{hp}} = \frac{\dot{Q}_t^{\text{hp} \rightarrow \text{sh}}}{\text{COP}_t^{\text{sh}}} + \frac{\dot{Q}_t^{\text{hp} \rightarrow \text{tank}}}{\text{COP}_t^{\text{dhw}}} \quad (3.6a)$$

$$\text{Electric power for the EH} \quad P_t^{\text{el}} = \frac{\dot{Q}_t^{\text{el} \rightarrow \text{sh}} + \dot{Q}_t^{\text{el} \rightarrow \text{tank}}}{\eta^{\text{el}}} \quad (3.6b)$$

$$\text{COP for space heating} \quad \text{COP}_t^{\text{sh}} = q^{\text{carnot}} \cdot \frac{T^{\text{H,sh}}}{T^{\text{H,sh}} - T_t^{\text{amb}}} \quad (3.6c)$$

$$\text{COP for the DHW tank} \quad \text{COP}_t^{\text{dhw}} = q^{\text{carnot}} \cdot \frac{T^{\text{H,tank}}}{T^{\text{H,tank}} - T_t^{\text{amb}}} \quad (3.6d)$$

$$\text{HP capacity constraint} \quad P_{\text{cap}}^{\text{hp}} \geq \frac{\dot{Q}_t^{\text{hp} \rightarrow \text{sh}}}{\text{COP}_t^{\text{sh}}} + \frac{\dot{Q}_t^{\text{hp} \rightarrow \text{tank}}}{\text{COP}_t^{\text{dhw}}} \quad (3.6e)$$

$$\text{EH capacity constraint} \quad P_{\text{cap}}^{\text{el}} \geq \frac{\dot{Q}_t^{\text{el} \rightarrow \text{sh}} + \dot{Q}_t^{\text{el} \rightarrow \text{tank}}}{\eta^{\text{el}}} \quad (3.6f)$$

where η^{el} is the EH efficiency, q^{carnot} is the HP Carnot efficiency, $T^{\text{H,sh}}$ and $T^{\text{H,tank}}$ are the hot source temperatures of the SH and DHW tank, respectively.

All parameters, variables, and their respective units are defined in Table 3.1.

3.2. Modeling technical flexibility

Table 3.1 – Variables definition. The decision variables are indicated with a ★ in the **V** columns. The rest are parameters.

	Variables	Set	Units	V	Descriptions
TIME	T	\mathbb{N}	-		number of time steps
	TS	\mathbb{R}_+^T	s		time steps
SYSTEM	P^{imp}	\mathbb{R}_+^T	W	★	imported power (from the grid)
	P^{exp}	\mathbb{R}_+^T	W	★	exported power (to the grid)
	P^{load}	\mathbb{R}_+^T	W		uncontrollable electricity consumption
	P^{cur}	\mathbb{R}_+^T	W	★	curtailed power
	T^{amb}	\mathbb{R}_+^T	K		ambient/external temperature
	c^{imp}	\mathbb{R}_+^T	CHF/J		import electricity tariff
	c^{exp}	\mathbb{R}_+^T	CHF/J		export electricity tariff
	L	\mathbb{N}	years		system lifetime
	r	\mathbb{R}	-		discount rate
PV	N	\mathbb{N}	-		number of PV configurations
	J	\mathbb{N}	-		number of roofs
	n^{mod}	\mathbb{N}^N	-	★	PV configurations, number of units
	b^{mod}	$\{0, 1\}^N$	-	★	PV configurations, presences
	b^{pv}	$\{0, 1\}$	-	★	PV installation, presence
	c_F^{PV}	\mathbb{R}_+	CHF		PV fixed cost
	c^{mod}	\mathbb{R}_+^N	CHF/W		PV configurations, specific costs
	$P_{\text{nom}}^{\text{mod}}$	\mathbb{R}_+^N	W		PV unit nominal powers
	P_t^{PV}	$\mathbb{R}_+^{T \times N}$	W		PV configuration unit generations
	A^{mod}	\mathbb{R}_+^N	m ²		PV configuration areas
	A^{roof}	\mathbb{R}_+^J	m ²		roofs areas
	γ^{PV}	\mathbb{R}	-		annual maintenance specific cost
BATTERY	E^{bat}	\mathbb{R}_+^T	J	★	energy stored in the battery
	$E_{\text{cap}}^{\text{bat}}$	\mathbb{R}_+^T	J	★	battery capacity
	α	$\{0, 1\}$	-		self-discharge coefficient
	$\eta^{\text{cha,dis}}$	$\{0, 1\}$	-		charge and discharge efficiency
	SOC_{init}	$\{0, 1\}$	-		initial state of charge
	$\text{SOC}_{\text{min,max}}$	$\{0, 1\}$	-		minimum and maximum allowable state of charge
	$\text{CR}^{\text{char,dis}}$	\mathbb{R}_+	W/kWh		charge and discharge C-rate
	c^{bat}	\mathbb{R}_+	CHF/J		battery specific cost
	c_F^{bat}	\mathbb{R}_+	CHF		battery fixed cost
	c_o^{bat}	\mathbb{R}_+	CHF/J		battery operational cost
	L^{bat}	\mathbb{N}	-		expected battery lifetime

Chapter 3. Technical flexibility at the building level

Table 3.1 – (continued)

	Variables	Set	Units	V	Descriptions
HP	P_{cap}^{hp}	\mathbb{R}_+	W	★	HP electric nominal power
	P_{cap}^{el}	\mathbb{R}_+	W	★	EH nominal power
	P^{hp}	\mathbb{R}_+^T	W	★	HP electric power
	P^{el}	\mathbb{R}_+^T	W	★	EH power
	\dot{Q}^{hp}	\mathbb{R}_+^T	W	★	HP thermal power
	COP	\mathbb{R}_+^T	W		HP coefficient of performance
	q^{carnot}	\mathbb{R}_+	-		Carnot non-ideality factor of the HP
	S_t	\mathbb{R}_+^T			HP starting up
	R_t	\mathbb{R}_+^T			HP running
	c^{start}	\mathbb{R}_+	CHF		HP start cost
	c^{run}	\mathbb{R}_+	CHF/s		HP run cost
	c^{hp}	\mathbb{R}_+	CHF/W		HP specific cost
	c^{el}	\mathbb{R}_+	CHF/W		EH specific cost
	η^{el}	\mathbb{R}_+	-		EH efficiency
DHW	$\dot{Q}^{hp \rightarrow tank}$	\mathbb{R}_+^T	W	★	HP thermal power to tank
	$\dot{Q}^{el \rightarrow tank}$	\mathbb{R}_+^T	W	★	EH thermal power to tank
	\dot{Q}^{DHW}	\mathbb{R}_+^T	W		DHW thermal power consumption
	T^{tank}	\mathbb{R}_+^T	K	★	tank temperature
	T^{room}	\mathbb{R}_+	K		room temperature (constant)
	$T^{H,tank}$	\mathbb{R}_+	K		hot source temperature of the DHW circuit
	$T_{min,max}^{tank}$	\mathbb{R}_+	K		hot water tank service temperature range
	C^{tank}	\mathbb{R}_+	J/K		thermal equivalent capacitance of the DHW tank
	R^{tank}	\mathbb{R}_+	K/W		thermal equivalent resistance of the DHW tank
BUILDING	$\dot{Q}^{hp \rightarrow sh}$	\mathbb{R}_+^T	W	★	HP thermal power to space heating
	$\dot{Q}^{el \rightarrow sh}$	\mathbb{R}_+^T	W	★	EH thermal power to space heating
	$\dot{Q}^{sh \rightarrow b}$	\mathbb{R}_+^T	W		thermal power from the space heating to building
	T^b	\mathbb{R}_+^T	K	★	building temperature
	T^{sh}	\mathbb{R}_+^T	K	★	space heating temperature
	$T^{H,sh}$	\mathbb{R}_+	K		hot source temperature of the space heating circuit
	$T_{min,max}^b$	\mathbb{R}_+^T	K		building comfort temperature range
	$T_{min,max}^{sh}$	\mathbb{R}_+^T	K		space heating service temperature range
	C^{sh}	\mathbb{R}_+	J/K		thermal equivalent capacitance of the SH circuit
	C^b	\mathbb{R}_+	J/K		thermal equivalent capacitance of the building
	R^{sh}	\mathbb{R}_+	K/W		thermal equivalent resistance of the space heating
	R^b	\mathbb{R}_+	K/W		thermal equivalent resistance of the building
	A_0	\mathbb{R}_+	m ²		equivalent horizontal building opening surface

To evaluate the technical flexibility, we need to evaluate the optimal size of each component modeled in the previous section and their optimal operation. This statement should turn into a mathematical optimization problem. Mixed-integer linear programming (MILP) is the most appropriate approach to solve such kind of problem. It allows finding the unique and optimal solution to the optimization problem, recalling that all equations of the previous section are linear. This approach is particularly suited for this application.

A generic MILP problem is formulated as follows:

$$\begin{aligned} \min_{x,y} \quad & f^T x + g^T y \\ \text{where} \quad & x \in \mathbb{R} \text{ and } y \in \mathbb{N} \\ \text{subject to:} \quad & Ax + By < b \\ & A_{eq}x + B_{eq}y = b_{eq} \end{aligned}$$

where f^T and g^T are the objective function coefficient vectors for the continuous and discrete decision variable x and y , respectively.

For our case, the objective function is to minimize the total expense over a given period, as defined in Equation 3.7. In this case, the total annualized cost ($TOTEX$, Equation 3.8) is the sum of the annual operating cost ($OPEX$) and the annualized investment cost ($CAPEX$). The latter is defined in Equation 3.10, with R being the capital recovery factor (defined in Equation 3.11) as a function of the annual discount rate, r , and the system lifetime, L . The ratio L/L^{bat} is an approximation representing the expected number of replacements of the battery over the entire system lifetime in the investment costs.

$$\begin{aligned} \min \quad & TOTEX \\ \text{for} \quad & n^{\text{mod}}, E_{\text{cap}}^{\text{bat}}, P_{\text{cap}}^{\text{hp}}, P_{\text{cap}}^{\text{el}}, \\ & P_{\text{cur}}, P_{\text{cha}}, P_{\text{dis}}, \\ & \dot{Q}^{\text{hp} \rightarrow \text{sh}}, \dot{Q}^{\text{hp} \rightarrow \text{tank}}, \\ & \dot{Q}^{\text{el} \rightarrow \text{sh}}, \dot{Q}^{\text{el} \rightarrow \text{tank}} \\ \text{subject to:} \quad & \text{Equations 3.1 to 3.6f} \end{aligned} \tag{3.7}$$

$$TOTEX = OPEX + R \cdot CAPEX \tag{3.8}$$

$$OPEX = \text{ox}^{\text{ge}} + \text{ox}^{\text{bo}} + \text{ox}^{\text{pm}} \tag{3.9}$$

$$CAPEX = \text{cx}^{\text{PV}} + \frac{L}{L^{\text{BAT}}} \cdot \text{cx}^{\text{bat}} + \text{cx}^{\text{hp}} + \text{cx}^{\text{el}} \tag{3.10}$$

$$R = \frac{r \cdot (1 + r)^L}{(1 + r)^L - 1} \tag{3.11}$$

Chapter 3. Technical flexibility at the building level

The OPEX comprises three parts (Equation 3.9): First, the costs associated with the exchange of energy with the grid. Second, the battery operation expenses consist of a cost, c_o^{bat} , proportional to the discharged energy of the battery. This parameter allows for reducing the intensity of usage of the battery, thus limiting the battery degradation (evaluated within a post-processing step). It can be considered as a tuning parameter of the model. Finally, the annual PV maintenance costs are proportional to the PV capacity. These costs are approximated by a fraction γ^{PV} of the PV capital cost. The definitions are given in Equations 3.12a to 3.12c.

$$\text{Grid exchanges} \quad \text{ox}^{\text{ge}} = \sum_{t=1}^T \left(P_t^{\text{imp}} \cdot c_t^{\text{imp}} - P_t^{\text{exp}} \cdot c_t^{\text{exp}} \right) \quad (3.12a)$$

$$\text{Battery operation} \quad \text{ox}^{\text{bo}} = \sum_{t=1}^T P_t^{\text{dis}} \cdot c_o^{\text{bat}} \cdot TS_t \quad (3.12b)$$

$$\text{PV maintenance} \quad \text{ox}^{\text{pm}} = \gamma^{\text{PV}} \cdot \text{cx}^{\text{PV}} \quad (3.12c)$$

Finally, the CAPEX is composed of the PV, battery, HP, and EH investment costs. The definitions of these costs are given in Equations 3.13a to 3.13d, where the unit cost of a configuration is proportional to the nominal power of a module, $P_{\text{nom},i}^{\text{mod}}$, and the price per watt, c_i^{mod} . A fixed cost of installing PV, c_F^{PV} , is also considered if the Boolean variable b^{PV} is equal to 1. Similarly, the cost of a battery is proportional to its capacity, $E_{\text{cap}}^{\text{bat}}$, and the specific cost (per J), c^{bat} , while the fixed cost, c_F^{bat} , is considered only if a battery is purchased (b^{bat} equal to 1). To account for the battery lifetime (L^{bat}) shorter than the system lifetime (L), the number of battery replacement is introduced with $\frac{L}{L^{\text{bat}}}$. The Boolean variables b^{PV} and b^{bat} need to switch from 0 to 1 when the number of purchased modules $\sum_{i=1}^N n_i^{\text{mod}}$ or the battery capacity $E_{\text{cap}}^{\text{bat}}$ is greater than zero. This is ensured in linear integer programming by adding the constraints formulated in Equations 3.14a and 3.14b, in which G is a sufficiently large number. The investment cost for the HP and EH, given in Equations 3.13c and 3.13d, are proportional to their capacity ($P_{\text{cap}}^{\text{hp,el}}$) and specific cost ($c^{\text{hp,el}}$ in CHF/W_{el})

$$\text{PV capital expense} \quad \text{cx}^{\text{PV}} = \sum_{i=1}^N n_i^{\text{mod}} \cdot P_{\text{nom},i}^{\text{mod}} \cdot c_i^{\text{mod}} + b^{\text{PV}} \cdot c_F^{\text{PV}} \quad (3.13a)$$

$$\text{Battery capital expense} \quad \text{cx}^{\text{bat}} = E_{\text{cap}}^{\text{bat}} \cdot c^{\text{bat}} + b^{\text{bat}} \cdot c_F^{\text{bat}} \quad (3.13b)$$

$$\text{HP capital expense} \quad \text{cx}^{\text{hp}} = P_{\text{cap}}^{\text{hp}} \cdot c^{\text{hp}} \quad (3.13c)$$

$$\text{EH capital expense} \quad \text{cx}^{\text{el}} = P_{\text{cap}}^{\text{el}} \cdot c^{\text{el}} \quad (3.13d)$$

$$\text{Battery investment Boolean variable} \quad E_{\text{cap}}^{\text{bat}} - G \cdot b^{\text{bat}} \leq 0 \quad (3.14a)$$

$$\text{PV investment Boolean variable} \quad n_i^{\text{mod}} - G \cdot b^{\text{pv}} \leq 0, i = 1 \dots N \quad (3.14b)$$

3.3 Comparing technical flexibility and behavioral flexibility

In this section, we applied such an optimization problem to the FLEXI 2 case study. As a reminder, the FLEXI 2 project consists in proposing two kinds of tariffs to a panel of households. Tariff T1 is a regular time-of-use tariff with the electricity rate lower between 11:00 and 15:00. Tariff T2 depends on the solar irradiance forecast, which can activate three low rate periods if enough solar hours are present. The three low rate periods are 10:00 to 13:00, 13:00 to 16:00, and 16:00 to 19:00 only during summertime.

For the estimation of the technical flexibility potential, we define an optimization problem aiming to optimize the size and operation of generic non-ideal storage. Although the approach is based on a battery, it could be applied to any storage technology that could be modeled using Equations 3.3a to 3.3f. We restricted the generic optimization problem, defined in Equation 3.7, to the following one without PV and thermal model:

$$\begin{aligned} \min \quad & TOTEX \\ \text{subject to:} \quad & \text{Equations 3.1 to 3.3f} \\ & \text{Equations 3.14a and 3.14b} \\ & \text{imposing no PV panel: } n_i^{\text{mod}} = 0 \quad i = [1 \dots N] \\ & \text{no power-to-heat: } P^x = 0 \quad x = [\text{hp}, \text{el}] \\ \text{using the definitions in:} \quad & \text{Equations 3.8 to 3.13d} \end{aligned} \quad (3.15)$$

The parameters of the optimization problem (reported in Table 3.2) have been selected keeping this aspect in mind and do not consist of relevant parameters for a particular electrochemical storage technology but are rather an indication of what a good storage technology may look like.

Table 3.2 – Parameter of the optimization problem

Parameter	Units	Value	Remark
c_t^{imp}	cts/kWh	31.45 or 12.45	depends on the time and the considered tariff (T1 or T2)
TS	s	900	
R	-	1/25	assuming no interest rate
c_o^{bat}	cts/kWh	5	
c^{bat}	CHF/kWh	150	
c_F^{bat}	CHF/kWh	0	
$\eta^{\text{cha,dis}}$	-	0.94	
$\text{SOC}_{\text{min,max}}$	-	[0.2,0.8]	
$\text{CR}^{\text{cha,dis}}$	kW/Wh	1	
α	-	0.04	
p^{load}	W		extracted from the FLEXI 2 smart meter measurements

Solving this optimization problem for each households of the FLEXI 2 experiment allows to compare the flexibility score achieved by the households (Equation 2.2) with its potential based on the disaggregation of their consumption (see Chapter 1) and the technical flexibility score obtained using the results of the optimization problem:

$$\begin{aligned}
 \text{Mean daily power:} \quad \bar{P}_{i,d}^{\text{day}} &= \frac{\sum_t P_{i,t}^{\text{imp}} \delta_{t,d}}{\sum_t \delta_{t,d}} \\
 \text{Mean power during low rate period:} \quad \bar{P}_{i,d}^{\text{flexi}} &= \frac{\sum_t P_{i,t}^{\text{imp}} \delta_{i,t,d}^{\text{flexi}}}{\sum_t \delta_{i,t,d}^{\text{flexi}}} \\
 \text{Flexi score:} \quad S_{i,d} &= \frac{\bar{P}_{i,d}^{\text{flexi}}}{\bar{P}_{i,d}^{\text{day}}} \quad (3.16)
 \end{aligned}$$

reminding $\delta_{t,d} = 1$ if time step t is in day d , and $\delta_{i,t,d}^{\text{flexi}} = 1$ if time step t is during a low rate period of day d for the i^{th} household (here subscript i denotes the household index for the sake of coherence with the previous chapter). Note that in the definition of the optimization problem, the household load consumption (in this chapter P^{load}) is uncontrollable.

In addition to the Flexi score, two other indicators are used in this analysis:

- The return on investment, defined as $\frac{\text{OPEX}^0 - \text{OPEX}}{\text{CAPEX}}$
- The battery autonomy ratio, defined as $\frac{E_{\text{cap}}^{\text{bat}}}{\text{mean daily consumption}}$

3.3. Comparing technical flexibility and behavioral flexibility

where $OPEX^0$ is the annual operating cost without the storage, i.e., $OPEX^0 = \sum_t P_t^{\text{load}} \cdot c_t^{\text{imp}} \cdot TS_t$.

The ratio between the battery capacity and the mean daily consumption, referred to as the battery autonomy ratio, gives the fraction of the mean daily consumption that could be covered by discharging the battery.

The storage capacity is plotted against the mean daily consumption in Figure 3.3a. The general trend indicates that the battery size scale linearly with the consumption and that larger batteries are installed when households face a regular time-of-use tariff (T1 has every day a low rate between 11:00 and 15:00) compared with the irregular T2. The battery autonomy ratio is pictured with the return on investment in Figure 3.3b. Again larger battery autonomy ratio is obtained with the T1 group. It also observed much higher profitability, which is linked to the fact the number of low rate periods for the second treatment is lower than for the first one.

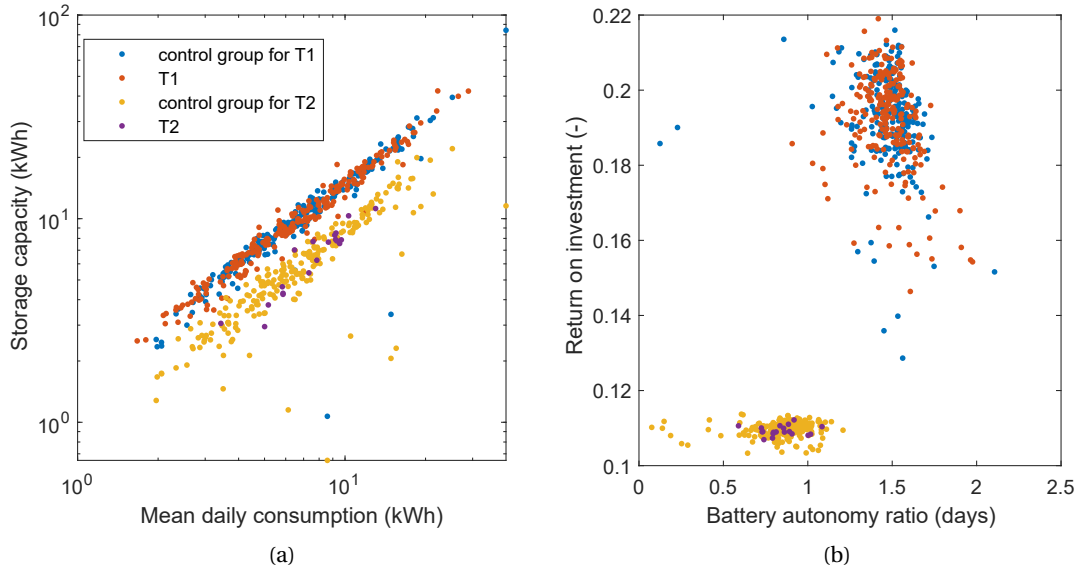


Figure 3.3 – Left: storage size vs. mean daily consumption. Right: return on investment vs. battery autonomy ratio

The comparison between the theoretical (obtained from the consumption disaggregation without considering any storage), achieved, and technical Flexi scores are available in Figure 3.4. Behavioral flexibility could theoretically increase the power, during the low rate period, up to 3 times the daily average power (corresponding to a theoretical Flexi score of 3). In contrast, the household achieved a Flexi score half-smaller. Technical flexibility is much more efficient, allowing to increase the power during a low rate period up to 6 times the average daily power (corresponding to a Flexi score of 6). The duration of the low rate period changes every day for treatment 2, explaining why the Flexi scores are smaller than the treatment 1 scores.

While these results do not question the pertinence of the technical flexibility, it is not meant to minimize the significance of behavioral flexibility, which can contribute to PV systems' flexibility. This analysis could not be made on the PV owners because the disaggregation of their consumption was not possible as none fill up the survey. However, it would be interesting to evaluate and compare the theoretical, technical, and achieved flexibility for this specific households group.

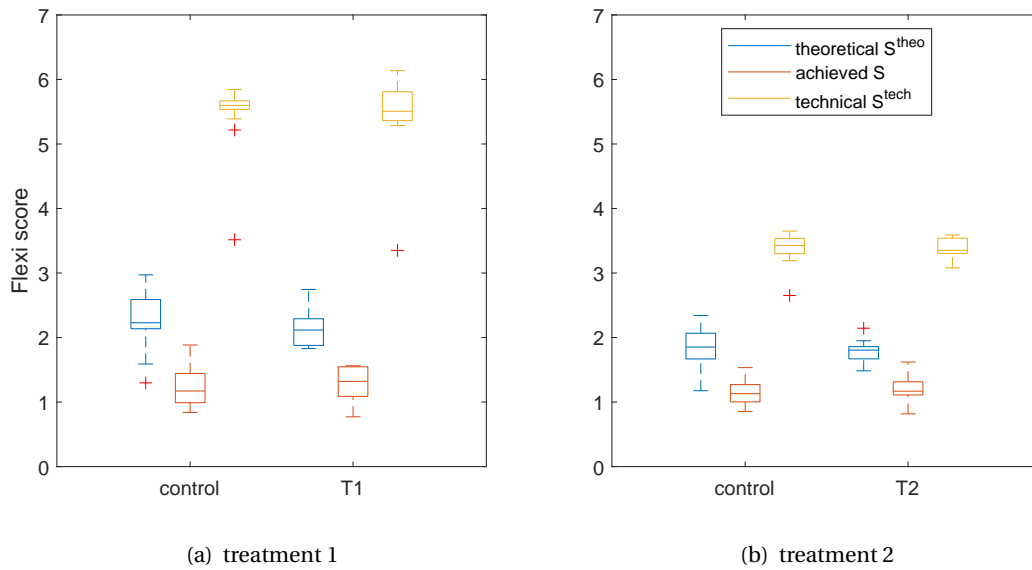


Figure 3.4 – Theoretical, achieved, and technical Flexi score for the control and treatment groups (considering the period during the experiment)

This section compared the technical flexibility potential with the behavioral flexibility potential. The results obtained in this section are heavily influenced by the storage technology cost assumptions of 150 CHF/kWh, which can be reached for electrochemical storage in the automotive industry but not yet for the residential sector. Besides, the market penetration of standalone battery technologies may be too slow to help Switzerland to reach its decarbonization target. The use of power-to-heat technologies is a more pragmatic approach, and the results shown in this section are encouraging.

The electrification of the buildings' heating system and the increasing usage of heat pumps offer a great opportunity for a cheap flexibility source. Thus, it is crucial to have quickly deployable energy management algorithms. The following will describe our contribution to this aspect.

3.4 A heuristic heat pump control algorithm

To fill the gap between energy system optimization and their real-life application, simple and efficient control algorithms are required. This section presents a heat pump (HP) heuristic control algorithm (HCA) and compares its performance with the optimal control.

The building energy management problem has attracted a wide range of research aiming to address this problem from various perspectives or using different techniques. Regarding thermal and electrical supply management, the first category is to use a convex formulation to get the absolute optimal solution. For instance, mixed-integer linear programming (MILP) can be used as in [Shiba et al., 1995, Ashouri et al., 2013, Harb et al., 2016, Beck et al., 2017] to determine the optimal size and operation of the components (i.e., of the HP, PV, battery, and thermal energy storage). This technique requires, however, linear or at least quadratic objective and constraint functions. The second approach is to use meta-heuristic optimization [Verhelst et al., 2010, Alimohammadisagvand et al., 2016, Renaldi et al., 2017, Angenendt et al., 2019]. Meta-heuristics typically focus on quickly getting a feasible (non-linear constraints are admissible) solution, but their optimality, in general, needs to be demonstrated. The advantage of using such a technique is to allow any kind of non-linearities in the input model. These first two categories are focused on the formulation of an optimization problem and how to solve it. The energy management problem can also be tackled from a control perspective.

Model predictive control is a well-known approach extensively used to solve energy management problems [Collazos and Maréchal, 2008, Vrettos et al., 2013, Zhao et al., 2015, Kuboth et al., 2019, Stadler et al., 2018]. This technique can be extended using dynamic optimization like in [Bastida et al., 2019]. This approach suffers from an extended complexity inherent to the fact that very accurate models are usually used and that the definition of the objective function is not so straightforward. The influence of the objective function formulation (despite aiming at the same conceptual goal) can indeed widely change the resulting operation [Verhelst et al., 2010]. For instance, instead of using the comfort temperature as hard bounds (often used in MILP approaches), a comfort penalty is integrated into the objective function [Anvari-Moghaddam et al., 2015]. The difficulty with such a method of combining heterogeneous metrics in the objective function is to find the appropriate weights so that the solution is a good trade-off between the various objectives.

Our approach for the HP control is to use a heuristic approach similar to [Riesen et al., 2017, Sánchez et al., 2019]. This approach has been recently identified [Schulz et al., 2020] as more appropriate in a short-term range due to the difficulty of the industry to embrace complex and emerging control methods like reinforcement learning [Rahimpour et al., 2020, Yan et al., 2020].

The proposed algorithm extends the basic formulation of [Sánchez et al., 2019] to encompass the control algorithm around a single indicator. The indicator puts in relation a possible action (like increasing the electricity fed to a HP) with the corresponding gain in operating expense and the heat production gain. Our heuristic control algorithm (HCA) evaluates this indicator

as often as needed and chooses the action which minimizes this indicator. Such an approach is novel because it does not require any parameters tuning and achieve a close-to-optimal control trajectory.

3.4.1 Description of the algorithm

The HCA's objective is to optimize the HP power consumption P_t^{hp} to meet the DHW and building heating needs while minimizing the *OPEX*. This power consumption profile is discretized with a power increment ΔP^{hp} . The algorithm's main steps, shown in Figure 3.5, are first to initialize temperatures, optimize the HP operation to meet the DHW needs, and finally, a second optimization is performed to meet the building heating demand.

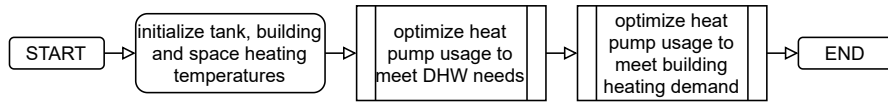


Figure 3.5 – Main steps of the HCA

The HCA, detailed in Figure 3.6, is used to optimize the HP usage to meet first the DHW, and second, the building heating demand. For the following, the word *tank* can be exchanged by *building*, as the approach is the same for both. At the beginning of the process, both HP and EH power profiles are set to zero. A first heat balance of the tank is carried out (thanks to Equations 3.4a to 3.6f), enabling to obtain the temperature profile of the tank over the entire time horizon. An indicator is then computed (Equation 3.17) for every possible increase of the HP electric power. If the tank temperature drops below the minimum temperature, a period P is defined, corresponding to the period during which the HP power should be increased to maintain the tank temperature in a given range $[T_{\min}^{\text{tank}}, T_{\max}^{\text{tank}}]$. If the HP is not already used at nominal power during the period P , then the HP power $P_{t_{\text{heat}}}^{\text{hp}}$ is increased by a power step ΔP^{hp} at the time t_{heat} corresponding to the minimum of the indicator. If the HP was already at maximum power during the period P , then the EH is used instead. A new heat balance is carried out to assess the tank's temperature rise from t_{heat} to the end of the time horizon. If the tank temperature is still too low, the loop starts again.

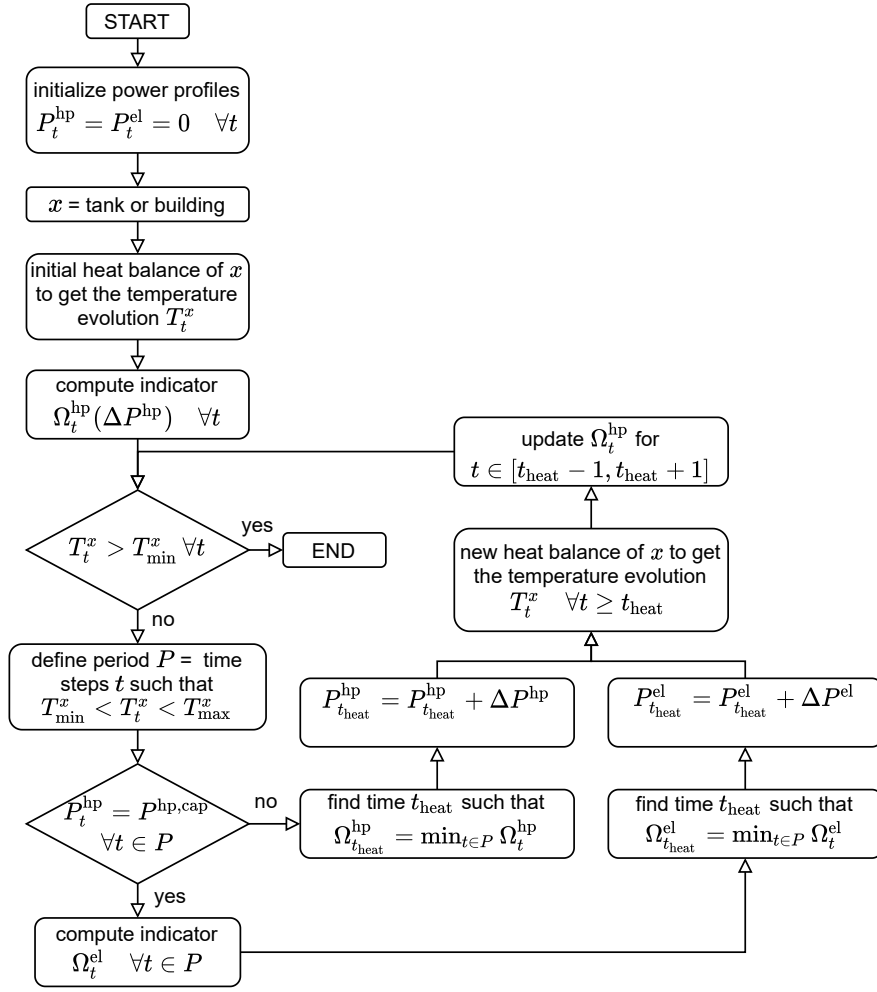


Figure 3.6 – Optimal HP and EH control

The HP indicator Ω_t^{hp} gives the cost of the produced heat. In other words, it is the ratio between the *OPEX* increase and thermal energy production increase due to the rise of the HP electricity consumption by ΔP^{hp} .

$$\Omega_t^{\text{hp}} = \frac{\Delta \text{OPEX}_t}{\Delta Q_t} \quad (3.17)$$

Here, the *OPEX* is the sum of two contributions. The first part, given by the power exchange

Chapter 3. Technical flexibility at the building level

with the grid, considers the import c_t^{imp} and export c_t^{exp} electricity tariffs.

$$OPEX_t = OPEX_t^{\text{grid}} + OPEX_t^{\text{hp}} \quad (3.18a)$$

$$OPEX_t^{\text{grid}} = \left(P_t^{\text{imp}} \cdot c_t^{\text{imp}} - P_t^{\text{exp}} \cdot c_t^{\text{exp}} \right) \cdot TS_t \quad (3.18b)$$

$$OPEX_t^{\text{hp}} = c^{\text{start}} \cdot S_t + c^{\text{run}} \cdot R_t \cdot TS_t \quad (3.18c)$$

The second part, $OPEX_t^{\text{hp}}$, depends on the HP operation and represents the wear of the compressor. It consists of two parts, a cost for each start-up of the HP and a second, proportional to the HP running time. The switching cost comes from the fact that switching on and off a HP causes mechanical wear and should be minimized. The running cost internalizes the HP has a finite lifetime, measured as the total operating hours. The running and starting costs are calculated by dividing the HP cost by 100'000 hours and 50'000 switchings respectively [Defalin SA, 2016]. The running R_t and starting S_t states are defined as followed.

$$R_t = \begin{cases} 1 & \text{if } P_t^{\text{hp}} > 0 \\ 0 & \text{otherwise} \end{cases} \quad (3.19)$$

$$S_t = \begin{cases} 1 & \text{if } R_{t-1} = 0 \cap R_t = 1 \\ 0 & \text{otherwise} \end{cases} \quad (3.20)$$

Finally, the $\Delta OPEX_t$ is given by the $OPEX$ difference when considering an increase of the HP power consumption by a power step ΔP^{hp} . This increase of the power consumption as an influence on the $OPEX_t^{\text{grid}}$ through Equation 3.1 and obviously on $OPEX_t^{\text{hp}}$ since R_t and S_t depend directly on P_t^{hp} .

$$\Delta OPEX_t = OPEX_t(P_t^{\text{hp}} + \Delta P^{\text{hp}}) - OPEX_t(P_t^{\text{hp}}) \quad (3.21)$$

The denominator of the indicator is based on the heat generated by the HP, \dot{Q}_t^{hp} , defined as :

$$\dot{Q}_t^{\text{hp}}(P_t^{\text{hp}}) = P_t^{\text{hp}} \cdot COP_t(P_t^{\text{hp}}) \cdot TS_t \quad (3.22)$$

Thus a variation of the heat generation driven by an increase of the HP consumption ΔP^{hp} can be expressed as :

$$\Delta \dot{Q}_t^{\text{hp}} = \dot{Q}_t^{\text{hp}}(P_t^{\text{hp}} + \Delta P^{\text{hp}}) - \dot{Q}_t^{\text{hp}}(P_t^{\text{hp}}) \quad (3.23)$$

$$= \left((P_t^{\text{hp}} + \Delta P^{\text{hp}}) \cdot \text{COP}_t(P_t^{\text{hp}} + \Delta P^{\text{hp}}) - P_t^{\text{hp}} \cdot \text{COP}_t(P_t^{\text{hp}}) \right) \cdot TS_t \quad (3.24)$$

In this work, the *COP* formulation, as defined in Equations 3.6c and 3.6d, was also implemented in the HCA. In this way, the *COP* is a parameter that does not depend on any decision variable. However, this is a simplistic assumption. Usually, the *COP* depends on the hot source temperature and the part-load ratio of the HP. The following formula gives an example of a non-linear formulation that could be easily implemented in the HCA.

$$\text{COP}_{\text{nonlin}}(T_t^{\text{amb}}, T_t^H, P_t^{\text{hp,n}}) = \text{COP}_{\text{lin}}(T_t^{\text{amb}}, T_t^H) \cdot f_c(P_t^{\text{hp,n}}) \quad (3.25)$$

with T_t^H , the tank T^{tank} or building T^{b} temperature. The linear part of the *COP* is only a linear function of the external temperature T^{amb} and hot source temperature T^H .

$$\text{COP}_{\text{lin}}(T_t^{\text{amb}}, T_t^H) = d_0 + d_1 \cdot T_t^{\text{amb}} + d_2 \cdot T_t^H \quad (3.26)$$

and f_c is the dependence of the HP efficiency on its part load ratio, here expressed with a sixth-order polynomial function extracted from [Genkinger and Afjei, 2011] (reproduced in [Sánchez et al., 2019]).

$$f_c(P_t^{\text{hp}}) = \sum_{n=1}^6 a_n \cdot (P_t^{\text{hp,n}})^n \quad (3.27)$$

Where $P_t^{\text{hp,n}}$ is the normalized HP power.

$$P_t^{\text{hp,n}} = \frac{P_t^{\text{hp}}}{P_{\text{cap}}^{\text{hp}}} \quad (3.28)$$

3.4.2 Reference design and optimal control definition

The reference design is obtained by derivation of Equation 3.7 and simply constraining the battery capacity to 0. The optimization problem is then given by:

$$\begin{aligned}
 & \min && TOTEX \\
 & \text{subject to:} && \text{Equations 3.1 to 3.6f} \\
 & && \text{and } E_{\text{cap}}^{\text{bat}} = 0 \\
 & \text{using the definition in:} && \text{Equations 3.8 to 3.13d}
 \end{aligned} \tag{3.29}$$

The solution to Equation 3.29 provides a reference value for n_i^{mod} , $P_{\text{cap}}^{\text{hp}}$, and $P_{\text{cap}}^{\text{el}}$ (distinguished from the optimization variable by the subscript "ref"). The solution to this problem also provides an optimal solution to the control problem. To ensure a fair comparison of the HCA and optimal control in a reasonable computing time, both MILP and HCA are run on shorter representative periods. This implies that the boundary conditions are the same for both algorithms. The MILP run on these periods only minimize the *OPEX* and force the PV, HP, and EH capacity to their reference values. In more details:

$$\begin{aligned}
 & \min && OPEX \\
 & \text{subject to:} && \text{Equations 3.1 to 3.6f} \\
 & && \text{and } E_{\text{cap}}^{\text{bat}} = 0 \\
 & && n_i^{\text{mod}} = n_{i,\text{ref}}^{\text{mod}} \\
 & && P_{\text{cap}}^{\text{hp}} = P_{\text{cap,ref}}^{\text{hp}} \\
 & && P_{\text{cap}}^{\text{el}} = P_{\text{cap,ref}}^{\text{el}} \\
 & \text{using the definition in:} && \text{Equations 3.9 and 3.12a}
 \end{aligned} \tag{3.30}$$

3.4.3 Benchmark

To benchmark the HCA performance, this algorithm is applied to several representative buildings. The methodology for selecting the set of representative buildings is described below. For each building in this set, typical periods are determined using time-series clustering based on the irradiance, temperature, electrical load, and DHW consumption. Then for each of these periods (and each building), the HP operation is solved using both the HCA and MILP formulation. Finally, key performance metrics are computed based on the operation results. This process is graphically summarized in Figure 3.7. The following will describe in more detail each of these steps.

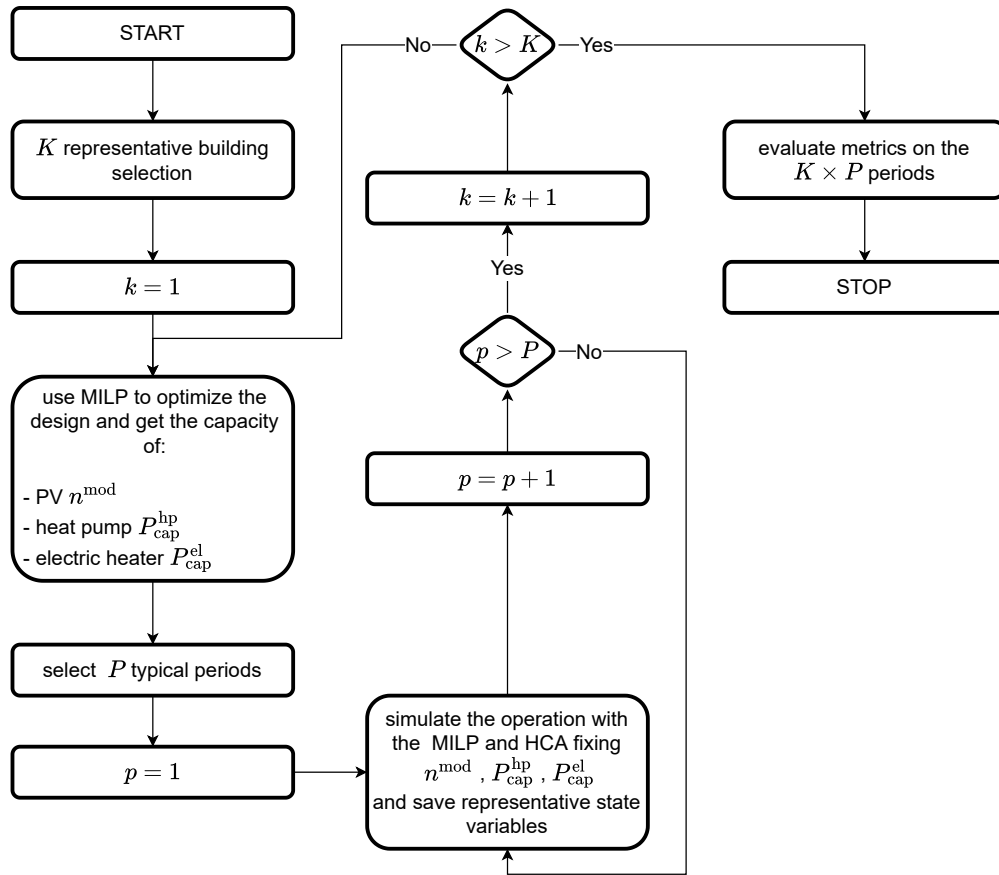


Figure 3.7 – Workflow of the benchmark process

The cantonal buildings registry (RCB) or its federal version (RegBL)¹ gives standard information about all the buildings in the canton (or Confederation for RegBL), like footprint area, number of levels, construction or renovation year, number of housing, etc. The RCB divides the buildings into six categories:

1010 provisional building

1021 single-family house

1025 multi-family building

1030 multi-family building with annex activities (like shops)

1040 building with partial usage for housing

1060 non-residential building

¹<https://www.housing-stat.ch/fr/accueil.html>

Chapter 3. Technical flexibility at the building level

Inspired by [Girardin et al., 2010], the building category, footprint area, the number of levels, number of housing, and the renovation year are combined with the SIA norm 2024 [SIA, 2015] to extract:

1. an estimation of the electrical, heat, and domestic hot water demand
2. the building's physical properties (heat transfer coefficient, i.e., thermal resistance, thermal capacity, etc. (see Table 3.1))

From the *solar roof*² data, the roofs' characteristics (area, azimuth, and tilt) are also known for each building. From this dataset of buildings, the most representative buildings are extracted for each building category. The *k-medoids* [Kaufman and Rousseeuw, 2009] algorithm is used to perform the clustering on the following set of features:

- number of housing
- number of levels
- renovation year
- height
- footprint area
- the ratio between the annual PV potential (extracted from *solar roof*) and the annual electricity demand
- the total heat demand (including DHW)

The number of medoids (representative building) is a parameter of the clustering. Finally, for all medoids, electrical and DHW load profiles are allocated using the annual energy demands. The electric profiles come from a load profiles database acquired during the FLEXI and FLEXI 2 projects (see Chapter 2 and [Perret et al., 2015, Perret et al., 2019]). The DHW load consumptions are generated from daily samples extracted from [Roux et al., 2018, Booyesen et al., 2019]. For these representative buildings, the PV, HP, and EH capacities are optimized simultaneously as their operations for one full year by solving the MILP problem depicted in Equation 3.29. To investigate the operational behavior of the HCA, typical periods have to be defined.

Following a similar approach, the selection of typical periods for a particular building consists in choosing a few representative period samples from a set of time-series samples. This

²<https://www.uvek-gis.admin.ch/BFE/sonnendach>

3.4. A heuristic heat pump control algorithm

approach, discussed in detail in [Kotzur et al., 2020], aims to mitigate the complexity of energy systems, by reducing the time dimension and number of variables. This partitioning of long time series into representative shorter samples is now a well-accepted technique [Suciu et al., 2018, Hoffmann et al., 2020, Cetinkaya et al., 2020]. The first step is, hence, to cut the time series into samples. In this work, each time-series sample is one week long. There are thus, 52 time-series samples for a particular building. Each sample consists of a $T^S \times F$ matrix, where T^S is the length of the time series (corresponding to one week in this case), and F is the number of considered features. For the latter, we choose the electrical load P^{load} , the DHW demand \dot{Q}^{DHW} , the horizontal global irradiance GHI , and the ambient temperature T^{amb} . Again, the *k-medoids* [Kaufman and Rousseeuw, 2009] algorithm is used to extract four representative weeks from the 52 available.

Once the design of a particular building in terms of technology capacity and the corresponding typical weeks are defined, the system operation is simulated. First, a reference operation is obtained by solving the MILP of Equation 3.30. Then the HCA is run. The relevant performance metrics can be computed for each typical week and each representative building.

The performance metrics are defined for each building $k \in [1 \dots K]$ and each typical period $p \in [1 \dots P]$. For easing the notation, the subscript k, p are dropped. The operator Σ denotes the operation $\sum_{t=1}^{T^S}$.

$$\text{Operating cost} \quad OPEX = \sum (P_t^{\text{imp}} \cdot c_t^{\text{imp}} - P_t^{\text{exp}} \cdot c_t^{\text{exp}}) T S_t \quad (3.31a)$$

$$\text{Heat generation} \quad Q_{u,s} = \sum Q_t^{u,s} \cdot T S_t \quad \forall u \in [\text{hp}, \text{el}], s \in [\text{sh}, \text{tank}] \quad (3.31b)$$

$$\text{HP running time ratio} \quad \text{HP}_{\text{run}} = \frac{\sum R_t \cdot T S_t}{\sum T S_t} \quad \text{with } R_t \text{ defined in 3.19} \quad (3.31c)$$

$$\text{HP switch on per day} \quad \text{HP}_{\text{switch}} = \frac{\sum S_t}{\sum T S_t / (24 \cdot 3600)} \quad \text{with } S_t \text{ defined in 3.20} \quad (3.31d)$$

$$\text{Temperature deviation} \quad \Delta \bar{T} = \frac{\sum |T_t^b - T^*|}{T^S} \quad \text{with } T^* = 19^\circ \text{C} \quad (3.31e)$$

The time needed for both algorithms to simulate the operation for a typical week is also recorded.

3.4.4 Case study

The cantonal building registry of the canton of Vaud has been used as the building dataset. Five representative buildings are extracted for each of the following categories

- Single-family house (cat 1021)
- Multi-family building (cat 1025)
- Non-residential building (cat 1060)

The resulting 15 representative buildings are pictured in Figure 3.8. In this figure, the exergy demand B_k (defined in Equation 3.32), which represents the equivalent mechanical energy demand, is plotted versus the floor area: the building footprint times the number of levels. The size of the disc represents the PV potential capacity.

$$B_k = \sum_{t=1}^T \left[P_{k,t}^{\text{load}} + \dot{Q}_{k,t}^{\text{DHW}} \left(1 - \frac{T^*}{T^{\text{dhw}}} \right) + Q_{k,t}^{\text{sh}} \left(1 - \frac{T^*}{T_k^{\text{sh}}} \right) \right] T S_t \quad \forall k = 1 \dots K \quad (3.32)$$

where $T^* = 19 + 273$ K, $T^{\text{dhw}} = 60 + 273$ K, and T_k^{sh} depends on the year of construction of the building, and vary between 35 and 50 °C.

As highlighted in Figure 3.8, single-family houses are relatively small compared with multi-family and non-residential buildings. Non-residential buildings can have a small building footprint but a high exergy demand, while multi-family buildings have the exergy demand scaling linearly with the building footprint. The reason behind this is that non-residential buildings have an energy consumption that is uncorrelated with their building footprint (such as industrial sites or shopping malls), while residential buildings energy demand scale typically with the living surface (the larger the surface, the more people and the higher the energy needs). The use of the exergy demand in this figure is simply to aggregate the electric consumption, the heat need for SH, and the DHW consumption in one metric.

The buildings' PV-related data are summarized in Table 3.4. The buildings' thermal parameters are summarized in Table 3.5. The costs for PV and HP are estimated for 2030 using the approach reported in [Bloch et al., 2019], while the HP and EH cost comes from [Fischer et al., 2016] and [Householdquotes, 2020]³. A standard flat tariff is considered (constant import and export rate at 21.02 and 8.16 cts/kWh respectively). The cost parameters and other standard parameters are reported in Table 3.3.

³<https://householdquotes.co.uk/electric-combi-boilers/>

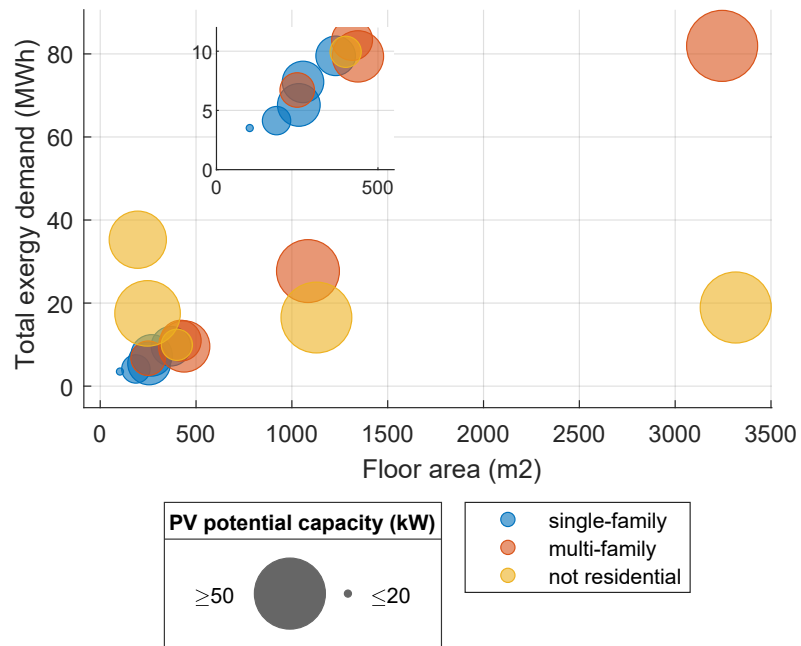


Figure 3.8 – Systems size given by their exergy consumption and buildings footage. The size of the disc indicates the PV potential capacity.

Table 3.3 – PV, HP, and system parameters

	Parameter	Unit	Value
PV	c_F^{PV}	CHF	10'050
	c^{mod}	CHF/W	0.83
	p_{nom}^{mod}	W	315
	p_t^{PV}	W	1
	A^{mod}	m ²	1.6
	γ^{PV}	-	0.5%
THERMAL	\bar{U}^{tank}	W/m ² K	1.0
	q^{carnot}	-	0.8
	η^{el}	-	0.99
	c^{hp}	CHF/W	1.5
	T^{amb}	K	2
	$T^{H,tank}$	°C	90
	$T_{min,max}^b$	°C	> 19
	T_{min}^{sh}	°C	5
	$T_{min,max}^{tank}$	°C	59-85
SYSTEM	T	-	3
	TS	s	900
	L	years	25
	r	-	3%
	c^{imp}	cts/kWh	21.02
	c^{exp}	cts/kWh	8.16
	p^{load}	W	4
	\dot{Q}_t^{DHW}	W	4

¹ Simulated using PVLIB for each configuration according to the modules parameters

² Extracted from weather data from *meteo-suisse*⁴.

³ 35040 for the design phase and 672 per periods for the simulations

⁴ Allocated for each building from a source of real measurement

3.4. A heuristic heat pump control algorithm

Table 3.4 – Building PV parameters

		$P_{\text{cap,pot}}^{\text{PV}}$ kW	A^{roof} m ²	# PV configurations -	# roofs -
HOUSE	1	28	211	5	5
	2	29	215	4	4
	3	19	141	2	2
	4	23	180	6	6
	5	29	225	6	6
MULTI FAMILY	6	26	195	6	6
	7	34	262	8	8
	8	43	314	4	1
	9	28	216	6	6
	10	96	716	3	3
COMMERCIAL	11	50	381	23	14
	12	110	803	4	1
	13	38	287	2	2
	14	45	337	2	2
	15	24	181	2	2

Table 3.5 – Building thermal parameters

		C^b $\frac{\text{kWh}}{\text{K}}$	C^{sh} $\frac{\text{kWh}}{\text{K}}$	U^b^* $\frac{\text{W}}{\text{K}}$	U^{sh}^* $\frac{\text{W}}{\text{K}}$	U^{tank}^* $\frac{\text{W}}{\text{K}}$	$T^{\text{H,sh}}$ $^{\circ}\text{C}$	$T_{\text{max}}^{\text{sh}}$ $^{\circ}\text{C}$	K_{sun} m^2	V^{tank}^{**} L	Floor area m^2
HOUSE	1	4.1	0.5	170	849	3.6	75	70	8	470	369
	2	4.5	0.4	207	616	2.9	75	70	10	341	268
	3	3.4	0.1	208	237	1.6	75	70	10	131	103
	4	3.1	0.1	153	291	2.3	60	55	5	237	186
	5	2.8	0.1	142	399	2.8	60	55	5	325	255
MULTI FAMILY	6	4.2	0.3	160	718	3.6	65	60	6	467	250
	7	4.9	0.2	182	616	5.3	60	55	5	819	438
	8	9.0	1.3	307	3115	9.6	65	60	12	2026	1084
	9	4.7	0.5	175	1207	5.1	65	60	7	785	420
	10	21.6	3.8	658	9325	20.0	65	60	26	6064	3245
COMMERCIAL	11	11.7	0.7	490	2320	2.6	60	55	20	277	1128
	12	25.8	2.1	977	6821	5.2	60	55	39	814	3316
	13	6.1	0.1	284	403	0.8	60	55	11	48	196
	14	7.7	0.3	344	487	0.9	75	70	20	61	247
	15	6.2	0.5	276	789	1.3	75	70	16	98	400

$$^* R^x = 1/U^x$$

$$^{**} C^{\text{tank}} = \rho c_p V^{\text{tank}} \quad \text{with } \rho = 1 \text{ kg/L, } c_p = 4.18 \cdot 10^3 \text{ J/kg}$$

3.4.5 Results

The designs obtained from the MILP are summarized in Figure 3.9. Note that the optimal PV capacity for each building appears to correspond to its maximum potential capacity reported in Table 3.4. For the single-family house and multi-family building, the HP capacity is larger than the EH. There is an apparent economic interest in investing in a HP rather than in an EH because, for every unit of electricity sent to the HP, one gets a lot more heat from the HP than from the EH. However, for rare peaks of DHW demand, it might be advantageous to invest in an EH because the specific investment cost is much lower. So for systems that may suffer from large heating peaks, it might be interesting to have a larger electrical capacity. For instance, non-residential buildings have significantly larger EH capacities.

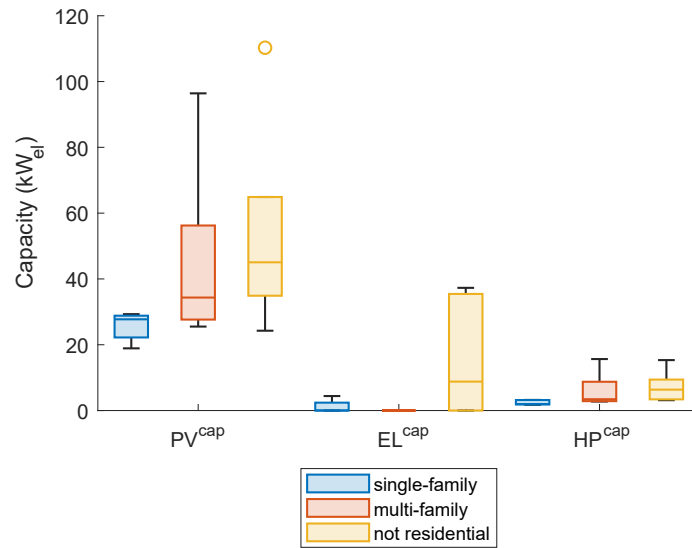


Figure 3.9 – PV, HP, and EH capacity given by the MILP

The operation is simulated for each typical week and each representative building. An example of the operation from the MILP and the HCA is represented in Figures 3.10 and 3.11, respectively. One may note that the MILP and HCA's operations are very similar. A closer look at Figure 3.11 highlights that the temperatures of the SH circuit and the hot water tank are higher than those given by the MILP (Figure 3.10). This means that the HCA generally generates more heat than the MILP, as shown in Figure 3.13 for the SH, and Figure 3.12 for the DHW.

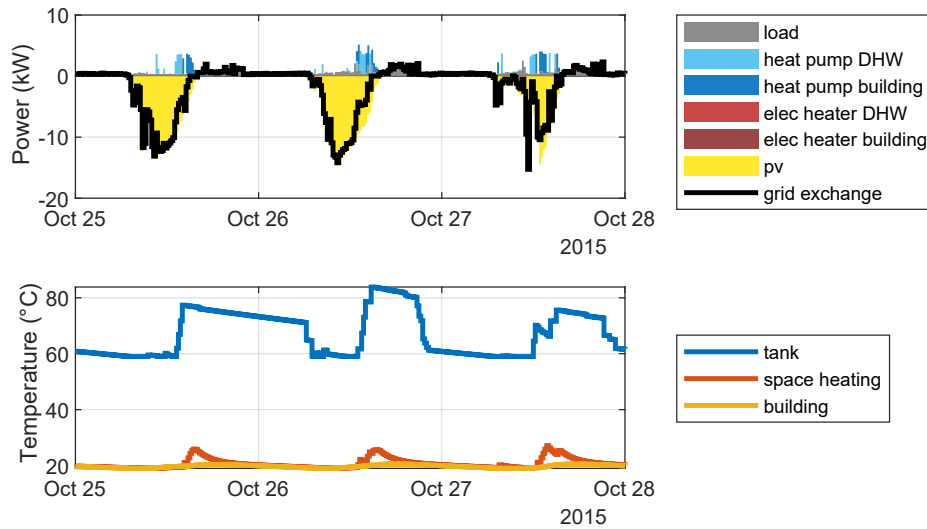


Figure 3.10 – Three-day operation example resulting from the MILP optimization

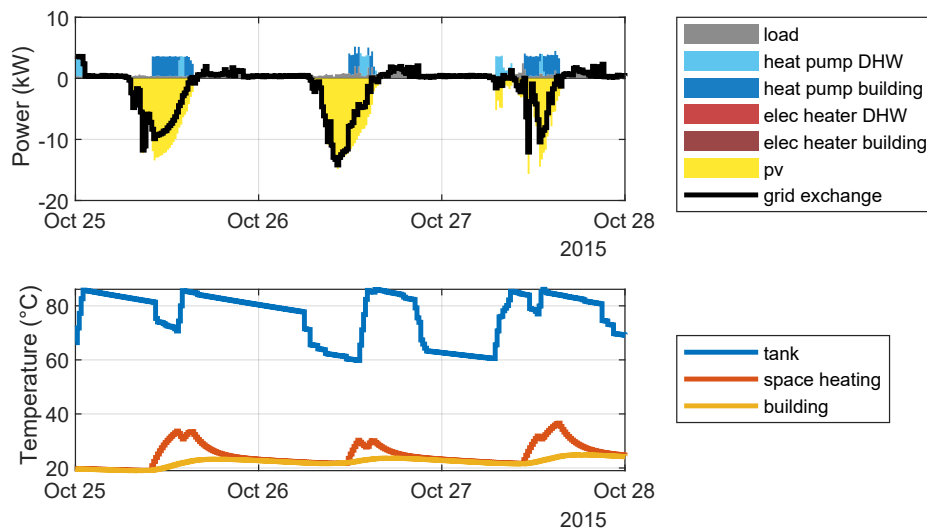


Figure 3.11 – Three-day operation example resulting from the HCA

The heat generated from the EH is negligible compared with the heat generated by the HP both for the SH and DHW as shown in Figures 3.12 and 3.13, respectively, even for the non-residential category where larger EH capacities are observed. This confirms the hypothesis that the EH only supports large peaks of heat demand. In Figures 3.12 and 3.13, the minimum heat required is also indicated. Three aspects can explain the difference between the minimum and actual heat generation. First, one should consider the tank heat loss. Second, the objective function is not to minimize the amount of heat consumed, but to minimize the operating

3.4. A heuristic heat pump control algorithm

cost. Finally, for the HCA only, the algorithm's non-optimality might induce this larger heat generation. The question arises if the HCA keeps the building warmer.

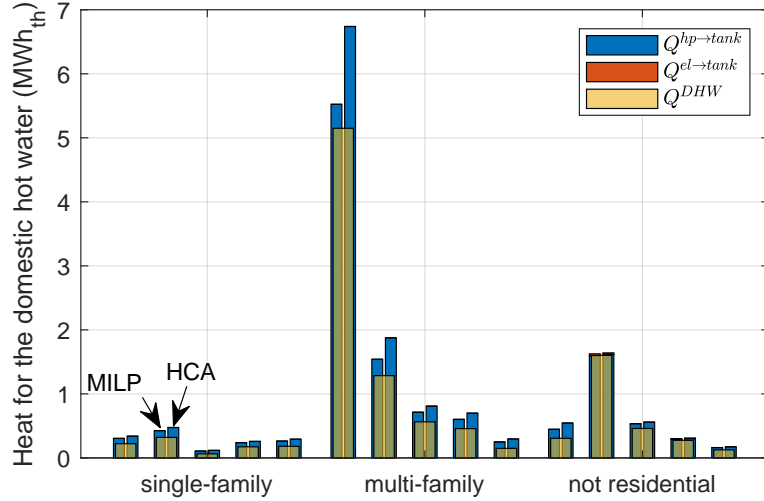


Figure 3.12 – Heat generation for DHW. $Q^{hp \rightarrow tank}$ is the heat generated by the HP, $Q^{el \rightarrow tank}$ is the heat generated by the EH (too small to be visible), Q^{DHW} is the DHW heat consumption. The left bars correspond to the MILP, and the right ones to the HCA.

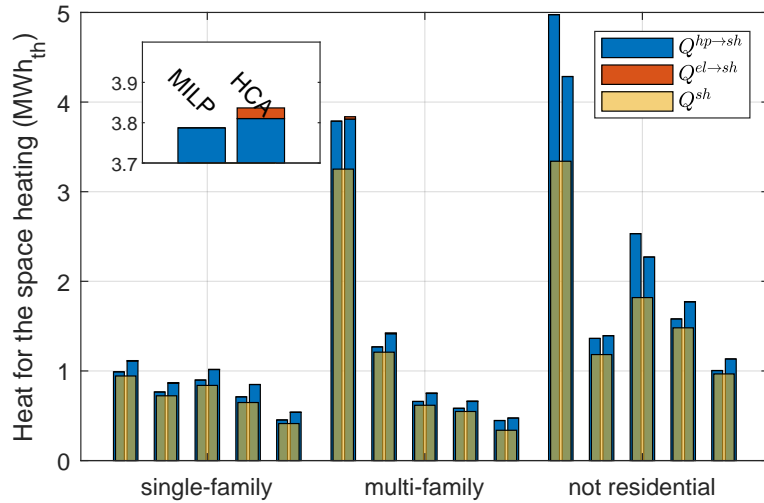


Figure 3.13 – Heat generation for space heating. $Q^{hp \rightarrow sh}$ is the heat generated by the HP, $Q^{el \rightarrow sh}$ is the heat generated by the EH (too small to be visible), Q^{sh} is minimum building heat consumption. The left bars correspond to the MILP, and the right ones to the HCA.

The mean temperature deviations are reported in Figure 3.14. Keeping in mind that those are the sum of the absolute temperature deviations from a target comfort temperature, the

HCA suffers from higher temperature deviations. They reach up to 2.5 °C (absolute value), which can be quite significant from the user's perspective. Nevertheless, these temperature deviations can come from the fact that the external temperature and solar gain can significantly increase the building temperature. Assuming that the MILP provides an optimal building temperature, the temperature deviations, in this case, reach up to 2 °C. In conclusion, the difference between the HCA and MILP is not so significant. Another aspect that may explain the higher temperature deviation of HCA is that the latter considers the running and switching cost of the HP.

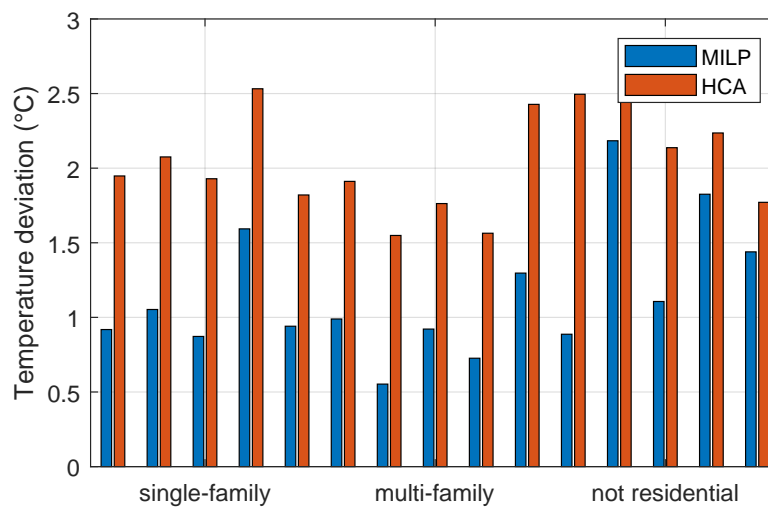


Figure 3.14 – Mean temperature deviations (°C).

The HCA takes into account the HP running time and aims to minimize it. In contrast, the MILP does not take into account this aspect in the objective function. Similarly, the MILP does not take into account the switching costs. Those are not integrated into the MILP objective function because this would require $2T$ additional Boolean decision variables and drastically increase the solving time. This leads to a much higher running time for the MILP than for the HCA, as highlighted in Figure 3.15. It might also explain why the HCA has a higher temperature deviation than the MILP. The MILP also has much higher switching per day than the HCA, as depicted in Figure 3.16, for the reason just explained. The switching and running costs are virtual costs that help to moderate the HP operation. The real cost of a HP is the investment cost that may be amortized on a shorter lifetime due to more intensive use. This aspect has not been further investigated. The only measurable cost is the operating cost.

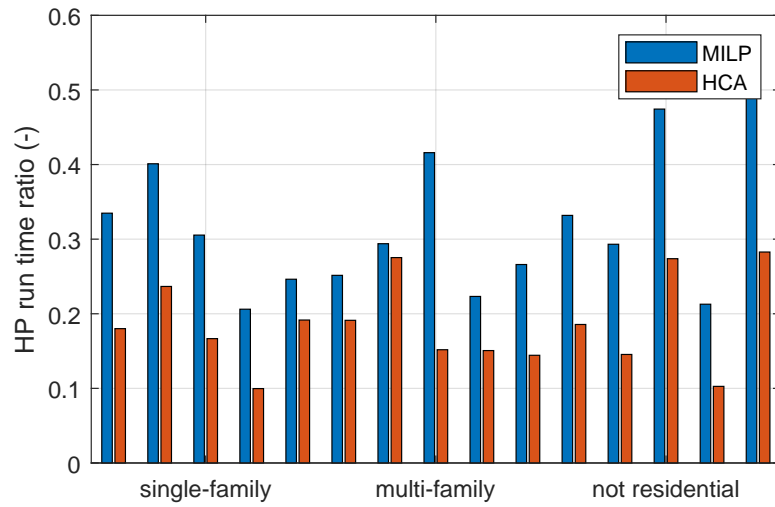


Figure 3.15 – HP running time ratio

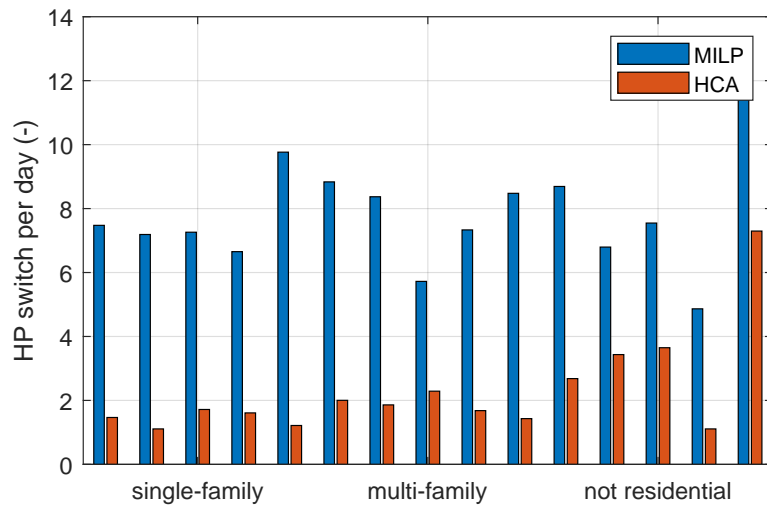


Figure 3.16 – Number of HP switching on per day

The operating costs for the 15 buildings and 4 periods (sorted by the ascending MILP *OPEX* value) are pictured in Figure 3.17. The blue line, representing the HCA, is very close to the MILP, showing very similar financial results in grid exchange. The total operating cost per building summed across all typical periods is reported in Table 3.6. The difference between the MILP and the HCA goes from 20 cts/day up to 2.55 CHF/day, for an *OPEX* ranging between -20 CHF/day and 20 CHF/day. The difference can even favor the HCA (the *OPEX* of the HCA is smaller than the MILP one). Despite the very tiny difference, these surprising results come from the fact that no constraints are applied to the HCA's space heating temperature. It

Chapter 3. Technical flexibility at the building level

happens that the HCA chooses to over-heat the SH circuit, self-consuming a little bit more PV energy, while the MILP would stop heating before breaking the temperature upper-bounds.

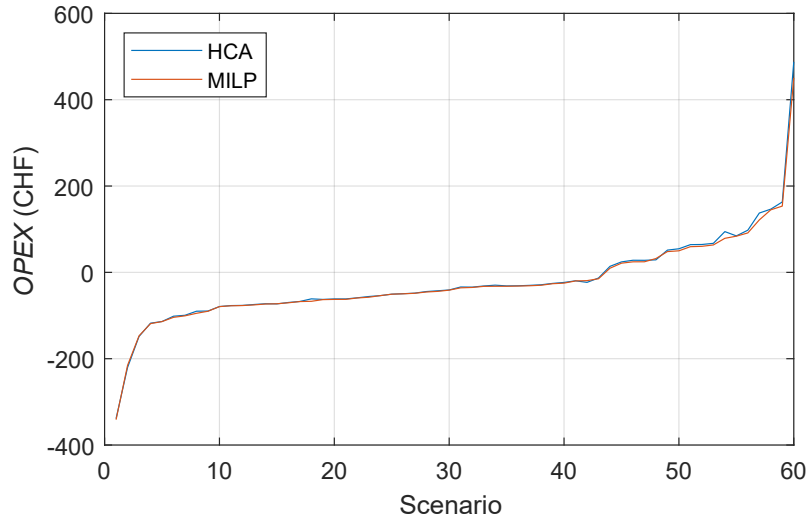


Figure 3.17 – *OPEX* value for all buildings and periods sorted by MILP *OPEX*

Table 3.6 – *OPEX* comparison (CHF/day)

		MILP	HCA	Δ
Single-family	1	-3.02	-2.77	0.26
	2	-4.63	-4.37	0.27
	3	-3.72	-3.55	0.17
	4	-4.69	-4.52	0.17
	5	-5.29	-5.11	0.19
Multi-family	6	-7.36	-7.24	0.12
	7	-5.27	-5.07	0.20
	8	-1.16	-0.44	0.71
	9	-2.47	-2.19	0.28
	10	19.53	22.08	2.55
Non-residential	11	-9.50	-9.53	-0.03
	12	-22.96	-22.98	-0.02
	13	5.57	5.68	0.12
	14	-5.09	-4.80	0.29
	15	-2.51	-2.31	0.19

Finally, the simulation times are reported in Table 3.7. The MILP problem is solved via GUROBI [Gurobi Optimization, 2019], a very efficient solver, whereas the HCA is a heuristic algorithm.

3.5. Impact of regulations on components size and profitability

For this reason, the simulation times are much higher for the HCA than for the MILP. However, the HCA can perform the control of a HP in a very short time compared with the period's length (one week). Moreover, the HCA can cope with all non-linear energy system models, making it suitable for a real implementation. Finally, the MILP requires advanced software to solve the optimization problem that is not required by the HCA. Indeed the HCA could be implemented on a simple micro-controller as a state machine.

Table 3.7 – Running time (s)

	Min	Max	Median	Mean
MILP	0.07	0.23	0.12	0.13
HCA	15.76	686.35	121.53	172.30

The results obtained in this section assume an optimal design for each of these buildings. However, regulations and technical constraints can make the decision-maker deviate from what was defined as optimal design. These regulations aim to achieve a particular goal, such as heat demand reduction. In turn, they can affect the technology size and the system profitability. The next section will investigate how a few selected regulations can affect the system operation and its profitability.

3.5 Impact of regulations on components size and profitability

In this section, we investigate the impact of three design regulations on the optimal design of PV systems. To lower the PV systems' impact on the grid, these regulations aim at increasing the storage capacity without any operational constraints. Compared to the HCA benchmark presented in the previous section, we consider this time the battery model, and test three design regulations:

- For each kW of installed PV capacity, a battery capacity of 0.75 kWh is installed.
- The building SH circuit provides thermal inertia corresponding to a time constant of 24h.
- The domestic hot water tank volume corresponds to 14 days of hot water consumption.

Noting that for a PV cost of 830 CHF/kW in 2030 (as assumed in the previous case study), all considered buildings have interest in covering their roofs. Hence, studying the effect of imposing the full coverage of all buildings' roofs with PV is not relevant in this context. Such a rule would not affect the final systems' design. However, with the other selected regulations, the optimal PV capacity may be impacted. It is worth investigating the impact of these regulations on the PV capacity, second the system profitability, and third the intensity of the grid interaction.

Chapter 3. Technical flexibility at the building level

The optimization problem, recalling the standard notation of this chapter, and including the regulation constraints, can be written as:

$$\begin{aligned} & \min && TOTEX \\ & \text{subject to:} && \text{Equations 3.1 to 3.6f} \\ & \text{using the definition in:} && \text{Equations 3.8 to 3.13d} \end{aligned} \quad (3.33)$$

For the 15 representative buildings presented in Section 3.4, the design and operation are solved sequentially for five distinct scenarios:

- A **reference** scenario, solving the problem of Equation 3.33, without additional constraints.
- A **large DHW tank** scenario, solving the problem of Equation 3.33, adjusting the size of the DHW tank to comply with the requirements of Equation 3.36.
- A **large SH inertia** scenario, adjusting C^{sh} so that it complies with the requirements of Equation 3.35.
- A **large storage** scenario, solving the problem of Equation 3.33 with the battery size constraints of Equation 3.34.
- A scenario mixing **all** three regulations.

The process is graphically summarized in Figure 3.18. From the optimization point of view, the regulation on the SH circuit and DHW tank capacities do not introduce any new constraint, but rather update the parameter values (see Equations 3.35 and 3.36).

$$\text{Battery size regulation} \quad E_{\text{cap}}^{\text{bat}} \geq e^{\text{bat}} \cdot \sum_{i=1}^N n_i^{\text{mod}} P_{\text{nom},i}^{\text{mod}} \quad (3.34)$$

$$\text{Building space heating circuit inertia} \quad C^{\text{sh}} R^{\text{sh}} = \tau^{\text{sh}} \quad (3.35)$$

$$\text{DHW tank volume} \quad V^{\text{tank}} = D \cdot \bar{V}^{\text{DHW}} \quad (3.36)$$

where $e^{\text{bat}} = 0.75 \text{ kWh/kW}$, $\tau^{\text{sh}} = 24\text{h}$, $D = 14$, and \bar{V}^{DHW} is the mean daily hot water consumption computed from \dot{Q}^{DHW} as follow:

$$\bar{V}^{\text{DHW}} = \frac{1}{N_{\text{days}}} \frac{\sum_{t=1}^T \dot{Q}_t^{\text{DHW}} T S_t}{\rho c_p (T^{\text{DHW},H} - T^{\text{cold}})}$$

with N_{days} number of days, $\rho = 1 \text{ kg/L}$, $c_p = 4.18 \text{ kJ/kg}$, $T^{\text{DHW},H} = 60^\circ\text{C}$, and $T^{\text{cold}} = 10^\circ\text{C}$.

3.5. Impact of regulations on components size and profitability

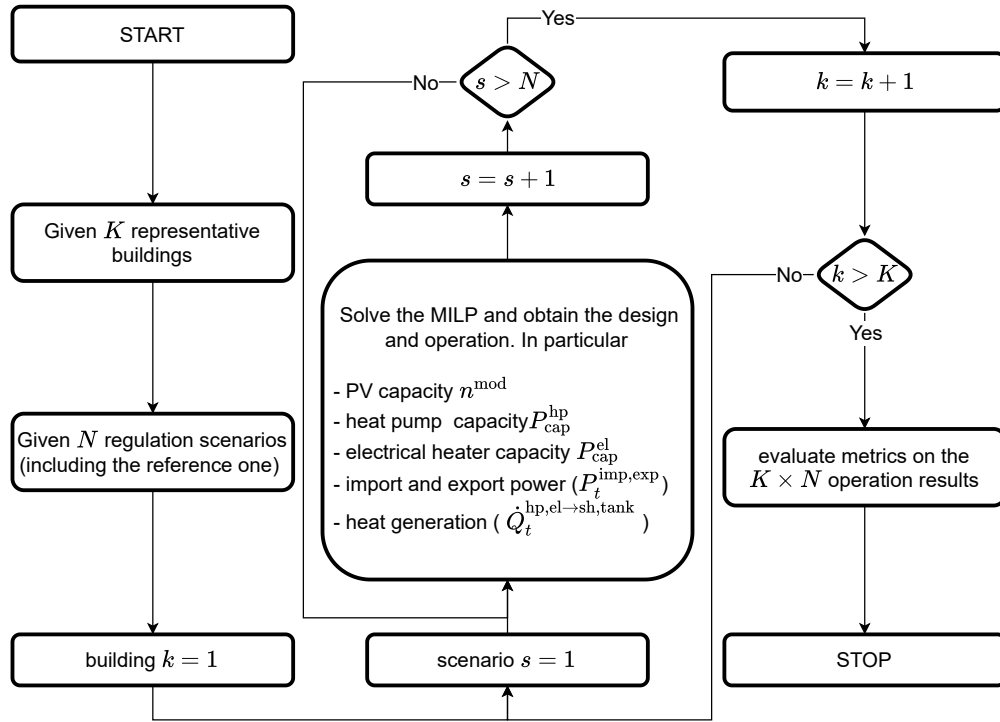


Figure 3.18 – Workflow of the methodology

The performance metrics aim to reflect the ultimate goals of this study. Recalling that the representative buildings can be quite different in terms of size, PV potential capacity, and magnitude of the consumption, the performance metrics aim to eliminate the magnitude of the raw number to allow comparison across the buildings. The performance indicators are the following:

- The PV hosting ratio, PV_{host} , is the ratio between the installed PV capacity and the maximum PV capacity that could be installed on the system's roofs (Equation 3.37a).
- The battery to PV capacity ratio, $E_{\text{cap}}^{\text{bat}*}$, is the ratio between the battery capacity in kWh and the PV capacity in kW (Equation 3.37b).
- The self-consumption, SC , is the share of the PV production directly consumed by the building (Equation 3.37c).
- The self-sufficiency, SS , is the share of the consumption covered by the flexible PV system (Equation 3.37d).
- The internal rate of return, IRR , is a financial metric of the system's profitability. It corresponds to the interest rate at which the net present value (NPV) is zero after the system lifetime (Equation 3.37f).

Chapter 3. Technical flexibility at the building level

- the heat consumption is the total heat generated by the power-to-heat technologies and consumed by the system (Equation 3.37h).
- the grid usage, defined for import GU^{imp} or export GU^{exp} , is the ratio between the maximum power at import or export and the maximum electrical demand (Equation 3.37i).

The mathematical derivations of those metrics are given below.

$$\text{PV hosting ratio} \quad PV_{\text{host}} = \frac{\sum_{i=1}^N n_i^{\text{mod}} P_{\text{nom},i}^{\text{mod}}}{\sum_{i=1}^N n_{\text{max},i}^{\text{mod}} P_{\text{nom},i}^{\text{mod}}} \quad (3.37a)$$

$$\text{Battery to PV capacity ratio} \quad E_{\text{cap}}^{\text{bat}*} = \frac{E_{\text{cap}}^{\text{bat}}}{\sum_{i=1}^N n_i^{\text{mod}} P_{\text{nom},i}^{\text{mod}}} \quad (3.37b)$$

$$\text{Self-consumption} \quad SC = \frac{\sum_t \left(\min(P_t^{\text{tot}}, P_t^{\text{exp}} - P_t^{\text{imp}} + P_t^{\text{tot}}) \right)}{\sum_t P_t^{\text{PV}}} \quad (3.37c)$$

$$\text{Self-sufficiency} \quad SS = \frac{\sum_t \left(\min(P_t^{\text{tot}}, P_t^{\text{exp}} - P_t^{\text{imp}} + P_t^{\text{tot}}) \right)}{\sum_t P_t^{\text{tot}}} \quad (3.37d)$$

$$\text{Total electrical demand} \quad P_t^{\text{tot}} = P_t^{\text{load}} + P_t^{\text{el}} + P_t^{\text{hp}} \quad (3.37e)$$

$$\text{Internal rate of return} \quad IRR = r \text{ such that } \sum_{y=1}^L \frac{CF_y}{(1+r)^y} = 0 \quad (3.37f)$$

$$\text{Cash flow} \quad CF_y = CAPEX_y + OPEX_y - OPEX_y^0 \quad (3.37g)$$

$$\text{Heat consumption} \quad \text{heat cons.} = \sum_t \sum_{u \in \{\text{hp}, \text{el}\}, s \in \{\text{sh}, \text{tank}\}} \dot{Q}_t^{u \rightarrow s} \cdot TS_t \quad (3.37h)$$

$$\text{Grid usage} \quad GU^{\text{imp}, \text{exp}} = \frac{\max_t P_t^{\text{imp}, \text{exp}}}{\max_t (P_t^{\text{load}} + P_t^{\text{heat}})} \quad (3.37i)$$

where P_t^{heat} is the minimum electrical power requires to heat the building and provide the DHW assuming a unitary efficiency. This is calculated by solving a simple optimization problem aiming to minimize the sum of the electric power consumed by the EH (and assuming $\eta^{\text{el}} = 1$).

The PV hosting ratio, self-consumption, self-sufficiency, and battery to PV capacity ratio distributions for all 15 buildings and the five scenarios are reported in Figure 3.19. As noticed, the PV price is low enough to enable full coverage for all buildings. For this reason, PV_{host} is equal to 1 for all systems and scenarios except for the large storage scenarios. Indeed the battery is not profitable and no systems install a battery. In the large storage scenario, which imposes a battery size of 0.75 kWh per kW of PV, the constraint linking the battery and PV capacity limits the latter because installing more PV requires installing a greater unprofitable battery. However, lowering the PV capacity and adding a battery increase self-consumption and self-sufficiency. The high self-sufficiency compared with the self-consumption indicates a fairly high PV penetration.

3.5. Impact of regulations on components size and profitability

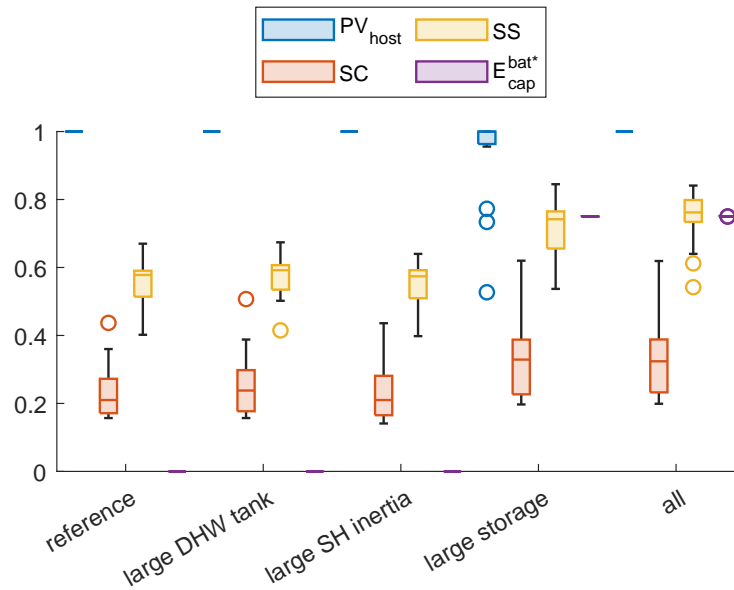


Figure 3.19 – PV hosting ratio, self-consumption, and self-sufficiency distributions for all scenarios

As shown in Figure 3.20a, increasing the DHW tank slightly lowers the need for power-to-heat capacity (both HP and EH). However, increasing the inertia of the SH allows getting rid (except for one system) of the EH by completely replacing this technology with a slightly larger HP. In Figure 3.20b, the metrics are normalized by their values in the reference scenario, allowing us to see the variations. Although the standard deviation is quite important, the *IRR* is slightly decreased when increasing the thermal inertia. This is especially more significant when increasing the SH circuit inertia. This regulation also increases the total heat consumption except for a few systems (still looking at Figure 3.20b). However, increasing the DHW tank volume requires more total heat consumption. Indeed the amount of water to keep hot is larger. Hence the loss is more significant in magnitude. In general increasing thermal inertia allows reducing the grid usage. However, this is very building-specific as increasing the SH thermal inertia increases the grid usage by more than 20% for some buildings while it reduces by up to 60% for an extreme case. Most of the considered systems have lowered their grid usage.

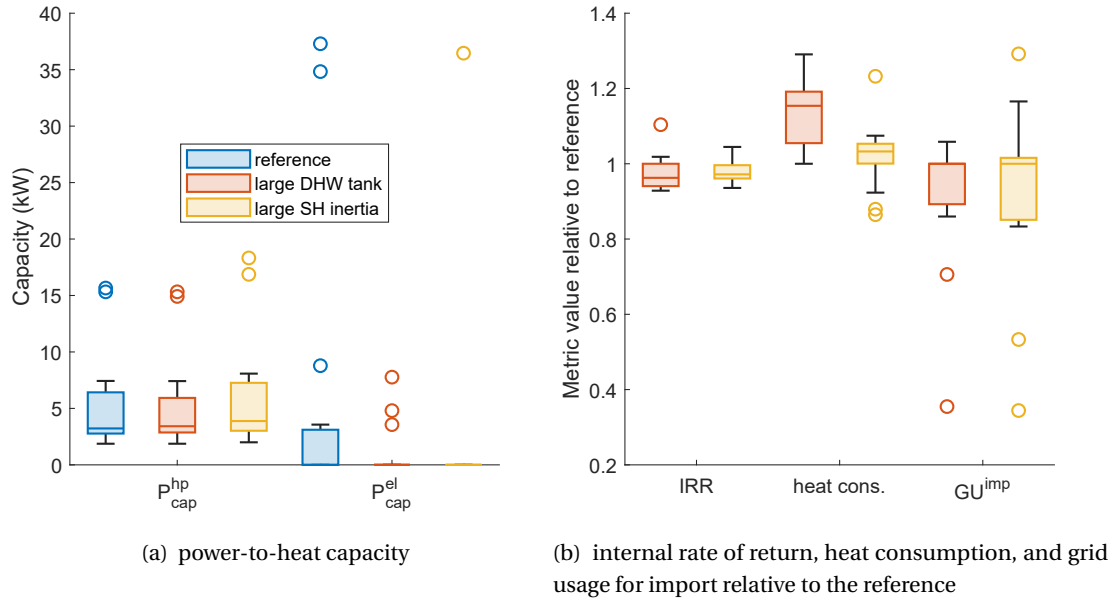


Figure 3.20 – Analysis of the regulations on thermal storage

The IRR , GU^{imp} , and GU^{exp} , normalized by their value under the reference case, are plotted in Figure 3.21. This figure highlights that increasing the thermal inertia does not affect the GU^{exp} , meaning that the thermal storage does not help to lower any PV power peak. However, adding a battery drastically increases the GU^{imp} . It is interesting to distinguish the GU when import or export, but from a network cable perspective, the ampacity limit is the same regardless of the current direction. Hence imposing storage will drastically increase the maximum current flowing through the line feeding the building. From an economic perspective, forcing storage, because it is by definition sub-optimal, lowers the profitability and the IRR of the systems⁵. In this sense combining all regulations has a significant impact as it lowers the IRR . However, all these systems remain profitable as the IRR are positive (an unprofitable system would have a negative IRR).

⁵As we will see in Chapter 4, these statements also depend on the electricity tariff.

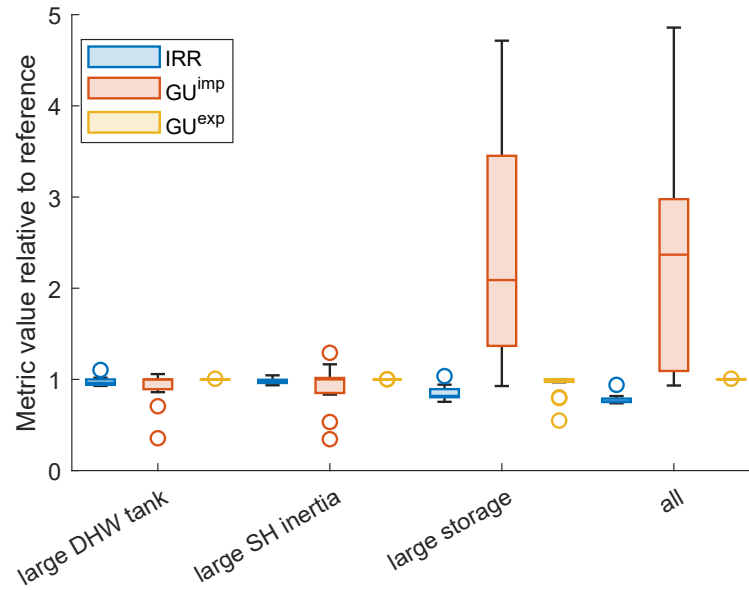


Figure 3.21 – Internal rate of return and grid usage metrics for all scenarios

This work highlights the fact that imposing batteries as a tool for naively gaining flexible power may have a detrimental effect on the system's profitability and reducing the stress on the distribution grid. Increasing the DHW tank and SH inertia helps to reduce the maximum import power while increasing the total heat consumption.

3.6 Conclusion

In this work, we propose a generic model of a PV system, considering curtailment, electric storage, and power-to-heat as ancillary flexibility technologies. We first investigate how technical flexibility (from a generic storage technology) compares with behavioral flexibility. Technical solutions may increase flexibility (measured by the Flexi score) by a factor of three compared with behavioral flexibility. To practically deliver this flexibility, we proposed a heuristic control algorithm (HCA) for managing a heat pump with a PV system. The HCA does not consider batteries, only a heat pump, as it is the most readily accessible source of flexibility in the residential sector. Our HCA is based on an indicator that relates, for all possible actions, the variations of the operating cost, and the variation of the produced heat. The algorithm's primary objective is to keep the temperature state variable in the imposed bounds. This ensures comfort in the building and the appropriate service temperature for the domestic hot water (DHW). A set of 15 building models was built to have a representative case study, and we benchmark this algorithm against the optimal control. We also used four typical periods of one week to simulate the HCA's behavior and compare it with the MILP one. Under the assumption of a perfect forecast, the HCA's performance is close to the optimal control. This perfect forecast assumption allows a true comparison of the algorithm performance

with optimal control. A real (imperfect) forecast leads to decreasing the HCA performance, but the influence of the forecast algorithm on the energy management control economic performance is minimal [Bloch, 2020]. Under perfect forecast, the differences between the HCA and MILP operating costs are negligible. The temperature deviations can sometimes be significant but stay in the same range as the MILP (recalling that no cooling is allowed, mostly due to the external temperature). The HCA, because it includes the running and switching costs of the HP, uses the HP more carefully, hence having a lower running time and number of switchings than the MILP. This should positively impact the lifetime of the HP in a real application. Although the HCA's computing time is much larger than the MILP, the HCA has a low computing burden when considering that we simulated one week of operation at 15 min time resolution. This makes the HCA suitable for a real deployment in a solar controller. Using the same case study of 15 representative buildings, we investigated the impact of regulations on their design, operation, and financial profitability. The results highlight that imposing a battery has several drawbacks as it significantly penalizes profitability while drastically increasing the intensity of the exchange with the grid. The main findings of this chapter are summarized in Table 3.8.

An alternative to design regulations is to set up the economic framework to influence the systems' design. In particular, tariffs have a significant influence on how the system will be designed and operated. The following chapter investigates this particular topic and elaborates on the PV systems' grid impact.

Table 3.8 – Technical flexibility results summary

Flexibility score comparison (median)			
	Achieved (-)	Theoretical (-)	Technical (-)
Constant time-of-use tariff (T1)	1.3	2.1	5.5
Variable time-of-use tariff (T2)	1.2	1.8	3.4
Heat pump control performance (average)			
	OPEX (CHF/day)	Comp. time (s)	Temp. dev (°C)
Heuristic control algorithm (HCA)	-22	172	2.06
Optimal control (MILP)	-25	0.13	1.15
Difference	3	172	0.91
Design regulation effect			
	PV hosting $\Delta(\%)$	Profitability IRR $\Delta(\%)$	Grid impact $\Delta(\%)$
large DHW tank	0	-3	0
large SH inertia	0	-2	+3
large storage	-7	-15	+139
all combined	0	-22	126

4 Using electricity tariffs to trigger flexibility

The economic framework has a significant impact on the adoption of PV and flexible technologies. In particular, tariffs have a prominent role in promoting investments in larger storage and power-to-heat technologies. This has major consequences on the grid impact. This chapter presents critical results on the impact of tariffs on PV systems' design and their grid impact. Besides, we discuss how the energy sector can use smart meter measurements in a privacy-preserving way.

Part of this section has been published in the following works:

Bloch, L., Holweger, J., Ballif, C., and Wyrsh, N. (2019). Impact of advanced electricity tariff structures on the optimal design, operation and profitability of a grid-connected PV system with energy storage. *Energy Informatics*, 2(1):16

and

Holweger, J., Bloch, L., Ballif, C., and Wyrsh, N. (2020a). Mitigating the impact of distributed PV in a low-voltage grid using electricity tariffs. *Electric Power Systems Research*, 189:106763

4.1 Introduction

The increasing usage of the grid, proportional to the maximum power exchanged, is one of the barriers to reach a high penetration of residential PV. Additionally, PV owners' current business model is to reduce their electricity bill thanks to self-consumption [Kubli, 2018], which raises social equity issues. Indeed the current tariff structures do not allow the network operator to recover grid costs from PV owners yet. At least, any compensation mechanism to recover grid cost from the PV production may reduce the attractiveness of PV investment [Huber et al., 2018]. To address these issues, carefully tailored demand-side management measures must be implemented to promote flexible PV energy systems while not penalizing PV technologies. As a tool, energy retail tariffs and grid fees could enable this flexibility. Regarding retail energy

tariffs, we can distinguish four different pricing strategies [Dutta and Mitra, 2017]:

Flat rate A common electricity tariff strategy, flat rate consists of a price proportional to the energy exchanged (i.e., in CHF/kWh). By definition, this tariff is constant through time.

Time-of-use Also common for larger residential consumers. A lower energy rate (CHF/kWh) typically applies during the night. In general, time-of-use tariffs have a variable rate according to the time of the day.

Critical peak pricing Similar to the time-of-use tariff, critical peak pricing sets a higher energy price (CHF/kWh) during periods of high demand, typically cooking time, on an everyday basis. An extension of this pricing policy is variable peak pricing which may consider daily variations of both the peak hours and the tariffs.

Real-time pricing The energy tariff is indexed with the spot energy market prices, for instance. Hence the energy tariff can vary on a 15- or 60-min basis.

Although network charges for the residential sector are mixed with the retail energy price in the form of a volumetric cost (CHF/kWh), alternative grid fees also exist [Azarova et al., 2018]:

Fixed charges A fixed annual price may depend on the power capacity of the connection point independent of both the energy consumption and the used power capacity.

Capacity based grid costs are paid on a monthly (or yearly) basis and based on the maximum measured power (CHF/kW). Usually, the capacity tariff is time-independent, but it can vary on a seasonal basis.

Block rate tariff An energy tariff (CHF/kWh) that varies according to the (averaged) power over a 15-min period. The energy tariff usually increases with the power interval, thus forming blocks. More details are given in Section 4.2.1.

In the early adoption of residential photovoltaics, feed-in tariffs' design was disputed to ensure a fair price for both the PV producer and the government. A high feed-in tariff incentivizes investment in distributed generation and transfers market price risk from investors to consumers [Devine et al., 2017]. [Ayompe and Duffy, 2013] analyzed various feed-in tariffs and proposed multiple (even continuous) tariffs at which household investment becomes profitable. They showed how current feed-in tariffs are often above the PV levelized cost of electricity, thus are over-subsidizing PV electricity. Appropriate tuning of the feed-in tariffs over a group of households limits this effect. The decreasing of the PV cost correlates with increasing PV penetration, thus sparking the need to re-think grid tariffs. [Huber et al., 2018] acknowledged this issue by claiming that the current way grid costs are charged promotes grid costs' desocialization. As predominantly wealthy households can invest in PV installations and equip their house with storage, their electricity consumption from the grid decreases until they become net

energy producers. In this way, their participation in covering the grid costs decreases, while lower-income households will have to cover a larger share of the grid costs. In [Bonbright et al., 1961], some basic guidelines of utility rate structure are stated. The most relevant of these requirements for energy distribution is that grid fees should be understandable and publicly acceptable. It should guarantee the minimum revenue to recover the investment cost in a "fair-return standard", discourage any wasteful use of the infrastructure, and ensure "fairness (...) in the apportionment of total costs of service among the different consumers".

Most of the adopted volumetric grid charge schemes (cost and revenue are proportional to the exchanged energy, as defined in [Hinz et al., 2018]) do not entirely satisfy this last rule. [Simshauser, 2016] showed that in terms of peak demand, PV owners have a grid usage similar to standard consumers. He proposed integrating a demand tariff (proportional to the maximum peak demand of a year), showing how such a tariff avoids an indirect subsidy to PV owners. [Schittekatte et al., 2018] have shown that high enough capacity-based charges, whose cost is proportional to the peak exchanged power, as defined in [Hinz et al., 2018], can over-incentivize investment in PV and batteries and might lead to inequity between passive consumers and prosumers. The risk described in the latter paper is that individual investment decisions might lead to over-investment in distributed renewable energy sources, which might cause an increase in the total system costs. In a world pushing toward decarbonization, incentivizing distributed renewable energy sources is a crucial lever. [Kubli, 2018] argues that promoting the diffusion of distributed PV comes with the promotion of self-consumption, hence reducing the volumetric exchange with the grid. The capacity-based tariff allows for appropriate re-allocation of the grid costs while promoting self-consumption. Still, it causes a re-distribution of the grid costs among consumers and prosumers.

However, one has to distinguish between grid fees and energy supply costs—the first aims to cover the distribution infrastructure cost. The second should represent the availability of a particular amount of energy at a specific time, given the overall demand. In most of the following reviewed papers, network charges are often considered together with energy supply charges. While the most adopted energy pricing mechanism is a simple flat rate (which includes grid fees in a volumetric way), the review [Dutta and Mitra, 2017] proposes an overview of dynamic pricing mechanisms. According to the authors, the primary motivation for introducing dynamic pricing of electricity is to avoid an unnecessary peak load that has to be covered by expensive production reserve capacity. In this way, time-of-use (TOU) and real-time pricing [Ashouri et al., 2015] are practical pricing mechanisms to encourage consumer demand to respond to a given price signal. The design of such a dynamic tariff is, however, not straightforward. This challenge is addressed by [Soares et al., 2019], who proposed a bi-level optimization approach to design TOU pricing while maximizing the retailer profit and modeling the reaction of a set of consumers to those prices.

Many authors also studied the impact of various network tariff schemes on the different stakeholders' revenues (or expenses). Starting with the grid operator, [Young et al., 2016] explored the impact of various PV penetration levels and energy efficiency measures (modeled as energy savings) on individual households' contribution to the network cost. The extension

of this work conducted by the same authors [Young et al., 2019] aims at modeling the impact of the use of residential batteries on the network revenue under various considered storage and PV capacity and under different tariff structures. The authors show that aiming to maximize self-consumption with a PV and battery system is beneficial for the network because it reduces the peak demand, thus the network cost.

Regarding the impact of grid tariffs on household energy bills, [Azarova et al., 2018] analyzed the effect of 11 hypothetical network tariffs on the energy bills of 765 households. Thanks to an appropriate investigation of the households' socio-economic data, the authors observed which socio-economic groups might benefit or suffer from different tariff structures. The authors highlighted the rising risk of inequity between consumers and prosumers with a relatively higher income. Focusing more specifically on the potential benefits to residential PV owners, [Darghouth et al., 2016] investigated how the evolution of the wholesale market design impacts the market price of electricity and, in turn, the bill savings of PV owners. Their work shows the trade-off between having an efficient market design and supporting distributed PV. [Ren et al., 2016] analyzed the financial benefit of a PV and battery system under nine different tariff scenarios combining three network components (fixed charges, capacity-based, and peak demand) and three retail energy components (flat, time-of-use, and critical peak price). The highest bill savings are achieved with capacity-based and critical peak price energy rates. [Borenstein, 2017] analyzed the effect of rebates and tax incentives on the net present value of US residential PV installations, showing that wealthier households get higher profitability from their PV installations than lower-income families due to their larger system sizes, higher consumption, and lower interest rates. As emerging business models arise, such as flexibility providers and aggregators of distributed energy storage systems to provide grid services, [Govaerts et al., 2018] studied the strategic operation of an aggregator of residential PV and energy storage systems under various distribution tariffs. The best profitability of a flexibility aggregator against an energy retailer is achieved under a capacity-based tariff. In the papers mentioned above, the authors used pre-defined scenarios of the system design. In other words, the authors performed a parametric analysis such as in [Schibuola et al., 2016], but no optimization to find the most appropriate design of the considered energy systems according to any financial metrics.

In this work, we use the capability of the PV system model presented in Chapter 3 and expand the objective function to include more advanced energy tariffs. This chapter investigates how tariff impacts the design of flexible PV systems and to which extent they can contribute to moderate the stress on the grid. In this sense, the chapter directly contributes to answering Research Question B) and provides good foundations to answer Research Question C) about mitigating grid reinforcement costs.

This chapter is divided into three parts. Section 4.2 investigates the impact of tariffs on the design and operation of a system with PV, battery, and power-to-heat units. This part aims to extend the objective function presented in Chapter 3 to include more advanced tariff structures. Before up-scaling this analysis to a whole network, the building loads and grid loads should be known. The roll-out of smart meters offers opportunities to use the actual

loads in the network for energy planning studies, but faces privacy issues. We address this issue by proposing, in Section 4.3, two methods to use smart meter data in a privacy-preserving way. The last part of this chapter (Section 4.4) aims to evaluate how tariffs can mitigate the stress on the grid of distributed PV and power-to-heat units.

4.2 Impact of tariffs on the design of a flexible PV system

To enable flexibility, technologies such as power-to-heat and battery energy storage are needed. The latter is particularly promising to increase the flexibility of PV systems. However, the economic viability of this technology is still under debate and depends strongly on the underlying electricity tariff structure [Milis et al., 2018].

This work aims to study the impact of the most up-to-date tariff structures provided by the literature on the optimal operation and design of a grid-connected residential PV-battery and heat pump system. First, an integrated optimization of both the component sizing and control, based on mixed-integer linear programming (MILP), is proposed. Then, appropriate performance metrics are defined, allowing us to assess how tariff structures can mitigate grid usage and prevent excessive power injection or withdrawal while preserving financial sustainability for the investor and user comfort.

4.2.1 Methodology

The methodology to optimize the system's design and control is based on the linear model introduced in Chapter 3. The system is composed of PV arrays, a battery, a heat pump, and its ancillary electric heater. As a reminder, the optimization's objective function is to minimize the total expense over a given period. In this case, the total annualized cost (*TOTEX*, Equation 3.8) is the sum of the annual operating cost (*OPEX*, Equation 3.9) and the annualized investment cost (*CAPEX*, Equation 3.10). The operating costs are composed of the maintenance costs, the battery operational cost, and grid exchange costs.

A The optimization problem

The contribution of this chapter is to extend the grid exchange components (Equation 4.1a) of the objective function to include new tariff structures. In particular, three kinds of tariff structure are defined: a volumetric tariff, a capacity tariff (the cost is proportional to the maximum power, evaluated monthly on both import and export), and a block rate tariff where the volumetric tariff depends on the power level at which the energy is exchanged. Volumetric tariffs are simply the product of the energy imported (or exported) and the corresponding import and export tariff ($c_t^{\text{imp,exp}}$ as depicted in Equation 4.1b). Note that a tariff can be constant in time, periodic over a day (or even a week), or even fully time-dependent. A capacity-based tariff is defined in Equation 4.1c where the maximum power P_m^{max} is determined based on constraints given in Equation 4.2, in which $\delta_{m,t}$ is a Boolean variable that takes the value

Chapter 4. Using electricity tariffs to trigger flexibility

one if the time t falls in month m , 0 otherwise.

$$\text{Grid exchange} \quad \text{ox}^{\text{ge}} = \sum_{g=\{\text{vol}, \text{pow}, \text{block}\}} \text{ox}_g^{\text{ge}} \quad (4.1a)$$

$$\text{Volumetric tariff} \quad \text{ox}_{\text{vol}}^{\text{ge}} = \sum_{t=1}^T \left[P_t^{\text{imp}} \cdot c_t^{\text{imp}} - P_t^{\text{exp}} \cdot c_t^{\text{exp}} \right] \cdot TS_t \quad (4.1b)$$

$$\text{Capacity tariff} \quad \text{ox}_{\text{pow}}^{\text{ge}} = \sum_{m=1}^M P_m^{\text{max}} \cdot c^{\text{pow}} \quad (4.1c)$$

$$\begin{aligned} \text{Block rate tariff} \quad \text{ox}_{\text{block}}^{\text{ge}} = & \sum_{t=1}^T \max_{k=1 \dots K} \left(P_t^{\text{imp}} \cdot a_k^{\text{imp}} \cdot TS_t + b_k^{\text{imp}} \right) \\ & - \sum_{t=1}^T \min_{k=1 \dots K} \left(P_t^{\text{exp}} \cdot a_k^{\text{exp}} \cdot TS_t + b_k^{\text{exp}} \right) \end{aligned} \quad (4.1d)$$

$$P_t^{\text{imp}} < \delta_{m,t} P_m^{\text{max}} \quad (4.2a)$$

$$P_t^{\text{exp}} < \delta_{m,t} P_m^{\text{max}} \quad (4.2b)$$

The block rate tariff is built by setting a tariff a_k between a power range $[p_{k-1}, p_k]$. It is created from a set of linear functions of slopes a_k and intercepts b_k . The parameters b_k can be found by the continuity of the function $\text{ox}_{\text{ge}}^{\text{block}}$ in p_k :

$$b_1 = 0 \quad (4.3a)$$

$$b_k = (a_{k-1} - a_k) \cdot TS \cdot p_{k-1} + b_{k-1} \quad \forall k > 1 \quad (4.3b)$$

An illustration of a three-block tariff is provided in Figure 4.1.

Note that the constraints formulated in Equation 4.1d are linear as the function $\min_{k=1 \dots K}$ and $\max_{k=1 \dots K}$ turns into a set of K linear inequalities as:

$$y = \min_{k=1 \dots K} f_k(x) \quad \longrightarrow \quad y \leq f_k(x) \quad \forall k = 1 \dots K$$

$$y = \max_{k=1 \dots K} f_k(x) \quad \longrightarrow \quad y \geq f_k(x) \quad \forall k = 1 \dots K$$

To wrap up, we define the optimization problem as the minimization of the total cost of ownership (*TOTEX*) subject to the aforementioned definitions, including the new tariffs

4.2. Impact of tariffs on the design of a flexible PV system

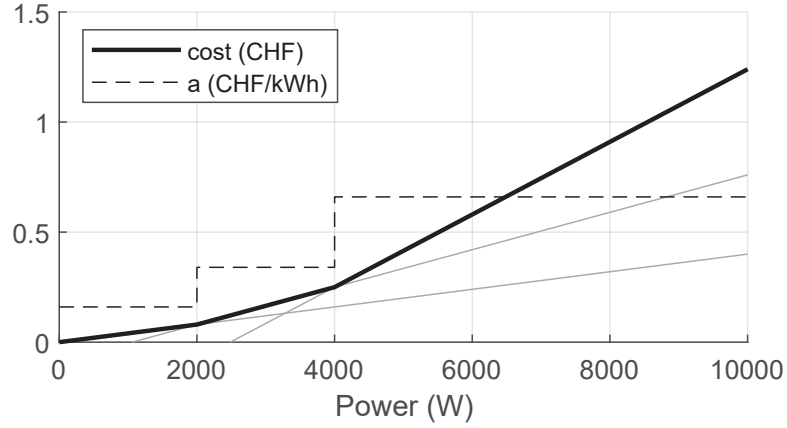


Figure 4.1 – Block rate tariff obtained by fixing the following tariff: $a = (0.16, 0.34, 0.66)$ CHF/kWh for the power ranges $([0-2], [2-4], [4-\infty])$ kW with a time step of 15 min.

structure and subject to the linear modeling equations developed in the previous chapter:

$$\begin{aligned} \min \quad & TOTEX = OPEX + R \cdot CAPEX \\ \text{where:} \quad & OPEX = ox^{ge} + ox^{bo} + ox^{pm} \\ & CAPEX = cx^{PV} + \frac{L}{L^{BAT}} \cdot cx^{bat} + cx^{hp} + cx^{el} \end{aligned} \quad (4.4)$$

and the definition in Equations 4.1a to 4.1d

subject to: Equations 3.1 to 3.6f

B Case study and scenario definition

To perform this study, a single-family house was selected in the Rolle area (Switzerland, the house's actual location is known from the author). It has essentially four roofs' orientation, and the total area is about 200 m². A top view of the house is pictured in Figure 4.2. The building has an electric demand of about 5 MWh per year and a heat demand of 11 MWh, including 2.8 MWh for domestic hot water. The details of the roofs are reported in Figure 4.2. The physical buildings' characteristics are extracted from the cantonal building registry, and the [SIA, 2015] norms, and reported in Table 4.1.

The PV and battery cost have been extracted from various market studies [IRENA, 2016, IRENA, 2017] and calibrated using the Swiss market data [SFOE, 2018]¹. The costs for the reference year 2030 are extrapolated using the approach described in [Bloch et al., 2019]. As heat pumps and electric heaters are mature technologies, we assume that their cost is not expected to change significantly in future years. The heat pump cost was extracted from [Fischer et al., 2016], while the electric heater cost comes from [Householdquotes, 2020]. An electric load and

¹<https://www.suisseenergie.ch/page/fr-ch/calculateur-solaire>



Figure 4.2 – Illustration of the house from map.geo.admin. Colors indicate suitability for solar energy. The table gives the orientations and area of each roof.

domestic hot water demand profile from another house (with similar size and characteristics) were used in this study. The system lifetime is assumed to be 25 years, and the interest rate 3%. All parameters are summarized in Table 4.1.

We investigate the system's optimal design and operation under five different tariff scenarios, inspired by the most up-to-date literature but never used in this context. The first and reference scenario is an actual tariff applied by the utility *Romande Energie*. It is a standard flat rate tariff in Switzerland with an energy rate of 21 cts/kWh (including grid fees and tax) [Romande Energie, 2019]. The second scenario is a fictive solar tariff that incentivizes households to consume more during midday when PV production is predominant. The third is a mirror of the continuous intraday price from the European power exchange spot market (EPEX²). The fourth is composed of a capacity-based tariff to cover the grid cost while constant volumetric tariffs are applied for the energy exchange. The last scenario consists of a block rate tariff. Each scenario's tariff is adjusted so that the grid cost and the energy retail cost (or revenue) are identical to the reference case when using the reference scenario's optimal design and operation. As no grid charge is defined for the spot market scenario, the EPEX market price is scaled so that the total cost of importing energy from the grid would stay the same when using the reference scenario system design. The same applies to the export price, which is the EPEX price scaled so that the export revenue would stay the same as for the reference scenario. Similarly, the block rate tariff does not contain any grid charge. The power threshold values and the tariff are scaled so that the total import cost remains approximately identical. The import/export tariff and grid charges are summarized for all scenarios in Table 4.2. The value indicates the tariff (per kWh) between the power interval specified in brackets for the block rate tariff. The negative value for the export price suggests that the system earns less money

²<https://www.epexspot.com/en/market-data/intradaycontinuous/intraday-table/-/CH>

4.2. Impact of tariffs on the design of a flexible PV system

Table 4.1 – System and building parameters. Note that $U = 1/R$.

	Param.	Unit	Value		Param.	Unit	Value
SYSTEM	T	-	35040		L	years	25
	M	-	12		L^{bat}	years	9
	TS	s	900		r	-	0.03
PV	N	-	8		SOC_{init}	-	0.7
	J	-	8		$\text{SOC}_{\text{min,max}}$	-	0-0.7
	c_F^{PV}	CHF	10'049	BATTERY	α	1/day	0.04
	c^{mod}	CHF/W	0.83		$\eta^{\text{cha,dis}}$	-	0.98
	$P_{\text{nom}}^{\text{mod}}$	W	315		$\text{CR}^{\text{char,dis}}$	1/h	1
	A^{mod}	m ²	1.63		c^{bat}	CHF/kWh	182
	γ^{PV}	-	0.5%		c_F^{bat}	CHF	0
					c_o^{bat}	CHF/kWh	10 ⁻⁶
HP	c^{hp}	CHF/W	1.5	EH	c^{el}	CHF/W	1.2
	q^{carnot}	-	0.8		η^{el}	-	0.99
BUILDING	C^{b}	kWh/K	14	SH	C^{sh}	kWh/K	1
	U^{b}	W/K	181		U^{sh}	W/K	524
	$T_{\text{min}}^{\text{b}}$	°C	19		$T_{\text{min}}^{\text{sh}}$	°C	5
					$T_{\text{max}}^{\text{sh}}$	°C	70
TANK	$T_{\text{min}}^{\text{tank}}$	°C	59				
	$T_{\text{max}}^{\text{sh}}$	°C	100				
	V^{tank}	L	291				

per additional kW above 4 kW feed to the grid than for lower injection power, corresponding to a negative slope of the third segment of the block rate tariff illustrated in Figure 4.1. It does not mean that the system is paying for injecting power above 4 kW unless the system is injecting at a power above 14.3 kW. To separate the effect of adding PV and batteries on the grid from the only presence of power-to-heat devices, we added a sixth scenario, in which no PV and battery is allowed. In this case, only the heat pump and electric heater size and operation are optimized. This scenario considers the same tariff as for the reference one. It only provides reference heat pump and electrical heater capacity values and their operation.

Table 4.2 – Scenarios and tariff structures

Scenario	Import (cts/kWh)	Export (cts/kWh)	Grid charges
Reference	9.26	8.16	11.76 cts/kWh
Solar tariff	11h-15h 4.48	7.13	11.76 cts/kWh
	15h-11h 9.35	9.26	11.76 cts/kWh
Spot market	EPEX scaled by 4.08	EPEX scaled by 1.62	-
Capacity	10.51	8.16	1.45 CHF/kW/month
Block rate tariff	16 [0-2]kW	15 [0-2]kW	-
	34 [2-4]kW	9 [2-4]kW	
	66.66 [4-∞]kW	-4.67 [4-∞]kW	
Thermal only	9.26	<i>no PV or battery</i>	11.76 cts/kWh

C Performance indicators

To assess the performance of the design and operation resulting from the optimization, a set of performance indicators is defined in Table 4.3. Some of them have been used earlier in this work but are mentioned here for completeness.

4.2.2 Results

The design and control optimization for each scenario is obtained by solving the MILP problem described in the previous section. The optimization problems are solved using GUROBI [Gurobi Optimization, 2019] with an Intel(R) Xeon(R) CPU E5-2630 v3 @ 2.40GHz processor with 8 Cores and 32GB of RAM. The optimization runtimes are about half an hour for the volumetric tariffs, whereas it takes about one hour to solve the capacity and 2 hours for the block rate scenarios. The only sizing of the heat pump and electric heater takes approximately 7 min.

Figure 4.3 illustrates the operation under the block rate tariff scenario. Both PV curtailment and the battery are widely used to minimize the cost. The amplitude of the grid exchange is minimal, and the import and export powers are likely to match with the power threshold of the block rate tariff (i.e., 2000 or 4000 W).

4.2. Impact of tariffs on the design of a flexible PV system

Table 4.3 – Performance indicators

Indicator	Description	Formula or symbol
PV hosted capacity	Ratio between the installed PV capacity and the potential PV capacity of the roof	$PV_{\text{host}} = \frac{\sum_{i=1}^N n_i^{\text{mod}} \cdot P_{\text{nom},i}^{\text{mod}}}{PV_{\text{potential}}}$
Energy curtailed ratio	Fraction of the total PV production curtailed	$PV_{\text{curt}} = \frac{\sum_t P_t^{\text{cur}}}{\sum_t P_t^{\text{PV}}}$
Battery autonomy ratio	Ratio between the installed battery capacity and the mean daily energy consumption	$Bat_{\text{auto}} = \frac{E_{\text{cap}}^{\text{bat}}}{\text{mean daily energy}}$
Battery lifetime	simulated battery lifetime using the degradation model of [Xu et al., 2018]	Bat life
Net present value of electricity	The net present value of the system for electricity provision, including investment and maintenance cost, battery replacement and cost of exchanging power with the grid ^a	$NPV^{\text{el}} = \sum_{y=1}^L \frac{cx_y^{\text{PV}} + cx_y^{\text{bat}} + ox_y^{\text{pm}} + ox_y^{\text{ge}}}{(1+r)^y}$
Net present value of heat	The net present value of the system for heat provision, cost of electricity for generating heat ^b	$NPV^{\text{heat}} = \sum_{y=1}^L \frac{cx_y^{\text{hp}} + cx_y^{\text{el}} + ox_y^{\text{heat}}}{(1+r)^y}$
Levelized cost of energy	The NPV of the PV and battery investment divided by the discounted electricity consumption	$LCOE = \frac{NPV^{\text{el}}}{\sum_{y=1}^L \frac{\sum_t P_t^{\text{tot}, TS_t}}{(1+r)^y}}$
Levelized cost of heat	The NPV of the power-to-heat investment divided by the discounted electricity consumption	$LCOH = \frac{NPV^{\text{heat}}}{\sum_{y=1}^L \frac{\sum_t (\dot{Q}_t^{\text{hp}} + \dot{Q}_t^{\text{el}}) \cdot TS_t}{(1+r)^y}}$
Discounted payback period	The time until the system achieves more savings (or revenue) with respect to a case where no investment was made	DPP
Self-consumption	Share of the PV production directly consumed by the system	$SC = \frac{\sum_t (\min(P_t^{\text{tot}}, P_t^{\text{exp}} - P_t^{\text{imp}} + P_t^{\text{tot}}))}{\sum_t P_t^{\text{PV}}}$
Self-sufficiency	Share of the load provided by the PV production	$SS = \frac{\sum_t (\min(P_t^{\text{tot}}, P_t^{\text{exp}} - P_t^{\text{imp}} + P_t^{\text{tot}}))}{\sum_t P_t^{\text{tot}}}$
Grid usage ratio	Ratio between the maximum import, export power, and the maximum load, including power-to-heat ^c	$GU^{\text{imp,exp}} = \frac{\max_t P_t^{\text{imp,exp}}}{\max_t P_{\text{thermal},t}^{\text{imp}}}$
Relative heat need	Ratio of the total heat generated and the minimum building heat demand	$Q' = \frac{\sum_t (\dot{Q}_t^{\text{hp}} + \dot{Q}_t^{\text{el}})}{\sum_t \dot{Q}_t^{\text{heat}}}$

^a The investment costs at $y = 1$ are defined in Equation 3.13. For the battery replacement, only the variable part is kept when computing cx^{bat} .

^b ox^{heat} is the cost of buying electricity for heat generation purposes, evaluated according to the corresponding tariff scenarios.

^c The maximum power $\max_t P_{\text{thermal},t}^{\text{imp}}$ refers to the "thermal only" scenario, which only considers the thermal model and discards investment in PV or battery technologies.

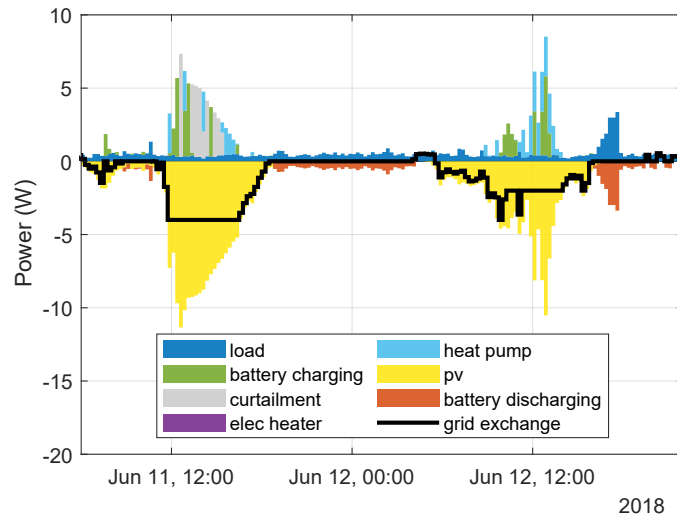


Figure 4.3 – Operation with the block rate tariff

All performance indicators defined in Table 4.3 have been evaluated for each scenario. Figure 4.4 shows the indicators related to the system design, Figure 4.5 shows those associated with the operating performance, and Figure 4.6 shows those related to economic performance. Due to the low cost of PV and the limited roof area, the maximum PV hosted capacity is reached for all cases but the block rate scenario (and the thermal only scenario, of course). The three first scenarios are based only on an energy tariff that does not give any incentive to curtail the PV generation. However, a few exceptions occur with the spot market tariff when prices are going negative and lead to PV generation's curtailment. In contrast, the block rate tariff scenario gives a financial incentive to curtail the PV generation when the total cost of exporting energy is too small. This leads to an energy curtailed ratio of 17%. Curtailment could also happen under the capacity tariff, but in this case, it is maybe more economical to convert it to heat. This requires thus a larger heat pump or electric heater capacity. As the latter is cheaper, there is an economic interest in producing heat (even with low efficiency) using this technology. The capacity-based tariff does not seem to encourage investment in the battery. Conversely, the solar and spot market scenario with higher tariff variations makes the use of a battery more profitable. All tariff scenarios lead to a heat pump capacity higher than for the thermal only scenario. Conversely, the higher electric heater capacity is observed for the thermal only scenario. The sizing of those capacities is only demand-driven for the thermal only scenario. As heat is cheaper to produce with a heat pump than an electric heater, the heat pump's optimal size is reached when it can cover almost all heat demands. The relatively large electrical heater covers the extreme peak demands. While for the other scenarios, the heat pump and electrical heater sizing are cost-driven. In those cases, the heat pump can be used as an additional flexibility tool to increase self-consumption, bringing more incentives to invest in a larger heat pump (and equally reducing the electric heater). The only exception to this explanation is the capacity scenario for the reasons explained above.

4.2. Impact of tariffs on the design of a flexible PV system

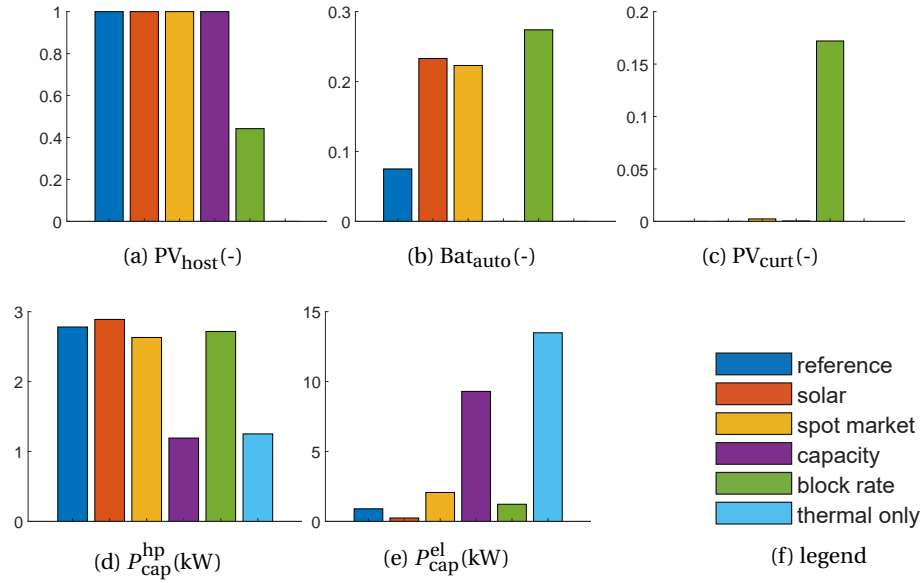


Figure 4.4 – Design metrics

As the PV capacity is smaller under the block rate scenario, self-consumption is the highest, as shown in Figure 4.5a. In these figures, horizontal (and possibly shaded bar) indicate the metric's value for the same design but without a battery. Figure 4.5a shows how much self-consumption is gained by investing in a battery. The solar and spot market tariff variations during the day also push to increase self-consumption. However, the spot market volatility can sometimes encourage more intensive use of the battery, leading to higher grid usages. Conversely, the battery is used to reduce the import grid usage under the block rate scenario. Only this tariff scenario allows decreasing both the import and export grid usage significantly using, as shown in Figure 4.3, a combination of PV curtailment and storage to flatten the grid exchanges. The relative heat needs are above one for all scenarios. This value is minimal for the thermal only scenario and accounts for the tank loss (we assume the tank does not dissipate its heat in the building). For all other scenarios, this metric somehow indicates the transfer of flexibility to power-to-heat.

As regards the economic performance indicators, the investment costs are quite similar. The block rate scenario being more dissuasive for PV induces slightly less total investment. Obviously, the PV and battery investments are more significant than only the heat pump and electric heater. All the advanced tariff scenarios show a higher revenue and a lower system *LCOE* than the loads-only scenario. The added value of the battery is pictured in Figure 4.6d (shaded area indicates the value obtained without the battery, it is displayed only for this figure for the sake of clearness). The greatest added value of the battery is observed for the block rate scenario. The levelized cost of heat accounts only for the discounted heat pump and electric heater investment costs. Hence the variations are much more minor than for the *LCOE*. It is cheaper for all advanced tariff scenarios (solar, spot market, capacity, and block rate), showing

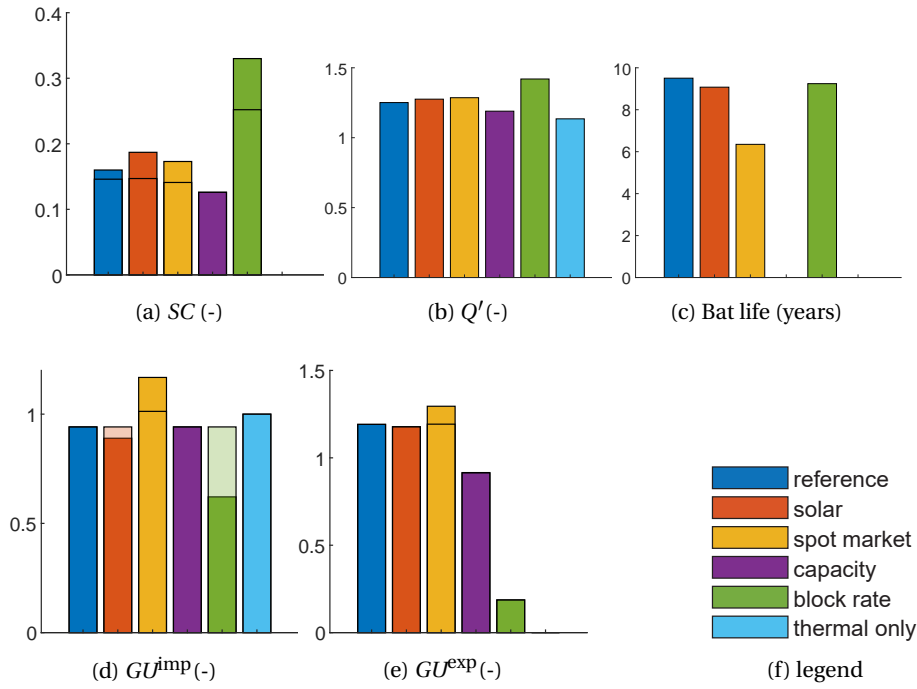


Figure 4.5 – Operation metrics

that the additional capacity contributes to reducing the cost of generating heat in all cases.

4.2.3 Discussion

The results highlight the profitability of investing in PV in all scenarios, while the benefit of investing in a battery is emphasized by dynamic prices that create a revenue opportunity. Simple capacity-based tariffs do not provide sufficient incentives to invest in a battery system if the maximum exchanged power is mostly determined by the PV injection power, which can be easily curtailed. Compared with a case with only power-to-heat units adequately sized, the grid usage at import is lowered by about 5 % by introducing PV while the grid usage at export increases by about 10%. The addition of a capacity-based tariff helps to moderate the grid usage, while a real-time pricing scheme from the EPEX intraday spot market significantly increases it. The main contributor to this usage is the battery, which, contrary to all others scenario, actually increase the grid usage because it is used for trading energy and not only for self-consumption purposes. The block rate tariff shows a very positive impact on the grid usage but penalizes the PV hosting. Indeed, as the marginal cost of exporting energy decreases with the export power, it reduces the attractiveness of installing a high PV capacity. By nature, this tariff prevents the overuse of the grid. A combination of the spot market tariff with a block rate tariff would be worth investigation, although it brings additional complexity. While volumetric tariffs are easy to understand and design for a distribution system operator, capacity tariffs already decrease accessibility for non-expert consumers. Regarding the block rate tariff, although our results show promising opportunities for demand-side management

4.3. Methodologies for creating realistic test cases for energy planners

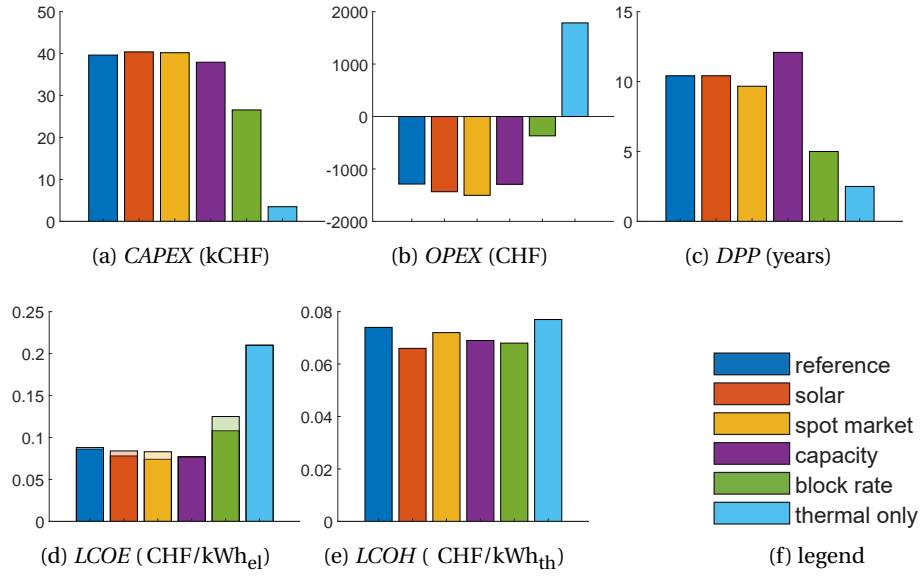


Figure 4.6 – economic metrics

and network management, there is a lack of knowledge on how to properly design such a tariff.

This section provided an in-depth presentation of the impact of tariffs on the optimal design and operation of a PV, battery, and power-to-heat system. We showed the complementarity or competition between the battery and power-to-heat technology and provided key insight to promote flexible PV systems. However, the framework of this study was just a single building. The following will show how these concepts apply to a more extensive set of buildings and how they impact the network. But before doing so, one must build realistic test cases. In particular, electric demand profiles are vital data that may be difficult to obtain. The following section will address this problem and propose two approaches to create realistic test cases for energy planners.

4.3 Methodologies for creating realistic test cases for energy planners

To assess the impact of distributed generation on distribution grids, the following general data are required.

- grid topology
- building characteristics
- weather conditions
- electric and heat demands

Whereas the three first elements can be found for most distribution grids in Switzerland, both electric and heat demands profiles are rarely available. Regarding electricity consumption, a few distribution system operators (DSO) have already replaced conventional meters with smart meters measuring the load at a resolution of 15 min. The use of the standard demand profiles (from SIA norms) is not a viable option since these profiles aggregated at the distribution grid level result in massive electricity demand peaks due to the lack of variances. This section aims to provide solutions to cope with this issue.

4.3.1 Load profiles allocation

The basic idea of the load profile allocation is to choose, from a sufficiently large load profiles dataset, the most appropriate load according to some knowledge of the network and consumers' characteristics. The first stage consists in selecting these load profiles according to their annual consumption magnitude. The loads are allocated to network locations according to prior knowledge of the consumers' annual consumption while ensuring the total network consumption is matched. A second stage is to deform the allocated load profiles so that the resulting load at the transformer is close enough to the measured transformer load, still keeping the annual energy consumption close to the original one. Thus, the developed methods consist in a two-stage optimization. In the first phase, a load profile is allocated to each meter. All profiles are tuned in the second phase to match potential additional network measurements. In particular, the sum of all the profiles should be as close as possible to the profile at the transformer (which is in most cases known).

A First stage optimization

The first stage optimization problem's overall idea is to consider the grid as a graph, formed by a set of nodes N , among which the set $N_L \subset N$ of nodes has unknown load profiles. The set $N_K \subset N$ contains measured load profiles. The root node (or transformer) is denoted as $N_P \subset N$. The reference dataset of load profiles is considered as virtual nodes J . Any load profile is assumed to be measured on the same time-span T . Finally, for each node $n \in N_L$ and $j \in J$ we define a load category $h_n \in H$. The sets' definitions are given in Table 4.4. The problem can be defined as connecting each node in N_L to a single node in J of the same load category (as pictured in Figure 4.7). The difference between the allocated annual energy of the reference load profile, E_n^{var} , and the one from the meter (assumed to be known for every node), E_j^{ref} , should be smaller than a given tolerance ϵ_E . In other words, the decision variable $\beta_{n,j}$ if greater than 0, allocates and scales the load profile j to the node n to have the allocated annual energy E_n^{var} close up to tolerance ϵ_E of the measured annual consumption of the node E_n^{ref} . The optimization's objective is to have the minimum scaling of the available load, i.e., $\beta_{n,j} \approx 1 \forall j \in J$. As pictured in Figure 4.7, a single available load profile may be allocated to more than one node in N_L . A parameter of the optimization problem k^h restricts the number of allocations for each load category. Most likely, the size of N_L will be much larger than the size of J . Thus, each load will be allocated more than once in the network.

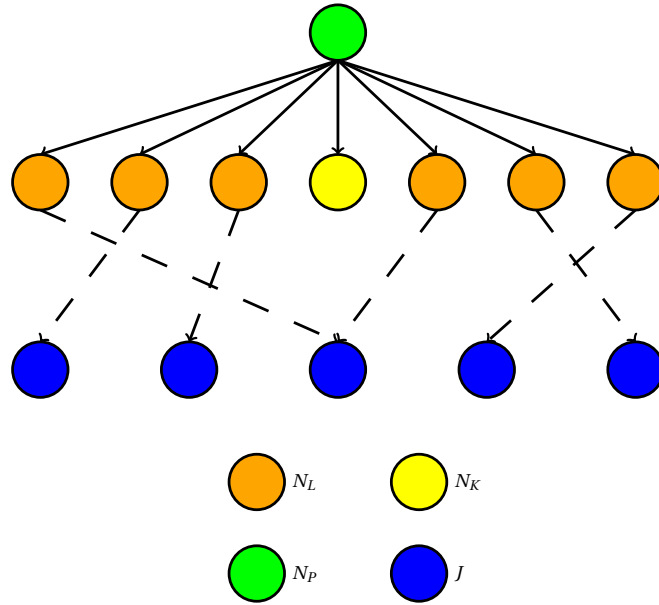


Figure 4.7 – Illustration of the first stage allocation

Table 4.4 – Networks topology and sets

Set	Subset of	Description
N	-	network nodes
H	-	load category
N_P	N	transformer node with measured load profiles
N_L	N	nodes with unknown load profiles
$N_L^{h \in H}$	N_L	nodes subset per load category
N_K	N	nodes with known load profiles
J		virtual nodes representing available load profiles from the dataset
$J^{h \in H}$	J	available load profiles subset per load category
T	-	time

The problem can be mathematically described as follow:

$$\text{The original allocated load} \quad E_n^{\text{org}} = \sum_{j \in J^h} \alpha_{n,j} E_j^{\text{ref}} \quad \forall n \in N_L^h, h \in H \quad (4.5a)$$

$$\text{The scaled allocated load} \quad E_n^{\text{var}} = \sum_{j \in J^h} \beta_{n,j} E_j^{\text{ref}} \quad \forall n \in N_L^h, h \in H \quad (4.5b)$$

$$\text{Scale is an allocation} \quad \alpha_{n,j} = \begin{cases} 0, & \text{if } \beta_{n,j} = 0 \\ 1, & \text{otherwise} \end{cases} \quad \forall n \in N_L^h, j \in J^h, h \in H \quad (4.5c)$$

$$\text{Node must have one load} \quad \sum_{j \in J^h} \alpha_{n,j} = 1 \quad \forall n \in N_L^h, h \in H \quad (4.5d)$$

$$\text{Constrained number of alloc.} \quad \sum_{n \in N_L^h} \alpha_{n,j} \leq k^h \quad \forall j \in J^h, h \in H \quad (4.5e)$$

$$\text{Annual energy error constr.} \quad \epsilon_E^2 \geq 1 - \frac{2 \cdot E_n^{\text{var}}}{E_n^{\text{ref}}} + \frac{(E_n^{\text{var}})^2}{(E_n^{\text{ref}})^2} \quad \forall n \in N_L \quad (4.5f)$$

And the optimization problem formulated as:

$$\begin{aligned} \min \quad & \sum_{n \in N_L} (E_n^{\text{org}})^2 - 2 \cdot E_n^{\text{org}} \cdot E_n^{\text{var}} + (E_n^{\text{var}})^2 \\ \text{for} \quad & \beta_{n,j} \\ \text{subject to:} \quad & \text{Equations 4.5a to 4.5f} \end{aligned} \quad (4.6)$$

Minimizing the objective function of Equation 4.6 implies having $\beta_{n,j}$ as close as possible to 1 $\forall j \in J$. Besides, having the constraints applied on subset N_L^h and performing restricted sum over J^h ensure the load category match without introducing any additional binary variable. All parameters and decision variables are described in Table 4.5.

B Second stage optimization

The second optimization aims to tune the allocated load profiles to match the resulting power profile at the transformer node, $P_{N_p,t}^{\text{var}}$ with the measured one $P_{N_p,t}^{\text{ref}}$, i.e., having the relative difference between both under a given tolerance ϵ_P . For this, a time step scale parameter defined as $\gamma_{n,t}$ can deform any allocated load profile $P_{n,t}^{\text{org}}$. Additionally, the constraints on the annual energy consumption still apply. The optimization problem's goal is to deform as little as possible the load profiles, hence having $\gamma_{n,t} \approx 1 \forall n \in N^L, t \in T$.

4.3. Methodologies for creating realistic test cases for energy planners

In mathematical forms, the problem translates as the following:

$$\text{Original load profile from 1}^{\text{st}} \text{ stage} \quad P_{n,t}^{\text{org}} = \sum_{j \in J} \alpha_{n,j} P_{j,t}^{\text{ref}} \quad \forall n \in N_L, t \in T \quad (4.7a)$$

$$\text{Deformed load profile} \quad P_{n,t}^{\text{var}} = \gamma_{n,t} P_{n,t}^{\text{org}} \quad \forall n \in N_L, t \in T \quad (4.7b)$$

$$\text{Resulting load at transformer} \quad P_{N_p,t}^{\text{var}} = \sum_{n \in N_L} P_{n,t}^{\text{var}} + \sum_{n \in N_K} P_{n,t}^{\text{ref}} \quad \forall t \in T \quad (4.7c)$$

$$\text{Allocated energy consumption} \quad E_n^{\text{var}} = \sum_{t \in T} P_{n,t}^{\text{var}} \cdot TS_t \quad \forall n \in N_L \quad (4.7d)$$

$$\text{Annual energy error constr.} \quad \epsilon_E^2 \geq 1 - \frac{2 \cdot E_n^{\text{var}}}{E_n^{\text{ref}}} + \frac{(E_n^{\text{var}})^2}{(E_n^{\text{ref}})^2} \quad \forall n \in N_L \quad (4.7e)$$

$$\text{Power error at transformer constr.} \quad \epsilon_P^2 \geq 1 - \frac{2 \cdot P_{N_p,t}^{\text{var}}}{P_{N_p,t}^{\text{ref}}} + \frac{(P_{N_p,t}^{\text{var}})^2}{(P_{N_p,t}^{\text{ref}})^2} \quad \forall t \in T \quad (4.7f)$$

Finally, the second stage optimization problem is defined as:

$$\begin{aligned} & \min \quad \sum_{n \in N_L} \sum_{t \in T} (P_{n,t}^{\text{org}})^2 - 2 \cdot P_{n,t}^{\text{org}} P_{n,t}^{\text{var}} + (P_{n,t}^{\text{var}})^2 \\ & \text{for} \quad \gamma_{n,t} \\ & \text{subject to:} \quad \text{Equations 4.7a to 4.7f} \end{aligned} \quad (4.8)$$

Table 4.5 – Variables and parameters definition. Column **S** indicates first stage or second stage optimization variables.

	S	Set	Dimension	Unit	Description
PARAMETERS					
DECISION VARIABLES					

4.3.2 Smart meter anonymization

An alternative approach to providing reliable cases study for grid planners is to use the actual smart meter data. The roll-out of smart meters in modern distribution networks offers opportunities for large dataset acquisition. However, to use smart meter data, the DSO's customers must give explicit consent, as stated by the Swiss data privacy law³:

“If the consent of the data subject is required for the processing of personal data, such consent is valid only if given voluntarily on the provision of adequate information. Additionally, consent must be given expressly in the case of processing of sensitive personal data or personality profiles”

Such explicit consent is, however, difficult to acquire. To comply with the law but still use these sensitive data, anonymization shall be guaranteed. In other words, the link between the data owner and the data shall be unequivocally broken, such as one should not be able to retrieve the original data owner from the processing of its data.

In our case, a smart meter, being identified by a unique identifier, is linked to a customer by its location (either a spot in the network or a physical building address). The link between the smart meter identifier, building address, and the network location (referred to as “a bus” in the following) is critical to perform network analysis or energy system optimization as presented in this thesis.

³Federal Act on Data Protection (Status as of 1 March 2019), art.4 al 5

4.3. Methodologies for creating realistic test cases for energy planners

This work proposes a smart meter anonymization method for network analysis (SMANET). The approach considers that the link between the smart meter id (i) and its network location (b) is known from the DSO metering service. Still, it cannot be communicated to the planners or any other third party for analysis purposes without the data owner's explicit consent. However, the smart meter measurements and network topology are available for the DSO network planning service. The basic idea of this method is to group smart meter measurements according to some characteristic features and provide, for each group, the network location list corresponding to the group's smart meters. In the graphical example of Figure 4.8, the meter id 1, 2, and 3 are grouped in A. They are located in network locations a, b, and c, respectively. From the network planner perspective, the only information accessible is that $i = 1, 2$, and 3 are in the same group as $b = a, b$, and c. It can arbitrarily choose to allocate the smart meter measurements 1 to the location a, b, or c, etc. The underlying assumption is that the smart meter measurements 1, 2, and 3 are electrically similar because they are in the same group. Hence inverting $i = 1$ and 2 at $b = a$ should have a minor impact on any further analysis performed by the network planner.

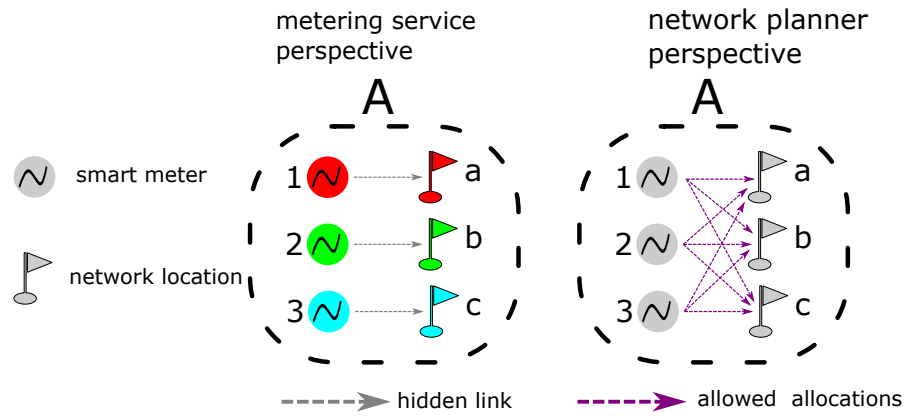


Figure 4.8 – Graphical description of the SMANET method

The workflow for setting up an anonymous allocation of smart meter data into a designated network is the following. The network planner receives the smart meter measurements $P_{i,t}$. The first task is to extract $K \geq 1$ relevant features $X_{i,k}$ $k = 1 \dots K$ for each measured load. The second task is to group the smart meters according to their features. The grouping, more commonly known as clustering, has one additional constraint compared with standard clustering methods. The number of clusters is not known in advance, and the population size inside a cluster is pre-determined. Such a task is referred to as partitioning in the literature. The population in each cluster should be more or less equal (balanced partitioning). At this stage, the metering service takes over and provides the list of buses for each meter group. Finally, the network planner randomly takes one permutation of this bus list to allocate each meter to a bus. This process is graphically pictured in Figure 4.9.

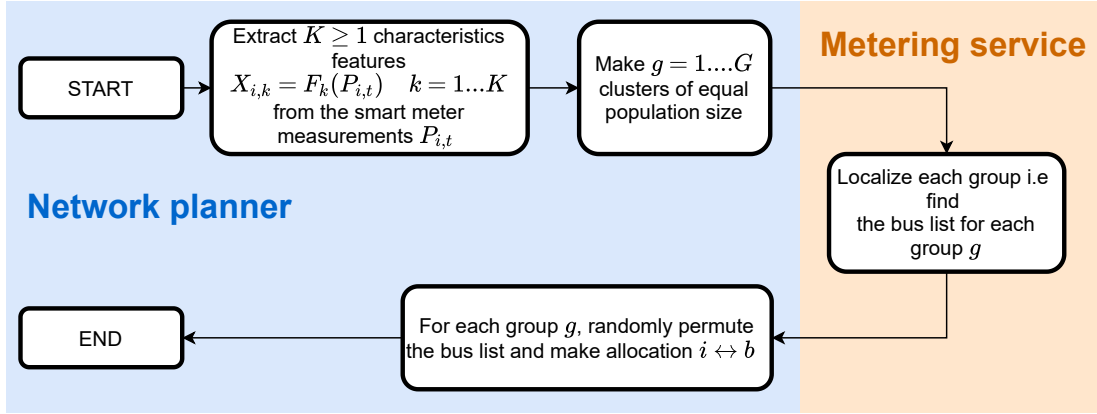


Figure 4.9 – Workflow of the SMANET method

The critical step in this process is to form groups of an equal number of elements. In the following, we investigate partitioning techniques and propose a suitable algorithm to perform the partitioning of the smart meter measurements into equal-size groups.

A Integer programming formulation of the partitioning problem

A generic formulation of the partitioning problem can be formulated using integer programming (IP). For a given dataset \mathbb{D} of N records and the similarity matrix $D[N \times N]$. An element $D_{u,v} \in [0, \infty)$ is a measure of the similarity between element u and v . We assume that this similarity measure respects the identity of indiscernibles ($D_{u,u} = 0$), is symmetric ($D_{u,v} = D_{v,u}$) and respects the triangle inequality ($D_{u,v} + D_{v,w} \geq D_{u,w}$). Typically such similarity metrics can be the Euclidian distance. Let x_u be a vector of K characteristics features. The similarity between two elements can be calculated as $D_{u,v} = \sqrt{\sum_{k=1}^K (x_{v,k} - x_{u,k})^2}$. In the following, we will consider such a similarity measure but any other similarity measure respecting the space metric properties is suitable.

The balanced partitioning problem consists in splitting the dataset into N_C clusters in which the numbers of records per cluster are equal for all clusters. One can deduce the prior relationship between the number of records per cluster and the number of clusters as:

$$m \leq \frac{N}{N_C} < m + 1 \Rightarrow m = \left\lfloor \frac{N}{N_C} \right\rfloor$$

where $\lfloor \cdot \rfloor$ is the floor function.

Let now see the dataset as a graph \mathbb{G} where \mathbb{S} is the set of edges that connect pairs of records (u, v) . To keep the full generality, let assume that the graph is coarse, i.e., some pairs (u, v) are not connected $((u, v), (v, u) \notin \mathbb{S})$. The edge weights are given by the similarity matrix D . The partitioning problem can be seen as connecting the records, or nodes of \mathbb{G} to form an

4.3. Methodologies for creating realistic test cases for energy planners

independent subgraph of \mathbb{G} containing between m and $m + 1$ element. The selection of an edge between two records is represented by variable $\delta_{u,v}$:

$$\delta_{u,v} = \begin{cases} 1 & \text{if records } u \text{ is in the same cluster as } v \\ 0 & \text{otherwise} \end{cases} \quad (4.9)$$

The variable $g_{c,u}$ keeps track of the belonging of records u to cluster c as :

$$g_{c,u} = \begin{cases} 1 & \text{if } u \text{ belong to cluster } c \\ 0 & \text{otherwise} \end{cases} \quad (4.10)$$

Using these definitions, we can formulate the balanced partitioning problem with the following constraints:

$$\mathbb{G} \text{ being coarse implies:} \quad g_{c,u} + g_{c,v} \leq 1 \quad \forall (u, v) \notin S \quad (4.11a)$$

$$\text{Each node must be in a cluster} \quad \sum_{c=1}^{N_C} g_{c,u} = 1 \quad \forall u = [1 \dots N] \quad (4.11b)$$

$$\text{Constraints cluster size} \quad m \leq \sum_{u=1}^{N_C} g_{c,u} \leq m + 1 \quad \forall c = [1 \dots N_C] \quad (4.11c)$$

$$u \in c \text{ and } v \in c \Leftrightarrow \delta_{u,v} = 1 \quad g_{c,u} + g_{c,v} - x_{u,v} \leq 1 \quad \forall (u, v) \in S \quad (4.11d)$$

$$u \in c \text{ and } v \notin c \Leftrightarrow \delta_{u,v} = 0 \quad g_{c,u} + (1 - g_{c,v}) - (1 - x_{u,v}) \leq 1 \quad \forall (u, v) \in S \quad (4.11e)$$

The optimization problem can be written as:

$$\begin{aligned} & \min && \sum_{(u,v) \in S} \delta_{u,v} \cdot D_{u,v} \\ & \text{for} && \delta_{u,v} \\ & \text{subject to:} && \text{Equations 4.11a to 4.11e} \end{aligned} \quad (4.12)$$

Figure 4.10a illustrates the results of partitioning a fully connected graph of 22 nodes into 7 clusters of 3 records. The partitioning into 3 records using such formulation is replicated for graphs with sizes ranging from 4 to 31 elements. For each problem, the time for solving is recorded and pictured in Figure 4.10b. This illustrates the issue with such formulation. The computation time increases exponentially with the graph size. One can estimate that solving problems containing about 100 records would be in the range of 10^8 years. There is hence a need for a faster partitioning method.

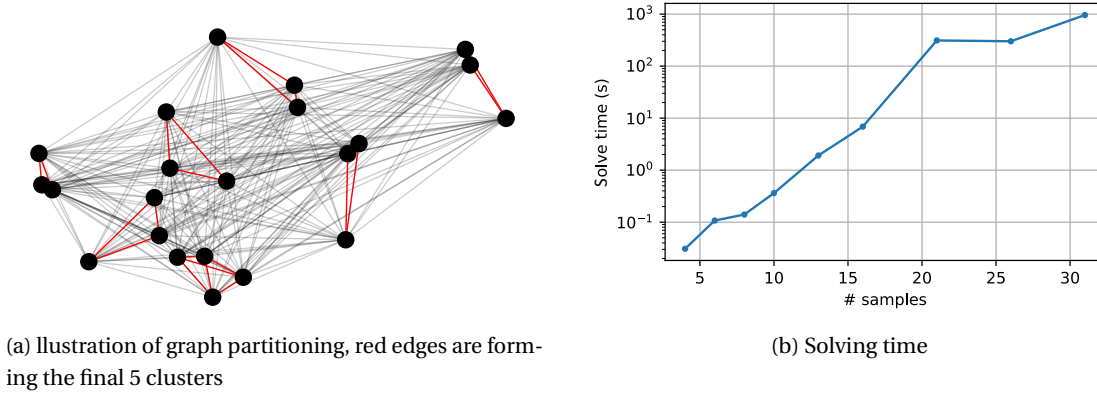


Figure 4.10 – Graph partitioning with integer programming

B Graph spectral partitioning

In modern computational science, graph partitioning is mainly used for balancing load and minimize scientific computation time [Schulz, 2015] (for instance, to solve a sizeable computational fluid dynamic problem in parallel, the discretized space domain is split into smaller pieces to be individually solved on several cores). Another application concerns route planning [Schulz, 2015]. Graph clustering is a particular application that aims to reveal intrinsic graph structure [Schulz, 2015].

Graph spectral partitioning is precisely described in [Schulz, 2015] as the connection between cuts in a graph and its second smallest eigenvalue. To understand this relation, we must remind a few properties of a graph. Let G be a graph of n nodes and $(i, j) \in S$, its set of edges. Three matrices are associated with such a graph. First, the adjacency matrix A of a weighted graph is defined as follow:

$$A_{i,j} = \begin{cases} 0 & \text{if } i = j \\ w_{i,j} & \text{otherwise} \end{cases}$$

Assuming the edge weight $w_{i,j}$ represents some sort of distance between two nodes, the adjacency matrix referred to the similarity matrix presented above. Second, the degree matrix is a diagonal matrix, where each element on its diagonal is the number of edges connecting this particular node:

$$D_{i,j} = \begin{cases} \deg(i) & \text{if } i = j \\ 0 & \text{otherwise} \end{cases}$$

Note that $\deg(i) = \sum_{(i,j) \in S} \delta_{i,j} = \sum_j \delta_{i,j}$ With: $\delta_{i,j} = 1$ if i is connected to j , 0 otherwise. Finally, the Laplacian matrix is defined as :

$$L = D - A$$

4.3. Methodologies for creating realistic test cases for energy planners

The Laplacian matrix has a few interesting properties. It is positive semi-definite and symmetric for an undirected graph.

Let's now assume we perform a cut in G in order to have two distinct graph $G_1 \subset G, G_2 \subset G, G_1 \cap G_2 = \emptyset$ represented by:

$$x_i = \begin{cases} 1 & \text{if } i \in G_1 \\ -1 & \text{if } i \in G_2 \end{cases}$$

The quadratic form of $x^T Lx$ gives:

$$x^T Lx = \sum_i \sum_j \delta_{i,j} x_i^2 - \sum_i \sum_j w_{i,j} x_i x_j \quad (4.13)$$

At this stage, note that:

$$\begin{aligned} x_i^2 &= 1 \\ x_i = x_j &\Rightarrow x_i x_j = 1 \quad (i, j) \text{ is an uncut edge} \\ x_i = -x_j &\Rightarrow x_i x_j = -1 \quad (i, j) \text{ is a cut edge} \end{aligned}$$

We can rewrite Equation 4.13 as:

$$x^T Lx = \underbrace{\sum_i \sum_j \delta_{i,j}}_{\text{number of edges in } G} - \sum_{(i,j) \text{ uncut}} w_{i,j} + \sum_{(i,j) \text{ cut}} w_{i,j} \quad (4.14)$$

Hence maximizing Equation 4.14 is equivalent to finding a cut that split G into two most distant parts. Due to the Laplacian matrix properties, this is equivalent to finding the highest eigenvalue and using the corresponding eigenvector to perform the cut (detailed derivations are given in [Schulz, 2015]). The spectral graph partitioning algorithm can be written as:

Algorithm 1: Spectral graph partition (SGP)

input : G a weighted graph

output: $G' = G_1 \cup G_2$ with $G_1 \subset G, G_2 \subset G$ distinct graphs, $G_1 \cap G_2 = \emptyset$

L : laplacian of G ;

v, λ eigenvectors and associated values of L ;

Get the maximum eigenvalue and associated vector: $v^{\max}, \lambda^{\max} = \max_{\lambda} \lambda$;

$m = \text{median}(v^{\max})$;

Construct cut vector x as: $x_i = \begin{cases} 1 & \text{if } v_i^{\max} \geq m \\ -1 & \text{if } v_i^{\max} < m \end{cases}$;

$G_1, G_2 = \text{cut}(G, x)$;

$G' = G' = G_1 \cup G_2$;

return G'

A graphical example of a single cut through a graph using the graph partitioning algorithm is pictured in Figure 4.11.

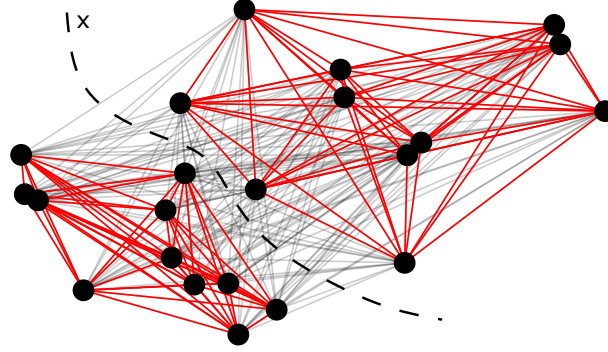


Figure 4.11 – Illustration of a single cut in a random graph, represented by its nodes (black dots) and edges (gray and red lines)

This approach can be used to successively cut the original graph into smaller partitions until the size of a sub-graph is smaller than $2k$ for k the desired graph size. The resulting clusters will have a size between k and $2k - 1$ as illustrated in Figure 4.12. For $k > 2$, this can lead to significant unbalance. To further reduce the imbalance, an IP formulation could be used when the next graph to cut has a relatively small number of nodes.

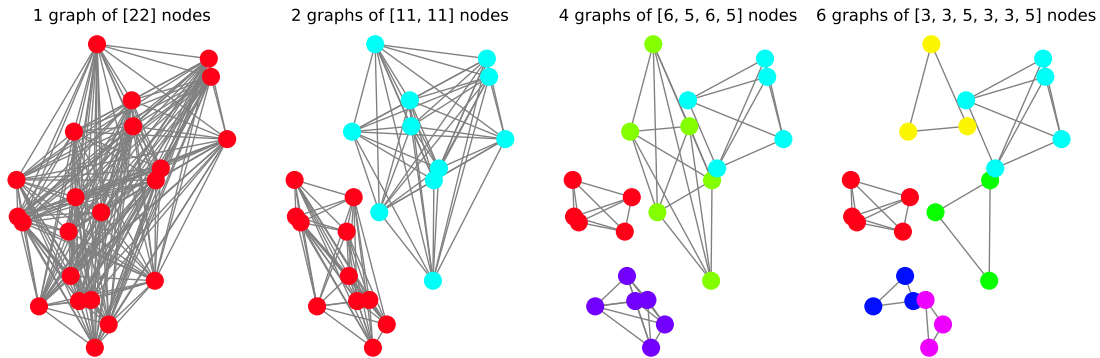


Figure 4.12 – Illustration of successive (from left to right) graph spectral partitioning

C Recursive graph spectral partitioning

The graph spectral partitioning has low complexity and ensures more or less balanced clusters when applied successively. On the opposite, the IP formulation of the graph partitioning problem provides the most optimal balancing of the graph partitioning, but the computational complexity makes it unusable for large graphs. To gain the best of the two worlds, we propose

the following recursive graph spectral partitioning (RGSP) algorithm:

Algorithm 2: Recursive spectral graph partition (RSGP)

input : G a weighted graph, k the desired partition size
output: $G' = \bigcup_{j=1}^J G_j$ with G_j a set of distinct graphs
 $G_j \subset G, G_l \cap G_k = \emptyset \quad l, k = [1 \dots J] \quad l \neq k$

$[G_1, G_2] = \text{SGP}(G)$: cut of G using spectral graph partition (Algorithm 1) ;
 G' : an empty graph ;
for i in $[1, 2]$ **do**
 N_i : number of nodes in G_i ;
 if $3k \leq N_i < 4k$ **then**
 G'_i : apply IP formulation to partition G_i (Equation 4.12) ;
 else if $N_i \geq 2k$ **then**
 $G'_i = \text{RSGP}(G_i)$;
 else
 $G'_i = G_i$;
 end
 $G' = G' \cup G'_i$;
end
return G'

The comparison of the partitioning of the 22 nodes graph into clusters of 3 records using SGP, RSGP, and IP is presented in Figure 4.13. In terms of unbalance ($\sum_g N_g - k$, with N_g the g^{th} partition size), the proposed RSGP algorithm lies in between the successive SGP algorithm and the IP optimization (RSGP's unbalance is 4 vs. 6 for SGP, and 1 for IP). However, the RSGP computing time does not increase exponentially with the number of nodes, as shown in Figure 4.14.

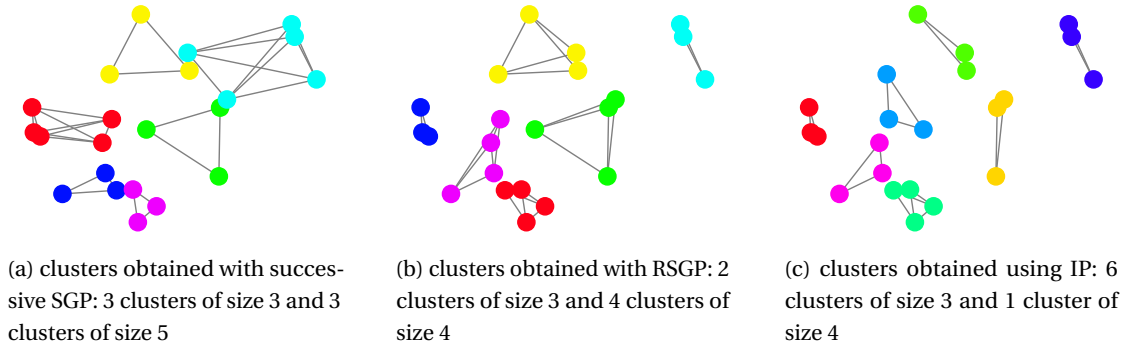


Figure 4.13 – Comparison of the partitioning on 22 nodes with the SGP, RSGP, and IP methods

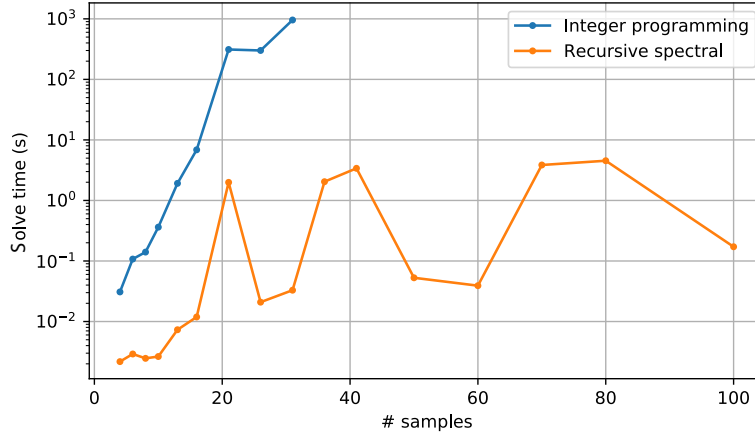


Figure 4.14 – Computation time comparison

Hence, the RGSP algorithm is suitable to partition large datasets into small groups of equal size and fulfill the requirements for grouping smart meter measurements for anonymization purposes. So far, the definition of the smart meter features (the record attributes) has not been discussed. Indeed the features selection depends on the ultimate goal of the study, as it will determine which load characteristics are significant and what is the similarity definition. Provided that the selected smart meter features (i.e., load characteristics) best reflect the analysis's end goal, the RGSP allows to reasonably assume that any replacement of one smart meter by another in the same group will provide similar results. In this section, we assume that the smart meter data are used for "network analysis" in general. For this specific end-use, we will discuss what are the most appropriate features.

4.3.3 Benchmark methodology

At this stage, we provided two methods for creating a real test case for network analysis:

- The load profiles allocation technique
- the load profiles anonymization technique

To validate these two approaches and compare their performances with respect to the final application, we solve the load-flow equation on six low-voltage networks of the Rolle area using reference loads. This set of loads are provided by smart meter measurements from *Romande Energie*. The locations of these loads are not known, but has been attributed for the purpose of this study. The load-flow problem allows us to calculate the buses voltage ($V_{b,t}$ $b \in \text{Bus set}$), lines current ($I_{l,t}$ $l \in \text{line set}$), and the power at the sub-station (transformer power P_i^{trafo} $i = [1...6]$) at all time $t \in T$. The load-flow is then solved using the loads resulting from both the load allocation technique and the anonymization technique. The performances of the two methods are measured using dedicated key performance indicators:

4.3. Methodologies for creating realistic test cases for energy planners

$$\text{Voltage magnitude mean square error} \quad \text{MSE}_{\text{vm}} = \sum_{t=1}^T \sum_{b=1}^B \frac{(V_b - V_b^{\text{ref}})^2}{B} \quad (4.15)$$

$$\text{Maximum transformer loading error} \quad E_{\text{maxTRL}} = \frac{P_{\text{max}}^{\text{trafo}} - P_{\text{max}}^{\text{trafo,ref}}}{P_{\text{max}}^{\text{trafo,ref}}} \quad (4.16)$$

$$\text{Maximum line loading error} \quad E_{\text{maxLNL}} = \frac{I_{\text{max}} - I_{\text{max}}^{\text{ref}}}{I_{l,t}^{\text{ref}}} \quad (4.17)$$

$$\text{Minimum voltage error} \quad E_{\text{minVM}} = \frac{V_{\text{max}} - V_{\text{min}}^{\text{ref}}}{V_{\text{min}}^{\text{ref}}} \quad (4.18)$$

where subscript min, max denotes the minimum/maximum over the time and element index (b for the buses, l for the lines, i for the transformers), superscript ref indicates the reference case values.

A Reference case

The DSO *Romande energy* deployed 600 smart meters in the Rolle area. Those data are not accessible for privacy reasons, as explained above. In this work, we assume that if at least 3 customers are metered by the smart meters for a given location in a network, aggregating the consumption to a single virtual smart meter is enough to preserve individual customers' privacy. This is typically the case for multi-family buildings. Those virtual meters have been located in their exact network location in the reference case (39 loads). In case two or more meters measure the same customers' consumption, they are also considered as one single smart meter and aggregated together (their location in the network is, however, not known). All other smart meter measurements have been allocated in the networks by using an estimation of building consumptions based on SIA norms. Finally, meters that appear to measure consumption and production (a PV system in a self-consumption scheme) have been discarded. Over the initial 600 smart meters, 257 consumption profiles (referred to as the smart meter measurements) are used in the reference case. The loads cover six low voltage networks, as shown in Figure 4.15.

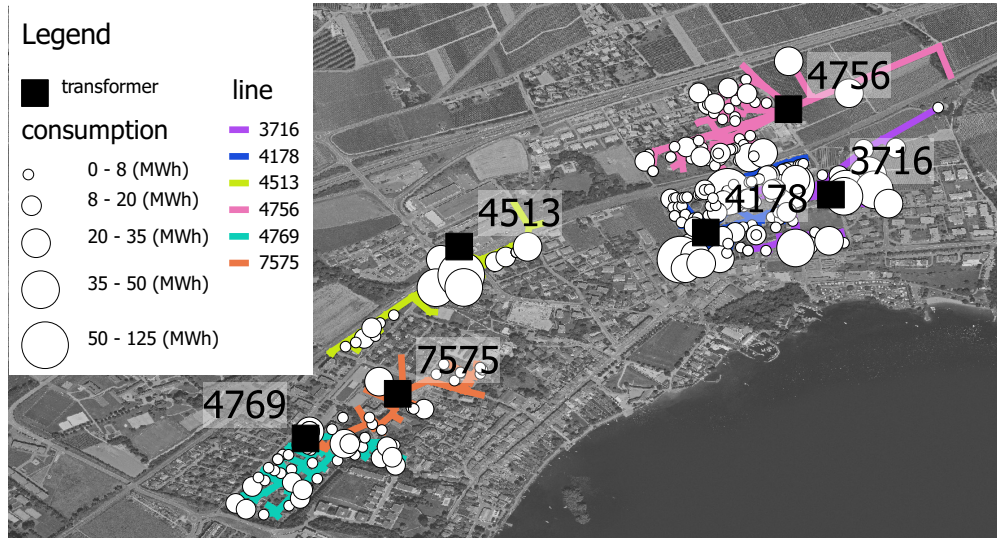


Figure 4.15 – Map of the six networks and reference loads annual consumption

B Load allocation database and parameters

For the load allocation method, a database of smart meter measurements is required. The loads are split into three categories, Apartment, House, and Not residential (hereafter Not res.). The loads' database gathers smart meter measurements from a large set of non-residential sites, the FLEXI [Perret et al., 2015], and FLEXI 2 [Perret et al., 2019] projects presented in Chapter 2. The number of loads in the database has to be compared with the number of loads present in each network and category, as reported in Table 4.6. The parameter k^h , representing the maximum number of allocation of a load in a particular network, is obtained by dividing the number of loads in the network by the number of loads in the database for a given category. All measurements have a resolution of 15 mins and cover one year. The energy and power tolerances for the allocation (ϵ_E and ϵ_P) are set to 5 and 1%, respectively.

4.3. Methodologies for creating realistic test cases for energy planners

Table 4.6 – Number of load per category (Not res. is not residential) and median annual consumption for each network (TR#, left side) and each database source (src. , right side)

TR #	Category	Network		Database		Src.
		# load	Median cons. (MWh)	# load	Median cons. (MWh)	
3716	Apartment	13	11.2	38	3.3	FLEXI
	House	15	5.4	46	4.4	
	Not res.	22	11.6	1	22.4	
4178	Apartment	9	20.2	44	2.1	FLEXI 2
	House	51	4.5	48	4.2	
	Not res.	6	10.0			
4513	Apartment	18	4.1			Not res.
	House	3	3.7			
	Not res.	9	11.0	3	407	
4756	Apartment	3	4.3			
	House	28	5.4			
	Not res.	18	9.9			
4769	Apartment	4	4.2			
	House	26	4.9			
	Not res.	14	12.5			
7575	Apartment	2	65.9			
	House	11	4.9			
	Not res.	5	5.1			

C Smart meter anonymization method

As stated in the reference case description, *Romande Energy* provided the 257 smart meter measurements located in the six sub-networks. To mimic a real case, the measurements' true locations are unknown except for the measurements grouping three or more customers (39 loads in total). For all other loads, the smart meter anonymization (SMANET) technique should be applied. The first step is to define the features of the loads. In a primary approach, the energy ($E_i = \sum_t P_{i,t} \cdot TS_t$), and maximum power ($P_i^{\max} = \max_t P_{i,t}$) are used as input features for the partitioning (the features are pictured in Figure 4.16a. The second step is to perform the partitioning using the recursive spectral graph partitioning method. For this step, the features are normalized to have zero mean and unity variance before calculated the distance matrix D . The target group size is set to three records. The resulting groups are pictured in Figure 4.16b.

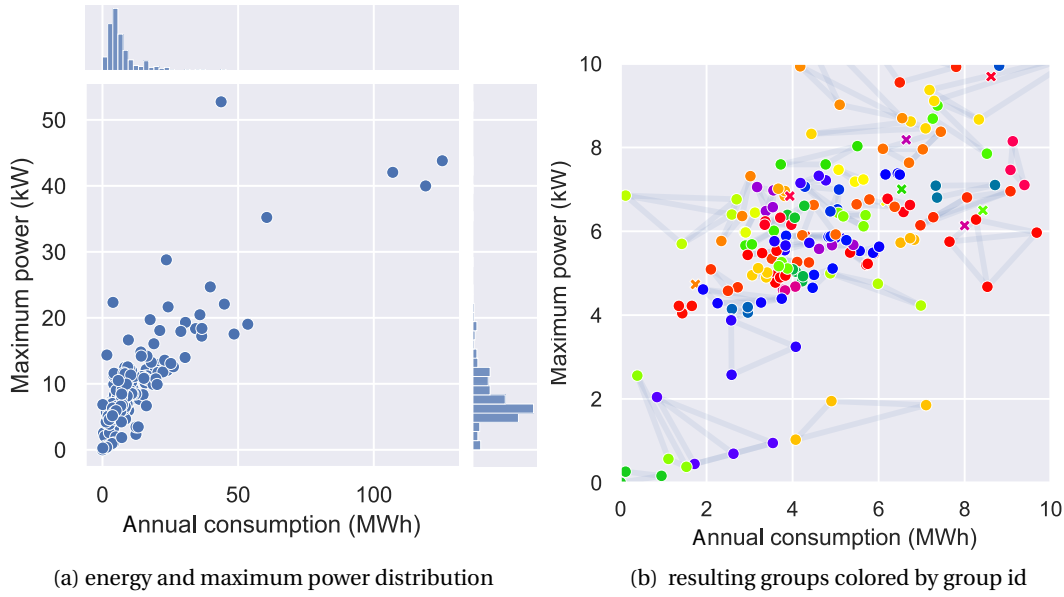


Figure 4.16 – Smart meter measurements features and results of the partitioning

D Features choice for SMANET

In a second approach, we intend to measure the impact of the feature choice on the load flow solution's accuracy. To do so, we defined five partitioning scenarios:

Energy and maximum power These are the same features as define just above, hereafter shortened "E + max P".

Energy Only the annual energy consumption is considered.

PCA From a set of features proposed by [Beckel et al., 2012], we perform a principal component analysis (PCA) and keep the first N components that explain 99% of the dataset variance.

Affinity Again, the Energy and maximum power are used as input features, but instead of the distance matrix, the affinity matrix is provided ($A_{i,j} = 1/D_{i,j}$). This implies in the formulation of the RGSP to find the partitioning with the largest intra-cluster variance.

One group instead of grouping the records by three, all records (except those measuring more than three customers) are put in a single group.

The resulting four additional partitioning scenarios are pictured in Figure 4.17. In these figures, we kept the projection on the Energy - max Power plane. This can lead to unnatural cluster representations as for the PCA scenarios (Figure 4.17b). Note that for the Energy scenarios (Figure 4.17a), the clusters are formed by vertical slicing of the dataset.

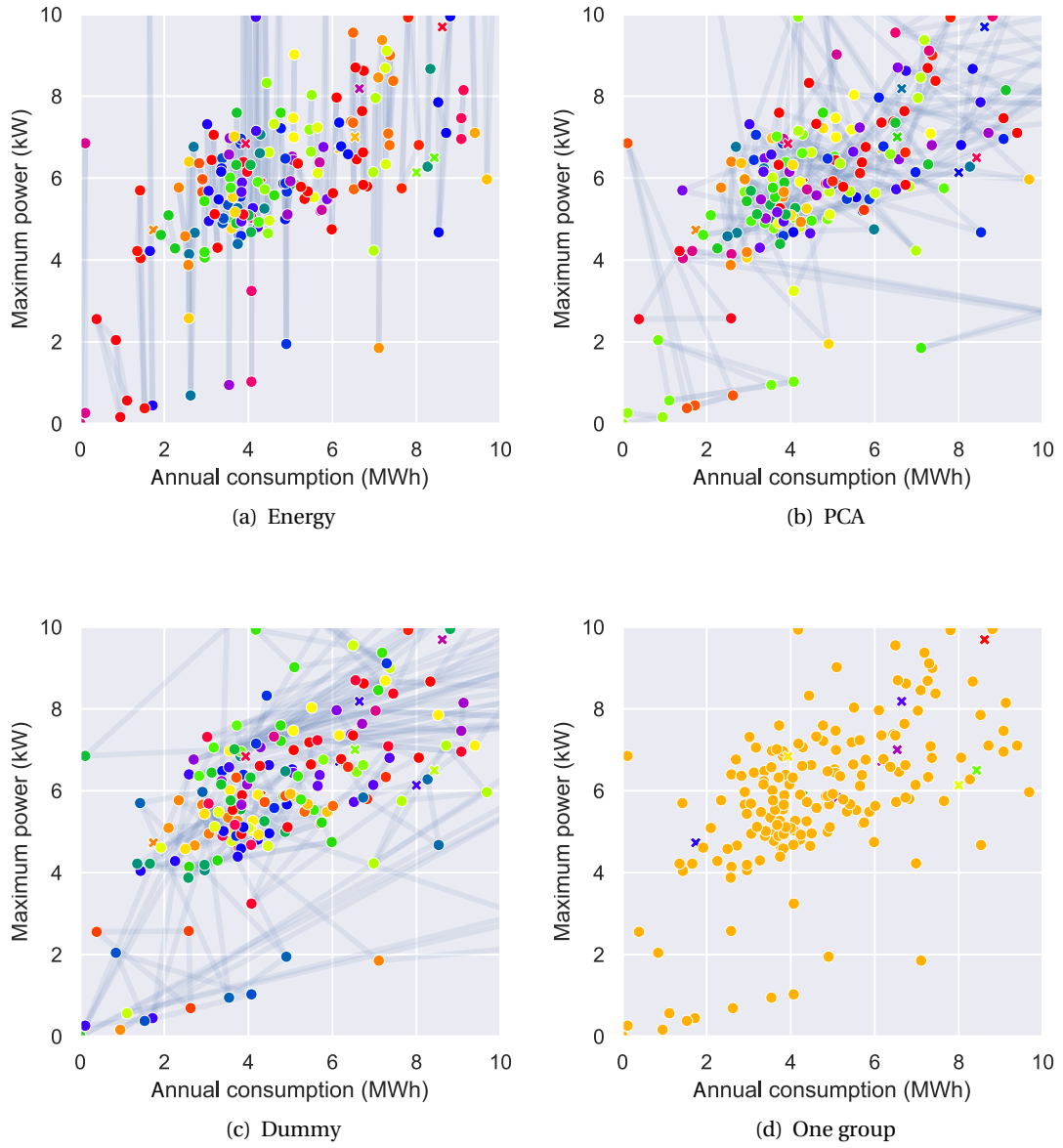


Figure 4.17 – Four additional partitioning scenarios. Measurements with more than three customers are marked with a \times .

As described in the workflow of the SMANET methodology Figure 4.9, the final stage is to randomly select one permutation of the buses per group and allocate each load to its bus. In this second part, to account for this method's stochastic nature, the load flow problem is solved 200 times each time with a new permutation of the buses-loads assignment.

To test the validity of the method, *Romande Energy* kindly agrees to participate in this experiment. To mimic a real application of this methodology, *Romande Energy* used the true

location of the load to get a reference solution of the load flow problem. Then, they applied the presented methodology and run 200 times the load flow simulation for each partitioning scenario.

4.3.4 Results

A Load allocation and SMANET comparison

The voltage error distribution across all times and all buses in the six networks are pictured in Figure 4.18. Both the allocation and the SMANET method give errors mostly below 0.002 pu, which are already sufficient for most network studies. The SMANET process seems to provide slightly smaller errors. These minor errors can be explained by the fact that during a large portion of the year, the active power demand is small compared with the network capacity (during the night, for instance), leading to a local voltage close to 1 pu.

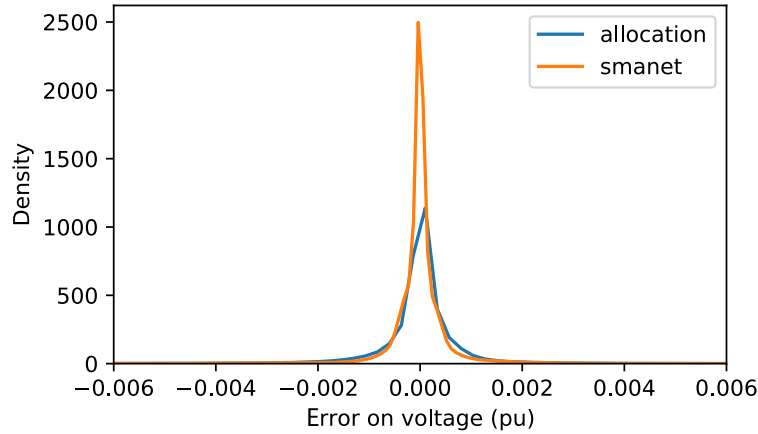


Figure 4.18 – Voltage error

To balance this effect, one must look at what is happening at the transformer nodes. The transformer's active power is plotted for the six networks for a particular day in Figure 4.19. This figure shows how the second stage optimization of the allocation method improves transformer state estimation accuracy compared with the first stage obtained power (blue dots). By definition, the maximum power deviation at the transformer should be smaller than 1%. For this reason, the allocated (stage 2) curve is very close to the true one. The resulting power at the transformer obtained with the SMANET method also leads to very good results. The quality of this method also lies in the fraction of the network loads that are given by the measure of more than the required three customers. In other words, for a network where all loads are multi-family buildings with more than three apartments, all loads' locations are known, and the network state estimation is very accurate (and there is no need for the anonymization methodology).

4.3. Methodologies for creating realistic test cases for energy planners

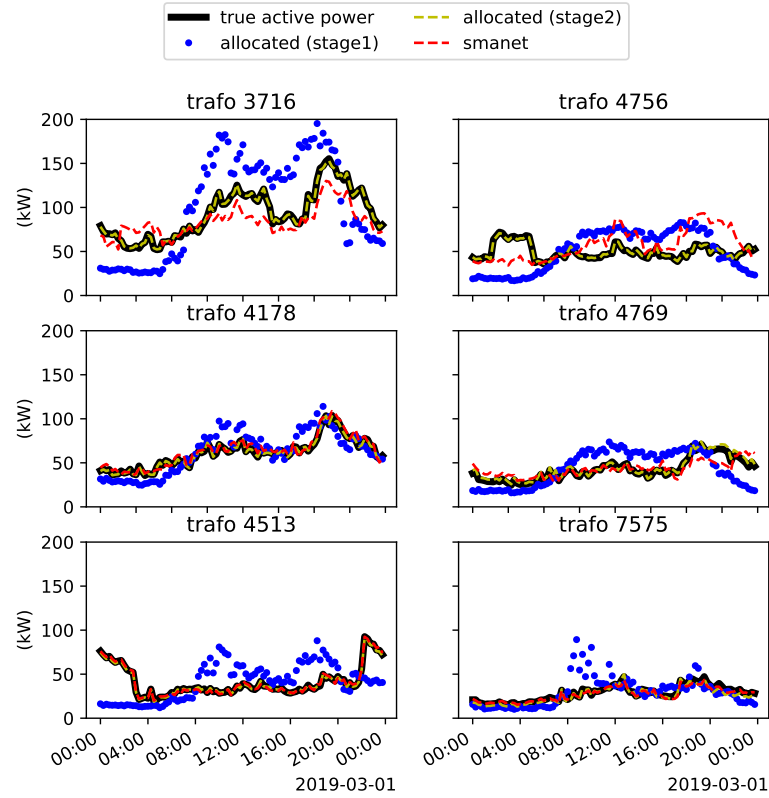
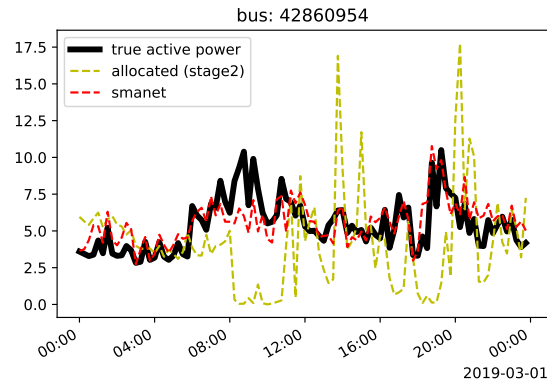
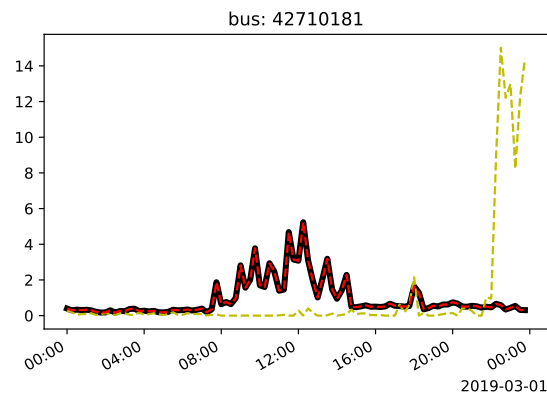


Figure 4.19 – Active power at the transformer nodes

Despite the good voltage accuracy for both methods, the local power allocated to a given network location (bus) is closer to the SMANET method than with the allocation method (Figure 4.20). The illustrative example of Figure 4.20b shows that the SMANET benefits from the network location knowledge in some cases. It also happens that by chance (1 out of 3), the load allocated to this bus is the actual original load of this bus.



(a) fully allocated load



(b) naturally anonymized load

Figure 4.20 – Example of active power at two buses

Finally, the key performance indicators are reported in Table 4.7. Again thanks to prior knowledge of the load locations, the SMANET method is slightly more accurate. The minimum voltage estimation error is below 3 % for both methods. The maximum transformer loading is underestimated by 19% for the SMANET methods versus 1.23 % for the allocation methods. The advantage of the allocation method on this metric is the constraints on the transformer's power that should be below 1% in this case. The additional 0.23% comes from the fact that no prior knowledge of the grid losses is used in the allocation (the transformer's power is assumed to be the sum of the network loads, neglecting the line losses). The accuracy of the SMANET methods also depends on the loads' final allocation, i.e., for a given bus, out of the three loads belonging to the corresponding group, which one is attributed to the bus. Besides, the loads' intra-group similarity is critical to have accurate network state estimation. In the following, this is discussed by evaluating the five partitioning scenarios and running, for each scenario, 200 times the load-flow simulation.

4.3. Methodologies for creating realistic test cases for energy planners

Table 4.7 – Performance indicators

	allocation	SMANET
MSE_{vm}	$6.33 \cdot 10^{-7}$	$3.20 \cdot 10^{-7}$
E_{maxTRL}	1.23 %	-18.90 %
E_{maxLNL}	1.83	$-5.46 \cdot 10^{-5}$
E_{minVM}	-2.76 %	0.16 %

B Features influence on SMANET accuracy

As mentioned, to have a clear overview of the SMANET accuracy, the load flows are solved several times with a new load-bus assignment. The key performance indicators are recorded for each iteration. Figure 4.21 pictures the mean square error value (calculated for all buses at all time for all iterations until the i^{th} iteration, and normalized by its value at the 200th iterations). This figure shows the convergence of the mean square error for all partitioning scenarios.

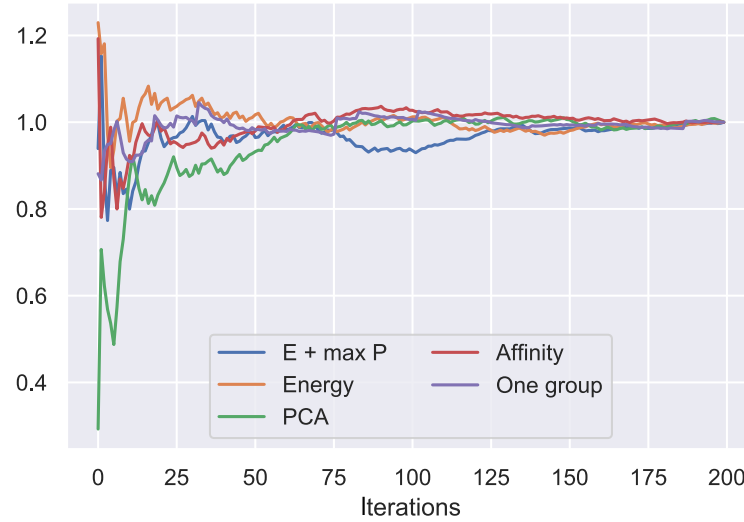


Figure 4.21 – MSE convergence

The voltage magnitude error (across all time, buses, and iterations) is plotted in Figure 4.22. Again the error is mostly smaller than 0.002 pu. Except for the Dummy and One group scenarios, the three other scenarios provide similar accuracy from this perspective.

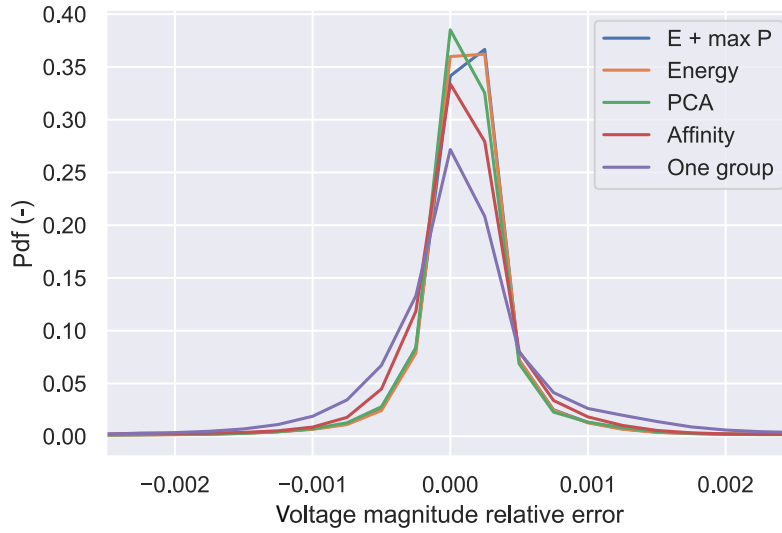


Figure 4.22 – Error on voltage magnitude

The mean square error of the voltage magnitude and its standard deviation (across iterations) are reported in Table 4.8. Again no significant differences are observed between scenarios, except for the Dummy and One group scenario that gives slightly larger MSE.

Table 4.8 – Mean squared error of the voltage magnitude for the five partitioning scenarios

	E + max P	Energy	PCA	Affinity	One group
Mean	$2.02 \cdot 10^{-8}$	$1.70 \cdot 10^{-8}$	$2.02 \cdot 10^{-8}$	$2.24 \cdot 10^{-8}$	$3.92 \cdot 10^{-8}$
Std	$7.66 \cdot 10^{-9}$	$6.84 \cdot 10^{-9}$	$9.05 \cdot 10^{-9}$	$7.18 \cdot 10^{-9}$	$1.68 \cdot 10^{-8}$

4.3.5 Discussion

In this work, two methods to use smart meters for network analysis are proposed. The first method is based on an allocation approach. First, the allocation is formulated as a mixed-integer problem to allocate loads from a database to the network locations based on the annual energy demand difference. Second, an adjustment stage deforms the original loads to match the power at the transformer. For estimating the transformer load, this method is the most appropriate.

The second method aims to anonymize the smart measurements extracted from a given set of networks by grouping the smart meter loads by three and linking this group to a set of three network locations (buses). The final load-bus allocation is achieved by randomly assigning a load to a bus in the considered group. This method could allow for stochastic analysis of the network stage (by randomly permuting the assignment). It could improve the quality of the

network analysis but at a higher computational burden.

Although both methods provide very similar results in terms of network state estimation accuracy, the SMANET approach should be preferred as soon as smart meter data are available inside a given network. When this is not the case, the allocation of smart meter measurements from an external network is a suitable solution. The allocation and SMANET approach could be combined. For the network locations where smart meters are installed, the SMANET approach could be used. For the network location where no smart meter is currently set up, smart meter data acquired outside the considered network(s) could be allocated to these locations. In such a case, it would be better to use load profiles from another network than just re-using the one measured in the network to avoid simultaneous peaks. If it is not possible, the second stage optimization of the allocation method should reduce this issue by deforming the loads.

Considering realistic loads in a network is a prerequisite to perform robust network analysis and energy planning study. The following section will use the allocated loads' method to study the effect of electricity tariffs on the network state facing high PV penetration.

4.4 Mitigating the impact of distributed PV using electricity tariffs

The decarbonization of Switzerland has essentially two requirements. First, provide clean and affordable electricity, which is known to imply massive investment in PV systems. Second, it needs the electrification of the building heating systems. Reaching the full PV potential in urban environments could lead to a system in which a significant fraction of the energy should be curtailed to cope with the network operating constraints. Optimal PV placement and orientation can moderate this issue by lowering the injection peak [Middelhaue et al., 2021], but their choice is mostly profit-driven. Similarly, the complete electrification of the building heating system may require investment in network reinforcement to ensure that the lines are suitably sized to distribute higher power. Although a central control of the heat pump is already widely used by DSOs (for load shedding during peak hours), PV curtailment is a promising solution. However, it could raise concerns about intrusiveness and discourage (potential) prosumers. An alternative approach to central control is to propose novel electricity pricing mechanisms that could help to mitigate the impact of distributed PV systems on the grid while allowing building owners to make profitable investments. This work aims to evaluate which advanced electricity tariff creates the best trade-off between these two objectives.

In this work, we investigate the effect of five different tariff scenarios on network operation when optimizing the design and operation of all buildings connected to that network, using the methodology developed in Chapter 3 and used in Section 4.2. The scenarios consider pure volumetric electricity tariffs, a mix of volumetric and capacity-based tariffs, or a block rate tariff. The optimization is run for a set of buildings in a sub-network of Rolle (Switzerland). The buildings' characteristics are known from a geographical information system and the Swiss building norms. The resulting loads and generations at each injection point allow for solving the load flow problem over a whole year to extract the voltage level and line loading

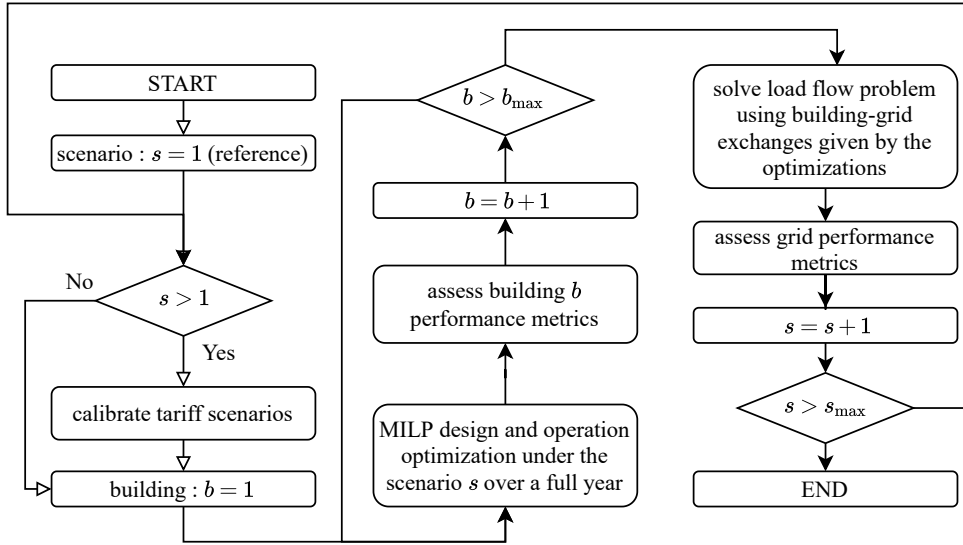


Figure 4.23 – Process workflow

distribution. Finally, these distributions are compared with a reference case to assess the effect of the selected tariffs.

4.4.1 Methodology

A General workflow

The methodology to assess the impact of distributed PV on a low-voltage grid consists in a two-step process, which is sequentially repeated for each tariff scenario. First, the design and operation of each building energy system are individually optimized using the MILP formulation of Equation 4.4 with the corresponding grid exchange cost. After each building optimization, the performance of the considered building is assessed. Once all buildings have been optimized, the load flow problem is solved for a distribution grid using the building-grid power exchanges resulting from the first step. Finally, the impact on the grid is assessed by evaluating dedicated grid performance metrics. The workflow of this process is illustrated in Figure 4.23. The first scenario ($s = 1$) serves as a reference scenario. The other scenarios' tariff parameters are calibrated such that the revenue of the DSO stays as close as possible to the revenue of the reference case. In this section, we do not distinguish between revenues for grid maintenance and energy retail.

B Case study and scenario definition

The case study is a district of Rolle. In particular, a low-voltage network and all related buildings connected to this network (exceptions are buildings with no known consumption or building characteristic data) are considered for this work. A map of the sub-network is



Figure 4.24 – Annual energy demand (heat assumed generated with a COP of 4) and PV potential capacity. Circles with the same size indicate a PV penetration of one.

pictured in Figure 4.24. This figure also shows the PV potential and annual energy demand with orange dashed and yellow circles. The map is made so that if the circles have the same size, it indicates a PV penetration close to one. The building size is determined by its floor area, which is approximated by the building footprint times the number of levels. The distribution of building floor area is pictured in Figure 4.25.

For each building in this network, the building and its roof characteristics are extracted from the cantonal registry of building⁴ and a geographical information system (namely *solar roof*⁵). The electric load profile is obtained using the allocation method presented in Section 4.3.1. The annual energy demand was obtained from *Romande Energy*, and the power at the transformer is measured using *Depsys Grid Eye*⁶ devices. The buildings' minimum temperature is assumed to be 19 °C. This is also the initial temperature. The tank's minimum temperature is 59 °C, and the initial temperature is 60 °C (the nominal temperature for domestic hot water is 60 °C according to the [SIA, 2015] norms). All other parameters that are building dependent are reported in Appendix C, Table C.1. The PV price, battery, corresponds to the estimated price of 2030 (using the method in [Bloch et al., 2019]). There is a fixed cost for PV of 10'049 CHF and a variable cost of 83 cts/W. The battery cost is 182 CHF/kWh without a fixed installation cost. The HP and EH costs are 1.5 and 1.2 CHF/W, respectively. All parameters are reported in Table 4.9.

⁴<https://www.housing-stat.ch/fr/accueil.html>

⁵<https://www.uvek-gis.admin.ch/BFE/sonnendach>

⁶<https://www.depsys.com/solutions/>

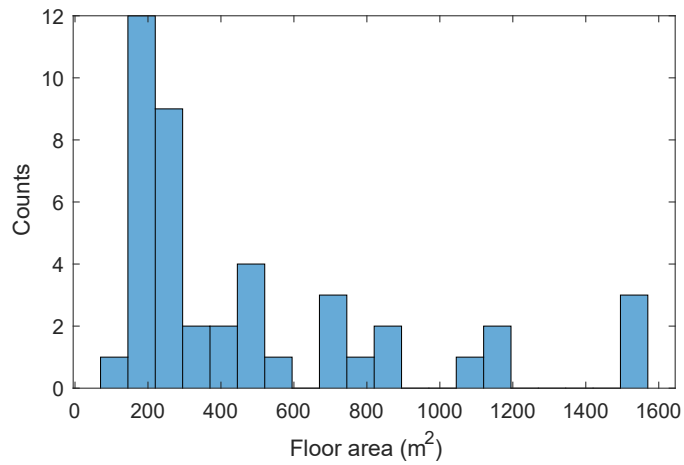


Figure 4.25 – Distribution of the building floor area

Table 4.9 – Technology and cost parameters

	Param.	Unit	Value		Param.	Unit	Value
SYSTEM	T	-	35040		L	years	25
	M	-	12		L^{bat}	years	9
	TS	s	900		r	-	0.03
PV	N	-	8	BATTERY	SOC_{init}	-	0.7
	J	-	8		$\text{SOC}_{\text{min,max}}$	-	0-0.7
	c_F^{PV}	CHF	10'049		α	1/day	0.04
	c_{mod}	CHF/W	0.83		$\eta^{\text{cha,dis}}$	-	0.98
	$P_{\text{nom}}^{\text{mod}}$	W	315		$\text{CR}^{\text{char,dis}}$	1/h	1
	A^{mod}	m ²	1.63		c^{bat}	CHF/kWh	182
	γ^{PV}	-	0.5%		c_F^{bat}	CHF	0
HP	c^{hp}	CHF/W	1.5	EH	c^{el}	CHF/W	1.2
	q^{carnot}	-	0.8		η^{el}	-	0.99
OTHER	$T_{\text{min}}^{\text{b}}$	°C	19				
	$T_{\text{min}}^{\text{tank}}$	°C	59				
	$T_{\text{max}}^{\text{sh}}$	°C	85				

4.4. Mitigating the impact of distributed PV using electricity tariffs

In this study, we defined five tariffs scenario:

reference a standard flat volumetric tariff. $c^{\text{imp}} = 21.02$ cts/kWh and $c^{\text{exp}} = 8.16$ cts/kWh.

solar a volumetric double tariff. The low rate tariff applies from 11:00 to 15:00 every day (local time). The ratio between the high and low rate is fixed to 1.57.

spot market a volumetric variable tariff. It is based on the continuous intraday price from the EPEX market data⁷).

capacity a mix between a volumetric and a capacity-based tariff.

block rate a piecewise linear cost function where the cost of buying/selling energy depends on the power at which it is exchanged.

In addition to these five scenarios, we consider two side scenarios, derived from the reference one, that help to compare the results:

only loads we consider neither PV nor battery, but instead, the optimization consists in sizing the heat pump and electric heater under the reference tariff scenario.

full PV this scenario just imposes all roofs being covered with the maximum PV potential, no battery, and again optimize the heat pump and electric heater capacity.

The tariff parameters are calculated based on the results of the reference scenario. Nevertheless, these parameters are reported in Table 4.10.

⁷EPEX price for 2018 <https://www.epexspot.com/en/market-data/intradaycontinuous/intraday-table/-/CH>

Table 4.10 – Tariff scenarios

Scenario	Description	Tariff (CHF cts/kWh)	
Reference	c_t^{imp} :	21.02	
	c_t^{exp} :	8.16	
Solar	$c_{t \in 11h:15h}^{\text{imp}}$:	14.61	
	$c_{t \in 11h:15h}^{\text{exp}}$:	7.15	
	$c_{t \notin 11h:15h}^{\text{imp}}$:	23.05	
	$c_{t \notin 11h:15h}^{\text{exp}}$:	11.24	
Spot market	c_t^{imp} :	EPEX*3.9867	
	c_t^{exp} :	EPEX*1.6547	
Capacity	c_t^{imp} :	14.12	
	c_t^{exp} :	11.52	
	c^{pow} :	5.41 CHF/kW/month	
Block rate	Power (kW)	a_k^{IMP}	a_k^{EXP}
	0 to 1	13.93	13.27
	1 to 2	15.33	11.87
	2 to 4	17.15	10.05
	4 to 6	19.51	7.68
	6 to 8	22.59	4.60
	8 to 10	26.59	0.61

C Performance indicators

The following list defines the performance metrics for the design and operation and the grid usage.

4.4. Mitigating the impact of distributed PV using electricity tariffs

PV hosting ratio	$PV_{\text{host}} = \frac{\sum_{i=1}^N n_i^{\text{mod}} P_{\text{nom},i}^{\text{mod}}}{\sum_{i=1}^N n_{\text{max},i}^{\text{mod}} P_{\text{nom},i}^{\text{mod}}}$	(4.19a)
Total electrical demand	$P_t^{\text{tot}} = P_t^{\text{load}} + P_t^{\text{el}} + P_t^{\text{hp}}$	
PV penetration	$PVP = \frac{\sum_t P_t^{\text{PV}}}{\sum_t P_t^{\text{tot}}}$	(4.19b)
PV curtailment	$PV_{\text{curt}} = \frac{\sum_t P_t^{\text{cur}}}{\sum_t P_t^{\text{PV}}}$	(4.19c)
Battery autonomy ratio	$Bat_{\text{auto}} = \frac{E_{\text{cap}}^{\text{bat}}}{\text{mean daily consumption}}$	(4.19d)
Self-sufficiency	$SS = \frac{\sum_t \left(\min(P_t^{\text{tot}}, P_t^{\text{exp}} - P_t^{\text{imp}} + P_t^{\text{tot}}) \right)}{\sum_t P_t^{\text{tot}}}$	(4.19e)
Relative heat need	$Q' = \frac{\sum_t (\dot{Q}_t^{\text{hp}} + \dot{Q}_t^{\text{el}})}{\sum_t \dot{Q}_t^{\text{heat}}}$	(4.19f)
Discounted payback time	$DPP = L \text{ such that } \sum_{y=1}^L \frac{CF_y}{(1+r)^y} = 0$	(4.19g)
Cash flow	$CF_y = CAPEX_y + OPEX_y - OPEX_y^0$	
Grid usage	$GU^{\text{imp,exp}} = \frac{\max_t P_t^{\text{imp,exp}}}{\max_t P_{\text{only loads}}^{\text{imp}}}$	(4.19h)

where \dot{Q}^{heat} is the minimum heat to fulfill for both space heating and domestic hot water demand, the $OPEX^0$ is the operating cost assuming no investment is made (assuming all heat demand is provided by an electric heater), and $P_{\text{only loads}}^{\text{imp}}$ is the maximum import power under the "only loads" scenario, which only solves the optimization for the heat pump and electric heater capacity (and their operation).

In addition to these metrics, we use normalization of the PV, battery, heat pump, and electric heater capacities with the building floor area. The corresponding metrics are denoted PV cap', Bat cap', HP cap', and EH cap' respectively. The floor area is defined as the building footprint area multiplied by the number of levels.

4.4.2 Results

The computation time statistics are reported in Section 4.4.2. The optimization time range between 2.4 up to 321 minutes (5 hours and 21 minutes). The most computational intensive scenario is the block rate scenarios with a median computing time just above 100 min. Solving the load flow problem is performed in 7 minutes for all scenarios, which is negligible compare with the 8 to 80 hours of optimization time.

Table 4.11 – Computation time statistics

Scenario	Building optimization				Load flow
	min [min]	max [min]	median [min]	total [h]	
Reference	3.7	57.3	13.6	11.8	6.6
Solar	2.4	41.6	11.3	8.8	6.6
Spot market	2.4	43.6	13.1	10.2	6.8
Capacity	31.8	147.2	90.4	60.6	6.6
Block rate	43.5	321.2	103.9	81.2	6.6

The normalized technology capacities are reported in Figure 4.26. The block rate leads to smaller PV capacity. As the marginal cost of exporting electricity decreases as a function of the export power (see Table 4.10), most of the time, high PV capacity systems will export energy at high power and sell energy at an unprofitable rate. Variable volumetric and capacity tariffs promote larger batteries, while the block rate scenario causes only slightly larger battery capacity than the reference scenario. Most systems have no electric heater in the reference solar and spot market scenario. However, capacity and block rate tariffs induce larger electric heater capacity, which compensates for reducing heat pump capacity for those scenarios.

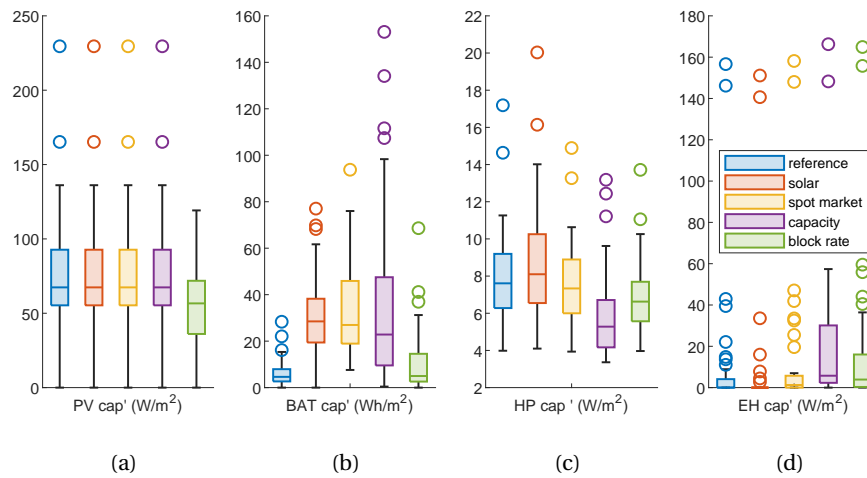


Figure 4.26 – Normalized technology capacities for all tariff scenarios

Figure 4.27 shows only the median, 25th and 75th quantile of each metric for each scenario. Instead of the floor area normalized PV and battery capacity, the PV hosting and battery autonomy ratio are used. This highlights that the 60 W/m² median value for the PV capacity corresponds to the maximum hosting capacity. As suggested, dynamic volumetric scenarios have a higher battery autonomy ratio. The median battery size increase from 5% of the daily consumption (recalling the definition of the battery autonomy ratio, Equation 4.19d) up to

4.4. Mitigating the impact of distributed PV using electricity tariffs

25% for the solar and spot market scenarios. From an operational point of view, this increase of flexibility capacity (observed for all technology compared to the reference case) induces an increase in the grid usage for volumetric tariffs. In contrast, it induces a decrease in grid usage (both import and export) for block rate and capacity tariffs. The discounted payback time, which accounts for the time to recover all investment (including the heat provision technologies), ranges from 7 to 10 years. This is quite optimistic because investing in heat pumps strongly reduces electricity consumption compared with using purely resistive heating.

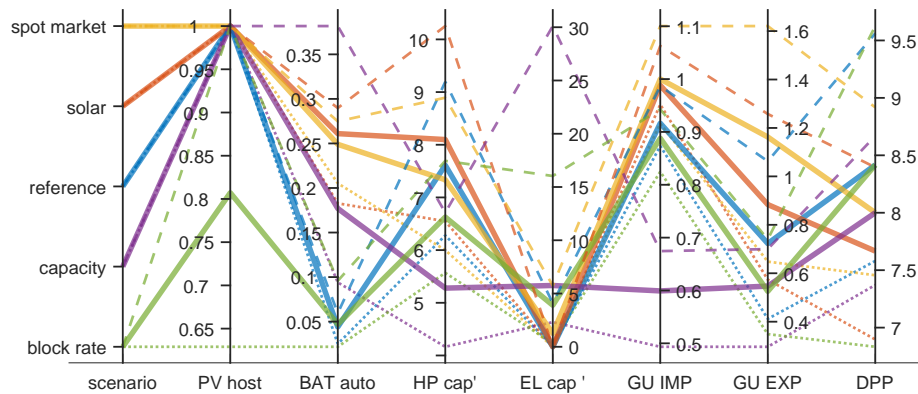


Figure 4.27 – Metrics as defined in Equation 4.19, in parallel coordinates. Solid lines are the median, dashed lines are the 75th percentile, and dotted lines are the 25th percentile.

The battery size tends to increase with the PV penetration, according to Figure 4.28, for volumetric-based tariffs. However, this is not so clear for the capacity-based and block rate scenarios. A previous work, considering only PV and batteries [Holweger et al., 2020a], shows that the battery autonomy ratio increases for PV penetration from 0 to 1.5 and decreases at higher PV penetration. This can also be seen in Figure 4.28. For all scenarios, the battery size helps to increase self-sufficiency, as highlighted by Figure 4.29.

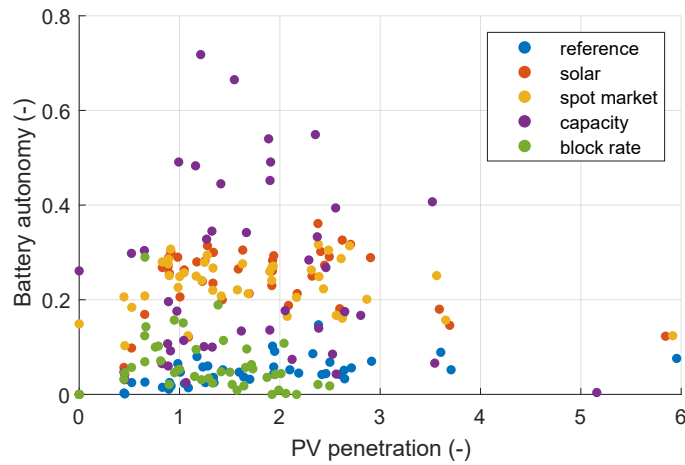


Figure 4.28 – Battery autonomy versus PV penetration

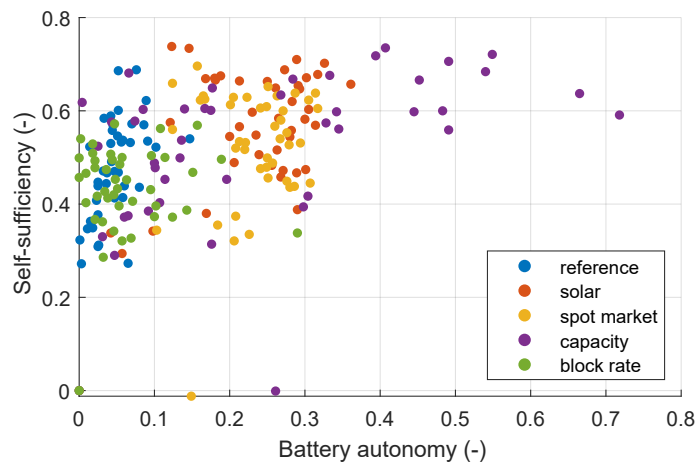


Figure 4.29 – Self-sufficiency level against the battery autonomy ratio

The relative heat need in Figure 4.30 compares the actual heat production and the minimum theoretical heat consumption. In this figure, the only loads scenario is plotted to highlight that the relative heat need ranges from 1.05 to 1.5. It essentially represents the tank losses. Indeed in this scenario, the objective function pushes to minimize the cost of providing heat. This metric increases when adding PV (full PV and reference scenarios), which implies that the building and tank are used as storage in a sub-optimal way (from the heat consumption perspective) to improve the objective functions. It is, even more, the case for the solar, spot market, capacity, and block rate scenarios (although the latter has a much smaller installed PV capacity).

4.4. Mitigating the impact of distributed PV using electricity tariffs

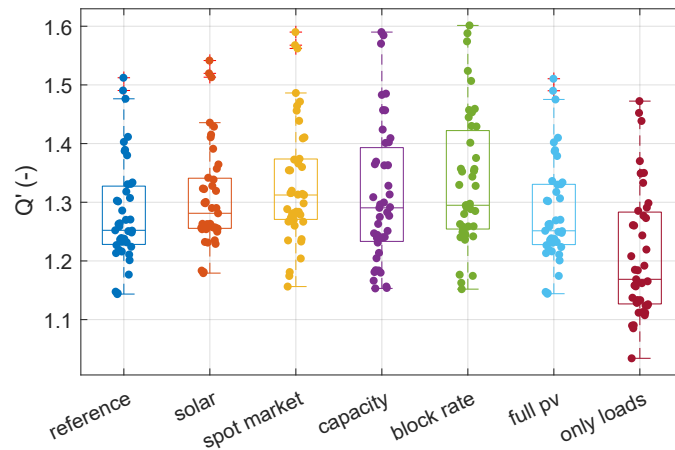


Figure 4.30 – Relative heat consumption

As highlighted in Figure 4.27, the grid usage intensity is dominated by the export. This can be explained in two ways. First, there are cases where an excess of PV production is injected into the grid. Second, there are cases where there are substantial price incentives to inject into the grid. The latter can typically explain why the spot market scenario has much higher grid usage for export than the reference scenario. On the opposite, block rate and capacity scenario have much smaller grid usage. The reason lies in the PV curtailment pictured in Figure 4.31 as a function of the PV penetration. For capacity and spot market scenario, the PV curtailment increase with the PV penetration. This is easily explained for the capacity tariff as the export power can be cheaply reduced by curtailment. For the spot market scenario, curtailment occurs when prices on the EPEX market are negative. No curtailment is observed for the other scenarios.

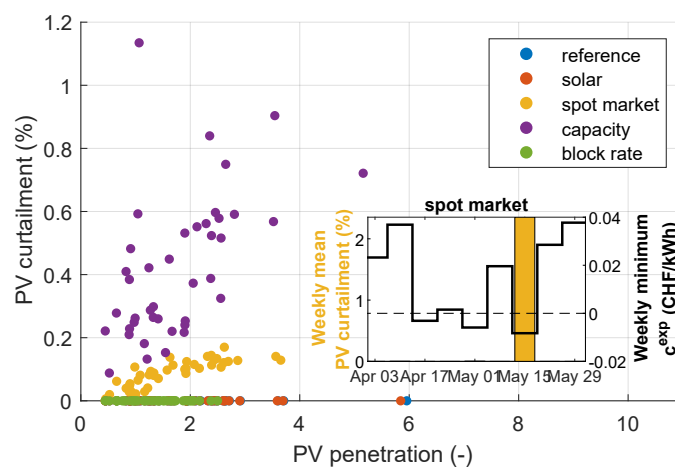


Figure 4.31 – Ratio of energy curtailed and PV penetration. In the inset, the bars are the weekly ratio of energy curtailed (left axis) and lines the weekly minimum c^{exp} (right axis).

To complete this analysis, Figure 4.32 pictures the grid usage for export against import. This allows splitting the systems in essentially three categories as a function of their grid usages. Starting from the top left quadrant, where $GU^{exp} > 1$ and $GU^{imp} < 1$, there are the energy exporters. Their use of the grid is dominated by their max export power. The energy traders increase grid usage both at import and export. Most of the systems under the variable tariff (solar and spot market) fall into this category. Finally, the low grid users have GU^{imp} and $GU^{exp} < 1$. Most systems under the capacity and block rate scenario are in this category. These observations lead to conclude that energy tariffs allow to shape customers' paradigms and strongly impact the way their system interacts with the grid.

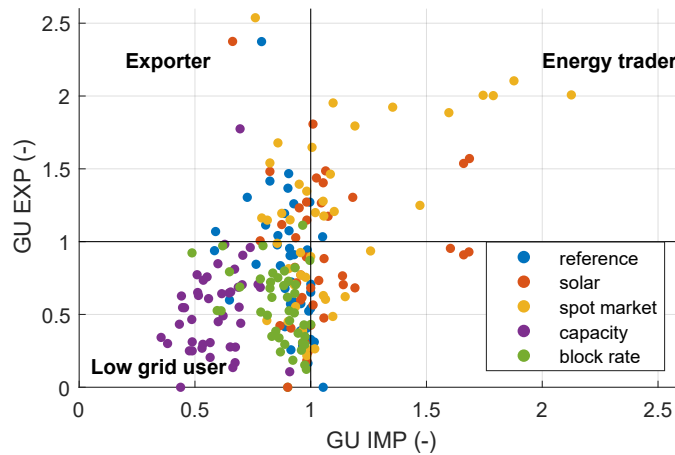


Figure 4.32 – Export grid usage ratio vs. import

Regarding the grid impact analysis of this study, Figure 4.33 shows the load duration curve measured at the transformer for all scenarios (including the full PV and only loads scenario). The cumulated installed PV capacity for each scenario is represented as a colored dot on the y-axis. The block rate reduces the total installed capacity to two-third of the potential capacity (from 1500 kW to 1000 kW). The other scenarios have almost the maximum PV potential capacity (this is why only the blue dots corresponding to the full PV case are plotted). All scenarios, including the only load scenarios, overload the 400 kW transformer capacity either when power is brought from the high-voltage side to the low voltage side (negative value) or, conversely, during excess PV production. Hence, the complete electrification of the building's heating systems requires grid reinforcement. The spot market scenario is the most demanding from the transformer perspective. In contrast, both capacity and block rate scenarios reduce stress on the transformer even when the network consumes energy (see the right inset).

This observation is confirmed by Figure 4.34. The line loading level is just below 60% in the worst case, indicating that the lines are well oversized compared with the transformer. Despite the slight difference between scenarios, one may note that the spot market has higher line loading than the reference. This converts into higher voltage deviation, as pictured in

4.4. Mitigating the impact of distributed PV using electricity tariffs

Figures 4.35a and 4.35b. In these figures, we distinguished the situation when there is local excess (when above 1 pu) or deficit (when below 1 pu) of energy. Again one can note that solar and spot market scenarios induce higher voltage deviation.

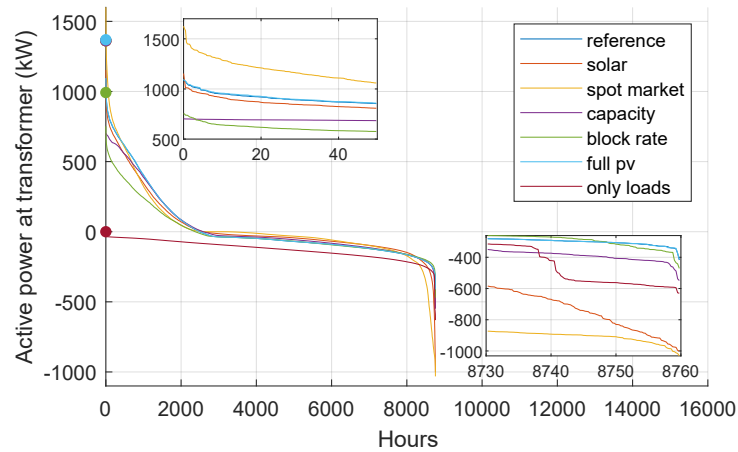


Figure 4.33 – Load duration curve at the transformer. Dots on the vertical axis indicate the total installed PV capacity per scenario. The nominal transformer capacity is 400 kW. Negative values indicate power flow from the high-voltage toward the low-voltage side.

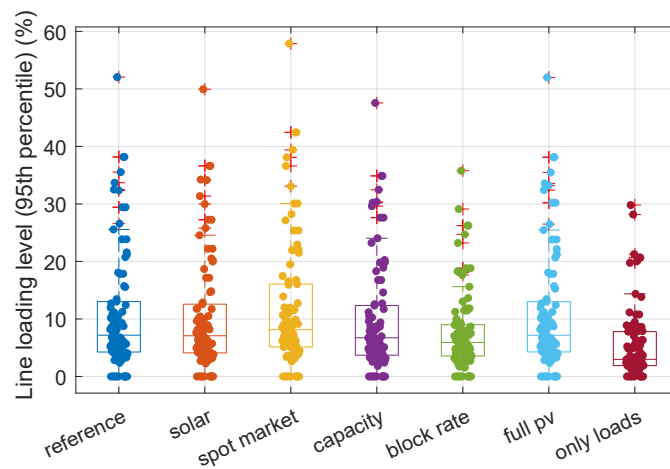
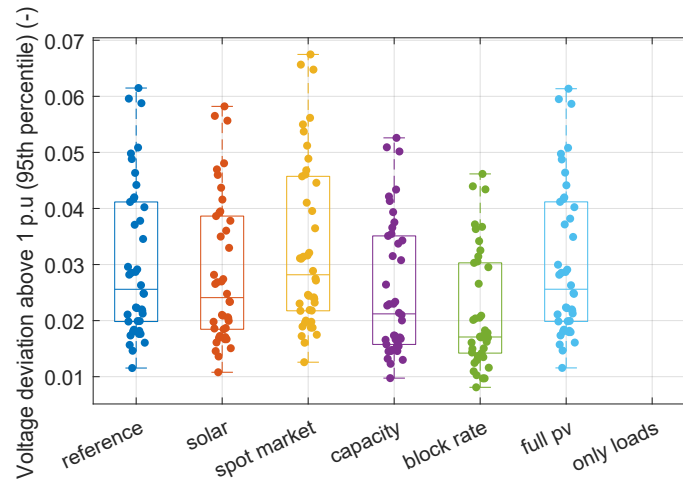
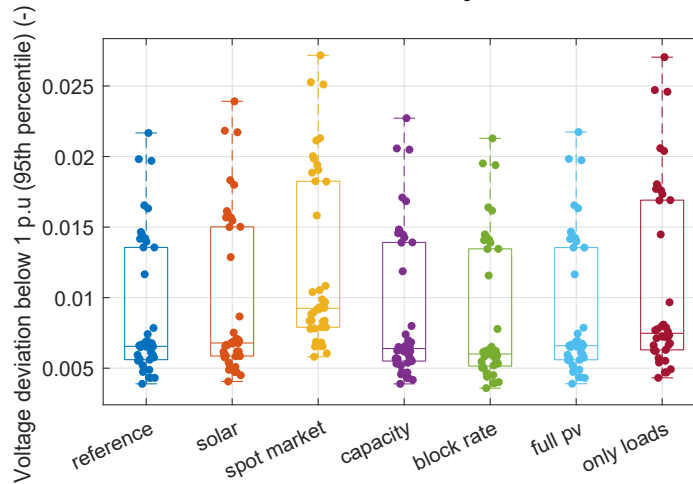


Figure 4.34 – 95th percentile of the line loading level



(a) When above 1 pu



(b) When below 1 pu

Figure 4.35 – Voltage deviation distribution

To conclude this analysis, the systems *LCOE* is plotted in Figure 4.36. It highlights that all systems but one (in the full PV scenario) are highly profitable, as their *LCOE* is below the 21.06 cts/kWh threshold (which corresponds to the reference retail electricity rate), represented by the horizontal dashed line. The only unprofitable system suffers from over-investing in PV. All tariff scenarios have *LCOE* smaller than the reference scenario, indicating that these tariff structures allow, assuming optimal control, better profitability for the customers. Conversely, this implies a loss in the DSO net revenues, as highlighted in Figure 4.37. The DSO revenues are the sum of the grid exchange cost across all systems. However, the block rate scenario, despite having a median *LCOE* smaller than the reference median *LCOE*, turns to have approximately the same or even slightly higher net DSO revenue. Despite the calibration, which ensures that the DSO's revenue remains the same, assuming the systems' design and operation are the reference scenario one, the net DSO revenues vary significantly from one scenario to another. The capacity tariff almost cut by half the DSO revenues compare to the

reference one. However, when comparing the only load scenario and the full PV or reference scenario, the latter cut almost by three the DSO revenues only with the addition of PV. This is related to the fact that less energy is sold to the end customers. The chosen methodology does not allow yet to split the share of the revenues allocated to the grid maintenance and energy retail.

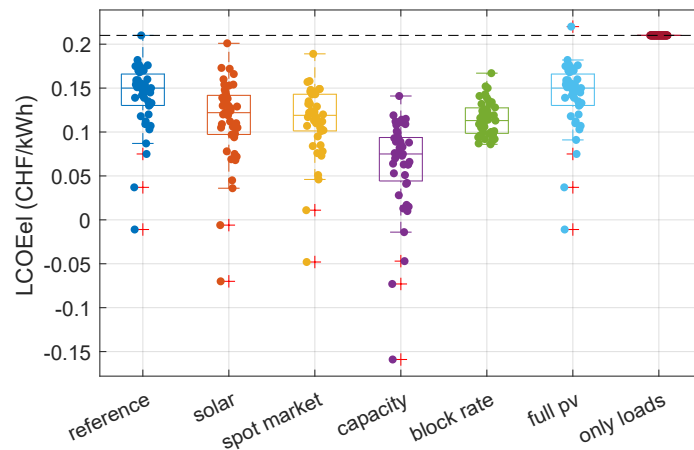


Figure 4.36 – Levelized cost of electricity demand per scenario

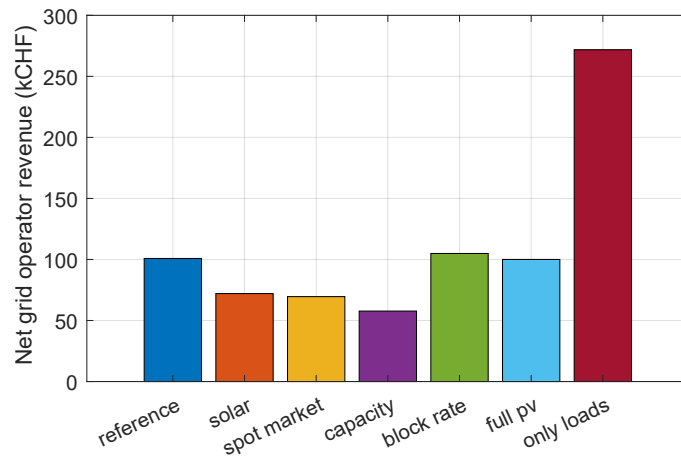


Figure 4.37 – Net revenue for the distribution system operator

4.5 Conclusion

In this chapter, we discussed the opportunity offered by electricity tariffs to promote flexible PV systems and how tariffs change customers' consumption paradigm and impact the grid stress state. To do so, an in-depth analysis was conducted on a single system to define the tariff structures and relevant key performance indicators properly. Three tariff structures

were considered: volumetric, capacity-based, and block rate tariffs. From these structures, four tariff scenarios were defined in addition to a reference scenario (using a standard tariff from *Romande Energy*) and a thermal-only scenario that aims to provide reference values for the heat pump and electric heater capacities. The four additional scenarios consider two time-of-use electricity tariffs, one mix of a capacity-based and volumetric tariff, and one block rate tariff. The investment in PV arrays promotes larger power-to-heat capacities to increase self-consumption using thermal inertia. The batteries' profitability comes from the variability of the electricity prices. However, variable volumetric tariffs increase the grid usage intensity. The contribution of the battery to lower the levelized cost of electricity is relatively small. The uncontrollable electric load should be known to up-scale this analysis to a more extensive set of buildings in a low-voltage network. In energy planning studies, the loads are often synthetic or generated from standard norms, but rarely actual loads from smart meters are used.

In the second part of this chapter, we proposed two methods to use smart meters for energy and network analysis. The first method considers a smart meter load profiles database and allocates them to the buildings at given network locations according to their (annual) energy consumption. Then, the assigned loads are deformed to match the low-voltage transformer active power measurements. The load profiles database consists of smart meter measurements either from the considered network or any other appropriate source.

The second method is a smart meter anonymization procedure we called SMANET. Even if a network were fully monitored by smart meters, the energy or grid planners would not be allowed to access these data for privacy-preserving reasons. Thus, one way to make these data available is to anonymize them. The allocation method presented above is an appropriate anonymization approach but relies on a potentially external load database and does not take advantage of any knowledge of the actual loads' locations. The SMANET's basic principle is to partition the loads (i.e., smart meter measurements) into small equal-size groups. For each group, the list of network locations corresponding to the loads is given in a randomized order. This allows a randomized loads-locations assignment, that preserves the load's anonymity (the exact location is not provided). In this work, we assumed that grouping loads by three is enough for privacy preservation. The task of finding the optimal partitioning of a set of records is not trivial. Hence, a method called recursive graph spectral partitioning (RGSP) was proposed. Both the allocation and SMANET methods were tested to assess whenever using such a load case would affect the network analysis results. It turns out that both provide good results in terms of voltage estimation. The allocation, by formulation, provides any arbitrary accuracy of the transformer load.

Once an appropriate test case of network loads was defined, it was possible to investigate the effect of tariffs on the design and operation of PV systems and their impact on a low-voltage grid.

The final part of this chapter presented how tariffs can mitigate the impact of distributed PV in a low-voltage grid by promoting flexibility and reasonable use of the grid. The insights obtained from this chapter's first part (at the building level) are confirmed in this broader study (at the grid level). Variable volumetric tariffs promote larger batteries and power-to-heat

capacities but also increase the stress on the grid. A capacity-based tariff changes the usage of the battery from energy trading to consumption peaks reduction. Injection peaks can be reduced either using the electric heater (which is a cheap, flexible capacity) or curtailment. The grid usage was effectively mitigated under the capacity and block rate scenarios. The latter also reduces the total PV capacity. This section's general conclusion is that tariffs can determine the intensity customers interact with the grid, thus mitigate voltage deviations, and lines or transformers loading. The main findings of this chapter are summarized in Table 4.12. Regarding the stress on the grid, all scenarios still violate at some point the transformer loading limit. Therefore, there is still a need for DSOs to balance between grid reinforcement and direct control of the system flexibilities. This aspect will be discussed in the following chapter.

Table 4.12 – Impact of tariffs, summary

Flat volumetric	Constant import and export tariff
Design impact:	<p><u>PV capacity</u> depends on <i>LCOE</i> and self-consumption.</p> <p>Battery capacity is a compromise between cost and self-consumption gain.</p> <p>Heat is mostly provided by a <u>heat pump</u> (sized according to the demand).</p>
Grid impact:	Mostly influenced by the installed <u>PV capacity</u>
Variable volumetric	Import and export tariff change along with time
Design impact:	<p>Minor influence on the <u>PV capacity</u>.</p> <p>The <u>battery</u> is used for trading energy. It charges when electricity is cheap , and discharge to avoid expensive energy import.</p> <p>The <u>heat pump</u> and <u>electric heater</u> might be oversized to use as effective flexibility sources.</p>
Grid impact:	Strongly increased by the battery usage, causing significant peak power as tariff changes.
Capacity-based	Charge according to the monthly maximum exchanged power. Can include a volumetric part.
Design impact:	<p><u>PV capacity</u> can be reduced if the PV penetration is so high that curtailment becomes too significant.</p> <p>Battery capacity fostered to cut import peak.</p> <p><u>Heat pump capacity</u> is reduced. <u>Electric heater</u> size increased to cover the extreme heat demand situation.</p>
Grid impact:	Effective reduction of the grid usage intensity.
Block rate	Import rate increases with power. Export rate decreases with power
Design impact:	<p><u>PV capacity</u> can be reduced for large systems as the feed-in rate is lower for high export power.</p> <p>The <u>battery</u> , <u>heat pump</u> and <u>electric heater</u> capacity are also reduced</p>
Grid impact:	Overall reduction of the line loading and voltage deviation. Transformer maximum loading is also reduced at a similar level to the capacity tariff, but the load duration curve is flatter.

5 Harvesting flexibility from a DSO perspective

As the power sector is shifting from centralized to distributed generation, flexibility is required, especially in low-voltage grids. This chapter presents how distribution system operators can harvest the flexibility available in the network from distributed flexible PV systems. Both behavioral and technical flexibility are potential sources to delay grid reinforcement and increase PV penetration. In this context, we present how energy communities increase the available flexibility. We also present how ideal behavioral flexibility could increase the PV hosting capacity. Finally, a discussion on the flexibility value is proposed.

Part of this work was reported in:

Holweger, J., Bloch, L., and Wyrsh, N. (2018). SCCER-FURIES - Determination of the flexibilisation potential of the electricity demand. ReEL D114b. Technical report, École Polytechnique Fédérale de Lausanne

5.1 Introduction

The deployment of distributed PV generation forces the distribution system operators (DSOs) to change their mission. In a centralized energy system, DSOs have to provide the infrastructure to deliver the energy requested by the end customers. In a distributed generation-based energy system, their role is to provide the infrastructure to allow the exchange of power inside the network and with the transmission grid. This is the necessary condition for a reliable access to energy for the end customers. The DSOs have to cope with the evolution of the energy demand and the deployment of distributed generation that may induce additional stress on their networks. The network has now to sustain any peak exchange regardless of the direction. This increases the complexity of maintaining the grid in a safe operating state. According to [Viral and Khatod, 2012], the main challenge with the increasing penetration of distributed generation is to keep the voltage level within acceptable bounds, as given by the voltage disturbance standard EN50160 [Markiewicz and Klajn, 2004], and to ensure that

the lines and transformers loading limits are not exceeded. Several approaches addressing this challenge are considered. Voltage regulation mechanisms can be applied either at the transformer (on-load tap changer) to directly influence the voltage level in the whole network [Agalgaonkar et al., 2014, Hashemipour et al., 2018], or locally using the inverter's reactive power capability [Viral and Khatod, 2012, Olivier et al., 2016, Olivier, 2018, Prionistis et al., 2021], as pictured in Figure 5.1. While it is already common practice to adjust the power factor of PV inverters (once and for all), dynamic adjustment of the reactive power by remote-control should become the standard for residential (< 1 MW) inverters in Europe [Bründlinger, 2020].

To increase the direct consumption of locally generated electricity, batteries [Massucco et al., 2021], power-to-heat [Hidalgo-Rodriguez and Myrzik, 2018], or any other flexible technologies can be used to help to operate the network safely. These uses of flexible technologies compete with grid reinforcement. Indeed, if the network cannot sustain the required load, grid reinforcement is the ultimate and costly way to avoid blackouts [Vu, 2018, Gupta et al., 2021]. Hence, the cost of implementing and using batteries, power-to-heat technologies, and remote-controlled inverters has to be balanced with the grid reinforcement costs. The underlying assumption is that the DSO has to pay for these flexible technologies or grid reinforcement. As shown in the previous chapter, distributed flexibility sources can be encouraged by appropriate economic and moral incentives. The technical and behavioral flexibility that prosumers will adopt while investing in a PV system could be harvested by the DSO to maintain a safe network operation. There is a lack of research in understanding what are the benefits of distributed flexibility compared to grid reinforcement and how to valorize it or reward prosumers for providing it.

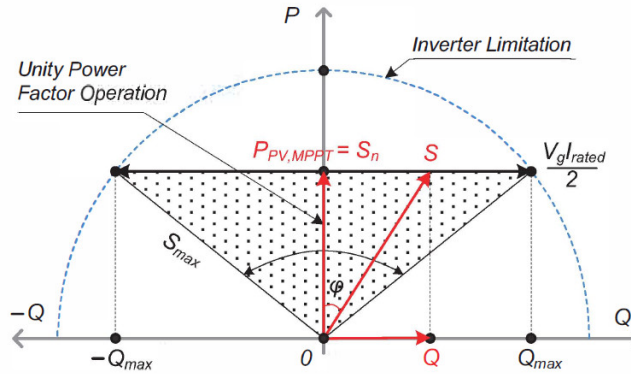


Figure 5.1 – Inverter active and reactive power (PQ) capability diagram from [Yang et al., 2015]

This chapter will propose some solutions and guidelines for DSOs to harvest the available distributed flexibility. In particular, we will investigate how energy communities can provide adequate support for enabling a high PV penetration with great flexibility to mitigate grid impact and possibly delay or minimize grid reinforcement. This concludes our contribution to Research Question B) about cost-effective flexibility. As energy communities are a motor for social innovation and citizen participation, we will investigate how behavioral flexibility can be harvested to increase the network maximum PV penetration and how this is econom-

ically competitive compared to PV generation curtailment. Finally, we will investigate how distributed (technical) flexibility can be harvested to maintain the network in safe operating conditions and reward this flexibility taking into account the avoided grid reinforcement cost. This chapter forms our essential contribution to Research Question C) about mitigating grid reinforcement costs.

5.2 Using energy community and spatial aggregation to enhance flexibility

Since 2018, Switzerland allows the creation of energy communities [Swissolar, 2019]¹. While it is not strictly restricted to PV systems, the main goal is to encourage investment in distributed renewable energy by allowing parties to group in a single entity, share the investment, and self-consume locally produced energy. Under the current Swiss regulation, two types of energy communities are considered. The first type of energy community is not a legal entity but rather a service that allows a multi-family building owner to sell directly the locally produced energy to its tenants². The minimum requirement is that the electricity is not sold at a higher price than what the tenants could get when purchased from the local energy retailer. This concept is a service for billing and counting energy relying on the principle that energy will be consumed locally. The second type of energy community is building owners, their parcel being adjacent (or possibly separated by a road or a river), that group under a single legal entity and determining a single connection point with the distribution network. All energy will be accounted for and charged based on the metering of this connection point. The subtle difference between both concepts is out of the scope of this thesis. The fundamental principle, common for both cases, is that energy communities are groups of energy systems co-located at the same place charged based on the metering of the energy exchange with a single grid connection point.

What remains unclear is if and how a DSO can use energy communities to limit its network stress under a high PV penetration. Hence, the purpose of this work is to investigate how aggregating energy systems to form energy communities can be profitable from the participant perspective, how it impacts the stress on the grid, and offer distributed flexible capacity.

5.2.1 Methodology

The proposed methodology aims to define community scenarios in a low-voltage grid and study the impact of the aggregation of PV-battery energy systems, under several tariff scenarios, on the system's design, and the grid impact. The communities are formed by aggregating buildings according to their proximity from a grid perspective, i.e., the distance of the lines

¹In french, "regroupements dans le cadre de la consommation propre" art 17 LEne <https://www.fedlex.admin.ch/eli/cc/2017/762/fr>.

²Under such circumstances, end-customers stay clients of the DSO and may choose to stay out of the energy community according to LApEl <https://www.fedlex.admin.ch/eli/cc/2007/418/fr>

connecting one building to another, hereafter referred to as line-distance. In this work, the Swiss regulatory framework allowing to form energy communities in particular proximity location conditions are ignored (for instance, the continuity of the parcel, which is part of the Swiss energy ordinance OEne art. 14 al.2³ are not considered). This aggregation is achieved by applying a clustering method on the building-to-building line distance matrix. Several community scenarios are generated by varying some clustering parameters, as described later on. Each community scenario u has a number B_u of systems (one or several aggregated buildings). For each system, the optimal battery size and operation are solved using the mixed-integer linear programming formulation described in Chapter 3.

Once all systems' design and operation are solved, the performance indicators and the grid impact indicators are calculated after solving the load flow problem. The sequence, system optimization - load flow and performance indicators calculation, is repeated for all community and tariff scenarios as pictured in Figure 5.2. The scenario with all systems being individual (no aggregation, hereafter referred to as "individual systems") and under the reference tariff is considered as the reference design and operation. To not bias the systems' profitability when changing the tariff, the latter is calibrated using this reference case.

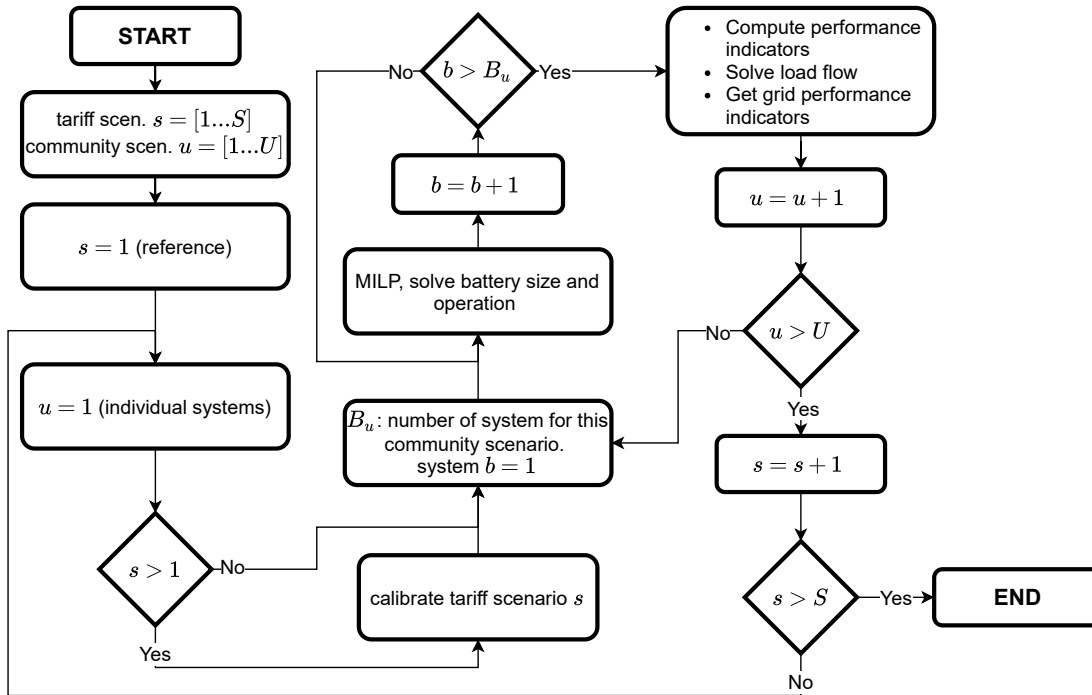


Figure 5.2 – Methodology workflow

³https://www.fedlex.admin.ch/eli/cc/2017/763/fr#art_14

A Buildings aggregation

The building aggregation is performed by applying clustering on the line-distance matrix D , i.e., the line-distance to connect one building to any other building by following only the existing electrical line. Representing the network as an undirected graph $G = (V, E)$ with the building point of connection to the grid as the graph vertices (V) and the lines are the graph edges (E). The line-distance matrix $D_{i,j}$ is built by finding the shortest path length to connect vertex i to j for all $(i, j) \in E$. This is achieved by applying the Dijkstra algorithm [Dijkstra, 1959]. The clustering is performed by applying the DBSCAN [Ester et al., 1996] algorithm. This algorithm's basic principle is to group the set of closely packed points in a high-density region, marking as outliers point lying in low-density areas.

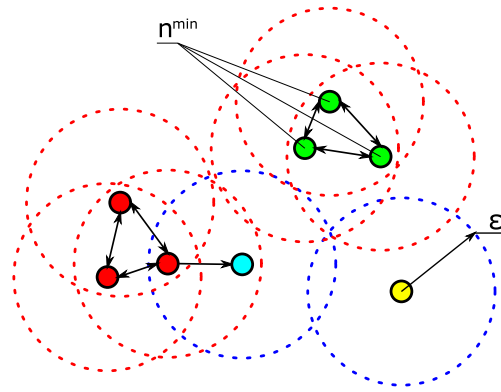


Figure 5.3 – Illustration of the principle of the DBSCAN algorithm

The algorithm essentially defines three types of points, as illustrated in Figure 5.3. :

a core point from which at least n^{\min} points (including itself) are within its boundary, formed by a radius of size ϵ such as the red and green points.

a non-core but reachable point that has less than n^{\min} core points in its boundary, like the blue point.

outliers non-core points that are not reachable like the yellow point.

After labeling each point in the dataset, clusters are formed by connected points. In the example of Figure 5.3, the red and blue points form a cluster, the green ones a second, while the orange point is an outlier.

This algorithm is used to aggregate the buildings. Fixing different values for the boundary radius (ϵ) leads to different aggregation levels, i.e., small ϵ will lead to a higher number of clusters of small size (smaller aggregation level), while high enough ϵ will lead to all buildings forming one single cluster. To define the community scenario, the following procedure is performed:

1. Initialize, iteration $k = 1$, $\epsilon^k = \epsilon^0 \gg \max(D)$ and $n^{\min} = 2$.
2. Run the DBSCAN algorithm and store the element cluster index g_i^k $i = 1 \dots B$ (B being the total number of buildings). Store the number of buildings per cluster N_g^k , $g = 1 \dots G^k$, with G^k the number of clusters for this iteration.
3. Update $\epsilon^{k+1} = r \cdot \epsilon^k$ with $r < 1$.
4. Iterate on k and return to the clustering step until the number of clusters corresponds to the number of buildings ($G^{k^{\text{end}}} = B$).

At each iteration, the parameter r decreases the boundary radius, thus increases the number of clusters. If r is close to (but smaller than) 1, the number of community scenarios can be pretty high, with several systems being very similar. Thus to reduce the number of community scenarios, we applied an additional *k-medoid* clustering step on the median and standard deviation of the number of buildings per cluster N_g^k . This step returns a vector of U indices k^u , $u = 1 \dots U$ corresponding to the selected DBSCAN clustering iteration. We make sure that the community scenario with all buildings labeled as independent systems ($k = k^{\text{end}}$) and all buildings grouped in the same cluster ($k = 1$) are in the selection.

B System optimization and tariff structure

As the purpose of this study is to evaluate how energy communities can act as a tool for DSO to mitigate the impact of a high PV penetration, we assumed for each building that any roof with a surface greater than 10 m² is fully covered with PV. Smaller roofs are not covered. This simplifies the optimization as the number of modules to be installed is not a decision variable. The optimization problem can be summarized as follow:

$$\begin{aligned}
 \min \quad & TOTEX = OPEX + R \cdot cx^{\text{bat}} \\
 \text{where:} \quad & OPEX = ox^{\text{ge}} + ox^{\text{bo}} \\
 & cx^{\text{bat}} = E_{\text{cap}}^{\text{bat}} \cdot c^{\text{bat}} + b^{\text{bat}} \cdot c_F^{\text{bat}} \\
 & ox^{\text{bo}} : \text{see Equation 3.12b} \\
 & ox^{\text{ge}} : \text{see the definitions in Equations 4.1a to 4.1c} \\
 \text{subject to:} \quad & \text{Equations 3.1 to 3.3f}
 \end{aligned} \tag{5.1}$$

As a reminder, the total PV production is the sum of roof-based PV production as $P_t^{\text{PV}} = \sum_{i=1}^N P_{t,i}^{\text{mod}} \cdot n_i^{\text{mod}}$ (Equation 3.2a). Although the buildings are aggregated into an energy community, the local PV production of a given roof $P_{t,i}^{\text{mod}} \cdot n_i^{\text{mod}}$ is injected at its original network injection point regardless of the community. The same applies to the uncontrollable load P_t^{load} . However, the installed battery inject or withdraw power at the most upstream injection point of the community. This implies assuming that for each community, a single (or none)

5.2. Using energy community and spatial aggregation to enhance flexibility

battery with a capacity $E_{\text{cap}}^{\text{bat}}$ will be installed in the building connected to the closest injection point to the transformer. The optimal location of the battery is not discussed in this work.

In this work, we consider only two tariff structures: Volumetric tariff (see Equation 4.1b in which the parameters are the import and export tariff along the time $(c_t^{\text{imp}}, c_t^{\text{exp}})$ and a capacity tariff (Equation 4.1c), which applies a capacity component c^{pow} to the monthly maximum exchanged power. The capacity component aims to cover the grid maintenance cost. The energy retail tariff and tax are included in the volumetric component. In the case of a purely volumetric tariff, the import tariff can be similarly split between the tax c^{tax} , the cost for the grid c_t^{grid} , and the energy retail price c_t^{buy} . The cost for exporting energy never internalizes any tax or grid cost and is, thus, equal to the energy retail cost c_t^{sell} . Keeping this in mind, we follow a slightly different approach than in Sections 4.2 and 4.4 to calibrate the tariff parameters as detailed below.

For a purely volumetric tariff, the calibration follows these steps:

- The volumetric tax c^{tax} is kept identical.
- The grid maintenance revenues are conserved, i.e., $C^{\text{grid},\text{old}} = \sum_b \sum_t P_{b,t}^{\text{imp}} c_t^{\text{grid},\text{new}}$.
- The revenue from buildings buying energy is conserved i.e., $C^{\text{buy},\text{old}} = \sum_b \sum_t P_{b,t}^{\text{imp}} c_t^{\text{buy},\text{new}}$.
- The cost from buildings selling energy is conserved i.e., $C^{\text{sell},\text{old}} = \sum_b \sum_t P_{b,t}^{\text{imp}} c_t^{\text{sell},\text{new}}$.
- The new overall costs for importing and exporting energy are $c_t^{\text{imp}} = c^{\text{tax}} + c_t^{\text{grid},\text{new}} + c_t^{\text{buy},\text{new}}$ and $c_t^{\text{exp}} = c_t^{\text{sell},\text{new}}$ respectively.

Note that $C^{\text{grid},\text{old}}$, $C^{\text{buy},\text{old}}$, and $C^{\text{sell},\text{old}}$ are the sum of the grid and energy retail (buying or selling) contributions of all buildings calculated using the reference tariff and each building import and export power.

In the case of a capacity tariff, the calibration follows the same steps as above except that the grid maintenance costs are conserved by applying $C^{\text{grid},\text{old}} = \sum_b \sum_m P_m^{\text{max}} c^{\text{pow},\text{new}}$, with P_m^{max} being the maximum monthly power exchanged (in the framework of mixed-integer programming, this refers to Equation 4.2). Tariff scenarios are calibrated only for the first community scenario (all systems being independent) and then applied to all other community scenarios.

C Performance indicators

The performance metrics aim to reflect the effect of aggregating systems on their design, operation, economic viability, and network impact. The indicators are split between the ones describing the system's performance and the ones representing the network impact. The

Chapter 5. Harvesting flexibility from a DSO perspective

following performance indicators are related to the system's design. They are defined for each system. To ease the notation, subscript b has been dropped.

$$\text{Battery autonomy ratio} \quad \text{Bat}_{\text{auto}} = \frac{E_{\text{cap}}^{\text{bat}}}{\text{building mean daily energy}} \quad (5.2a)$$

$$\text{Cumulative energy stored} \quad E^{\text{stored}} = \sum_b \sum_t P_t^{\text{cha}} \cdot TS_t \quad (5.2b)$$

$$\text{\# of daily cycles} \quad \text{Bat}^{\text{cycles}} = \frac{E^{\text{stored}}}{E_{\text{cap}}^{\text{bat}} \cdot \text{\# simulated days}} \quad (5.2c)$$

$$\text{Investment cost} \quad \text{CAPEX} = \text{cx}^{\text{PV}} + \text{cx}^{\text{bat}} \quad (5.2d)$$

$$\text{System net present value} \quad \text{NPV} = \sum_{y=1}^L \frac{\text{cx}_y^{\text{PV}} + \text{cx}_y^{\text{bat}} + \text{ox}_y^{\text{pm}} + \text{ox}_y^{\text{ge}}}{(1+r)^y} \quad (5.2e)$$

$$\text{Levelized cost of electricity} \quad \text{LCOE} = \frac{\text{NPV}}{\sum_{y=1}^L \frac{\sum_t P_t^{\text{load}} \cdot TS_t}{(1+r)^y}} \quad (5.2f)$$

$$\text{Internal rate of return} \quad \text{IRR} = r \text{ such that } \text{NPV} = 0 \quad (5.2g)$$

The network impact indicators are related to the network state variable obtained by solving the load flow problem. Those are: the bus voltage magnitude $V_{i,t}$ $i \in \mathbb{B}$, \mathbb{B} being the set of network buses, the line current $I_{l,t}$ $l \in \mathbb{L}$, \mathbb{L} being the set of network lines, and the active power at the transformer P_t^{trafo} (positive is power flowing outward the network). We thus define the following grid impact indicators:

$$\text{Min. and max. bus voltage} \quad V_i^{\text{min,max}} = \min_t / \max_t V_{i,t} \quad (5.3a)$$

$$\text{Fraction of overloaded lines} \quad F^{\text{ol-lines}} = \frac{\sum_l \delta_l^{\text{ol}}}{|\mathbb{L}|} \quad (5.3b)$$

$$\delta_l^{\text{ol}} = \begin{cases} 1 & \text{if } \max_t I_{l,t} > I_l^{\text{max}} \\ 0 & \text{otherwise} \end{cases}$$

$$\text{Network self-consumption} \quad \text{SC} = \frac{\sum_t \left[\min \left(\sum_b P_{b,t}^{\text{load}}, P_t^{\text{trafo}} + \sum_b P_{b,t}^{\text{load}} \right) \right]}{\sum_b \sum_t P_{b,t}^{\text{PV}}} \quad (5.3c)$$

$$\text{Network self-sufficiency} \quad \text{SS} = \frac{\sum_t \left[\min \left(\sum_b P_{b,t}^{\text{load}}, P_t^{\text{trafo}} + \sum_b P_{b,t}^{\text{load}} \right) \right]}{\sum_b \sum_t P_{b,t}^{\text{load}}} \quad (5.3d)$$

5.2.2 Case study

This analysis is performed on the Rolle area's low-voltage grid already presented in Section 4.4. We choose $U = 5$ community scenarios where the number of clusters, hereafter referred as communities, ranges from $B^u = 42$ (each building are independent) to $B^u = 1$ (all building forms a single community). The resulting community scenarios are pictured in Figure 5.4. A careful reader might note that in Figure 5.4a, there might be two or more adjacent buildings with the same color. The reason comes from our conception of a building as an energy system connected to a single network injection point. The geographical information system used to produce these maps might consider a slightly different definition.

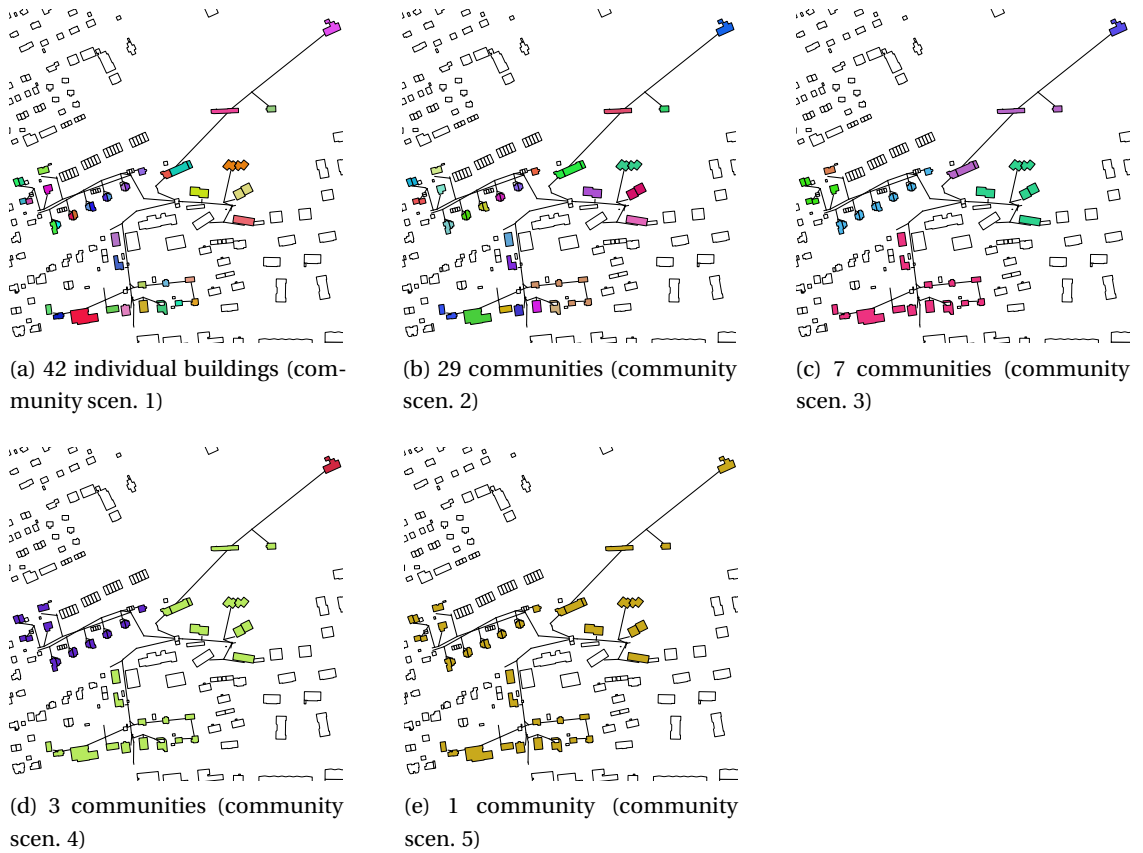


Figure 5.4 – Community aggregation scenarios. Each community has its own color.

The number of buildings per community is plotted in Figure 5.5 as a function of the aggregation level (represented by the number of communities for each community scenario). For instance, the first scenario, corresponding to all buildings being independent systems, consists of 42 communities with one building. The variance in the number of buildings between clusters can be pretty significant when the aggregation level increases. For instance, the 4th community scenario consists of 3 communities of 1, 18 and 23 buildings. This community size imbalance should not affect the outcomes of this study, as from a modeling point of view, they are

perfectly equivalent energy systems, their available PV capacity and energy consumption being different.

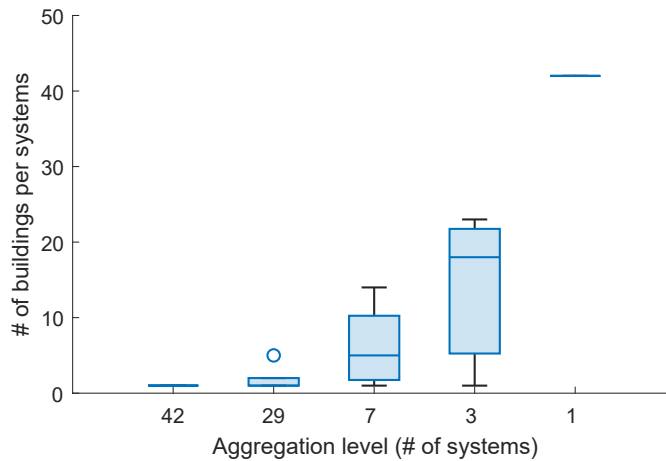


Figure 5.5 – Distribution of the number of buildings per community

We define three tariff scenarios: the first serves as a reference. It is a standard flat volumetric tariff. The second is the variable volumetric tariff mirroring the variation of the spot market price (same as in Section 4.4). The third is a capacity-based tariff with a volumetric component, hereafter referred to as capacity tariff. A block rate tariff was initially considered in this study but was found to be irrelevant in this system aggregation context for the following reasons. First, using the calibration approach, which distinguishes the grid maintenance cost from the energy retail cost, was hardly applicable to a block rate structure. Second, a block rate structure assumes a certain energy price for a given power level. With the combination of several buildings, up to the whole network, the average power at which the energy is exchanged increases. Thus, there are risks that the block rate structure ends up being seen from the optimization problem as a simple flat volumetric tariff with a high import rate and very low export rate. This raises numerous questions about the construction and versatility of a block rate that is out of this work's scope. Therefore, it was decided not to consider a block rate structure in this context.

5.2. Using energy community and spatial aggregation to enhance flexibility

Table 5.1 – Tariff scenarios

Scenario	Description	Tariff (CHF cts/kWh)
Reference	c_t^{imp} :	21.02
	c_t^{exp} :	8.16
Spot market	c_t^{imp} :	2.69 + EPEX*3.2928
	c_t^{exp} :	EPEX*1.5830
Capacity	c_t^{imp} :	11.95
	c_t^{exp} :	8.16
	c^{pow} :	3.32 CHF/kW/month

For each building in this network, the roof characteristics come from a geographical information system (namely *solar roof*⁴). The electric load profile is obtained using the allocation method presented in Section 4.3.1. Except for the thermal part, which is not considered in this study, the buildings and roofs parameter corresponds to the one described in Appendix C, Table C.1. The PV and battery costs are the ones estimated for 2030 using the method presented in [Bloch et al., 2019]. The cost and technical parameters are summarized in Table 5.2.

Table 5.2 – System, PV and battery parameters

	Param.	Unit	Value	Param.	Unit	Value
SYSTEM	T	-	35040	L	years	25
	M	-	12	L^{bat}	years	9
	TS	s	900	r	-	0.03
BATTERY	SOC_{init}	-	0.7	$\text{CR}^{\text{char,dis}}$	1/h	1
	$\text{SOC}_{\text{min,max}}$	-	0-0.7	c^{bat}	CHF/kWh	182
	α	1/day	0.04	c_F^{bat}	CHF	0
	$\eta^{\text{cha,dis}}$	-	0.98	c_o^{bat}	CHF/kWh	10^{-6}
PV	c_F^{PV}	CHF	10'049	c^{mod}	CHF/W	0.83
	$P_{\text{nom}}^{\text{mod}}$	W	315			

⁴<https://www.uvek-gis.admin.ch/BFE/sonnendach>

5.2.3 Results

From the design perspective, recalling that the installed PV capacity is set at its maximum potential, the battery size is the only free design variable. The total installed battery capacity (sum of all communities' battery capacity) is reported in Figure 5.6. The number of installed batteries is also reported on the right axis. While the number of batteries is always equal to the number of communities, we see two different trends for the total installed battery capacity. The spot market tariff promotes larger battery capacity (as reported in Chapter 4). The battery capacity increases with the aggregation level while it reduces for the reference and capacity scenario. Interestingly, in the first community scenario (42 community), the total installed battery capacity is more significant for the capacity scenario than for the reference scenario, while it is the opposite when reaching a high aggregation level (with only one system). This is due to the battery usage that differs between the reference and capacity scenario. In the first one, the battery helps increase self-consumption while reducing the import or export peak power for the second. When aggregating loads, such import peaks become less significant and are easily covered by the total PV generation.

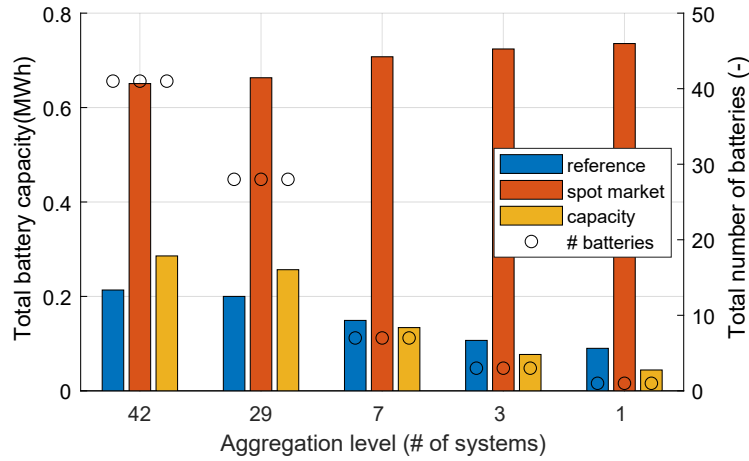


Figure 5.6 – Total installed battery capacity and number of batteries (right axis)

The distribution of battery autonomy ratio reported in Figure 5.7 emphasizes that the battery is used for different purposes at the system level. Indeed, for the reference scenario, the median decrease from 0.2 to 0.035 for the last community scenario, the spread decreasing simultaneously. For the spot market scenario, the median stays slightly above 0.3 for all community scenarios. The battery size is proportional primarily to the energy demand of the community in this case. For the capacity scenario, the battery autonomy ratio being influenced by the maximum peak demand rather than the annual energy consumption, the median decreases as for the reference, but the variance stays much larger. To better understand this change of battery usage paradigm, one should look at the battery operation.

5.2. Using energy community and spatial aggregation to enhance flexibility

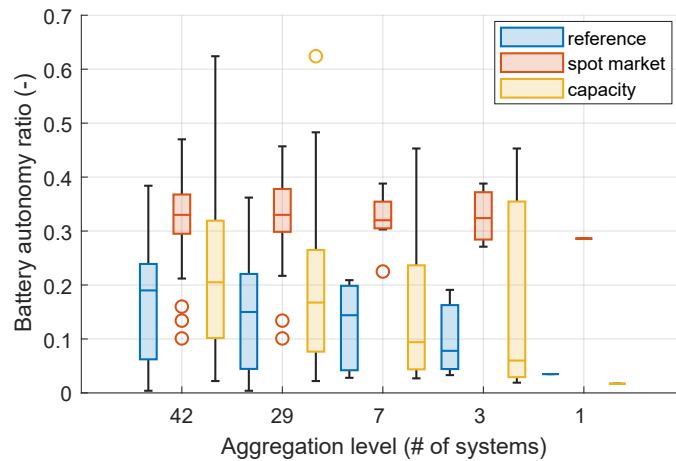


Figure 5.7 – Distribution of battery autonomy ratio

The cumulative energy stored in the batteries (Figure 5.8) shows a similar trend to the total installed battery capacity (Figure 5.6). However, the values are three orders of magnitude higher, indicating a high number of charging-discharging cycles. The average number of daily cycles per day is plotted in Figure 5.9. It is below 0.8 for the reference and decreases with the aggregation level. Conversely, the daily cycle number increases for the capacity and ends up at approximately one cycle per day. This number is much higher for the spot market scenario, but its medians vary around 1.5 cycles per day. From these observations, we can deduce that the battery usage becomes less intensive for the reference tariff as the aggregation level increases. It stays approximately constant for the spot market scenario and increases for the capacity tariff as smaller batteries are used to limit all demand peaks.

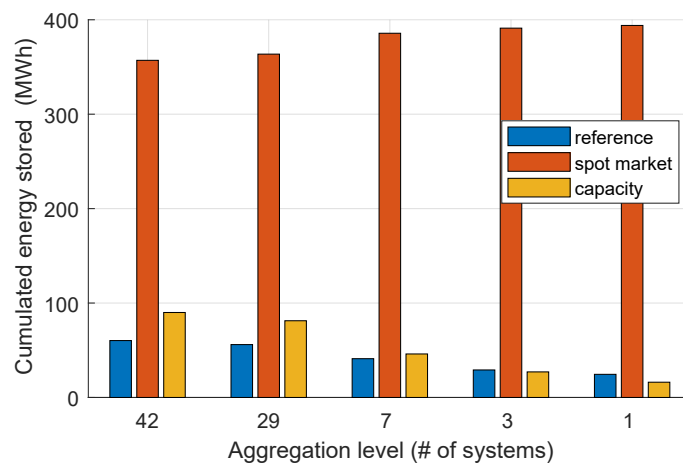


Figure 5.8 – Cumulated energy stored in the batteries

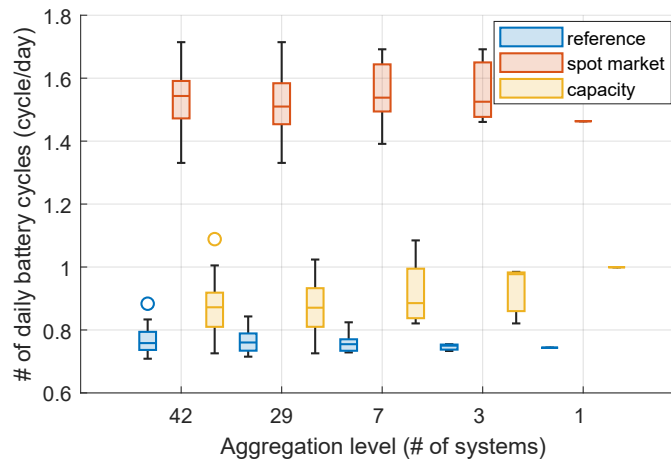


Figure 5.9 – Mean number of daily cycles distribution

From an economic perspective, the total investment costs are similar when comparing tariff scenarios, as highlighted in Figure 5.10. Most of the capital expenditure is on PV installations and a small part on the battery. The aggregation of the buildings reduces the total capital cost. This is explained by the fact that the fixed cost c_F^{PV} is applied precisely once per community. This is a direct consequence of the optimization problem modeling choices. A more appropriate choice would have been to decrease the variable cost c^{mod} with the installed capacity (being known in advance as we fixed it to the maximum) as economies of scale. However, a more detailed model of PV module price and batch discount is outside the scope of this work. It can be reasonably assumed that the fixed cost covering the administrative and engineering costs is applied only once for a community and does not scale with the system's size.

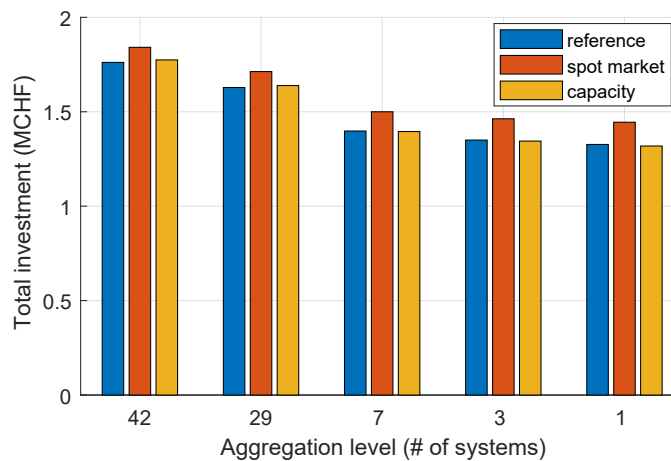


Figure 5.10 – Total investment costs

The benefits of lowering the total investment cost directly affect the levelized cost of electricity

5.2. Using energy community and spatial aggregation to enhance flexibility

(*LCOE*), as shown in Figure 5.11. In most cases, the *LCOE* is below 0.2 CHF/kWh, which is approximately equal to the reference retail energy tariff. A few communities may experience a *LCOE* above this value for the capacity scenario. As the number of communities decreases and the aggregation level increases, all communities experience a *LCOE* in the range of 0.1 CHF/kWh. This figure also highlights that building aggregation may significantly impact the overall cost of energy of individuals building owners. For instance, when all 42 buildings are independent, negative *LCOE* can be encountered, indicating a highly profitable investment. If these systems group with others to form a larger community and the grid exchange costs are purely shared on an energy basis, their profitability will decrease. This observation is also highlighted in Figure 5.12. The internal rate of return (*IRR*) might decrease for some buildings owner when aggregating. This statement depends highly on how the costs and benefits are shared inside each community. The metrics here only reflect the global performance. This issue was acknowledged by [Abada et al., 2020], who studied the energy community's stability. An energy community is stable if any participant leaving the community will lower his profit. We do not consider this aspect in this study.

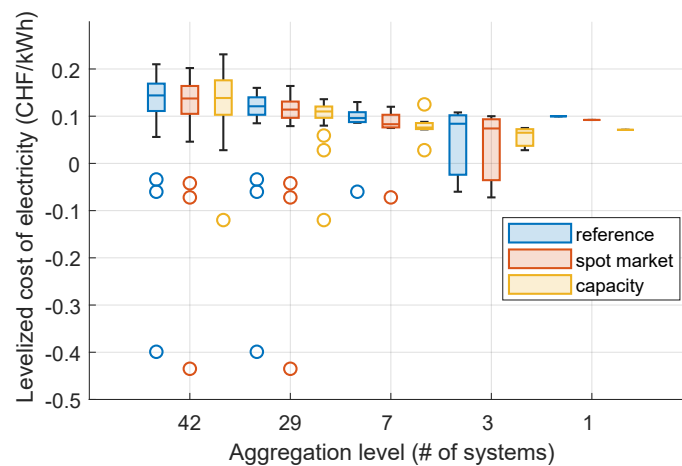


Figure 5.11 – Levelized cost of electricity served

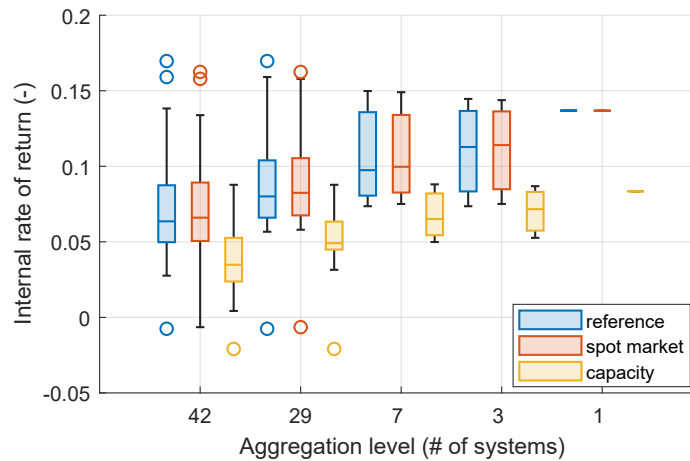
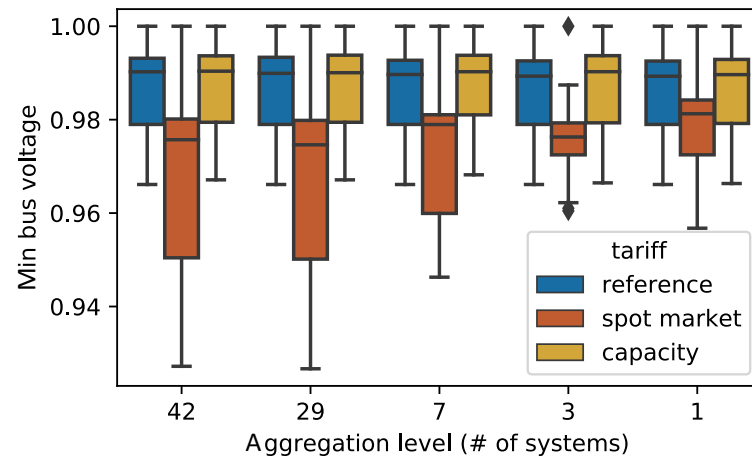


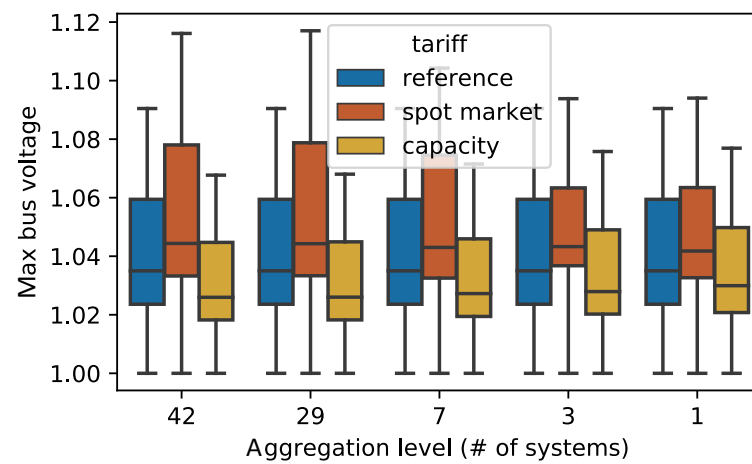
Figure 5.12 – Internal rate of return

The impact of aggregation on the bus voltage deviation (reported in Figure 5.13) is much smaller than the impact of the tariff itself from the grid perspective. However, for the spot market tariff, which has a highly negative impact on the grid, the aggregation of the buildings benefits to the grid voltage level as the minimum bus voltage increase and the maximum bus voltage decrease with the aggregation level. However, Figure 5.14 highlights that the fraction of overloaded lines increases with the aggregation level. This is because larger batteries are installed at their respective injection point without considering the grid capabilities to sustain such a load. If such installations would be made in practice, one should choose either a more appropriate battery location and a more optimal community grid connection point or retrofit the lines.

5.2. Using energy community and spatial aggregation to enhance flexibility



(a) minimum



(b)

Figure 5.13 – Bus voltage

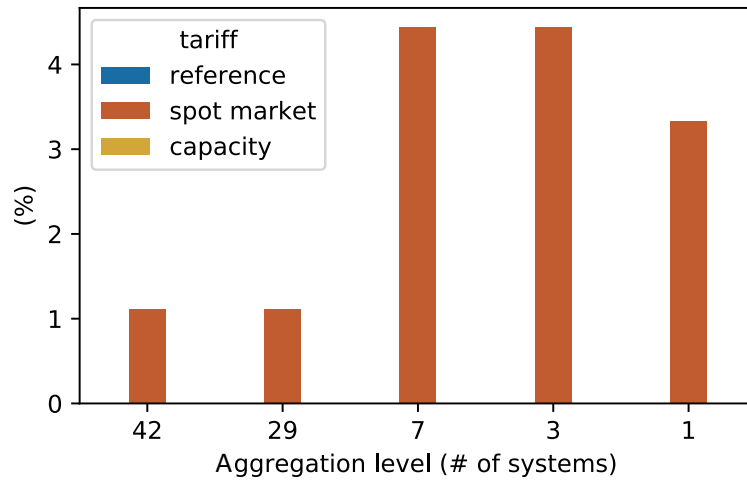


Figure 5.14 – Fraction of overloaded lines

The network-level self-sufficiency and self-consumption are barely affected by the aggregation level, as shown in Figure 5.15. A slight decrease in self-consumption and self-sufficiency can be observed for the reference and capacity tariff, while the opposite trend is observed for the spot market scenario.

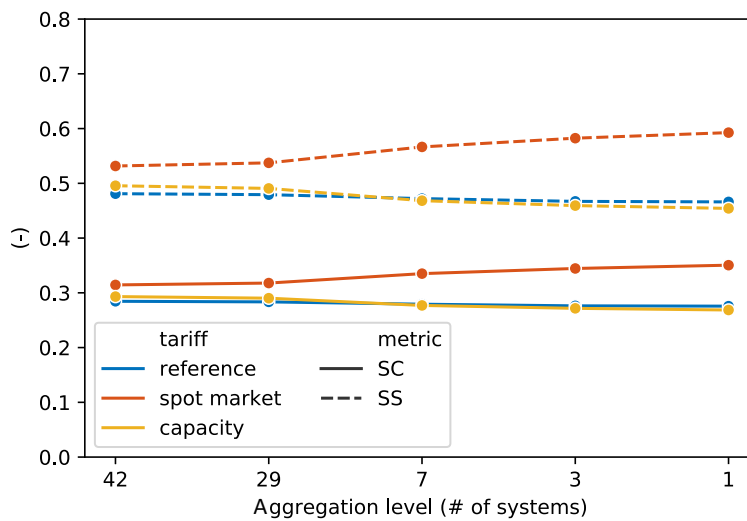


Figure 5.15 – Self-consumption (SC) and Self-sufficiency (SS) at the transformer level

Finally, the load duration curves at the transformer are plotted in Figure 5.16. In more detail, Figure 5.16b shows only the load duration curve for the first community scenario, while Figures 5.16a and 5.16c shows all tariffs and community scenarios. As highlighted in Section 4.4, the tariffs impact more significantly the load duration curve. However, the aggregation level tends to increase the loads both when the network is injecting and consuming power for the

spot market scenario.

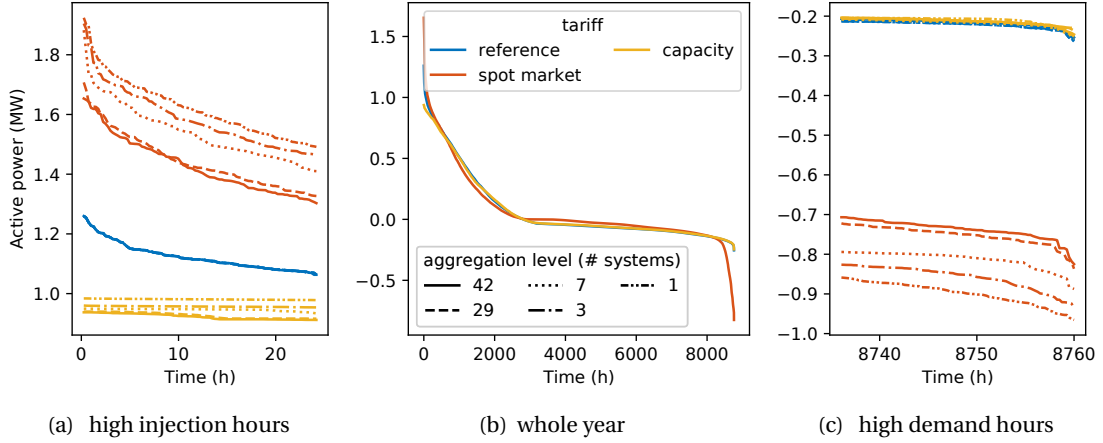


Figure 5.16 – Load duration curve

5.2.4 Discussion

Energy communities are now a well-known concept. Their role in the energy transition is defined as a motor for social innovation [Caramizaru and Uihlein, 2019], reducing energy poverty and providing ground for smart-technology innovation. Energy communities are well coupled with the concept of microgrid, which describes the underlying infrastructure for the distribution of energy [Aghamolaei et al., 2020]. Our work investigated the impact of the aggregation of systems (the most basic system being a single independent building) on their design, operational performances, and impact on the network's operational state.

The formation of energy communities is performed based on the inter-building distance. Instead of the geographical distance, the line length is used as a distance metric. As the line length is a Euclidian distance, the resulting line distance respects the fundamental metric properties, particularly the triangle inequality. However, clustering does not need a true metric as a similarity measure [Chang et al., 2016, Ackermann et al., 2010], but this is desirable for our problem to make sure the clusters are formed based on their geographical properties. A distance metric based on the line impedance would first not necessarily respect the triangle inequality criterion, second not ensure that the resulting community groups consist of geographically close buildings. We could have embedded the line properties and any building features such as energy consumption, PV potential, or socio-demographic information in a new clustering problem. However, the complexity of such a problem would be challenging. Besides, energy communities are entities formed by neighbor citizens and driven by a common interest in sharing resources. Therefore, the assumption that energy communities are formed according to their geographical proximity seems reasonable.

From a DSO perspective, the outcome of this work can be summarized in the following

statements. First, individual grouping customers to form energy communities does not mitigate the grid stress. At best, the impact of a high PV penetration is the same at any aggregation level. Second, the impact of a high PV penetration is more efficiently mitigated using electricity tariffs than forming energy communities. Finally, energy communities can favor more flexibility of the PV system if the appropriate tariff is applied. Variable tariffs, for instance, offer economic incentives to increase the storage capacity, which is itself favored by the aggregation of systems. There is, however, an opposition between two counteracting facts. Under variable tariffs, system aggregation increases the network's flexibility, but their usage increases the grid's stress. There is, however, a case in which this situation could be favorable. Assuming a few energy communities contain a sufficient storage capacity, the cost for deploying remote control of these flexible assets would be lower than the deployment of remote control for plenty of small individual assets.

The interest of energy communities also relies on the social interaction that the community members may have [Caramizaru and Uihlein, 2019, Bauwens et al., 2016, Geels et al., 2017]. If directed toward energy conservation [Geiger et al., 2019] or self-consumption, such interaction may have an interesting effect on the community performance. The following section investigates how DSOs can harvest these behavioral changes to increase the PV penetration in low-voltage grids.

5.3 Potential of ideal behavioral flexibility to increase the PV penetration in a low-voltage grid

A vital issue for the fast deployment of PV in a low-voltage grid is the mismatch between the load and instantaneous PV generation that may create a high reverse power flow. Namely, as high PV generation occurs during the day while the load remains low, the power flow can be reversed from the low-voltage grid to the medium-voltage one and can break the transformer capacity limit.

Demand-side management is a promising solution to increase the penetration of solar energy in a low-voltage network. As presented in Chapter 3, the principle is to encourage customers to shift their load toward high PV generation periods in exchange for a financial reward. As experienced in this thesis, time-of-use tariffs can be used as an incentive. We denote "ideal behavioral flexibility" the people's theoretical ability to intentionally shift and change consumption habits under a financial or moral incentive. It contains any household appliance except the ones explicitly considered as technical flexibility sources (batteries and power-to-heat). Although all those appliances could be automated, we still consider it as the households' consumption behavior. The open question is: does the grid benefit from this flexibility in the context of increasing PV penetration?

In this work, we aim to evaluate how ideal behavioral flexibility can increase the network PV hosting capacity. To this end, we leverage on the previous results of the theoretically available

5.3. Potential of ideal behavioral flexibility to increase the PV penetration in a low-voltage grid

flexibility presented in Section 2.4.2.

5.3.1 Methodology

The general idea of the methodology is to obtain the available shiftable energy (or power) in the network at any point in time and use it to cut the excess PV generation to keep the power at the transformer within its capacity limit. The reference PV generation is calculated by assuming all roofs are covered with PV. We define a scaling factor $n > 0$, which linearly scales this PV generation profile ($n = 1$ corresponds to the generation with all roofs covered). The maximum value of n , such that the available flexibility can successfully keep the overall injection power below the transformer capacity, give the maximum PV generation, thus PV penetration. To do so, we assume:

1. The PV generation is the sum of the generation of all available roofs and can be scaled by any real number $n \in \mathbb{R}^+$.
2. The network PV hosting capacity is limited only by the reverse power flow at the transformer. Line ampacity and bus voltage constraints are not considered.
3. The ideal behavioral flexibility can be freely shifted during the day, making sure the daily energy consumption is conserved.

More precisely, the power at the transformer for a given scale n is given by:

$$P_t = L_t - n \cdot G_t \quad \forall t \in T \quad (5.4)$$

where L_t is the total network load, and G_t the total PV generation (assuming all roof covered). Negative values of P are injection power to the upper grid level and correspond to excess PV generation. The maximum value of n ensuring that the injection power will be below the transformer capacity limit, i.e., $P_t > P^{\text{lim}} \quad \forall t \in T$ ($P^{\text{lim}} < 0$), is given by:

$$n^0 = \min_t \frac{L_t - P^{\text{lim}}}{G_t} \quad (5.5)$$

Using the aforementioned assumptions, we can split L_t between its unshiftable U_t and shiftable S_t component (Equation 5.6) in order to bring the available shiftable power S_t inside a target period where we have the injection power exceeding the transformer capacity. The third assumption constrains the daily energy consumption to be conserved (no inter-day load shifting). Introducing the daily load $L_{d,h}$, available shiftable power $S_{d,h}$ generation $G_{d,h}$, and injection power $P_{d,h}$ for all days $d \in D$, and hours $h \in H$, we update the original load by adding flexibility as:

$$\text{Original load} \quad L_{d,h} = U_{d,h} + S_{d,h} \quad (5.6)$$

$$\text{Power at the transformer} \quad P_{d,h} = L_{d,h} - n \cdot G_{d,h} \quad (5.7)$$

$$\text{Target period} \quad \delta_{d,h} = \begin{cases} 1 & \text{if } P_{d,h} < P^{\text{lim}} \\ 0 & \text{otherwise} \end{cases} \quad (5.8)$$

$$\text{Optimal distribution of the shiftable energy} \quad e_h = \frac{\delta_{d,h} P_{d,h}}{\sum_{h'} \delta_{d,h'} P_{d,h'}} \quad (5.9)$$

$$\text{New load with flexibility} \quad L_{d,h}^{\text{flex}} = U_{d,h} + e_h \cdot \left(\sum_{h'} S_{d,h'} \right) \quad (5.10)$$

Using this new load $L_{d,h}^{\text{flex}}$ the maximum value of the PV generation scale for the considered day is given by:

$$n_d = \min_h \frac{L_{d,h}^{\text{flex}}(n) - P^{\text{lim}}}{G_{d,h}} \quad (5.11)$$

At this stage, an iterative process is needed as n_d depends on a guess value of n . This can be easily solved by any gradient-free optimization algorithm, given the fact that the search interval is bounded (n^0 is the lower bounds. If $n^0 < 1$, an appropriate upper bounds for n is 1). In our case, we obtained the final value of n_d using the golden-section search algorithm [Forsythe et al., 1977].

The final value of the PV generation scale is given by taking the minimum of the n_d :

$$n^* = \min_d n_d \quad (5.12)$$

To give some perspective to this value, some additional metrics are calculated as follow:

$$\text{PV penetration} \quad PVP = \frac{\sum_{d,h} L_{d,h}^{\text{flex}}}{n \cdot \sum_{d,h} G_{d,h}^*} \quad (5.13)$$

$$\text{PV self-consumption} \quad SC = \frac{\sum_{d,h} \min(L_{d,h}^{\text{flex}}, G_{d,h}^*)}{\sum_t G_{d,h}^*} \quad (5.14)$$

$$\text{PV self-sufficiency} \quad SC = \frac{\sum_t \min(L_{d,h}^{\text{flex}}, G_{d,h}^*)}{\sum_t L_{d,h}^{\text{flex}}} \quad (5.15)$$

with $G_{d,h}^* = n^* \cdot G_{d,h}$

Note that for low insulation day, the PV generation can be low, or even null, which results in

5.3. Potential of ideal behavioral flexibility to increase the PV penetration in a low-voltage grid

no excess PV generation. In such case, the target period in which the shiftable power will be shared (previously defined in Equation 5.8) is slightly redefined as:

$$\delta_{d,h} = \begin{cases} 1 & \text{if } (P_{d,h}^* < P^{\text{lim}}) \text{ else} \\ 1 & \text{if } L_{d,h} < G_{d,h}^* \\ 0 & \text{otherwise} \end{cases} \quad (5.16)$$

recalling $P_{d,h}^* = L_{d,h} - G_{d,h}^*$.

5.3.2 Case study and available shiftable power

The presented methodology is applied to the Rolle low-voltage network introduced in Section 5.2.2. The loads are assigned using the allocation method presented in Section 4.3.1. The disaggregation algorithm presented in Chapter 1 has been applied to the initial load that served for the allocation to extract the share of shiftable power. As the *device usage prediction* algorithm gives at each point in time the amount of easily, hardly, and not shiftable energy (converted into power), we considered the shiftable power as being the sum of the easily and hardly shiftable power. This gives a representative idea of the theoretical available flexible power. As the allocation process described in Section 4.3.1 involved some scaling (possibly intraday) of the original loads to generated the final allocated load, we assumed that the share of shiftable energy is conserved at all points in time. Thus, the original shiftable power is scaled as the corresponding original load.

The PV generation was simulated assuming a full coverage of all roofs with an area greater than 10 m² and an annual irradiance greater than 1000 kWh/m². The resulting total PV capacity available is 1250 kW and generates approximately 1500 MWh per year. In comparison, the total consumption of the network is 720 MWh. The transformer has a nominal capacity of 400 kW.

5.3.3 Results

Applying this methodology, the maximum PV generation scale from Equation 5.5 gives $n = 0.353$, ($P^{\text{lim}} = -400$ kW), which corresponds to a PV penetration of 73%.

The worst day in terms of reverse power flow at the transformer is reported in Figure 5.17. The reverse power just reaches the transformer capacity limit in the afternoon.

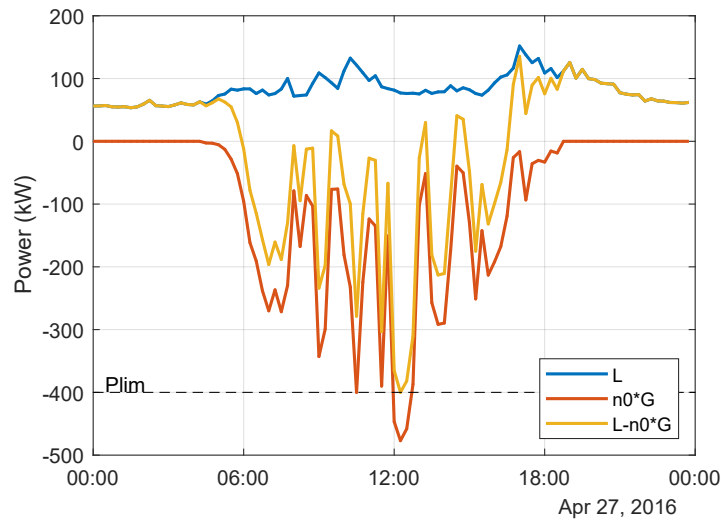


Figure 5.17 – Load L and generation G during the day with the highest reverse power flow

Using the theoretical shiftable power, the PV generation can be further scaled up to a new value of $n = 0.424$, corresponding to a PV penetration of 87%. This is possible under the assumption that the amount of shiftable energy is moved into the period of high injection preventing the reverse power at the transformer to go below -400 kW, as illustrated in Figure 5.18. This figure also highlights that the shiftable power is reduced relatively homogeneously either before or after the target periods. To achieve these results, households must be aware of the foreseen requirements to increase their consumption, delaying any energy-intensive morning activities and anticipating the evening activities. This condition relies on the assumption of having, first, a good communication canal with the households, second, a good forecast of both load and PV generation. Besides, such a perfect synchronization between the PV generation and flexible load seems unrealistic without technical measure, which challenges the assumption that this flexibility is purely behavioral.

5.3. Potential of ideal behavioral flexibility to increase the PV penetration in a low-voltage grid

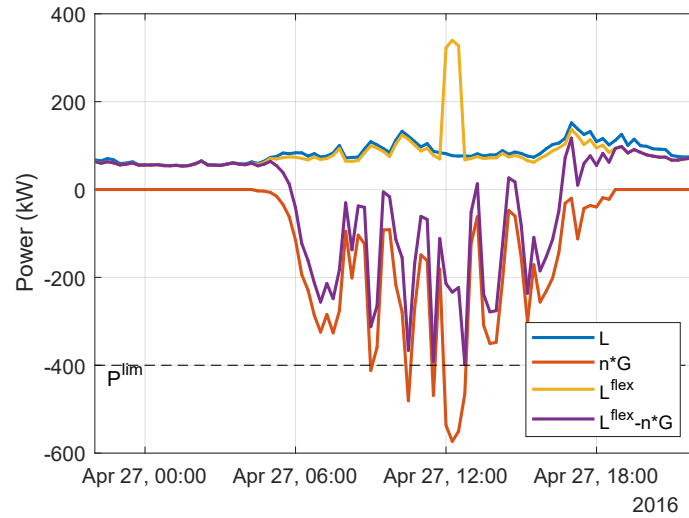


Figure 5.18 – Load L and generation G during the day with the highest injection

To get an estimation of the value of ideal behavioral flexibility, we defined an average cost of the electricity consumed. It takes into account the cost of importing energy, the gains from selling excess PV energy, the average price of a kWh of PV production (the levelized cost of PV energy, $LCOE^{PV}$), and normalizes by the total network consumption:

$$C = \frac{E^{\text{imp}} \cdot c^{\text{imp}} - E^{\text{exp}} \cdot c^{\text{exp}} + E^{\text{PV}} \cdot LCOE^{PV}}{E^{\text{load}}} \quad (5.17)$$

where E^{PV} is the total PV generated energy (for a given scale n), $E^{\text{imp}, \text{exp}}$ are the total imported and exported energy (at the transformer level, for the same scaling), and E^{load} is the total network energy consumption.

Re-using the simple flat tariff from *Romande Energy* with $c^{\text{imp}} = 21.02$ cts/kWh, $c^{\text{exp}} = 8.16$ cts/kWh, and assuming a levelized cost of electricity using 2030 price of 15 cts/kWh, the average cost of electricity can be calculated either at the maximum PV penetration (PVP) without taking flexibility into account, or at the increased one thanks to the flexibility. These costs and the PV penetration, self-consumption, and self-sufficiency are reported in Table 5.3 for both cases.

Table 5.3 – Scores without and with the flexibility

	PVP	SC [%]	SS [%]	C [cts/kWh]
Without flex	72.6	49.8	36.1	20.7
With flex	87.3 (+20%)	49.6 (-0.4%)	43.1 (+20%)	20.9 (+0.9%)

These results highlight that ideal behavioral flexibility allows for a relative increase of the

Chapter 5. Harvesting flexibility from a DSO perspective

PV penetration by about 20%. The decrease in self-consumption is negligible, but the increase in self-sufficiency is remarkable. The average cost of electricity also increases by about 0.2 cts/kWh and indicates that with the foreseen PV price of 2030, it will not be economically interesting to achieve such a high penetration. Note that the optimal PV capacity, considering the ideal behavioral flexibility, has not been investigated in this work.

A *LCOE* sensitivity analysis is performed to see the effect of the PV cost on the profitability of ideal behavioral flexibility. The average electricity price normalized by the import tariff ($\frac{C}{c_{\text{imp}}}$) is plotted against the PV *LCOE* normalized by the export price ($\frac{LCOE^{\text{PV}}}{c^{\text{exp}}}$) in Figure 5.19. Three different curves can be observed in this figure, the blue curve shows the case without flexibility, at a *PVP* of 73%, the red curve with flexibility, at a *PVP* of 87%, and the yellow curve at the same penetration level but using curtailment instead of flexibility. From this graph, several insights are gained: First, curtailing without flexibility becomes profitable if the PV *LCOE* drops significantly compared with the export price. Second, it will always be more interesting to use flexibility (assuming it is free) than curtailment. Finally, the increase of PV penetration gained by ideal behavioral flexibility becomes profitable only if the PV *LCOE* gets smaller than 1.8 times the cost of exporting energy in this case study. The thin vertical dashed line represents the ratio $\frac{LCOE^{\text{PV}}}{c^{\text{exp}}}$ calculated for the PV 2030 price and shows that such a high PV penetration is not profitable.

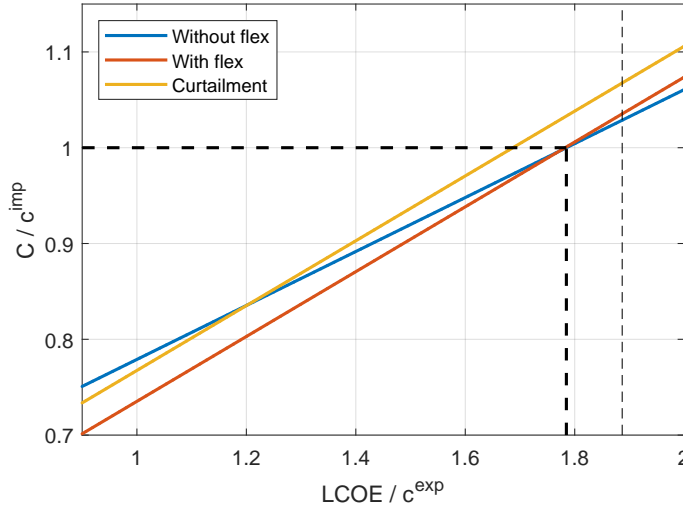


Figure 5.19 – Electricity cost evolution normalized by the import tariff c^{imp} as a function of the *LCOE* normalized by the export tariff c^{exp} . The thin vertical line indicates the situation with the 2030 price. The thick dash lines just represent the threshold for flexibility profitability.

5.3.4 Discussion

In Chapter 2, we investigated the potential for load shifting of households and commented on how to trigger the available flexibility potential. This section pushed the reflection to

investigate how a DSO can benefit from this flexibility to increase the PV penetration in a low-voltage grid. To this end, the theoretical shiftable power extracted from the disaggregation of the household load using the method presented in Chapter 1 is used. We investigated if the shiftable power could be coordinated to lower reverse power at the transformer and avoid transformer capacity breaking. The results highlight that a 20% relative increase of PV penetration is possible. The underlying assumption that households may move freely their energy to match with the PV generation is optimistic and need further discussions. For instance, even at a network scale, it is hard to ensure a perfectly synchronized load shifting to match the excess PV generation. Similarly, some load shifting activities may induce energy conservation, as highlighted by the field trial results presented in Section 2.4 (the opposite is also possible). This, however, should not affect the PV hosting capacity but may have a significant effect on the self-consumption and self-sufficiency metric.

The sensitivity analysis on the PV $LCOE$ allows us to outline that flexibility is a better choice than curtailment. However, the profitability of the resulting high PV penetration depends on the ratio between the PV $LCOE$ and the export power. If this ratio is lower than 1.2, the 83% PV penetration becomes profitable despite the curtailment. However, using flexibility enables one to reach profitability much sooner (at a ratio $\frac{LCOE^{PV}}{c_{exp}} = 1.78$). The value of the flexibility underlay here in the gain of time for the PV price to reach the break-even point to enable such high PV penetration.

This work primarily focused on ideal behavioral flexibility, without taking into account the technical flexibility coming from storage that may be a large source of flexibility. Besides, the findings set the basement for further research on the value of flexibility. To address these aspects, the following section investigates how DSOs can use remote-controlled technical flexibility assets to avoid grid reinforcement.

5.4 Harvesting the flexibility of PV systems

The line ampacity breaking, reverse power flow, and voltage rise can be easily mitigated by curtailment of the excess of PV (or other renewable-based) generation. However, this solution has a cost and is often considered as something to avoid as most as possible. Besides on-load tap changer and PV inverter reactive power capabilities, a third possibility is to add electrochemical storage to inject or absorb active power and thus mitigate the local energy surplus [Hashemipour et al., 2018]. The optimal placement of such storage assets for voltage regulation is also a current research question addressed in [Yong et al., 2018], for instance. When addressing the voltage-regulation problem, one cannot neglect either the line ampacity constraints or the transformer capacity constraints. However, the cost of generation or the cost of exchanging energy is not always explicitly integrated within the optimization problem formulation.

Another branch of the literature focuses more specifically on the optimal economic dispatch of distributed generation (including PV or other renewable-based generation and storage).

Such a problem is often referred to as the *optimal power flow* problem. As an example, [Hlalele et al., 2020] investigate the optimal dispatch plan under renewable generation constraints, i.e., the renewable-based generation cannot be freely curtailed. Similar constraints are considered in [Drabecki, 2019], which included the knowledge of existing stakeholders contracts that constraints the minimum and maximum generation at some specific network location. In [Nazari-Heris et al., 2019], the total cost of exchanging energy between microgrids is considered as the objective function of the optimal power flow problem. The authors consider that the DSOs' role is to regulate microgrids interactions to ensure their supply of energy and a safe network operation.

If no solution of the economic dispatch plan or optimal power flow problem can be found, or that such solution would lead to an inappropriate amount of energy being curtailed, the final solution is to perform grid reinforcement. However, grid reinforcement costs are not straightforward to estimate, as demonstrated in [Scheidler et al., 2018, Vu, 2018]. These costs directly drive the need for flexibility in an active distribution network. Several works investigated how a flexibility market can be created [Cruz et al., 2018, Jin et al., 2020]. Different pricing schemes are proposed to encourage participation in such markets and ensure fair retribution of the benefits [Mamounakis et al., 2019, Tsaousoglou et al., 2019]. In this literature study, the demand for flexibility and its value is often considered as an input parameter. The pricing mechanism is often similar to the retail-energy market, i.e., placing energy-based price bids [Olivella-Rosell et al., 2018].

The present work aims to complement the above literature by comparing the cost of the required flexibility with the cost of grid reinforcement. A new capacity-based pricing for flexibility is also proposed. Critical periods are defined when the network constraints are violated and call for flexibility. The DSO acts as a central dispatch planner and exploits the available flexibility to resolve the violation while maximizing the PV generation. This is formulated as an optimal power flow problem. The estimated reinforcement cost needed to avoid network constraints violations is compared to the cost for the prosumers to provide this flexibility.

5.4.1 Methodology

This study aims to compare the cost of providing flexibility to resolve network constraints violations with the cost of grid reinforcement in the framework of increasing PV penetration. To this end, the methodology consists of the following procedure:

1. The systems' optimal design and operation are obtained for a given PV penetration level.
2. The resulting grid power exchanges are inserted in a load flow problem simulation to evaluate the network constraints violations.
3. One or several consecutive violations of the network constraints are considered as intervention periods (IPs). The IPs are augmented with one 15-min time step before

and after the violation periods. This ease the optimization problem. Also, if the time between two consecutive IPs is shorter than 1h, the IPs are merged. For each IP, an optimal power flow problem is formulated to maximize the total PV generation and resolve these violations.

4. The resulting modified grid exchange profile is used to calculate the sum of the systems' operating costs ($OPEX^{opf}$).
5. The cost of providing the required flexibility is defined as the difference between the $OPEX$ after the DSOs intervention ($OPEX^{opf}$) and the original one ($OPEX^0$).
6. The cost of providing flexibility is compared with the grid reinforcement cost estimated from the initial load flow.

This procedure is repeated for several PV penetration levels and available flexibility capacity scenarios.

A Flexibility assets determination

For a given PV penetration level, the flexibility asset capacities are determined by solving an optimization problem and minimizing each PV system's total cost of ownership. In this work, we considered that the PV system flexibility could be provided by either active power curtailment, inverter reactive power capability, and the absorption or injection of active power using electrochemical storage. Hence, the optimization aims to find the appropriate battery capacity for each system, given an energy tariff. At the same time, the system's optimal operation is extracted.

The corresponding optimization is the same as the one proposed in Section 5.2. In this work, we consider only a variable volumetric tariff. Hence the optimization problem of a given system design can be formulated as:

$$\begin{aligned}
 \min \quad & TOTEX = OPEX + R \cdot cx^{bat} \\
 \text{where:} \quad & OPEX = ox^{ge} + ox^{bo} \\
 & cx^{bat} = E_{cap}^{bat} \cdot c^{bat} + b^{bat} \cdot c_F^{bat} \\
 & ox^{bo} : \text{see Equation 3.12b} \\
 & ox^{ge} = \sum_{t=1}^T (P_t^{imp} \cdot c_t^{imp} - P_t^{exp} \cdot c_t^{exp}) \\
 \text{subject to:} \quad & \text{Equations 3.1 to 3.3f}
 \end{aligned} \tag{5.18}$$

B Load flow and optimal power flow problem and intervention periods

The resulting grid exchange profiles ($P^{\text{imp}} - P^{\text{exp}}$) of all systems considered in a given network are used to solve the load-flow problem and extract potential violation of the network constraints. As a reminder, the load flow problem can be formulated as:

$$\text{Active power} \quad P_{i,t} = V_{i,t} \sum_{k=1}^n V_{k,t} (G_{ik} \cos(\theta_{i,t} - \theta_{k,t}) + B_{ik} \sin(\theta_{i,t} - \theta_{k,t})) \quad (5.19a)$$

$$\text{Reactive power} \quad Q_{i,t} = V_{i,t} \sum_{k=1}^n V_{k,t} (G_{ik} \sin(\theta_{i,t} - \theta_{k,t}) - B_{ik} \cos(\theta_{i,t} - \theta_{k,t})) \quad (5.19b)$$

$$\text{Line impedance} \quad Y_{ik} = G_{ik} + jB_{ik} = \frac{1}{R_{ik} + jX_{ik}} \quad (5.19c)$$

$$\text{Line current} \quad I_{ik,t} = Y_{ik} (V_{i,t} - V_{k,t}) \quad (5.19d)$$

where $P, Q_{i,t}$ are the active and reactive power bus injection at bus $i \in \mathbb{B}$, $V_{i,t}$ is the voltage magnitude, θ_i is the voltage angle, and $R_{ik}, X_{ik} (ik) \in \mathbb{L}$ are the line resistance and reactance respectively, j being the imaginary number.

The load flow equations (Equations 5.19a to 5.19d) are valid for all considered time step $t \in T$ which are considered independent.

The PV system are colocated with the load and battery at buses $i \in \mathbb{S} \subset \mathbb{B}$. We consider only the active power injection, which is possible only at these buses. For all other buses, the active and reactive power is equal to zero at all times. The injection power at the system bus is deduced from the solution of the optimal design and operation problem (Equation 5.18) as :

$$P_{i,t} = P_{i,t}^{\text{exp}} - P_{i,t}^{\text{imp}} \quad \forall i \in \mathbb{S}, \quad t \in T \quad (5.20a)$$

$$P_{i,t} = 0 \quad \forall i \notin \mathbb{S}, \quad t \in T \quad (5.20b)$$

$$Q_{i,t} = 0 \quad \forall i \in \mathbb{B}, \quad t \in T \quad (5.20c)$$

The voltage network constraints can be defined as the following:

$$\text{Voltage constraints} \quad V^{\text{low}} < V_{i,t} < V^{\text{up}} \quad (5.21a)$$

$$\text{Line ampacity limit} \quad I_{ik,t} < I^{\text{max}} \quad (5.21b)$$

$$\text{Transformer capacity} \quad S_t^{\text{tr}} = |V_{n^0,t} \cdot I_{n^0 n^1,t}| < \quad (5.21c)$$

where $V^{\text{low,up}}$ are the voltage lower and upper bounds, I^{max} is the line rated current, n^0 is the transformer low-voltage side node, S_t^{tr} is the transformer apparent power, and $S^{\text{tr,max}}$ is the rated transformer capacity.

An intervention period (IP) is a set of consecutive time steps when one or more network constraints (Equations 5.21a to 5.21c) are not satisfied. During this IP, the DSO can use the available flexibility to resolve the violations and keep the network safe. To this end, we formulate an optimal power problem (OPF) aiming to maximize the whole PV generation and constraining the DSO to minimize the effect of its intervention on the system's future operation. Namely, a constraint is applied to the battery state of charge so that the grid exchange profile after the IP is not disturbed. This constraint ensures that at the end of the IP, the state of charge corresponds to the one extracted from the original optimal operation (solution of the optimization defined in Equation 5.18):

$$\text{Battery state of charge constraints} \quad E_{i,t}^{\text{bat,OPF}} = E_{i,t}^{\text{bat}} \quad \text{for } t = [\text{IP}^{\text{start}}, \text{IP}^{\text{end}}] \quad i \in \mathbb{S} \quad (5.22)$$

where $E_{i,t}^{\text{bat,OPF}}$ is the battery energy decision variable of the OPF problem and $E_{i,t}^{\text{bat}}$ of battery energy extracted from the solution of Equation 5.18, and $\text{IP}^{\text{start, end}}$ are the first and last IP time step. Note that there can be any number P of IPs, which are independent OPF problems.

The OPF formulation is derived from POWERMODELS [Coffrin et al., 2018], which contains a battery model slightly different than the one exploited in this thesis: The battery energy balance (Equation 5.23a) is the same as the one considered in Chapter 3 (Equation 3.3a), except no self-discharge is considered here. The energy stored in the battery is constrained by upper and lower bounds (Equation 5.23b). Equation 5.23c ensures no simultaneous charge or discharge of the battery. The battery, through its inverter, is allowed to inject or absorb reactive power (Equations 5.23d and 5.23e). It also considers a constant power loss (active and reactive) P, Q_i^{loss} . The bus reactive power injection is constrained by Equation 5.23f. Finally, the maximum charge or discharge power is constrained by the maximum apparent injection

power (Equation 5.23g) and the maximum injection current (Equation 5.23h).

$$E_{i,t+1}^{\text{bat}} - E_{i,t}^{\text{bat}} = TS \left(\eta^{\text{cha}} P_{i,t+1}^{\text{cha}} - \frac{1}{\eta^{\text{dis}}} P_{i,t+1}^{\text{dis}} \right) \quad (5.23a)$$

$$E_{\min}^{\text{bat}} \leq E_{i,t}^{\text{bat}} \leq E_{\max}^{\text{bat}} \quad (5.23b)$$

$$P_{i,t}^{\text{dis}} \cdot P_{i,t}^{\text{cha}} = 0 \quad (5.23c)$$

$$P_{i,t}^{\text{bat,bus}} + (P_{i,t}^{\text{dis}} - P_{i,t}^{\text{cha}}) = P_i^{\text{loss}} + R_i * |I_{i,t}^{\text{bat}}|^2 \quad (5.23d)$$

$$Q_{i,t}^{\text{bat,bus}} = j \cdot Q_{i,t}^{\text{bat}} + Q_{i,t}^{\text{loss}} + X_i * |I_{i,t}^{\text{bat}}|^2 \quad (5.23e)$$

$$Q_i^{\text{bat,min}} \leq Q_{i,t}^{\text{bat,bus}} \leq Q_i^{\text{bat,max}} \quad (5.23f)$$

$$\sqrt{P_{i,t}^{\text{bat,bus}^2} + Q_{i,t}^{\text{bat,bus}^2}} \leq S^{\text{bat,max}} \quad (5.23g)$$

$$|I_{i,t}^{\text{bat}}| = \frac{\sqrt{P_{i,t}^{\text{bat,bus}^2} + Q_{i,t}^{\text{bat,bus}^2}}}{V_{i,t}} \leq I^{\text{bat,max}} \quad (5.23h)$$

where E^{bat} is the battery stored energy, $P^{\text{dis,cha}}$ is the battery charging and discharging power, $\eta^{\text{dis,cha}}$, its corresponding efficiencies, $E_{\max,\min}^{\text{bat}}$ corresponds to the min and max state of charge, $P, Q^{\text{bat,bus}}$ are the active and reactive power bus injection, $P^{\text{loss}}, Q^{\text{loss}}$ are constant power loss, Q^{bat} is a slack reactive power variable bounded by upper and lower bounds, $Q^{\text{bat,max}}$ and $Q^{\text{bat,min}}$, R and X are the injection resistance and reactance, and I^{bat} is the injection current.

Combining the storage flexibility with the PV systems and their inverter capabilities, the bus injection power constraints can be written as follow:

$$\text{Active power at system bus} \quad P_{i,t} = P_{i,t}^{\text{PV}} - P_{i,t}^{\text{cur}} + P_{i,t}^{\text{bat,bus}} - P_{i,t}^{\text{load}} \quad \forall i \in \mathbb{S}, t \in T \quad (5.24a)$$

$$\text{Reactive power at system bus} \quad Q_{i,t} = Q_{i,t}^{\text{PV}} + Q_{i,t}^{\text{bat,bus}} \quad \forall i \in \mathbb{S}, t \in T \quad (5.24b)$$

$$\text{Active power at all other bus} \quad P_{i,t} = 0 \quad \forall i \notin \mathbb{S}, t \in T \quad (5.24c)$$

$$\text{Reactive power at all other bus} \quad Q_{i,t} = 0 \quad \forall i \notin \mathbb{S}, t \in T \quad (5.24d)$$

$$\text{Curtailement limit} \quad P_{i,t}^{\text{cur}} \leq P_{i,t}^{\text{PV}} \quad \forall i \in \mathbb{S}, t \in T \quad (5.24e)$$

$$\text{Inverter reactive power} \quad -q_r^{\text{max}} \cdot P_{i,t}^{\text{PV}} < Q_{i,t}^{\text{PV}} < q_r^{\text{max}} \cdot P_{i,t}^{\text{PV}} \quad \forall i \in \mathbb{S}, t \in T \quad (5.24f)$$

where $P_{i,t}^{\text{load}}$ is the uncontrollable load, $Q_{i,t}^{\text{PV}}$ is the PV inverter reactive power injection, and q_r^{max} is the inverter reactive power capability measured in VAR/W.

Finally, the formulation of the OPF problem can be written as:

$$\begin{aligned}
 & \min_{P_{i,t}^{\text{cur}}, P_{i,t}^{\text{cha}}, P_{i,t}^{\text{dis}}, Q_{i,t}^{\text{bat,bus}}, Q_{i,t}^{\text{PV}}} \sum_{i \in \mathbb{S}, t \in [\text{IP}^{\text{start}} \dots \text{IP}^{\text{end}}]} - (P_{i,t}^{\text{PV}} - P_{i,t}^{\text{cur}}) \\
 & \text{where: } P_{i,t}^{\text{PV}} \text{ is calculated in Equation 3.2a} \\
 & \text{and the number of installed modules is fixed} \\
 & \text{subject to: load flow equations: Equations 5.19a to 5.21c} \quad (5.25) \\
 & \text{storage constrains: Equation 5.22} \\
 & \text{storage model: Equations 5.23a to 5.23h} \\
 & \text{bus power balance: Equations 5.24a to 5.24d} \\
 & \text{PV inverter flexibility: Equations 5.24e and 5.24f}
 \end{aligned}$$

The objective function is to maximize the net PV generation, which is equivalent to minimizing the curtailment. The formulation above is closer to the traditional literature's formulation [Chatzivasilieiadis, 2018, Coffrin et al., 2018, Hlalele et al., 2020].

C Cost assessment

Once a satisfying solution is obtained for all IPs, the resulting total operating cost is calculated with the modified grid exchange power and compared with the original operating cost:

$$\text{New OPEX} \quad OPEX_i^{\text{OPF}} = \sum_{i \in \mathbb{S}} \sum_{t=1}^T \left(P_{i,t}^{\text{imp,OPF}} \cdot c_t^{\text{imp}} - P_{i,t}^{\text{exp,OPF}} \cdot c_t^{\text{exp}} \right) \quad (5.26)$$

$$\text{Original OPEX} \quad OPEX_i^0 = \sum_{i \in \mathbb{S}} \sum_{t=1}^T \left(P_{i,t}^{\text{imp}} \cdot c_t^{\text{imp}} - P_{i,t}^{\text{exp}} \cdot c_t^{\text{exp}} \right) \quad (5.27)$$

$$\text{Cosf of flexibility provision} \quad \Delta OPEX = \sum_i OPEX_i^{\text{OPF}} - OPEX_i^0 \quad (5.28)$$

where, again, superscript OPF denotes the variable's value obtained by solving Equation 5.25 on all IPs. The values of these variables outside the IPs are the ones of the initial optimal design and operation problem (Equation 5.18). This is ensured by the continuity of the battery's state of charge of Equation 5.22.

The difference between these two operating costs defines the cost for flexibility provision (Equation 5.28). This cost is finally compared with the cost of grid reinforcement estimated

Chapter 5. Harvesting flexibility from a DSO perspective

using the solution of the load flow:

$$\text{Total annualized reinforcement cost} \quad C_{\text{reinf}} = R^{\text{grid}} \cdot (C_{\text{reinf,line}} + C_{\text{reinf,trafo}}) \quad (5.29a)$$

$$\text{Line reinforcement cost} \quad C_{\text{reinf,line}} = \sum_{(l) \in \mathbb{L}} \delta_l \cdot c^{\text{line}} \cdot d_l \quad (5.29b)$$

$$\text{Transformer reinforcement cost} \quad C_{\text{reinf,trafo}} = \delta_{tr} \cdot c^{\text{trafo}} \cdot \left(\max_t S_t^{\text{tr}} \right) \quad (5.29c)$$

$$\text{Line reinforcement needed} \quad \delta_l = \begin{cases} 1 & \text{if } \max_t I_{l,t} > I^{\text{max}} \\ 0 & \text{otherwise} \end{cases} \quad (5.29d)$$

$$\text{Transformer reinforcement needed} \quad \delta_{tr} = \begin{cases} 1 & \text{if } \max_t S_t^{\text{tr}} > S^{\text{tr,max}} \\ 0 & \text{otherwise} \end{cases} \quad (5.29e)$$

$$\text{Annuity factor} \quad R^{\text{grid}} = \frac{r^{\text{grid}} \cdot (1 + r^{\text{grid}})^{L^{\text{grid}}}}{(1 + r^{\text{grid}})^{L^{\text{grid}}} - 1} \quad (5.29f)$$

where c^{line} is the cost of replacing a line per unit of length, d_l is the line length, c^{trafo} is the cost of replacing a transformer per unit of capacity.

D Other performance indicators

In addition to the operating costs, which determines the cost of providing the flexibility, a few other performance indicators are defined in order to have a better understanding of the flexibility requirements and how it is delivered (in the following, operator $\sum_p = \sum_{p=1}^P$ is the sum of over all IPs, and $\sum_t = \sum_{t=1}^T$ is the sum over all time steps):

$$\text{Intervention period duration} \quad \Delta \text{IP}_p = \text{IP}_p^{\text{end}} - \text{IP}_p^{\text{start}} \quad p = 1 \dots P \quad (5.30a)$$

$$\text{Total intervention time} \quad \text{TIP} = \sum_p \left(\text{IP}_p^{\text{end}} - \text{IP}_p^{\text{start}} \right) \quad (5.30b)$$

$$\text{Cumulative energy stored} \quad E^{\text{stored}} = \sum_{i \in \mathbb{S}} \sum_t P_t^{\text{cha}} \cdot T S_t \quad (5.30c)$$

$$\text{Mean battery absolute deviation} \quad \Delta P^{\text{bat}} = \frac{\sum_{i \in \mathbb{S}} \sum_t \left| P_{i,t}^{\text{bat,OPF}} - P_{i,t}^{\text{bat}} \right|}{|\mathbb{S}| T} \quad (5.30d)$$

$$\text{PV inverter } \cos \phi \quad \cos \phi_{i,t} = \frac{P_{i,t}^{\text{PV,OPF}} - P_{i,t}^{\text{cur,OPF}}}{\sqrt{\left(P_{i,t}^{\text{PV,OPF}} - P_{i,t}^{\text{cur,OPF}} \right)^2 + Q_{i,t}^{\text{PV}2}}} \quad (5.30e)$$

5.4.2 Case study

We applied the presented methodology on the *CIGRE* low-voltage grid [CIGRE et al., 2009]. This is a simplified model of a three-phase European low-voltage grid, as pictured in Figure 5.20. Such a case study is a standard, representative case open for the research community. We consider the load and generation are balanced on the three phases to meet the above OPF formulation. In the original set-up, no PV generation or storage is present in the network, and only a daily profile is given for the load. Hence, we adapted this case study and assumed each load is a physical building with some roofs potentially covered by PV modules. We arbitrarily picked some loads from the FLEXI [Perret et al., 2015] and FLEXI 2 [Perret et al., 2019] projects and inserted them in the network. The buildings' characteristics (especially the roof area and orientation which determines the PV capacity and generation profile) are picked from the solar roof database⁵. The buildings are matched with the load according to their annual energy consumption estimated using the [SIA, 2015] norm. We assumed a time-of-use electricity tariff with a low rate during the night and weekend and a high rate during the day, as reported in Table 5.4. We estimated the cost of the battery for 2030, using the approach of [Bloch et al., 2019], is equal to 182 CHF/kWh. The transformer cost is assumed to be 60 CHF/kVA, and the line replacement cost 70 CHF/m [Zhang et al., 2013]. The lifetime of the grid components lifetime is assumed to be the same as the one of the transformers, estimated at 30 years by [Behi et al., 2017]. We assumed that only the PV inverter can provide reactive power up to 0.4 VAr/W [Bründlinger, 2020]. All parameters and corresponding values are reported in Table 5.5.

⁵<https://www.uvek-gis.admin.ch/BFE/sonnendach>

Chapter 5. Harvesting flexibility from a DSO perspective

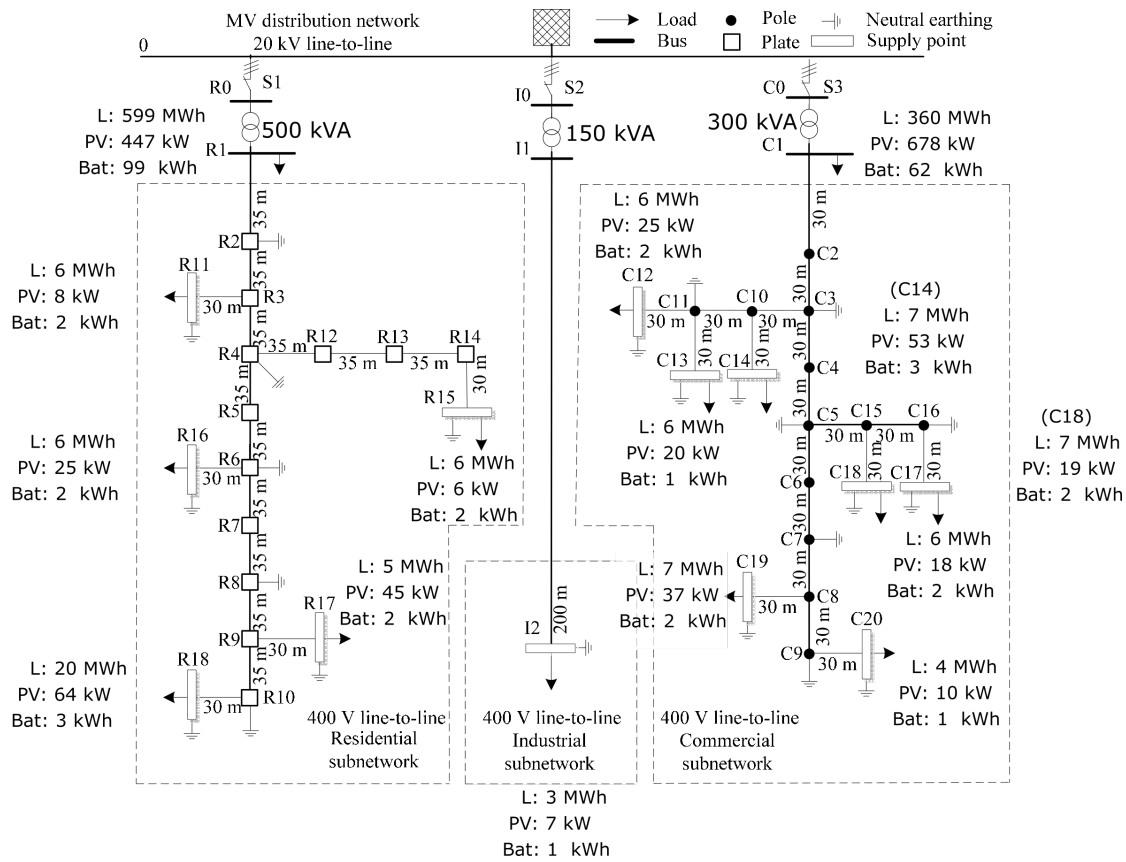


Figure 5.20 – Illustration of the CIGRE Low-voltage network adapted from [CIGRE et al., 2009]

Table 5.4 – Tariff

	Hours	Tariff (cts/kWh)
c^{imp}	Mon-Fri 06h-22h	23.92
	Mon-Fri 22h-06h	15.16
	Sat-Sun all-day	15.16
c^{exp}		8.16

5.4. Harvesting the flexibility of PV systems

Table 5.5 – System, PV, and battery parameters

	Param.	Unit	Value	Param.	Unit	Value
SYSTEM	T	-	35040	L	years	25
	M	-	12	L^{bat}	years	9
	TS	s	900	r	-	0.03
BATTERY, INVERTER	SOC_{init}	-	0.7	$\text{CR}^{\text{char,dis}}$	1/h	1
	$\text{SOC}_{\text{min,max}}$	-	0-0.7	c^{bat}	CHF/kWh	182
	α	1/day	0.04	c_F^{bat}	CHF	0
	$\eta^{\text{cha,dis}}$	-	0.98	c_o^{bat}	CHF/kWh	10^{-6}
	p^{loss}	MW	0	R	Ω	0
	Q^{loss}	MVAr	0	X	Ω	0
	$Q^{\text{bat,min,max}}$	MVAr	0	q_r^{max}	MVAr/MW	0.4
NETWORK	$V^{\text{low,up}}$	pu	0.95-1.05			R0-R1:500
	I^{max}	kA	1	$S^{\text{tr,max}}$	kVA	I0-I1:150
						C0-C1:300
	r^{grid}	-	0.03	c^{trafo}	CHF/kVA	60
	L^{grid}	years	30	c^{line}	CHF/m	70

The annual energy demand, maximum PV capacity, and corresponding battery capacity (obtained by solving Equation 5.18, with this maximum PV capacity and tariff) are reported in Table 5.6. The total annual energy demand is about 1000 MWh/year. The maximum installed PV and battery capacity is 1500 kW and 263 kWh, respectively. To evaluate the effect of an increasing PV penetration on the cost of providing flexibility and grid reinforcement, the PV capacity is slowly increased from 10% up to 100% of the maximal capacity (determine by the roof area). In this way, we define eight PV penetration scenarios. For each scenario, the number of modules is adjusted to prevent unrealistically small installation. In more details, the minimum number of modules that can be installed is determined as:

$$n_i^{\text{mod}} \geq \frac{R \cdot c_F^{\text{PV}}}{G_i} \cdot c^{\text{imp}} - R \cdot P_i^{\text{mod}} \cdot c^{\text{mod}} \quad (5.31)$$

where R is the annuity factor defined in Equation 3.11, c_F^{PV} the fixed cost of an installation, $G_i = \sum_t P_{i,t}^{\text{PV}} \cdot TS_t$ with $P_{i,t}^{\text{PV}}$ the modules generation power, P_i^{mod} is the module nominal power and c^{mod} is the PV variable cost.

The meaning of Equation 5.31 can be interpreted as the minimum number of modules to reach a $LCOE^{\text{PV}}$ below the import tariff c^{imp} (taken as 23.92 cts/kWh).

The resulting scenarios are reported in Figure 5.21. In this figure, the PV hosting ratio (define as the ratio between installed capacity and the maximum PV capacity) is also represented and

Chapter 5. Harvesting flexibility from a DSO perspective

the PV network hosting ratio, which compares the installed PV capacity with the transformer's capacity. As we have three transformers, the reference transformer capacity is the sum of the capacity, i.e., 0.95 MVA.

Table 5.6 – Systems data

	Annual demand (MWh)	PV max capacity (kW)	Battery capacity (kWh)
R1	598.97	447.09	141.13
R11	6.09	8.19	2.89
R15	6.13	6.30	2.18
R16	5.58	24.89	2.48
R17	5.29	44.74	2.30
R18	19.82	64.27	4.71
I2	2.88	6.93	1.21
C1	360.34	678.35	87.96
C12	5.89	19.53	1.39
C13	11.73	40.64	4.83
C14	7.02	53.25	3.69
C17	5.84	17.64	2.37
C18	6.56	18.90	3.10
C19	7.34	36.86	2.65
C20	3.59	10.08	1.09
Total	1053.08	1477.69	263.97

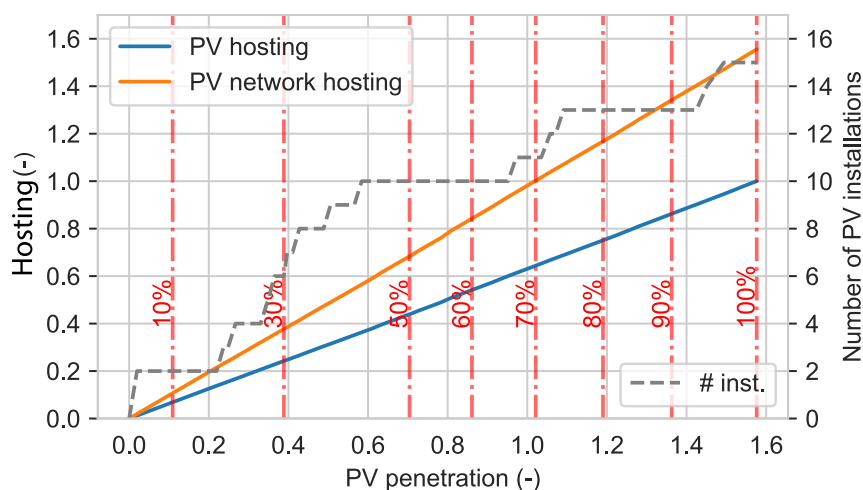


Figure 5.21 – PV hosting and PV network hosting ratio (left axis) and number of installed systems (right axis, maximum is 15 systems). The red dashed lines are the selected PV penetration scenarios. The numbers indicated in red are the scalings used to vary the PV capacity.

Finally, for each of the eight PV penetration scenarios, the load flow, and OPF problem are solved without considering the storage capacities. As a consequence, to cope with the grid constraints, only curtailment can be used. This will provide an additional comparison point for assessing the cost of flexibility provision.

5.4.3 Results

The solution of the load flow problem provides the essential information for the flexibility requirements. Figure 5.22 illustrates a particular day of the 100% PV capacity scenario. The blue curves in Figure 5.22a are the load-flow problem results for both the max transformer loading (over the three transformers) and the maximum bus voltage (over the entire set of buses). As one observed, both transformer loading and bus voltage violate the network constraints (represented with the horizontal black dashed line). Hence, there is a need for a DSO intervention to remotely control the PV inverters and batteries available in the network. Figures 5.22b and 5.22c illustrate the operation of one particular system. As one can see in Figure 5.22b, the PV generation is relatively high, and the battery is used to charge from PV energy at the end of the day to discharge and reduce the grid exchange during the evening, especially just before 22:00 when electricity is still at its high rate. The results of the OPF (Figure 5.22c) highlights that the DSO has to curtail a significant fraction of the PV energy while using the battery to limit curtailment at its minimum. Note that the operation at the end of the day (and in the morning) is precisely the same as the original. This is due to the constraints on the state of charge that ensure the operation's continuity and limit any future impact of the DSO intervention. This constraint is graphically illustrated in Figure 5.23. The original state of charge (in blue) and the "after OPF" state of charge coincide during the whole day except during the IP, where the battery is used to self-consume PV energy and avoid a small fraction of curtailment. As a result, the "after OPF" transformer loading and bus voltage (in orange) in Figure 5.22a stay nicely below their upper limits.

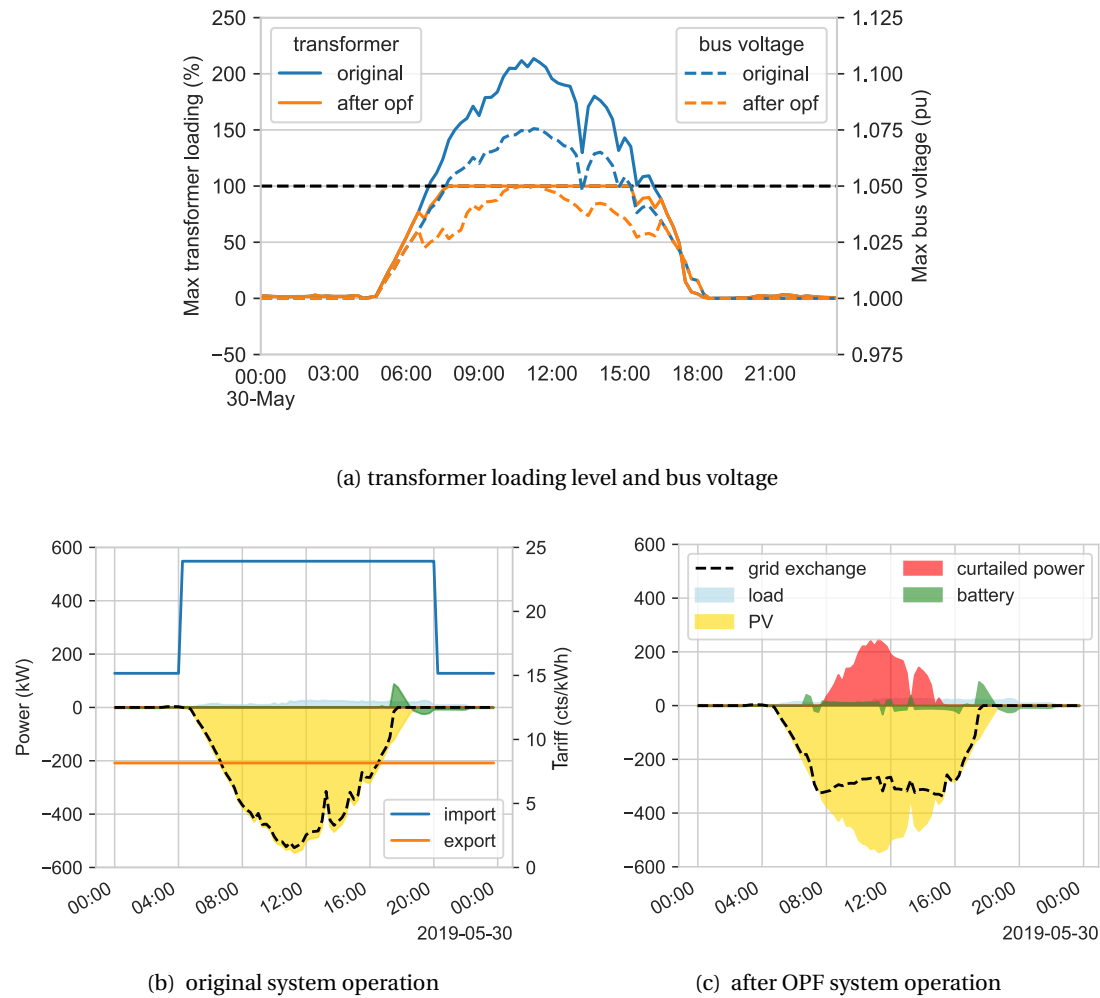


Figure 5.22 – Illustration of the network and one system active power along a day, for the 100% PV capacity scenario

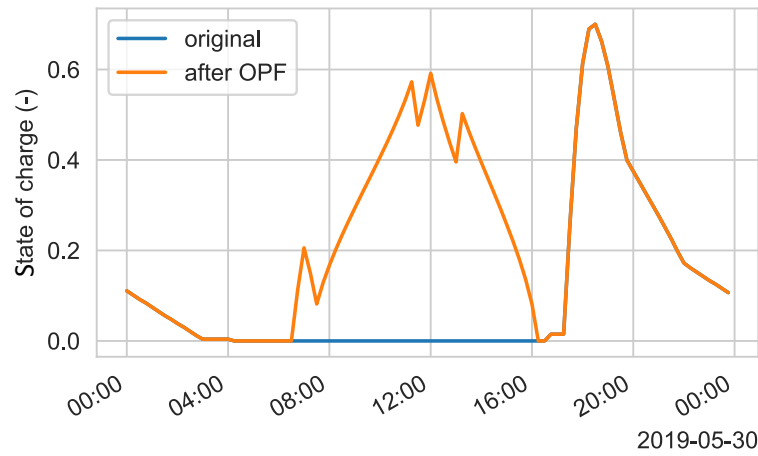


Figure 5.23 – State of charge evolution during a day. Note how the state of charge after the OPF comes back to its originally scheduled value.

The IPs length for the eight PV penetration scenarios and the case with or without storage are compared in Figure 5.24. A tiny difference can be observed between these two cases. An IP can reach up to 10 h, with a mean value reaching more than 4 h at the highest penetration scenario. The total intervention time for the case with storage is also indicated, increasing linearly from a 70% PV penetration ratio and reaching almost 1400 h at 160% PV penetration.

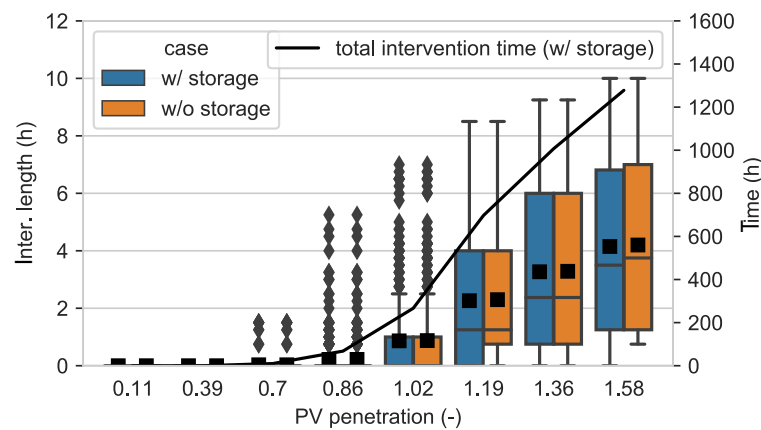


Figure 5.24 – Duration distribution (left axis). Averages are indicated with a square and outliers with a diamond. The total intervention time is on the right axis.

Table 5.7 summarizes the type of network constraints violations for each PV penetration. The use of storage slightly reduces the amount of time but not the magnitude of the maximum violations. Network violations occur starting with a PV penetration of 70%, with transformer overloading. No current ampacity breaking has been observed. Bus over-voltage occurs starting at a PV penetration of 120%.

Chapter 5. Harvesting flexibility from a DSO perspective

Table 5.7 – Summary of the network violations. Differences between the case with and without storage are indicated in **bold**.

	Transformer overloading				Bus over-voltage			
	time (h)		max (%)		time (h)		max (pu)	
	w/o storage	w/ storage	w/o	w/	w/o	w/	w/o	w/
PV penetration	0.11	-	-	-	-	-	-	-
	0.39	-	-	-	-	-	-	-
	0.70	5	5	110	-	-	-	-
	0.86	44	44	134	-	-	-	-
	1.02	175	173	158	-	-	-	-
	1.19	530	523	186	30	29	1.06	1.06
	1.36	804	799	215	442	439	1.07	1.07
	1.58	1060	1044	246	850	846	1.09	1.09

To understand how much DSO is using the battery, Figure 5.25 highlights the difference between the cumulative energy stored with the original operation and after DSO intervention. The difference becomes significant from a PV penetration around 1. The mean battery deviated power is relatively stable to 4 kW.

The DSO can also use the PV inverter reactive power capabilities. Figure 5.26 pictures the distribution of the $\cos \phi$ of the PV inverter for the maximum PV penetration scenario. Mostly there is no reactive power injection except for a particular system with a $\cos \phi$ regularly close to 0.93.

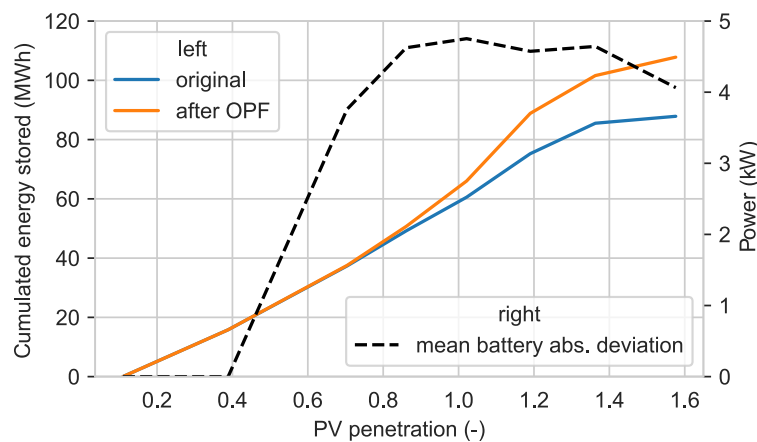


Figure 5.25 – Cumulative energy stored (left axis) and mean battery deviated power (right axis)

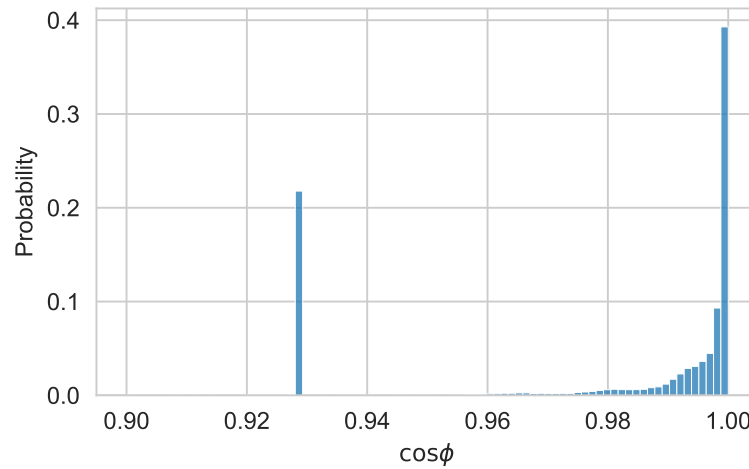


Figure 5.26 – Distribution of the $\cos \phi$ value during intervention time

The last resource for coping with grid constraints is PV production curtailment. This is also the objective function of the OPF problem. Table 5.8 reports the value of the energy curtailed for the case with or without storage and the PV production. The ratio of energy curtailed represents at most 8% of the PV annual production (at the maximum PV penetration). Using storage allows a significant reduction of the amount of energy to curtail.

Table 5.8 – Energy curtailed and PV production

PV penetration	Energy curtailed (MWh)		Generation (MWh)
	w/ storage	w/o storage	
0.11	0	0	115
0.39	0	0	409
0.70	0	0	742
0.86	0	1	907
1.02	0	8	1076
1.19	3	32	1253
1.36	14	77	1435
1.58	49	139	1660

Although the PV curtailment is small, the DSO intervention's financial impact, namely the cost of flexibility provision, has to be compared with the cost of grid reinforcement. Figure 5.27 highlights that the cost of providing flexibility is smaller when using storage than without it (the latter corresponds to the curtailment cost). As the grid reinforcement cost is quite difficult to predict, the grid reinforcement cost is scaled and reported to the transformer's specific cost. The bold black dashed line corresponds to a reference transformer value of 60 CHF/kVA. Any colored dashed line shows the reinforcement cost scaled between 0.2 (12 CHF/kVA) and

2 (120 CHF/kVA). This allows estimating in which penetration level range is the distributed flexibility competitive with grid reinforcement. In this case, curtailing is competitive until PV penetration between 0.9 and 1.2 while adding storage in the flexibility port-folio allows being competitive until a PV penetration of 1.2 or further. Distributed flexibility is readily competitive until reaching the maximum PV capacity assuming a grid reinforcement cost above 90 CHF/kVA

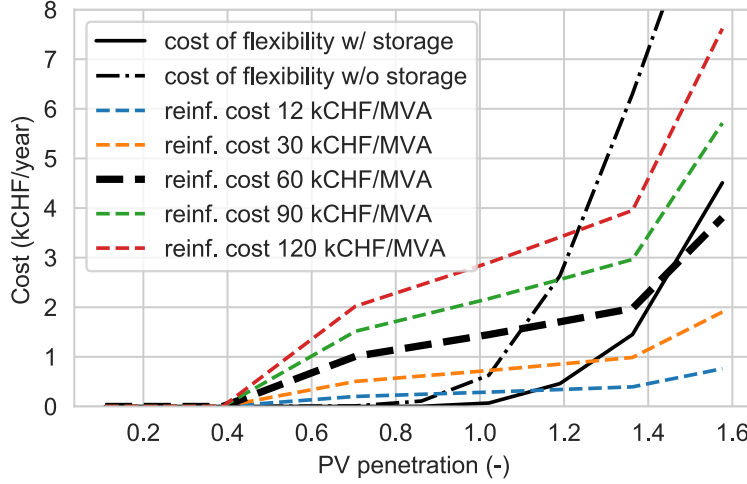


Figure 5.27 – Total cost of flexibility

Recalling that optimal design and operation ensure the battery's profitability under a given tariff, the flexibility cost corresponds to the compensation by the DSOs for having controlled the PV systems. A small margin can serve as additional compensation to bring acceptance for such policy and cover any additional cost for remote control or additional battery degradation (which was not estimated here). In the following, we investigate two possible mechanisms, one energy-based reward, and one capacity-based reward.

The flexibility cost margin is the difference between the cost of grid reinforcement and the cost of flexibility. Hence, it corresponds to the benefits made by DSO for avoiding grid reinforcement. To redistribute these benefits to the customers, one could imagine having energy-based or a capacity-based flexibility cost, i.e.:

$$C^{\text{flex,margin}} = C_{\text{reinf}} - \Delta OPEX \quad (5.32)$$

$$C_{\text{energy}}^{\text{flex,value}} = \frac{C^{\text{flex,margin}}}{\sum_i \sum_{t \in \cup_p} IP_p (P_{i,t}^{\text{cha,OPF}} + P_{i,t}^{\text{cur}}) \cdot TS_t} \quad (5.33)$$

$$C_{\text{capacity}}^{\text{flex,value}} = \frac{C^{\text{flex,margin}}}{\sum_i PV_i^{\text{cap}} + E_{\text{cap},i}^{\text{bat}} \cdot CR_i^{\text{dis}}} \quad (5.34)$$

where PV_i^{cap} is the installed PV capacity and $E_{\text{cap},i}^{\text{bat}} \cdot CR_i$ is the battery rated power capacity (i.e., maximum charge and discharge power, assuming equal).

The evolution of the energy-based flexibility value with increasing PV penetration for a case with or without storage and varying grid reinforcement cost is plotted in Figure 5.28. Due to the discontinuous nature of the grid reinforcement cost, at low PV penetration, an energy-based flexibility reward would lead to a high cost and then decreases with the PV penetration. The energy-based flexibility value would indeed reduce to an insignificant value at high PV penetration, raising some concerns about the viability of such schemes. Indeed as the need for flexibility involve more and more energy to be either curtailed or shifted by the battery, and the flexibility being more and more reduced as the cost of providing flexibility increase, the resulting energy-based flexibility value decreases very quickly. The alternative capacity-based flexibility value is reported in Figure 5.29. As one can observe, this reward scheme offers a wide range of conditions in which the flexibility value is positive and substantial. The case without storage offers a sharp drop as observed for the energy-based flexibility value for a similar reason. However, considering storage enables a flexibility value of about half of the grid reinforcement cost between 70% and 100% PV penetration.

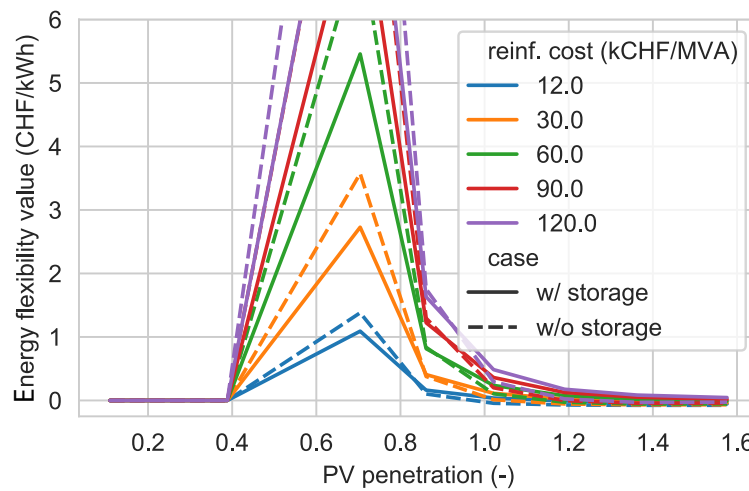


Figure 5.28 – Flexibility cost margin normalized by the shifted energy

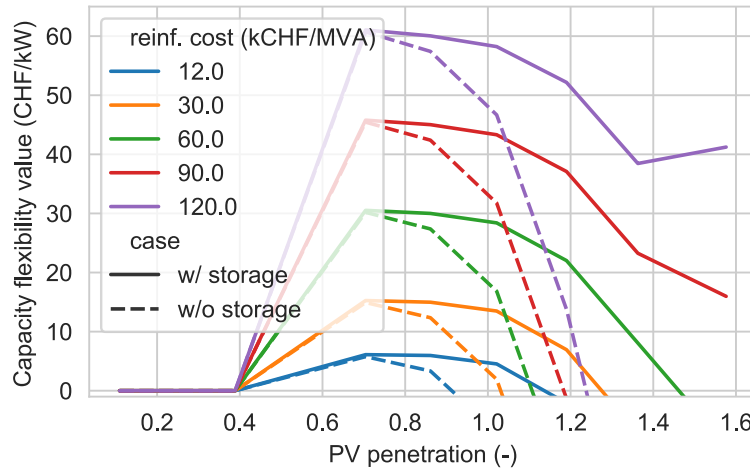


Figure 5.29 – Flexibility cost margin normalized by the installed PV capacity

5.4.4 Discussion

In this work, the PV penetration was used as a reference metric to compare the hosted PV capacity with the network capacity. The choice of this metric relies on the assumption that networks are designed to sustain the maximum consumption power. In this particular case, as the network is composed of three substations, it is most appropriate to use the PV penetration than the ratio between the PV capacity and the sum of the transformers' capacity. The latter could be a relevant metric as well.

The results highlight that flexibility is profitable over grid reinforcement when the PV penetration approaches 50% until about 110%. Although an upscaling of these numbers is not straightforward, it gives some perspective on the economic advantage of distributed flexibility over grid reinforcement in the context of the Swiss energy transition. In 2050, it is expected that Switzerland will consume 76 TWh of electricity covered, amongst others, by 34 TWh of PV. This is a PV penetration of "only" 45%. Thus the current study contributes to ensuring the feasibility of this goal from a system integration point of view. Nevertheless, it is by far relevant to focus on what is happening at higher PV penetration, which can typically occur in rural or suburban areas. Hence, such study should replicate on different network topology ranging from dense urban to rural areas. One could expect that grid reinforcement might quickly be the best option in rural areas as flexibility would be more appropriate in an urban context. Our findings contrast with those of [Gupta et al., 2021], who do not explicitly consider flexibility in their deployment scenario for PV, heat pumps, and electric vehicles. Our approach differs in two ways. First, smart active power curtailment is considered. Second, the battery size is optimized according to each systems leading to a network with 0.2 kW (or kWh) of battery power (or energy, in our case) capacity per kW of PV paid by the building owners, while [Gupta et al., 2021] consider a battery power capacity equal to the PV capacity paid by the DSO. Thus, our findings complement the work of [Gupta et al., 2021] and by adding that the 11 Billion CHF

needed for grid reinforcement can be lowered. For the share of the low-voltage networks, those with a PV penetration above 45%, might benefit from the flexibility and reduce the total cost for grid reinforcement. To converge to a coherent assessment of the Swiss situation, our approach should be extended with electric vehicles and heat pumps.

In this work, we proposed to remunerate flexibility by compensating for the additional cost induced by the DSO intervention. By definition, this quantity is positive as the decision variable deviates from the optimal control trajectory. In an actual implementation, under the no-storage case, this assumption is realistic as the most optimal control of a PV system is to always inject at the maximum available generation power. Under a storage scenario, this optimal control assumption is questionable but could be the ground for a fair posterior calculation of the flexibility compensation. In more details, let us assume that for a particular day, the DSO had to activate the charging of a battery to ease the network from excess PV generation. The next day, knowing precisely the past PV generation and load, the DSO could calculate the optimal battery control trajectory and pays the difference in operating cost between the optimal control version and the actual operating cost of the considered day.

To redistribute the avoided grid flexibility cost, the most adopted approach is an energy-based remuneration scheme [Mamounakis et al., 2019, Olivella-Rosell et al., 2018, Jin et al., 2020], but our results show that such a flexibility value decreases very quickly with the PV penetration. Hence, using such compensation schemes, and giving that the avoided cost (about 1000 CHF/year) being small compared with the total expense for energy provision (1 GWh/year times 0.21 cts/kWh is about 200'000 CHF/year), the energy-based flexibility value would not be an appropriate signal to foster acceptance of DSO controlled assets. However, a capacity-based compensation scheme presents more advantages. Under such a mechanism, the value of flexibility is more constant while distributed flexibility stays competitive compared to grid reinforcement. Its value corresponds to a one-time payment of 30 CHF/kW of installed PV and battery capacity if the DSO is allowed to control this system. This is a 10% percent additional subsidy to the 290 CHF/kW⁶ of the unique retribution from the current Swiss PV encouragement scheme. This could potentially cover the additional cost of a remote controller. This flexibility value is a compensation for letting the DSO control the battery and does not consist in a mandatory contribution to the profitability of the battery. Indeed, the battery size is determined by an optimization problem that does not take into account future income from the DSO's intervention. There is still an open question on the quantification of the DSO-induced battery degradation. Especially at high PV penetration, the DSO's interventions increase the number of cycles (or the total energy stored) by about 15% at a penetration of 120%. This is still moderate but may raise concerns as larger PV penetration leads to a more significant increase in the battery DSO usage.

The flexibility provision cost, defined as the difference between an original and new *OPEX*, heavily relies on the tariffs. This opens the path of new research questions about the interaction between the tariff structure (which impacts the system's design and operation, thus the grid

⁶Appendix 2.1, ch2.3 of OEnER

reinforcement needs and flexibility requirements) and the cost of providing the flexibility. In particular, capacity-based tariffs and block-rate tariffs may be particularly interesting as their ability to reduce the grid's stress can be conjugated with harvesting the particularly high battery capacity they incentivize.

5.5 Conclusion

This chapter aims to propose solutions and guidelines for distribution system operators (DSOs) to harvest the distributed flexibility offered by PV systems. Distributed PV systems offer new opportunities for DSO to delay investment in grid reinforcement. As a general outline of this work, we can state a few recommendations for DSOs. First, the constitution of energy communities is beneficial from a PV deployment perspective as it allows to reduce investment costs and increase the social welfare of the communities. In contrast, it does not bring any advantages from the grid perspective and even slightly increases the grid's stress without offering more flexibility capacity. However, there is an advantage of grouping flexible assets into fewer, larger capacities. From a grid management perspective, there is more gain in offering suitably tailored electricity tariffs that reduce the stress on the grid and promote additional flexibility capacity, in the forms of batteries, for instance, than encouraging energy communities. Second, ideal behavioral flexibility may be an excellent opportunity for DSOs to increase the PV penetration up to 20% theoretically. Although this concept is challenging to put into practice and might show being unreliable, behavioral change in consumption habits helps and, as such, is worth being promoted. Third, there is a case for distributed flexibility as a competitive alternative to grid reinforcement. In the path toward a high PV penetration in our low-voltage grids, leveraging the available flexibility is an excellent opportunity to delay grid investment. It implies a compensation mechanism to ensure no pejoration of the PV systems' financial stability. We propose a simple mechanism where the DSO compensates the economic loss implied by the remote control of the energy management. The remote control cost can be covered by the benefits of avoiding grid-reinforcement costs and can be a one-time contribution to the PV systems investment.

More precisely, this chapter started with an investigation of the effect of aggregating systems to form energy communities on the grid stress. We compared several community scenarios, from no-aggregation (all individual buildings) to one large energy community for the whole network under three tariff scenarios. For each case, the optimal battery size and operation were determined while PV was assumed to be fixed at its maximum to ensure a maximal PV penetration. The results highlight that energy communities have a negligible negative effect on the grid impact, which can be compensated by electricity tariffs. The major advantages of forming energy communities are the reduction of the total investment cost and the reduction of the flexibility assets that can be controlled by DSOs.

Then we investigated to which extent ideal behavioral flexibility can increase the network PV hosting capacity. We used the *device usage prediction* algorithm to disaggregate households'

smart meter measurements and get the shiftable energy potential. Their loads were allocated into a low-voltage network. The maximum PV hosting capacity of the network was determined by ensuring that the maximum reverse power flow of the transformer did not exceed its capacity. The shiftable power was freely moved into the critical periods to reduce excess PV generation peaks. An iterative process allowed to extract the maximum PV hosting capacity, which can be increased by 20% by harvesting ideal behavioral flexibility.

Finally, we looked at the value of the flexibility in a framework where the DSO can control the flexible assets, namely batteries, of distributed PV systems, to maintain a safe network's operation. We evaluated the cost of providing the required flexibility to keep the network in safe operating bounds by calculating the difference between the original operating cost given by optimal control and the operating cost associated with the DSO interventions. The cost of providing flexibility was compared with the grid reinforcement cost. Any positive difference between them is referred to as the flexibility value. We highlighted that distributed flexibility is profitable until a PV penetration of 100-145% depending on the grid reinforcement costs.

To summarize the essential findings of this chapter, we compare the behavioral and technical flexibility provision cost with the grid reinforcement cost under different PV penetration in Table 5.9. The costs are normalized by the total network consumption to allow a comparison.

A capacity-based reward mechanism, to encourage PV system owners to provide such remote-controlled flexibility, was found to be more adapted than an energy based reward mechanism.

This statement contrasts with the demand-side management remuneration schemes that were proposed at the beginning of this thesis. Indeed a remunerative incentive to foster household flexibility usually takes the form of energy-based remuneration schemes (variable tariffs, for instance). The interesting alternative capacity-based remuneration schemes could be applied to a household demand-side management program. As an idea, households could propose a particular capacity they can reduce (or increase). They are paid if they have been able to achieve the proposed power reduction or increase respectively during a particular event. These reflections close the loop of this thesis and lead to the conclusion.

Table 5.9 – Cost of flexibility summary

	Unit	Behavioral ¹		Technical ²		
PV penetration	(%)	73 ^a	87	70 ^a	145	158
PV capacity	(kW)	440 ^a	530	650 ^a	1360	1480
Consumption	(MWh)	720		1060		
Flexibility provision cost[*]	(cts/kWh)	0 ^b	0 ^b	≈ 0	0.26	0.43
Avoided grid reinforcement cost[†]	(cts/kWh)	0	0.14	0.01	0.26	0.36
Flexibility profitability (yes/no)		yes		yes	no	

¹ Study realized on the Rolle case study

² Study realized on the *CIGRE* test case

$$* = \frac{\Delta OPEX}{\text{Consumption}}$$

$$† = \frac{C_{\text{reinf}}}{\text{Consumption}}$$

^a Estimated maximum PV penetration without requiring flexibility

^b Ideal behavioral flexibility is assumed to be free in this analysis

6 Conclusion

“Solving the climate crisis is the greatest and most complex challenge that Homo sapiens have ever faced. The main solution, however, is so simple that even a small child can understand it. We have to stop our emissions of greenhouse gases.

Either we do that or we don’t.” [Thunberg, 2019]

Summary

This thesis aims to contribute to global climate change mitigation by proposing significant contributions to foster a large penetration of renewable energy, particularly photovoltaics (PV).

As distributed PV is expected to be one of the pillars of the energy transition, flexibility requirements will increase, especially at the district scale. Under high unbalance between local generation and demand, low-voltage grids may experience over-voltage, line ampacity, and transformer capacity breaking. To cope with this challenge, this thesis aims to provide insights to promote PV systems flexibility and use these assets to mitigate the grid impact of large-scale deployment of PV systems and delay grid reinforcement.

In Switzerland, most of the distributed PV will be installed on roof-tops. The consequence of the generation decentralization is to enforce the households and the private sector’s role as distributed energy producers. The households’ ability to adapt their power demand is, thus, of primary relevance. We investigated, in Chapter 1, the household’s flexibility potential by proposing an analytic method to disaggregate the smart meter consumption measurements into appliance categories. The *device usage prediction* (DUE) algorithm is based on a Markov model of the household activity chain, which infers, based on the power measurements, which activities are occurring, and which appliances are activated. We benchmarked this algorithm against four state-of-the-art algorithms. The DUE being an unsupervised algorithm, it performs similarly from a disaggregation perspective but does not suffer from an exponential increase of the computation time with the dataset’s size.

Chapter 6. Conclusion

In Chapter 2, this algorithm was used to disaggregate a panel of households' smart meter measurements to evaluate their flexibility potential. This potential was compared with their reactions to time-of-use tariffs in the context of a field experiment. Two groups of households were submitted to two different treatments. First, a time-of-use tariff with a low rate during 11:00-15:00 was applied. The second tariff consisted in a low rate, applied either between 10:00 and 13:00, 13:00-16:00, or 16:00-19:00. The decision to activate low rate periods relied on the weather forecast and depended on solar insolation during these periods. If enough solar insolation was expected, a low rate period was scheduled for the corresponding period. The households were informed by SMS one day in advance of the activation of the low rate periods. The households' reaction was measured using a dedicated score comparing the average power during low rate periods with the average daily power. The variation of this score and the mean daily consumption variation were compared with a control group (receiving no incentive or information). The observed behavior change is low but still perceptible. A significant fraction of the households receiving the incentives increased their flexibility score compared with the control group. The achieved flexibility potential, assessed by comparing the measured flexibility score with a theoretical score using the disaggregation tool DUE, lies between 30 and 90%.

The flexibility potential of new PV adopters was also assessed in Chapter 2. In the context of PV systems in self-consumption schemes, the challenge is that smart meters do not measure the households' consumption but the net exchange of energy with the grid. Hence, a dedicated methodology was proposed to estimate the actual households' consumption from smart meter measurements and simulated PV generation. The drawback of this method is that it overestimates the PV self-consumed energy. A quantification of this error was performed to have a critical view of the results. To minimize the effect of this bias, the analysis was also restricted to clear-sky days only. Instead of the self-consumption ratio, we proposed a normalized self-consumption (NSC) metric that allows comparing systems with various PV penetration (or PV size) on a comparable basis. The results highlighted a significant consumption behavior change for PV adopters compared with the control group.

The behavioral flexibility potential was compared, in Chapter 3, with the technical flexibility. There is no doubt that any technical measure, particularly storage, can multiply by three the average power demand during a particular period of interest compared with behavioral flexibility. The model presented in Chapter 3 considers either storage (electrochemical) and power-to-heat (namely, heat pumps and electric heater). This model can be translated into a linear optimization problem. The decision variables are the design variable (PV capacity, storage size, power-to-heat capacities) and the system's operation ones (ultimately the import and export power, constraints by the power balance, and technology constraints). This model was used to assess the effectiveness of design regulation to enforce PV systems flexibility. The results highlighted that imposing a minimum battery size per PV capacity unit can deteriorate PV adoption, grid impact, and financial consequence.

A heuristic heat pump control algorithm (HCA) was proposed in Chapter 3. The algorithm

is based on optimizing an indicator that compares the variation, by a given action, of the operating cost with the heat produced. Besides the proposition of this novel, practical, and easily implementable algorithm, a comparison between this algorithm and the optimal control closes the gap between energy planning (which concerns the design of energy systems and some estimation of their operation) and the energy management problem. This work highlighted that the proposed control algorithm performs similarly to the optimal control.

One of the primary results of this thesis was presented in Chapter 4. The electricity tariff is a relevant lever to promote PV systems flexibility and mitigate the impact of a large PV penetration. At the building level, the system design and operation were studied to understand how it adapts to advanced tariff structures. The battery usage changes from "increasing self-consumption" to "energy trading" when switching from a flat to a variable tariff. In contrast, the battery is used to cut consumption peak under capacity tariffs. The addition of PV increases the heat pump capacity, but it is marginally affected by a tariff change, except for the capacity tariff. The electric heater capacity is adapted to the heat demand and complements the heat pump capacity. We also introduced a block rate tariff in which the energy tariff depends on the power level at which it is exchanged. In particular, the energy rate increases with the import power. Conversely, the export tariff decreases when the export power increases. In our example, this tariff significantly penalizes the PV penetration. Nevertheless, the design of block rate tariffs is challenging, and other designs might mitigate this effect. More specific research is needed on that matter. These results are up-scaled to a low-voltage network hosting about 40 buildings with a PV potential of 1.5 MW. The conclusions at a single building level are easily transposed to a large set of buildings. For buildings with a significant PV penetration, curtailment and electric heaters are used under capacity tariffs to cut peak export power. The tariff strongly impacts the grid usage intensity. Indeed, variable tariffs lead to more intensive grid exchanges, which turn into more significant voltage deviations, line, and transformer loading. Again a block rate tariff promotes smaller PV installation, thus reduce the impact on the grid. In contrast, a capacity tariff allows installing the full PV potential (as for all other volumetric tariffs) and significantly reduces the grid impact.

To up-scale the study from a single building to a whole network case, appropriate building load scenarios are needed. Smart meter measurement could be particularly suitable, but the privacy-preserving consideration does not allow direct use of such a precious data source. We addressed this challenge, in Chapter 4, by proposing two approaches for using smart meter data while hiding to the final data user, the customers' location, thus respecting its privacy. The first approach is based on the allocation of smart meter measurements (possibly obtained in a different network). Those are normalized to match the annual energy consumption at the building level (either known or estimated from a static approach) and deformed so that the grid load's aggregation meets the transformer active power measurements. The second approach relies on the assumption that substituting any load by one presenting similar electric characteristics will produce relevant results from a grid impact perspective. Thus, we proposed a *smart meter anonymization technique for network analysis* (SMANET) that groups load measurements by three according to their electrical characteristics. The three

Chapter 6. Conclusion

grid locations are provided on a group basis, hence guaranteeing privacy preservation. The two approaches were tested in a reference case study. The results highlight that both methods have specific advantages and drawbacks. In particular, the SMANET method allows a better accuracy on the local voltage deviation than the allocation, while the latter shows a greater accuracy regarding transformer loading. The feature selection for the grouping phase of the SMANET approach has little influence on its performance.

In Chapter 5, we described how a distribution system operator (DSO) could harvest the available flexibility potential. First, we showed that the aggregation of systems to create energy communities is not an effective approach to mitigate the impact of a large PV penetration compared to electricity tariffs. Furthermore, the system aggregation may lead to more severe voltage deviation and peak transformer loading. Second, we showed that behavioral flexibility could significantly contribute to the maximum network PV hosting capacity. Finally, we showed how distributed flexibility could be harvested to resolve grid network constraint violations by allowing a DSO to control curtailment and storage in the available PV systems. The resulting over-cost induced by the controlled system's non-optimal trajectory is paid to the system owner and represents the flexibility cost. This cost was then compared with grid reinforcement. We showed that the value of flexibility, defined as the benefits of applying such scheme instead of grid reinforcements, represents about half the cost of grid reinforcement, i.e., about 30 CHF/kW.

Thus, we contribute to addressing the challenge of integrating a high PV penetration by promoting flexibility for PV systems in the following way:

- We showed that behavioral flexibility has low but measurable effectiveness. However, it may raise customers' interest in their energy consumption and drive energy savings. We highlighted how households' shiftable energy could match local PV production (Chapter 2) and increase the PV network hosting capacity (Section 5.3).
- We proposed a disaggregation algorithm suitable for low smart meter measurement resolution (15 min), providing valuable insights for DSO and energy retailer customers (Chapter 1).
- We showed that tariffs are promising tools to promote systems flexibility (Sections 3.5 and 4.2). They offer some economic advantages over design regulations.
- We demonstrated how tariffs define customers' interactions with the electrical network and mitigate the impact of a high PV penetration (Section 4.4).
- We proposed two approaches to exploit smart meters data for network planning purposes while coping with privacy preservation regulations (Section 4.3).
- We showed that aggregating systems to form energy communities does not contribute to mitigating grid impact (Section 5.2).

6.1. Policy recommendations for the promotion of distributed PV in Switzerland

- We proposed an approach to estimate the flexibility value and a remuneration scheme for the distributed flexibility (Section 5.4).

6.1 Policy recommendations for the promotion of distributed PV in Switzerland

This thesis presented evidence that PV systems flexibility is a vital component for successfully integrating a large share of renewable energy in Switzerland. This section aims to contribute to future energy-related political debates to translate the findings into concrete actions.

6.1.1 Citizen involvement in the energy transition

Switzerland has a direct democracy. The citizen's political involvement is high and strategic decisions can be influenced through democratic instruments, such as popular federal initiatives and referenda. This emphasizes that the energy transition cannot be achieved without the citizen's strong support and participation. So many aspects of the Swiss CO₂ emission are related to citizen behaviors and choices. As depicted in the Swiss energy perspective for 2050 [SFOE, 2021], the massive integration of renewable energy must receive wide acceptance. In this respect, PV energy already enjoys good support from the population. However, only a minor fraction of the population has access to this technology. Only one third¹ of the Swiss households owns their dwelling. This means that only this share can decide to invest and install PV if their financial means are sufficient. Self-consumption communities only concern tenants of buildings whose owners have environmental concerns.

There is a bias in the access to distributed renewable energy. First, it is currently only for the wealthiest who can invest either for their own use or for their tenants as a long-term financial investment. There is a need to provide broader access to PV technology for the following reasons. First, it emphasizes redistribution of wealth created by local energy production, thus enforcing a more social energy transition. Second, it unlocks the households' flexibility potential by fostering energy consumption/production awareness. Thus, it promotes investment and acceptance of flexible technologies.

In this context, the creation of energy communities is particularly relevant. This thesis showed that such spatial aggregation does not significantly impact the network compared with a case without aggregation. However, energy communities can leverage social innovation to promote energy conservation and behavioral flexibility. An innovative business model could consider the community as a cooperative, with shareholders sharing a fraction of the initial investment cost, the rest being covered by external funding. The cost and benefits shall be shared to promote adequacy between the demand and local energy production and energy conservation.

¹<https://www.bfs.admin.ch/bfs/en/home/statistics/construction-housing.html>

These recommendations can also encourage the acceptance of other renewable energy sources. In particular, most wind energy projects experienced a low acceptance in Switzerland. Promoting citizen involvement by constituting citizen-owned energy communities to invest in wind energy has a great potential to increase the acceptance and chance of success to harvest the potential of this energy source.

6.1.2 Comments on the current Swiss framework

Decarbonization scenarios for Switzerland imply to install typically between 34 and 50 GW of PV capacity by 2050 [SFOE, 2021, Nordmann, 2019]. The current Swiss energy and electricity provision laws include a few mechanisms to promote renewable energy source investments. The future revision of the energy and electricity provision law includes a complete liberalization of the retail energy market, including for small customers. This future regulation includes a base energy provision mechanism constituted of 100% Swiss and renewable energy. This deregulation offers vast opportunities for local energy markets, which would enable peer-to-peer energy trading. Those can be beneficial to offer universal access to cheap PV energy.

The provision of flexibility as a service by end-customers is at least considered in the new law project, though no instrument to promote such flexibility is described. There is currently a high risk that this flexibility cannot be harvested due to a lack of technical measures to ensure that DSO can access these opportunities. Future grid codes might include guidelines and minimum specific requirements for the flexibility of PV systems. Allowing peak shaving can be an appropriate measure to delay grid investments, but it should be remunerated to maintain the PV systems' financial profitability. The federal electricity commission could propose a base mechanism to regulate such compensation, for instance, following the principles presented in this thesis.

6.1.3 Toward 50 GW PV capacity in Switzerland

To reach 50 GW PV capacity by 2050, Switzerland should install about 34 GW on buildings (single-family, multi-family, commercial, and industrial buildings), 5 GW on agricultural land, another 5 GW on public service space (public transport station, highway-side, etc.) and a remaining 6 GW on other ground [Nordmann, 2019, Swissolar, 2020] ([Remund et al., 2019], account for about 3GW in the alps). According to *Swissolar*², 460 MW were installed in 2020, pushing the total installed PV capacity to 3 GW. The newly installed PV capacity is about 300 MW/year (average 2013-2019). To reach 50 GW by 2050, we should install about 1500 MW/year.

To reach such a pace, we should make sure the PV installations cover the whole suited roof

²<https://www.swissolar.ch/fr/services/medias/news/detail/n-n/rekordzubau-bei-der-schweizer-photovoltaik-2020/>

6.1. Policy recommendations for the promotion of distributed PV in Switzerland

area. Figure 6.1 shows the yearly installed PV capacity³ (blue bar) and the PV potential that could have been installed on the corresponding roofs, assuming a module efficiency of 17% and only roofs with more than 1000 kWh/m²/year irradiance⁴. This figure highlights that only 40% of the potential is covered with PV. Hence, there is an urgent need to encourage a complete coverage of the roof's potential when new installations are planned. However, the current economic context and PV cost make it hardly profitable to install a large PV plant in a self-consumption scheme. Moreover, most DSOs or installers do not encourage complete roof coverage. For these reasons, there must be incentives for all actors (from private households to energy companies) to make sure most of the available space is covered with PV. The current pitfall is that those small- to mid-size installations will surely last until 2030-2040, making the unexploited roof area out of reach for future PV installation. It is indeed unlikely that building owners will upgrade their installation except maybe for covering other non-exploited roofs.

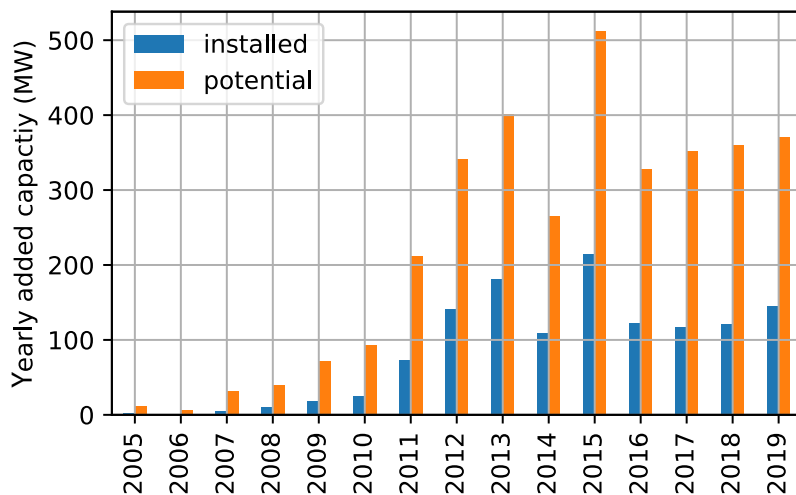


Figure 6.1 – Yearly installed capacity and the corresponding roof potential (assuming a module efficiency of 17% and only roofs with an irradiance > 1000 kWh/m²)

To ensure that a large installation is also cost-effective, virtual energy communities can provide a suitable business case even in self-consumption schemes. Virtual energy communities should allow anyone, tenants, companies, or public entities, to co-invest in a large PV plant in their neighborhood, which will then cover their energy needs. Participants in such virtual energy communities should pay only a fraction of the electricity tariff grid share when they self-consume the PV production. Using such a mechanism allows decoupling the PV investment from the energy market, and leverage on a social acceptance of clean, affordable, and local

³Only the installation with capacity above 30 kW or in feed-in remuneration at cost scheme or that volunteer for the source of electricity certification, integrated or attached on rooftops, source: <https://opendata.swiss/en/perma/e5a00bdb-5022-4856-ad4a-d1afe7bf38b0@bundesamt-fur-energie-bfe>

⁴Method and data from *solar roof* <https://opendata.swiss/en/perma/b614de5c-2f12-4355-b2c9-7aef2c363ad6@bundesamt-fur-energie-bfe>

energy.

Another reason that may prevent the roll-out of large PV installations is the financial aspect. The initial investment cost and capital cost may discourage building owners from covering their entire roof. The financial challenge can be harvested by cheap access to capital. One or more dedicated institutions (public pension funds, national bank) can provide this to offer the financial condition to drive distributed PV investments.

The Swiss Federal Office for Energy assumed a PV penetration of about 45% by 2050 (34 TWh PV generation to cover 76 TWh of national consumption). Assuming this penetration occurs mainly in residential and district scales, our findings emphasize the feasibility of this target, provided that flexibility encouragement mechanisms exist.

6.2 Conclusions and perspectives

This thesis highlights the role of the residential sector in providing part of the required flexibility to integrate a large share of PV energy in low voltage grids. This section presents the main messages and perspectives.

First, despite the low households' reaction to time-of-use tariffs, their potential flexibility is still significant. Our results highlighted that PV adopters have a more significant consumption behavior change. Hence, there is an unexplored gap to evaluate how remunerative and moral incentives can be combined and offered to any households (including those with no access to PV) to foster this new flexibility potential. For instance, allowing households to co-invest in a neighbor PV plant, and remunerating them according to their self-consumption level could create the incentive to more significantly change consumption habits. In addition, such a scheme would offer broader access to PV energy, even for tenants, and greater inclusion of citizens in the energy transition. To push even further the harvesting of the household behavioral flexibility, DSOs could offer a direct flexibility service by asking people to increase or suddenly lower their consumption by direct notification on their mobile phone. Despite the low households' flexible capacity compared with technical means, such a measure would open the acceptance for more intrusive demand-side management measures and increase the citizen role in the decarbonization of the power sector.

To promote the flexibility of PV systems, tariffs are a promising tool to enable an economically viable deployment of flexible technologies such as storage, thus promoting larger flexible capacities. In particular, variable tariffs are particularly effective to foster larger battery sizes but should be used with care, as the usage of those batteries may significantly impact the network. In comparison, capacity-based tariffs allow the installation of large batteries, especially for systems with prominent consumption peaks, and reduce grid stress. Finally, block rate tariff is a promising grid structure as it strongly reduces the grid usage intensity, but its complexity may raise concerns about its acceptance. However, such a structure is already in use in the water supply. The only remaining blocking point is a solid theoretical background

on designing such an electricity tariff, keeping in mind such a structure can be detrimental for the PV deployment. There is currently a lack of research in this field.

Distributed flexibility has the potential to be harvested by DSOs to deal with punctual network constraint violations. The most straightforward approach is active power curtailment, but its cost can be higher than grid reinforcement. Providing the conditions that allow owners to invest in flexible technologies, such as batteries, reduces the cost of providing flexibility. It could enable DSOs to use such flexibility instead of grid reinforcement, as it can be a competitive solution, depending on the network capacity and PV penetration. The role of power-to-heat in this context should also be evaluated and probably increase the overall profitability of distributed flexibility. There is some methodological challenge that should be addressed in such case. In particular, providing a generic distributed flexibility model allowing to skip the modeling of individual technologies (battery, heat pump, and electric heater) should be addressed. To enforce our conclusion on the profitability, one should evaluate, from a social welfare perspective, the overall cost of an increasing PV penetration (including grid reinforcement, cost of flexibility, and overall cost of electricity) to evaluate the best economic strategy according to the network topology, and geographical situation.

Our findings highlight that a capacity-based remuneration scheme for enabling remote-control flexibility assets is the most appropriate. It would consist in a one-time payment contribution of about 30 CHF per kW of installed PV and battery capacity. Further research should be conducted to increase the robustness of this number, especially for a wider variety of network topologies. As the grid charges are calculated according to the total network maintenance and investment cost of a DSO entire operating area, such remuneration scheme should be estimated similarly, i.e., considering the grid reinforcement and flexibility cost of the same operating area.

Such a scheme also promotes larger installation, which can be achieved by aggregating systems into energy communities. In such a way, the installed PV capacity and battery capacity are more significant, and the DSO needs to control only a few medium-capacity assets instead of a large number of small ones. This also fosters the role of citizens as investors in the energy transition. The negligible negative network impact of energy communities is here balanced by the economic advantage given by the reduction of the investment cost (including remote-control cost). The flexibility cost competitiveness of energy communities compared to individual systems deserves further investigation.

Future work should consider the impact of additional flexibility sources such as the sector coupling between electricity, heat, and gas network at the district scale. In addition, further research should focus on the long-term evolution of distributed PV, flexibility sources, and network investment. In particular, a clear road map for implementing 50 GW PV capacity and the requirements for flexibility and grid reinforcement at the district scale should be produced.

6.3 Summary for distribution system operators and policymakers

Recommendation I:

Promoting consumer behavior change regarding the adequacy between their consumption and local PV generation is worth considering. It paves the way for energy savings and the acceptance of more flexible technologies.

Recommendation II:

Non-intrusive load monitoring can be a valuable service to provide insights on flexibility potential and energy savings. It can be performed offline from smart meter measurements by distribution system operators.

Recommendation III:

Electricity tariffs can effectively complement regulations to foster PV system flexibility. Variable energy tariffs are particularly effective in encouraging larger storage capacity but should be treated with care as it increases the grid stress. Capacity tariffs promote a more reasonable exchange with the grid.

Recommendation IV:

Block rate tariffs may be the ultimate tool to encourage flexibility of PV systems. Still, it should be mainly designed according to the energy system size (PV capacity and consumption power intensity).

Recommendation V:

Distributed flexibility is more economical than simple curtailment of the PV production and should be favored over grid reinforcement when it makes the most sense.

Recommendation VI:

Encouraging energy communities allows securing investment in large PV plants to cover the community needs. It also lowers investment costs and aggregate flexibility. A mechanism to encourage flexibility is a one-time subsidy of 30 CHF/kW to install remote control. By doing so, energy communities will have a positive impact on the grid and PV deployment.

A FLEXI 2 survey

Bienvenue au questionnaire du projet Flexi

Le projet Flexi est une étude scientifique qui vise à déterminer la flexibilité de la demande d'électricité. L'objectif est de savoir dans quelle mesure la consommation peut être déplacée vers le milieu de la journée, afin d'utiliser au mieux l'énergie photovoltaïque qui est produite pendant cette période.

Planair, l'**EPFL** et l'**Université de Neuchâtel** sont les partenaires du projet, qui bénéficie également du soutien logistique de **La Goule** (votre fournisseur d'électricité) et du soutien financier de l'**Office Fédéral de l'Énergie**.

Pour répondre au questionnaire en totalité, il faut compter **environ 5 minutes**. Vous avez la possibilité d'interrompre le questionnaire et d'y revenir. Vos réponses seront sauvegardées.

Nous vous remercions d'avance.

Informations relatives au traitement des données :

- *Les informations collectées au travers de ce questionnaire et les consommations d'électricité (ci-après : les données) seront traitées de façon strictement anonyme et confidentielle.*
 - *Les données seront utilisées uniquement pour des analyses scientifiques menées par des chercheurs académiques.*
 - *Les données relatives à la consommation d'électricité ne seront pas traitées en temps réel.*
 - *Les participants peuvent en tout temps demander l'effacement de leurs données.*
 - *En fin d'étude, seules des données anonymisées seront conservées.*
-

Vous habitez...

☐ un appartement

☐ une maison

Vous êtes...

☐ locataire

☐ propriétaire

Votre logement comprend...

	0	1	2	3	4	5 ou plus
Pièces	<input type="radio"/>	<input type="radio"/>	<input type="radio"/>	<input type="radio"/>	<input type="radio"/>	<input type="radio"/>
Salles de bain / toilettes	<input type="radio"/>	<input type="radio"/>	<input type="radio"/>	<input type="radio"/>	<input type="radio"/>	<input type="radio"/>
Autres (p. ex.: cave, grenier, véranda, ...)	<input type="radio"/>	<input type="radio"/>	<input type="radio"/>	<input type="radio"/>	<input type="radio"/>	<input type="radio"/>

Quelle est la surface habitable de votre logement ?

_____ m²

Comment le chauffage de votre logement fonctionne-t-il ?

Plusieurs réponses possibles.

- ☐ Électricité
 - ☐ Mazout
 - ☐ Gaz
 - ☐ Pompe à chaleur
 - ☐ Chauffage à distance
 - ☐ Bois
 - ☐ Autre (précisez) : _____
 - ☐ Je ne sais pas
-

Comment l'eau de votre logement est-elle chauffée ?

Plusieurs réponses possibles.

- ☐ Électricité
 - ☐ Mazout
 - ☐ Gaz
 - ☐ Pompe à chaleur
 - ☐ Chauffage à distance
 - ☐ Bois
 - ☐ Autre (précisez): _____
 - ☐ Je ne sais pas.
-

Parmi les appareils suivants, lesquels possédez-vous ?
Ne pas tenir compte des équipements collectifs de l'immeuble.

Cuisine

- ☐ Réfrigérateur
- ☐ Congélateur séparé du réfrigérateur
- ☐ Cuisinière électrique
- ☐ Four traditionnel
- ☐ Four micro-ondes
- ☐ Lave-vaisselle
- ☐ Robot cuisine
- ☐ Bouilloire électrique
- ☐ Machine à café
- ☐ Mixer
- ☐ Presse-agrumes électrique

Appareils ménagers

- ☐ Lave-linge
- ☐ Sèche-linge
- ☐ Aspirateur
- ☐ Fer à repasser
- ☐ Humidificateur / évaporateur / aquarium

Multimédia

- ☐ Télévision

- ☐ Box TV
- ☐ Lecteur DVD
- ☐ Console de jeux vidéo
- ☐ Chaîne hifi / radio / dock station
- ☐ Cadre photo numérique
- ☐ Ordinateur fixe
- ☐ Ordinateur portable
- ☐ Modem internet
- ☐ Tablette
- ☐ Téléphone fixe (y.c. sans fil)
- ☐ Téléphone portable
- ☐ Imprimante / scanner

Salle de bain

- ☐ Sèche-cheveux
 - ☐ Rasoir électrique
 - ☐ Brosse à dent électrique
-

Combien des appareils suivants possédez-vous ?

	1	2	3	4	5 ou plus
Télévision(s)	<input type="radio"/>	<input type="radio"/>	<input type="radio"/>	<input type="radio"/>	<input type="radio"/>
Console(s) de jeux vidéo	<input type="radio"/>	<input type="radio"/>	<input type="radio"/>	<input type="radio"/>	<input type="radio"/>
Ordinateur(s) fixe(s)	<input type="radio"/>	<input type="radio"/>	<input type="radio"/>	<input type="radio"/>	<input type="radio"/>
Ordinateur(s) portable(s)	<input type="radio"/>	<input type="radio"/>	<input type="radio"/>	<input type="radio"/>	<input type="radio"/>

À quelle fréquence utilisez-vous les appareils suivants ?

☐ Lave-vaisselle _____ fois par semaine

☐ Lave-linge _____ fois par semaine

Quelle proportion d'ampoules basse consommation utilisez-vous dans votre domicile ?

☐ Moins de 25%

☐ 25-49%

☐ 50-74%

☐ 75% ou plus

Voici une série d'affirmations concernant l'environnement. Pouvez-vous indiquer dans quelle mesure vous êtes en accord ou en désaccord avec chacune d'entre elles ?

	Pas du tout d'accord	Plutôt pas d'accord	Partagé(e)	Plutôt d'accord	Entièrement d'accord
Cela me préoccupe quand je pense aux conditions environnementales dans lesquelles nos enfants et petits-enfants devront probablement vivre.	<input type="radio"/>	<input type="radio"/>	<input type="radio"/>	<input type="radio"/>	<input type="radio"/>
Si les choses continuent ainsi, nous allons bientôt vivre une catastrophe écologique majeure.	<input type="radio"/>	<input type="radio"/>	<input type="radio"/>	<input type="radio"/>	<input type="radio"/>
Lorsque je lis dans le journal ou vois à la télévision des reportages sur les problèmes environnementaux, je suis souvent indigné(e) ou en colère.	<input type="radio"/>	<input type="radio"/>	<input type="radio"/>	<input type="radio"/>	<input type="radio"/>
Il y a des limites à la croissance économique, et notre monde industrialisé les a déjà dépassées ou n'est pas loin de les atteindre.	<input type="radio"/>	<input type="radio"/>	<input type="radio"/>	<input type="radio"/>	<input type="radio"/>
De nos jours, la plus grande partie de la population continue à se comporter de façon irresponsable vis-à-vis de l'environnement.	<input type="radio"/>	<input type="radio"/>	<input type="radio"/>	<input type="radio"/>	<input type="radio"/>
À mon avis, les problèmes environnementaux et leur impact sont présentés de façon très exagérée par les écologistes.	<input type="radio"/>	<input type="radio"/>	<input type="radio"/>	<input type="radio"/>	<input type="radio"/>

Les responsables politiques restent encore aujourd'hui beaucoup trop passifs par rapport à l'environnement.

Nous devrions tous être prêts à modérer notre train de vie pour protéger l'environnement.

Il faut absolument que des mesures soient prises en faveur de la protection de l'environnement, même si cela nuit à l'emploi.

☐☐☐☐☐☐☐☐☐☐☐☐☐☐☐

Combien pensez-vous que coûte 1 kilowattheure (kWh) d'électricité en Suisse (en moyenne) ?
Indiquez votre meilleure estimation.

_____ centimes

Que pensez-vous des affirmations suivantes ?

	Vrai	Faux	Je ne sais pas
La plus grande partie de l'énergie consommée dans un ménage suisse sert au chauffage.	<input type="radio"/>	<input type="radio"/>	<input type="radio"/>
Les émissions de CO2 jouent un rôle crucial dans le réchauffement climatique.	<input type="radio"/>	<input type="radio"/>	<input type="radio"/>
Abaissier la température de 1°C permet de réduire la consommation d'énergie liée au chauffage d'environ 6%.	<input type="radio"/>	<input type="radio"/>	<input type="radio"/>
Le charbon est une source d'énergie renouvelable.	<input type="radio"/>	<input type="radio"/>	<input type="radio"/>
Les centrales hydroélectriques représentent 10% de la production totale d'électricité en Suisse.	<input type="radio"/>	<input type="radio"/>	<input type="radio"/>

Savez-vous que *La Goule* propose des prestations de centrale photovoltaïque clés en main ?

☐ Oui

☐ Non

Combien de personnes y a-t-il dans votre ménage ?

	0	1	2	3	4	5	6	plus de 6
Femmes (18 ans ou +)	<input type="radio"/>	<input type="radio"/>	<input type="radio"/>	<input type="radio"/>	<input type="radio"/>	<input type="radio"/>	<input type="radio"/>	<input type="radio"/>
Hommes (18 ans ou +)	<input type="radio"/>	<input type="radio"/>	<input type="radio"/>	<input type="radio"/>	<input type="radio"/>	<input type="radio"/>	<input type="radio"/>	<input type="radio"/>
Filles (< 18 ans)	<input type="radio"/>	<input type="radio"/>	<input type="radio"/>	<input type="radio"/>	<input type="radio"/>	<input type="radio"/>	<input type="radio"/>	<input type="radio"/>
Garçons (< 18 ans)	<input type="radio"/>	<input type="radio"/>	<input type="radio"/>	<input type="radio"/>	<input type="radio"/>	<input type="radio"/>	<input type="radio"/>	<input type="radio"/>

Combien de personnes de chaque catégorie y a-t-il dans votre ménage ?

	0	1	2	3	4	5	6	plus de 6
Travailleur plein- temps (90-100%)	<input type="radio"/>	<input type="radio"/>	<input type="radio"/>	<input type="radio"/>	<input type="radio"/>	<input type="radio"/>	<input type="radio"/>	<input type="radio"/>
Travailleur temps partiel (50-80%)	<input type="radio"/>	<input type="radio"/>	<input type="radio"/>	<input type="radio"/>	<input type="radio"/>	<input type="radio"/>	<input type="radio"/>	<input type="radio"/>
Travailleur temps partiel (< 50%)	<input type="radio"/>	<input type="radio"/>	<input type="radio"/>	<input type="radio"/>	<input type="radio"/>	<input type="radio"/>	<input type="radio"/>	<input type="radio"/>
Écolier / étudiant	<input type="radio"/>	<input type="radio"/>	<input type="radio"/>	<input type="radio"/>	<input type="radio"/>	<input type="radio"/>	<input type="radio"/>	<input type="radio"/>
Retraité	<input type="radio"/>	<input type="radio"/>	<input type="radio"/>	<input type="radio"/>	<input type="radio"/>	<input type="radio"/>	<input type="radio"/>	<input type="radio"/>
Sans emploi	<input type="radio"/>	<input type="radio"/>	<input type="radio"/>	<input type="radio"/>	<input type="radio"/>	<input type="radio"/>	<input type="radio"/>	<input type="radio"/>
Autre	<input type="radio"/>	<input type="radio"/>	<input type="radio"/>	<input type="radio"/>	<input type="radio"/>	<input type="radio"/>	<input type="radio"/>	<input type="radio"/>

Combien de personnes de votre ménage travaillent régulièrement de nuit ou le week-end ?

	0	1	2	3	4	5	6	plus de 6
Nuit	<input type="radio"/>	<input type="radio"/>	<input type="radio"/>	<input type="radio"/>	<input type="radio"/>	<input type="radio"/>	<input type="radio"/>	<input type="radio"/>
Week- end	<input type="radio"/>	<input type="radio"/>	<input type="radio"/>	<input type="radio"/>	<input type="radio"/>	<input type="radio"/>	<input type="radio"/>	<input type="radio"/>

De quel type est votre ménage ?

- ☐ Famille / Couple
 - ☐ Famille monoparentale
 - ☐ Co-location
 - ☐ Autre
-

Quel est le niveau d'éducation le plus élevé dans votre ménage ?

- ☐ École obligatoire
 - ☐ Formation professionnelle élémentaire
 - ☐ École de formation générale
 - ☐ Apprentissage (CFC)
 - ☐ Maturité (gymnasiale ou professionnelle)
 - ☐ Formation professionnelle supérieure
 - ☐ Haute école spécialisée HES / HEP
 - ☐ Université / EPF
-

Quel est le revenu mensuel brut (en CHF) de votre ménage ?

- ☐ moins de 2'000
 - ☐ 2'000-3'999
 - ☐ 4'000-5'999
 - ☐ 6'000-7'999
 - ☐ 8'000-9'999
 - ☐ 10'000-11'999
 - ☐ 12'000-13'999
 - ☐ 14'000 ou plus
 - ☐ Je ne souhaite pas répondre
 - ☐ Je ne sais pas
-

Vous êtes...

- ☐ une femme
 - ☐ un homme
-

Quel est votre âge ?

- ☐ moins de 18
- ☐ 18-29
- ☐ 30-39
- ☐ 40-49
- ☐ 50-59
- ☐ 60-69
- ☐ 70 ou plus
-

Merci pour votre participation

Le sondage auquel vous venez de participer fait partie d'un projet scientifique dont le but est d'analyser la flexibilité de la demande d'électricité. Les informations collectées au travers de ce questionnaire ainsi que vos consommations d'électricité seront traitées de façon strictement anonyme et confidentielle. Elles seront utilisées uniquement pour des analyses scientifiques menées par des chercheurs académiques. Pour signifier votre accord, veuillez s'il vous plaît **cocher la case "lu et approuvé" ci-dessous**.

Dans le cadre du projet, votre ménage pourrait être sélectionné afin de participer à une expérience particulière, dans laquelle un numéro de téléphone portable serait utilisé pour vous transmettre des informations par SMS. Dans cette optique, nous vous prions de bien vouloir indiquer une adresse électronique et, le cas échéant, si vous seriez disposé-e à communiquer votre numéro de téléphone portable pour les besoins de l'expérience.

Votre adresse électronique et votre numéro de téléphone ne seront utilisés que dans le cadre du projet scientifique en cours et ne seront en aucun cas transmis à des tiers.

- ☐ Lu et approuvé
- ☐ Adresse électronique : _____
- ☐ Disposé-e à communiquer un numéro de téléphone portable pour les besoins futurs de l'expérience.

B FLEXI 2 PV owner survey

Projet FLEXI – Étude scientifique sur la consommation d'électricité

Afin de pouvoir réaliser cette étude sur les habitudes de consommation électrique des ménages possédant une installation photovoltaïque, nous avons besoin de quelques renseignements supplémentaires concernant votre installation.

***Obligatoire**

Données personnelles

1. **Prénom ***

2. **Nom ***

3. **Adresse ***

Installation photovoltaïque

Précisions sur votre installation photovoltaïque

4. **Date de l'installation**

Exemple : 15 décembre 2012

5. **Nombre d'orientations**

Si votre installation couvre par exemple les faces est et ouest, veuillez choisir 2.
Une seule réponse possible.

1	2	3	4	5
<input type="radio"/>	<input type="radio"/>	<input type="radio"/>	<input type="radio"/>	<input type="radio"/>

6. Puissance installée

Puissance installée des modules en W (exemple : 3000W). Si vous ne savez pas, vous pouvez préciser le nombre de modules (exemple : 10mod). En cas de multiple orientations, merci de séparer les réponses par une virgule (exemple E et W : 2000W,2000W)

7. Orientation

Azimut de l'orientation de votre installation, par exemple 180 pour sud (0:N, 90:E, 135:SE, 180:S, 225:SW, 270:W). En cas de multiple orientations, merci de séparer les réponses par une virgule (exemple E et W : 90,270)

8. Inclinaison

Inclinaison de votre installation/toit (0:plat, 90:vertical). En cas de multiple orientations, merci de séparer les réponses par une virgule (exemple E et W : 20,35)

9. Disposez-vous du devis de votre installation photovoltaïque ?

Nous serions intéressé par la partie technique de ce document détaillant le nombre et type de module, onduleur, etc. Si vous disposez de ce document, merci de l'envoyer par mail à lionel.bloch@epfl.ch. De même si vous avez une photo de votre installation.

Une seule réponse possible.

☐ Oui

☐ Non

Données de production photovoltaïque

Nous avons besoin de ces données pour déterminer quel est la part de votre production que vous consommez.

10. Disposez-vous de l'historique de votre production solaire sous forme de fichiers ?

Si oui, merci de l'envoyer par mail à lionel.bloch@epfl.ch.

Une seule réponse possible.

☐ Oui

☐ Non

11. Disposez-vous d'un portail pour permettant de visualiser votre production photovoltaïque et accepter vous de nous en transmettre l'accès ? *

Si oui, nous reprendrons contact par mail.

Une seule réponse possible.

☐ Oui

☐ Non

Note

12. Remarque

C Rolle buildings parameters

Table C.1 – Rolle buildings' parameters

EGID	Footage m ²	A^{roof} m ²	C^{b} kWh/K	C^{sh} kWh/K	U^{b} W/K	U^{sh} W/K	A_0^{sun} m ²	$T_{\text{max}}^{\text{sh}}$ °C	U^{tank} W/K	V^{tank} L
829040	1158	560	46	5.99	472	2663	23	70	7.8	1475
829041	291	505	33	0.65	653	599	26	55	2.7	308
829043	262	196	15	2.09	337	771	17	60	2.6	277
829044	165	125	7	0.28	96	258	3	55	2.1	210
829045	267	130	11	0.41	111	376	3	55	3.8	499
829046	156	139	9	0.27	133	244	4	55	2.0	199
829047	158	139	9	0.27	125	247	4	55	2.1	201
829048	267	144	11	0.41	111	376	3	55	3.8	499
829049	198	89	8	1.02	116	455	6	70	2.4	252
829050	474	132	19	0.81	211	741	7	55	4.3	604
829051	201	103	8	1.04	118	462	6	70	2.4	256
829052	201	99	8	1.04	118	462	6	70	2.4	256
829053	294	120	12	0.50	146	460	5	55	3.1	375
829054	201	109	8	0.34	118	314	4	55	2.4	256
829055	201	96	8	0.34	118	314	4	55	2.4	256
829056	201	96	8	0.34	112	314	4	55	2.4	256
829057	456	220	18	0.77	204	713	7	55	4.2	581
829058	130	52	8	0.55	88	374	3	60	2.3	243
829059	714	444	40	3.17	469	1408	27	70	5.0	755
829062	1125	250	27	4.76	262	3233	10	60	9.9	2102
829063	1100	226	26	4.66	242	3161	10	60	9.7	2056
829066	1544	411	46	2.36	411	2173	11	55	12.2	2885
829067	204	109	8	0.35	114	319	4	55	2.4	260
829080	844	208	25	1.29	248	1188	7	55	8.1	1577
829081	848	206	25	1.30	249	1193	7	55	8.2	1585
829082	1532	380	46	6.49	416	4402	17	60	12.1	2863
829691	372	196	15	1.92	179	856	9	70	3.7	474
829692	250	260	15	1.06	178	718	7	60	3.6	467

Appendix C. Rolle buildings parameters

Table C.1 – (continued)

EGID	Footage m ²	A^{roof} m ²	C^{b} kWh/K	C^{sh} kWh/K	U^{b} W/K	U^{sh} W/K	A_0^{sun} m ²	$T_{\text{max}}^{\text{sh}}$ °C	U^{tank} W/K	V^{tank} L
829693	1568	1146	88	6.96	852	3093	49	70	8.4	1658
829694	579	360	23	2.45	222	1664	9	60	6.3	1082
829695	422	278	25	1.79	236	1213	9	60	5.1	789
829696	333	142	13	1.41	145	957	6	60	4.4	622
829697	460	381	26	1.03	282	946	11	55	3.7	486
829698	184	126	11	0.95	181	423	9	70	2.3	234
829700	210	149	13	1.09	190	483	9	70	2.5	268
829713	228	201	14	1.18	181	524	9	70	2.6	291
3104398	327	183	13	0.50	119	460	3	55	4.3	611
3104405	246	303	10	0.42	102	385	3	55	2.8	313
3104571	720	327	29	1.10	285	1013	8	55	7.3	1346
3104580	270	151	11	0.46	149	422	5	55	3.0	344
280065226	465	226	19	2.41	233	1070	11	70	4.2	592
280082734	714	294	28	2.87	435	1159	15	55	5.8	948
280091601	753	257	30	1.15	288	1060	8	55	7.5	1407

Bibliography

- [Abada et al., 2020] Abada, I., Ehrenmann, A., and Lambin, X. (2020). On the Viability of Energy Communities. *The Energy Journal*, 41(1).
- [Ackermann et al., 2010] Ackermann, M. R., Blömer, J., and Sohler, C. (2010). Clustering for metric and nonmetric distance measures. *ACM Transactions on Algorithms*, 6(4):1–26.
- [Agalgaonkar et al., 2014] Agalgaonkar, Y. P., Pal, B. C., and Jabr, R. A. (2014). Distribution voltage control considering the impact of pv generation on tap changers and autonomous regulators. *IEEE Transactions on Power Systems*, 29(1):182–192.
- [Aghamolaei et al., 2020] Aghamolaei, R., Shamsi, M. H., and O'Donnell, J. (2020). Feasibility analysis of community-based PV systems for residential districts: A comparison of on-site centralized and distributed PV installations. *Renewable Energy*, 157:793–808.
- [Alhamoud et al., 2014] Alhamoud, A., Ruettiger, F., Reinhardt, A., Englert, F., Burgstahler, D., Bohnstedt, D., Gottron, C., and Steinmetz, R. (2014). SMARTENERGY.KOM: An intelligent system for energy saving in smart home. In *39th Annual IEEE Conference on Local Computer Networks Workshops*, pages 685–692. IEEE.
- [Alhamoud et al., 2015] Alhamoud, A., Xu, P., Englert, F., Reinhardt, A., Scholl, P., Boehnstedt, D., and Steinmetz, R. (2015). Extracting human behavior patterns from appliance-level power consumption data. In *European Conference on Wireless Sensor Networks*, pages 52–67. Springer.
- [Alimohammadisagvand et al., 2016] Alimohammadisagvand, B., Jokisalo, J., Kilpeläinen, S., Ali, M., and Sirén, K. (2016). Cost-optimal thermal energy storage system for a residential building with heat pump heating and demand response control. *Applied Energy*, 174:275–287.
- [Allcott, 2011] Allcott, H. (2011). Rethinking real-time electricity pricing. *Resource and Energy Economics*, 33(4):820–842. Special section: Sustainable Resource Use and Economic Dynamics.
- [Angenendt et al., 2019] Angenendt, G., Zurmühlen, S., Rücker, F., Axelsen, H., and Sauer, D. U. (2019). Optimization and operation of integrated homes with photovoltaic battery energy storage systems and power-to-heat coupling. *Energy Conversion and Management: X*, 1(January):100005.
- [Ansari et al., 2016] Ansari, B., Shi, D., Sharma, R., and Simoes, M. G. (2016). Economic analysis, optimal sizing and management of energy storage for PV grid integration. In *2016 IEEE/PES Transmission and Distribution Conference and Exposition (T&D)*, volume 2016-July, pages 1–5, Dallas, TX, USA. IEEE.
- [Anvari-Moghaddam et al., 2015] Anvari-Moghaddam, A., Monsef, H., and Rahimi-Kian, A. (2015). Cost-effective and comfort-aware residential energy management under different pricing schemes and weather conditions. *Energy and Buildings*, 86:782–793.

Bibliography

- [Ashouri et al., 2013] Ashouri, A., Fux, S. S., Benz, M. J., and Guzzella, L. (2013). Optimal design and operation of building services using mixed-integer linear programming techniques. *Energy*, 59:365–376.
- [Ashouri et al., 2015] Ashouri, A., Stadler, P., and Marechal, F. (2015). Day-ahead promised load as alternative to real-time pricing. In *2015 IEEE International Conference on Smart Grid Communications (SmartGridComm)*, pages 551–556. IEEE.
- [Ayompe and Duffy, 2013] Ayompe, L. and Duffy, A. (2013). Feed-in tariff design for domestic scale grid-connected PV systems using high resolution household electricity demand data. *Energy Policy*, 61:619–627.
- [Azarova et al., 2018] Azarova, V., Engel, D., Ferner, C., Kollmann, A., and Reichl, J. (2018). Exploring the impact of network tariffs on household electricity expenditures using load profiles and socio-economic characteristics. *Nature Energy*, 3(4):317–325.
- [Babacan et al., 2017] Babacan, O., Ratnam, E. L., Disfani, V. R., and Kleissl, J. (2017). Distributed energy storage system scheduling considering tariff structure, energy arbitrage and solar PV penetration. *Applied Energy*, 205:1384–1393.
- [Bastida et al., 2019] Bastida, H., Ugalde-Loo, C. E., Abeysekera, M., Qadrdan, M., Wu, J., and Jenkins, N. (2019). Dynamic modelling and control of thermal energy storage. *Energy Procedia*, 158:2890–2895.
- [Batra et al., 2014] Batra, N., Kelly, J., Parson, O., Dutta, H., Knottenbelt, W., Rogers, A., Singh, A., and Srivastava, M. (2014). NILMTK. In *Proceedings of the 5th international conference on Future energy systems*, volume 12, pages 16838–16866. ACM.
- [Batra et al., 2016] Batra, N., Singh, A., and Whitehouse, K. (2016). Gemello. In *Proceedings of the 22nd ACM SIGKDD International Conference on Knowledge Discovery and Data Mining - KDD '16*, pages 431–440, New York, New York, USA. ACM.
- [Bauwens et al., 2016] Bauwens, T., Gotchev, B., and Holstenkamp, L. (2016). What drives the development of community energy in europe? the case of wind power cooperatives. *Energy Research & Social Science*, 13:136–147.
- [Beck et al., 2017] Beck, T., Kondziella, H., Huard, G., and Bruckner, T. (2017). Optimal operation, configuration and sizing of generation and storage technologies for residential heat pump systems in the spotlight of self-consumption of photovoltaic electricity. *Applied Energy*, 188:604–619.
- [Beckel et al., 2014a] Beckel, C., Kleiminger, W., Cicchetti, R., Staake, T., and Santini, S. (2014a). The ECO data set and the performance of non-intrusive load monitoring algorithms. In *Proceedings of the 1st ACM Conference on Embedded Systems for Energy-Efficient Buildings - BuildSys '14*, pages 80–89.
- [Beckel et al., 2012] Beckel, C., Sadamori, L., and Santini, S. (2012). Towards automatic classification of private households using electricity consumption data. In *Proceedings of the Fourth ACM Workshop on Embedded Sensing Systems for Energy-Efficiency in Buildings - BuildSys '12*, page 169. ACM.
- [Beckel et al., 2014b] Beckel, C., Sadamori, L., Staake, T., and Santini, S. (2014b). Revealing household characteristics from smart meter data. *Energy*, 78:397–410.
- [Behi et al., 2017] Behi, B., Arefi, A., Pezeshki, H., and Shahnian, F. (2017). Distribution transformer lifetime analysis in the presence of demand response and rooftop PV integration. *Renewable Energy and Environmental Sustainability*, 2:27.

- [Bianchi, 2006] Bianchi, M. A. (2006). Adaptive modellbasierte prädiktive Regelung einer Kleinwärmepumpenanlage. *Eidgenössischen Technischen Hochschule Zürich*, Doctoral thesis 16892:14–18.
- [Biansoongnern and Plangklang, 2016] Biansoongnern, S. and Plangklang, B. (2016). Nonintrusive load monitoring (NILM) using an Artificial Neural Network in embedded system with low sampling rate. In *2016 13th International Conference on Electrical Engineering/Electronics, Computer, Telecommunications and Information Technology, ECTI-CON 2016*, pages 1–4.
- [Billauer, 2012] Billauer, E. (2012). peakdet: Peak detection using MATLAB (non-derivative local extremum, maximum, minimum).
- [Birt et al., 2012] Birt, B. J., Newsham, G. R., Beausoleil-Morrison, I., Armstrong, M. M., Saldanha, N., and Rowlands, I. H. (2012). Disaggregating categories of electrical energy end-use from whole-house hourly data. *Energy and Buildings*, 50:93–102.
- [Bloch et al., 2020a] Bloch, L., Girardin, L., Holweger, J., and Middelhaue, L. (2020a). SCCER JA-RED - A list of possible ancillary services for enhanced grid operation and implementation of the most effective ones at the RE demo site - Deliverable 1.2.3. Technical report, École Polytechnique Fédérale de Lausanne, EPFL Valais/Neuchâtel.
- [Bloch et al., 2019] Bloch, L., Holweger, J., Ballif, C., and Wyrsh, N. (2019). Impact of advanced electricity tariff structures on the optimal design, operation and profitability of a grid-connected PV system with energy storage. *Energy Informatics*, 2(1):16.
- [Bloch et al., 2020b] Bloch, L., Holweger, J., and Wyrsh, N. (2020b). SCCER-FURIES - Deployment recommendation for large penetration of PV and distributed storage. Technical report, École Polytechnique Fédérale de Lausanne.
- [Bloch et al., 2017] Bloch, L., Holweger, J., Wyrsh, N., Tommasi, H., and Girardin, L. (2017). SCCER JA-RED - Description of the multi-energy demonstration system in the RE demo site - Deliverable 1.2.1. Technical report, École Polytechnique Fédérale de Lausanne, EPFL Valais/Neuchâtel.
- [Bloch, 2020] Bloch, L. B. (2020). *Optimal path to a high share of distributed PV in low-voltage distribution grids*. PhD thesis, Ecole Polytechnique Fédérale de Lausanne.
- [Blooming and Carnovale, 2006] Blooming, T. and Carnovale, D. (2006). Application of IEEE STD 519-1992 harmonic limits. In *Conference Record of 2006 Annual Pulp and Paper Industry Technical Conference*, pages 1–9. IEEE.
- [Bonbright et al., 1961] Bonbright, J. C., Daniels, A. L., and Kamerschen, D. R. (1961). *Principles of public utility rates*. Columbia University Press New York.
- [Bonfigli et al., 2017] Bonfigli, R., Principi, E., Fagiani, M., Severini, M., Squartini, S., and Piazza, F. (2017). Non-intrusive load monitoring by using active and reactive power in additive Factorial Hidden Markov Models. *Applied Energy*, 208(August):1590–1607.
- [Bonfigli et al., 2015] Bonfigli, R., Squartini, S., Fagiani, M., and Piazza, F. (2015). Unsupervised algorithms for non-intrusive load monitoring: An up-to-date overview. In *2015 IEEE 15th International Conference on Environment and Electrical Engineering (EEEIC)*, pages 1175–1180. IEEE.
- [Boogen et al., 2017] Boogen, N., Datta, S., and Filippini, M. (2017). Demand-side management by electric utilities in Switzerland: Analyzing its impact on residential electricity demand. *Energy Economics*, 64(Supplement C):402–414.

Bibliography

- [Booyesen et al., 2019] Booyesen, M., Engelbrecht, J., Ritchie, M., Apperley, M., and Cloete, A. (2019). How much energy can optimal control of domestic water heating save? *Energy for Sustainable Development*, 51:73–85.
- [Borenstein, 2017] Borenstein, S. (2017). Private Net Benefits of Residential Solar PV: The Role of Electricity Tariffs, Tax Incentives, and Rebates. *Journal of the Association of Environmental and Resource Economists*, 4(S1):S85–S122.
- [Bründlinger, 2020] Bründlinger, R. (2020). Grid Codes in Europe - Overview on the current requirements in European codes and national interconnection standards. Technical Report January, AIT, Vienna.
- [Callahan, 2004] Callahan, D. (2004). *The Cheating Culture: Why More Americans Are Doing Wrong to Get Ahead*. Harcourt.
- [Caramizaru and Uihlein, 2019] Caramizaru, A. and Uihlein, A. (2019). Energy communities : an overview of energy and social innovation. Technical report, European Commission, Ixelles.
- [Cetinkaya et al., 2020] Cetinkaya, U., Avcı, E., and Bayindir, R. (2020). Time series clustering analysis of energy consumption data. In *2020 9th International Conference on Renewable Energy Research and Application (ICRERA)*, pages 409–413.
- [Chang et al., 2016] Chang, C. S., Liao, W., Chen, Y. S., and Liou, L. H. (2016). A mathematical theory for clustering in metric spaces. *IEEE Transactions on Network Science and Engineering*, 3(1):2–16.
- [Chatzivasileiadis, 2018] Chatzivasileiadis, S. (2018). Lecture Notes on Optimal Power Flow (OPF). Technical Report September, Technical University of Denmark.
- [Child et al., 2019] Child, M., Kemfert, C., Bogdanov, D., and Breyer, C. (2019). Flexible electricity generation, grid exchange and storage for the transition to a 100% renewable energy system in Europe. *Renewable Energy*, 139:80–101.
- [CIGRE et al., 2009] CIGRE, Strunz, K., Abbey, C., Andrieu, C., Campbell, R. C., and Fletcher, R. (2009). Benchmark Systems for Network Integration of Renewable and Distributed Energy Resources. Technical Report July, CIGRE.
- [Coffrin et al., 2018] Coffrin, C., Bent, R., Sundar, K., Ng, Y., and Lubin, M. (2018). Powermodels.jl: An open-source framework for exploring power flow formulations. In *2018 Power Systems Computation Conference (PSCC)*, pages 1–8.
- [Collazos and Maréchal, 2008] Collazos, A. and Maréchal, F. (2008). Predictive optimal management method for the control of polygeneration systems. In Braunschweig, B. and Joulia, X., editors, *Computer Aided Chemical Engineering*, volume 25 of *Computer Aided Chemical Engineering*, pages 325–330. Elsevier.
- [Cruz et al., 2018] Cruz, M. R., Fitiwi, D. Z., Santos, S. F., and Catalão, J. P. (2018). A comprehensive survey of flexibility options for supporting the low-carbon energy future. *Renewable and Sustainable Energy Reviews*, 97(September):338–353.
- [Darby, 2018] Darby, S. J. (2018). Smart electric storage heating and potential for residential demand response. *Energy Efficiency*, 11(1):67–77.
- [Darghouth et al., 2016] Darghouth, N. R., Wiser, R. H., and Barbose, G. (2016). Customer economics of residential photovoltaic systems: Sensitivities to changes in wholesale market design and rate structures. *Renewable and Sustainable Energy Reviews*, 54:1459–1469.

- [Deetjen et al., 2018] Deetjen, T. A., Vitter, J. S., Reimers, A. S., and Webber, M. E. (2018). Optimal dispatch and equipment sizing of a residential central utility plant for improving rooftop solar integration. *Energy*, 147:1044–1059.
- [Defalin SA, 2016] Defalin SA (2016). FURION heat pumps. <http://pompyfurion.pl/en/index>. Accessed on 2017.12.23.
- [Denholm and Margolis, 2007] Denholm, P. and Margolis, R. M. (2007). Evaluating the limits of solar photovoltaics (pv) in electric power systems utilizing energy storage and other enabling technologies. *Energy Policy*, 35(9):4424 – 4433.
- [Devine et al., 2017] Devine, M. T., Farrell, N., and Lee, W. T. (2017). Optimising feed-in tariff design through efficient risk allocation. *Sustainable Energy, Grids and Networks*, 9:59–74.
- [Dijkstra, 1959] Dijkstra, E. W. (1959). A note on two problems in connexion with graphs. *Numerische Mathematik*, 1(1):269–271.
- [Dong et al., 2013] Dong, H., Wang, B., and Lu, C. T. (2013). Deep sparse coding based recursive disaggregation model for water conservation. *IJCAI International Joint Conference on Artificial Intelligence*, pages 2804–2810.
- [Drabecki, 2019] Drabecki, M. (2019). Obtaining feasibility of power flows in the deregulated electricity market environment. *Przegląd Elektrotechniczny*, 1(10):46–49.
- [Dutta and Mitra, 2017] Dutta, G. and Mitra, K. (2017). A literature review on dynamic pricing of electricity. *Journal of the Operational Research Society*, 68(10):1131–1145.
- [Eid et al., 2019] Eid, C., Grosveld, J., and Hakvoort, R. (2019). Assessing the costs of electric flexibility from distributed energy resources: A case from the Netherlands. *Sustainable Energy Technologies and Assessments*, 31:1–8.
- [Elhamifar and Sastry, 2015] Elhamifar, E. and Sastry, S. (2015). Energy Disaggregation via Learning Powerlets and Sparse Coding. In *Proceedings of the Twenty-Ninth AAAI Conference on Artificial Intelligence Pattern*, pages 629–635.
- [Enslin and Heskes, 2004] Enslin, J. and Heskes, P. (2004). Harmonic Interaction Between a Large Number of Distributed Power Inverters and the Distribution Network. *IEEE Transactions on Power Electronics*, 19(6):1586–1593.
- [Esa et al., 2016] Esa, N. F., Abdullah, M. P., and Hassan, M. Y. (2016). A review disaggregation method in Non-intrusive Appliance Load Monitoring. *Renewable and Sustainable Energy Reviews*, 66:163–173.
- [Ester et al., 1996] Ester, M., Kriegel, H.-P., Sander, J., and Xu, X. (1996). A density-based algorithm for discovering clusters in large spatial databases with noise. In *Proceedings of the Second International Conference on Knowledge Discovery and Data Mining*, KDD'96, page 226–231. AAAI Press.
- [Faustine et al., 2017] Faustine, A., Mvungi, N. H., Kaijage, S., and Michael, K. (2017). A Survey on Non-Intrusive Load Monitoring Methodies and Techniques for Energy Disaggregation Problem. *arXiv:1703.00785 [cs]*.
- [Filippini, 2011] Filippini, M. (2011). Short- and long-run time-of-use price elasticities in swiss residential electricity demand. *Energy Policy*, 39(10):5811 – 5817. Sustainability of biofuels.
- [Fischer et al., 2016] Fischer, D., Lindberg, K. B., Madani, H., and Wittwer, C. (2016). Impact of PV and variable prices on optimal system sizing for heat pumps and thermal storage. *Energy and Buildings*, 128:723–733.

Bibliography

- [Fischer et al., 2014] Fischer, D., Toral, T. R., Lindberg, K. B., Wille-Haussmann, B., and Madani, H. (2014). Investigation of Thermal Storage Operation Strategies with Heat Pumps in German Multi Family Houses. *Energy Procedia*, 58:137–144.
- [FOEN, 2021] FOEN (2021). Switzerland's greenhouse gas inventory.
- [Forsythe et al., 1977] Forsythe, 1917-1972, G. E., Malcolm, M. A., and Moler, C. B. v. (1977). *Computer methods for mathematical computations*. Englewood Cliffs (N.J.) : Prentice-Hall.
- [FSO, 2020] FSO (2020). Swiss Earnings Structure Survey. Technical report, Federal Statistical Office, Neuchâtel.
- [Geels et al., 2017] Geels, F. W., Sovacool, B. K., Schwanen, T., and Sorrell, S. (2017). The socio-technical dynamics of low-carbon transitions. *Joule*, 1(3):463–479.
- [Geiger et al., 2019] Geiger, N., Swim, J. K., and Glenna, L. (2019). Spread the green word: A social community perspective into environmentally sustainable behavior. *Environment and Behavior*, 51(5):561–589.
- [Gellings, 1985] Gellings, C. W. (1985). The Concept of Demand-Side Management for Electric Utilities. *Proceedings of the IEEE*, 73(10):1468–1470.
- [Genkinger and Afjei, 2011] Genkinger, A. and Afjei, T. (2011). EFKOS – Effizienz kombinierter Systeme mit Wärmepumpe. Technical report, Federal office for energy.
- [Gershuny and Sullivan, 2017] Gershuny, J. and Sullivan, O. (2017). United Kingdom Time Use Survey, 2014-2015. *Centre for Time Use Research, University of Oxford, UK Data Service*.
- [Girardin, 2012] Girardin, L. (2012). A GIS-based Methodology for the Evaluation of Integrated Energy Systems in Urban Area. *École Polytechnique Fédérale de Lausanne*, Doctoral thesis 5287:100–101.
- [Girardin et al., 2010] Girardin, L., Marechal, F., Dubuis, M., Calame-Darbellay, N., and Favrat, D. (2010). EnerGis: A geographical information based system for the evaluation of integrated energy conversion systems in urban areas. *Energy*, 35(2):830–840.
- [Goutte and Vassilopoulos, 2019] Goutte, S. and Vassilopoulos, P. (2019). The value of flexibility in power markets. *Energy Policy*, 125:347–357.
- [Govaerts et al., 2018] Govaerts, N., Bruninx, K., and Delarue, E. (2018). Impact of Distribution Tariff Design on the Profitability of Aggregators of Distributed Energy Storage Systems. In *15th International Conference on the European Energy Market (EEM)*, pages 1–5, Łódź, Poland. IEEE.
- [Gupta et al., 2021] Gupta, R., Pena-Bello, A., Streicher, K. N., Roduner, C., Thöni, D., Patel, M. K., and Parra, D. (2021). Spatial analysis of distribution grid capacity and costs to enable massive deployment of PV, electric mobility and electric heating. *Applied Energy*, 287(October 2020):116504.
- [Gurobi Optimization, 2019] Gurobi Optimization, L. (2019). Gurobi optimizer 8.1, reference manual.
- [Hakell et al., 2015] Hakell, B., Fisher, G., and Hersey, A. (2015). Setting the Benchmark for Non Intrusive Load Monitoring : A Comprehensive Assessment of AMI-based Load Disaggregation. Technical report, Pecan Street.
- [Halvgaard et al., 2012] Halvgaard, R., Poulsen, N. K., Madsen, H., and Jørgensen, J. B. (2012). Economic model predictive control for building climate control in a smart grid. In *2012 IEEE PES Innovative Smart Grid Technologies (ISGT)*, pages 1–6. IEEE.

- [Harb et al., 2016] Harb, H., Reinhardt, J., Streblow, R., and Müller, D. (2016). Mip approach for designing heating systems in residential buildings and neighbourhoods. *Journal of Building Performance Simulation*, 9(3):316–330.
- [Hart, 1992] Hart, G. W. (1992). Nonintrusive appliance load monitoring. *Proceedings of the IEEE*, 80(12):1870–1891.
- [Hashemipour et al., 2018] Hashemipour, N., Niknam, T., Aghaei, J., Farahmand, H., Korpas, M., Shafie-Khah, M., Osorio, G. J., and Catalao, J. P. S. (2018). A linear multi-objective operation model for smart distribution systems coordinating tap-changers, photovoltaics and battery energy storage. In *2018 Power Systems Computation Conference (PSCC)*. IEEE.
- [Hay and Davis, 1978] Hay, J. E. and Davis, J. A. (1978). Calculation of the solar radiation incident on inclined surfaces. In *Proceedings first Canadian Solar Radiation Data Workshop, Toronto, Ontario, Canada 1978*.
- [He et al., 2016] He, K., Stankovic, L., Liao, J., and Stankovic, V. (2016). Non-Intrusive Load Disaggregation using Graph Signal Processing. *IEEE Transactions on Smart Grid*, 9(3):1739–1747.
- [Heussen et al., 2010] Heussen, K., Koch, S., Ulbig, A., and Andersson, G. (2010). Energy storage in power system operation: The power nodes modeling framework. In *2010 IEEE PES Innovative Smart Grid Technologies Conference Europe (ISGT Europe)*, pages 1–8. IEEE.
- [Hidalgo-Rodriguez and Myrzik, 2018] Hidalgo-Rodriguez, D. I. and Myrzik, J. (2018). Optimal operation of interconnected home-microgrids with flexible thermal loads: A comparison of decentralized, centralized, and hierarchical-distributed model predictive control. *20th Power Systems Computation Conference, PSCC 2018*.
- [Hinterstocker et al., 2017] Hinterstocker, M., Schott, P., and von Roon, S. (2017). Evaluation of the effects of time-of-use pricing for private households based on measured load data. In *2017 14th International Conference on the European Energy Market (EEM)*, pages 1–6. IEEE.
- [Hinz et al., 2018] Hinz, F., Schmidt, M., and Möst, D. (2018). Regional distribution effects of different electricity network tariff designs with a distributed generation structure: The case of Germany. *Energy Policy*, 113(November 2017):97–111.
- [Hlalele et al., 2020] Hlalele, T. G., Naidoo, R. M., Zhang, J., and Bansal, R. C. (2020). Dynamic Economic Dispatch with Maximal Renewable Penetration under Renewable Obligation. *IEEE Access*, 8(May):38794–38808.
- [Hoffmann et al., 2020] Hoffmann, M., Kotzur, L., Stolten, D., and Robinius, M. (2020). A review on time series aggregation methods for energy system models. *Energies*, 13(3):641.
- [Holweger et al., 2021a] Holweger, J., Ballif, C., and Wyrsh, N. (2021a). Assessing the cost of distributed flexibility versus grid reinforcement in low-voltage networks. Manuscript in preparation.
- [Holweger et al., 2020a] Holweger, J., Bloch, L., Ballif, C., and Wyrsh, N. (2020a). Mitigating the impact of distributed PV in a low-voltage grid using electricity tariffs. *Electric Power Systems Research*, 189:106763.
- [Holweger et al., 2021b] Holweger, J., Bloch, L., Ballif, C., and Wyrsh, N. (2021b). Privacy-preserving methods for smart meters based network simulations. Manuscript in preparation.
- [Holweger et al., 2018] Holweger, J., Bloch, L., and Wyrsh, N. (2018). SCCER-FURIES - Determination of the flexibilisation potential of the electricity demand. ReEL D114b. Technical report, École Polytechnique Fédérale de Lausanne.

Bibliography

- [Holweger et al., 2020b] Holweger, J., Bloch, L., and Wyrsh, N. (2020b). SCCER-FURIES - Definition of optimal control of DHW for self-consumption strategies. Technical report, École Polytechnique Fédérale de Lausanne.
- [Holweger et al., 2019] Holweger, J., Dorokhova, M., Bloch, L., Ballif, C., and Wyrsh, N. (2019). Unsupervised algorithm for disaggregating low-sampling-rate electricity consumption of households. *Sustainable Energy, Grids and Networks*, 19:100244.
- [Hondo and Baba, 2010] Hondo, H. and Baba, K. (2010). Socio-psychological impacts of the introduction of energy technologies: Change in environmental behavior of households with photovoltaic systems. *Applied Energy*, 87(1):229 – 235.
- [Householdquotes, 2020] Householdquotes (2020). Electric Combi Boilers: A Cost-Effective Way To Heat Small Homes?
- [Hoyer, 2012] Hoyer, P. (2012). Non-negative sparse coding. In *Proceedings of the 12th IEEE Workshop on Neural Networks for Signal Processing*, pages 557–565. IEEE.
- [Huber et al., 2018] Huber, J., Richter, B., and Weinhardt, C. (2018). Are consumption tariffs still up-to-date? An operationalized assessment of grid fees. In *15th International Conference on the European Energy Market, EEM*, volume 2018-June, pages 1–5, Łódź, Poland. IEEE.
- [IEA, 2019] IEA (2019). Energy Transitions Indicators.
- [Infras et al., 2020] Infras, Prognos, and TEP Energy (2020). Analyse des schweizerischen Energieverbrauchs 2000 - 2019 nach Verwendungszwecken. Technical Report October, Swiss federal office for energy.
- [IRENA, 2016] IRENA (2016). The power to change: solar and wind cost reduction potential to 2025. Technical report, International Renewable Energy Agency.
- [IRENA, 2017] IRENA (2017). Electricity storage and renewables: Costs and markets to 2030. Technical report, International Renewable Energy Agency, Abu Dhabi.
- [IRENA, 2018] IRENA (2018). Power System Flexibility for the Energy Transition, Part 1: Overview for policy makers. Technical report, International Renewable Energy Agency, Abu Dhabi.
- [IRENA, 2020] IRENA (2020). Renewable Power Generation Costs in 2019. Technical report, International Renewable Energy Agency.
- [Jin et al., 2020] Jin, X., Wu, Q., and Jia, H. (2020). Local flexibility markets: Literature review on concepts, models and clearing methods. *Applied Energy*, 261(January):114387.
- [Johnson and Willsky, 2013] Johnson, M. J. and Willsky, A. S. (2013). Bayesian Nonparametric Hidden Semi-Markov Models. *Journal of Machine Learning Research*, 14(Feb):673–701.
- [Kaufman and Rousseeuw, 2009] Kaufman, L. and Rousseeuw, P. J. (2009). *Finding groups in data: an introduction to cluster analysis*, volume 344. John Wiley & Sons.
- [Kelly, 2017] Kelly, J. (2017). UK Domestic Appliance Level Electricity(UK-DALE-2017)-Disaggregated appliance/whole house power.
- [Kelly and Knottenbelt, 2015a] Kelly, J. and Knottenbelt, W. (2015a). Neural NILM: Deep neural networks applied to energy disaggregation. In *Proceedings of the 2nd ACM International Conference on Embedded Systems for Energy-Efficient Built Environments*, pages 55–64. ACM.

- [Kelly and Knottenbelt, 2015b] Kelly, J. and Knottenbelt, W. (2015b). The UK-DALE dataset, domestic appliance-level electricity demand and whole-house demand from five UK homes. *Scientific Data*, 2(1):150007.
- [Kepplinger et al., 2016] Kepplinger, P., Huber, G., and Petrasch, J. (2016). Field testing of demand side management via autonomous optimal control of a domestic hot water heater. *Energy and Buildings*, 127:730–735.
- [Kim et al., 2011] Kim, H., Marwah, M., Arlitt, M., Lyon, G., and Han, J. (2011). Unsupervised Disaggregation of Low Frequency Power Measurements. In *Proceedings of the 2011 SIAM International Conference on Data Mining*, pages 747–758. Society for Industrial and Applied Mathematics, Philadelphia, PA.
- [King et al., 2004] King, D. L., Boyson, W. E., and Kratochvil, J. A. (2004). Photovoltaic array performance model. Technical Report November, Sandia National Laboratories, Albuquerque.
- [Koenig, 2011] Koenig, M. (2011). Knowledge management in theory and practice (2nd ed.). *JASIST*, 62:2083.
- [Kolter et al., 2010] Kolter, J. Z., Batra, S., and Ng, A. Y. (2010). Energy disaggregation via discriminative sparse coding. In *Advances in Neural Information Processing Systems*, pages 1153–1161.
- [Kolter and Johnson, 2011] Kolter, J. Z. and Johnson, M. J. (2011). REDD: A Public Data Set for Energy Disaggregation Research. In *Workshop on Data Mining Applications in Sustainability (SIGKDD)*, San Diego, CA, volume 25, pages 59–62.
- [Kolter et al., 2012] Kolter, Z., Jaakkola, T., and Kolter, J. Z. (2012). Approximate Inference in Additive Factorial HMMs with Application to Energy Disaggregation. *Proc. Int. Conf. Arti. Intell. Statist.*, XX:1472–1482.
- [Kondziella and Bruckner, 2016] Kondziella, H. and Bruckner, T. (2016). Flexibility requirements of renewable energy based electricity systems - A review of research results and methodologies. *Renewable and Sustainable Energy Reviews*, 53:10–22.
- [Koroleva et al., 2019] Koroleva, K., Melenhorst, M., Novak, J., Herrera Gonzalez, S. L., Fraternali, P., and Rizzoli, A. E. (2019). Designing an integrated socio-technical behaviour change system for energy saving. *Energy Informatics*, 2(S1):30.
- [Kotzur et al., 2020] Kotzur, L., Nolting, L., Hoffmann, M., Groß, T., Smolenko, A., Priesmann, J., Büsing, H., Beer, R., Kullmann, F., Singh, B., Praktiknjo, A., Stolten, D., and Robinius, M. (2020). A modeler's guide to handle complexity in energy system optimization.
- [Kubli, 2018] Kubli, M. (2018). Squaring the sunny circle? On balancing distributive justice of power grid costs and incentives for solar prosumers. *Energy Policy*, 114:173–188.
- [Kuboth et al., 2019] Kuboth, S., Heberle, F., Weith, T., Welzl, M., König-Haagen, A., and Brüggemann, D. (2019). Experimental short-term investigation of model predictive heat pump control in residential buildings. *Energy and Buildings*, 204.
- [Kumar and Chandra, 2017a] Kumar, K. and Chandra, M. G. (2017a). An intuitive explanation of graph signal processing-based electrical load disaggregation. In *2017 IEEE 13th International Colloquium on Signal Processing & its Applications (CSPA)*, pages 100–105. IEEE.
- [Kumar and Chandra, 2017b] Kumar, K. and Chandra, M. G. (2017b). Event and feature based electrical load disaggregation using graph signal processing. In *2017 IEEE 13th International Colloquium on Signal Processing & its Applications (CSPA)*, pages 168–172. IEEE.

Bibliography

- [Kumar et al., 2016] Kumar, K., Sinha, R., Chandra, M. G., and Thokala, N. K. (2016). Data-driven electrical load disaggregation using graph signal processing. In *2016 IEEE Annual India Conference (INDICON)*, pages 1–6. IEEE.
- [Lauinger et al., 2016] Lauinger, D., Caliandro, P., Van herle, J., and Kuhn, D. (2016). A linear programming approach to the optimization of residential energy systems. *Journal of Energy Storage*, 7:24–37.
- [Leijonmarck, 2015] Leijonmarck, E. (2015). Exploiting temporal difference for energy disaggregation via discriminative sparse coding. Master's thesis, KTH, Mathematical Statistics.
- [Liang et al., 2010] Liang, J., Ng, S. K. K., Kendall, G., and Cheng, J. W. M. (2010). Load Signature Study—Part I: Basic Concept, Structure, and Methodology. *IEEE Transactions on Power Delivery*, 25(2):551–560.
- [Liao et al., 2014] Liao, J., Elafoudi, G., Stankovic, L., and Stankovic, V. (2014). Non-intrusive appliance load monitoring using low-resolution smart meter data. In *2014 IEEE International Conference on Smart Grid Communications (SmartGridComm)*, pages 535–540. IEEE.
- [Liu et al., 2018] Liu, C., Akintayo, A., Jiang, Z., Henze, G. P., and Sarkar, S. (2018). Multivariate exploration of non-intrusive load monitoring via spatiotemporal pattern network. *Applied Energy*, 211(December 2017):1106–1122.
- [Mairal et al., 2009] Mairal, J., Bach, F., Ponce, J., and Sapiro, G. (2009). Online dictionary learning for sparse coding. In *Proceedings of the 26th Annual International Conference on Machine Learning*, pages 689–696, New York, New York, USA. ACM Press.
- [Makonin and Popowich, 2015] Makonin, S. and Popowich, F. (2015). Nonintrusive load monitoring (NILM) performance evaluation. *Energy Efficiency*, 8(4):809–814.
- [Mamounakis et al., 2019] Mamounakis, I., Efthymiopoulos, N., Vergados, D. J., Tsaousoglou, G., Makris, P., and Varvarigos, E. M. (2019). A pricing scheme for electric utility's participation in day-ahead and real-time flexibility energy markets. *Journal of Modern Power Systems and Clean Energy*, 7(5):1294–1306.
- [Manivannan et al., 2017] Manivannan, M., Najafi, B., and Rinaldi, F. (2017). Machine Learning-Based Short-Term Prediction of Air-Conditioning Load through Smart Meter Analyticsan intu. *MDPI Energies*, 10.
- [Markiewicz and Klajn, 2004] Markiewicz, H. and Klajn, A. (2004). Voltage Disturbances Standard EN50160. Technical report, Lonardo Power Quality Initiative, Wroclaw.
- [Massucco et al., 2021] Massucco, S., Pongiglione, P., Silvestro, F., Paolone, M., and Sossan, F. (2021). Siting and Sizing of Energy Storage Systems: Towards a Unified Approach for Transmission and Distribution System Operators for Reserve Provision and Grid Support. *Electric Power Systems Research*, 190:106660.
- [Middelhaue et al., 2021] Middelhaue, L., Baldi, F., Stadler, P., and Maréchal, F. (2021). Grid-Aware Layout of Photovoltaic Panels in Sustainable Building Energy Systems. *Frontiers in Energy Research*, 8:317.
- [Middelhaue et al., 2018] Middelhaue, L., Bloch, L., Girardin, L., Stadler, P. M., Holweger, J., and Tommasi, H. (2018). SCCER-FURIES - Design of Sizes for Buildings Energy Systems as a Function of the Grid Evolution - Deliverable 1.4.1a. Technical report, École Polytechnique Fédérale de Lausanne, EPFL Valais/Neuchâtel.

- [Middelhaue et al., 2019] Middelhaue, L., Bloch, L., Holweger, J., Stadler, P. M., and Girardin, L. (2019). SCCER JA-RED - Detailed evaluation of the grid operation bottlenecks and load shifting potential for the reference system - Deliverable 1.2.2. Technical report, École Polytechnique Fédérale de Lausanne, EPFL Valais/Neuchâtel.
- [Milis et al., 2018] Milis, K., Peremans, H., and Van Passel, S. (2018). Steering the adoption of battery storage through electricity tariff design. *Renewable and Sustainable Energy Reviews*, 98(September):125–139.
- [Mulder et al., 2013] Mulder, G., Six, D., Claessens, B., Broes, T., Omar, N., and Mierlo, J. V. (2013). The dimensioning of PV-battery systems depending on the incentive and selling price conditions. *Applied Energy*, 111:1126–1135.
- [Nazari-Heris et al., 2019] Nazari-Heris, F., Mohammadi-ivatloo, B., and Nazarpour, D. (2019). Network constrained economic dispatch of renewable energy and CHP based microgrids. *International Journal of Electrical Power & Energy Systems*, 110:144–160.
- [Nordmann, 2019] Nordmann, R. (2019). *Le plan solaire et climat*. Favre SA, Lausanne.
- [Olivella-Rosell et al., 2018] Olivella-Rosell, P., Lloret-Gallego, P., Munné-Collado, Í., Villafila-Robles, R., Sumper, A., Ottessen, S. Ø., Rajasekharan, J., and Bremdal, B. A. (2018). Local flexibility market design for aggregators providing multiple flexibility services at distribution network level. *Energies*, 11(4):1–19.
- [Olivier, 2018] Olivier, F. (2018). *Solutions for integrating photovoltaic panels into low-voltage distribution networks*. PhD thesis, Liège Université.
- [Olivier et al., 2016] Olivier, F., Aristidou, P., Ernst, D., and Van Cutsem, T. (2016). Active Management of Low-Voltage Networks for Mitigating Overvoltages Due to Photovoltaic Units. *IEEE Transactions on Smart Grid*, 7(2):926–936.
- [O’Shaughnessy et al., 2018] O’Shaughnessy, E., Cutler, D., Ardani, K., and Margolis, R. (2018). Solar plus: Optimization of distributed solar PV through battery storage and dispatchable load in residential buildings. *Applied Energy*, 213:11–21.
- [Paetz et al., 2013] Paetz, A.-G., Kaschub, T., Jochem, P., and Fichtner, W. (2013). Load-shifting potentials in households including electric mobility - A comparison of user behaviour with modelling results. In *2013 10th International Conference on the European Energy Market (EEM)*, pages 1–7. IEEE.
- [Parson et al., 2012] Parson, O., Ghosh, S., Weal, M., and Rogers, A. (2012). Non-Intrusive Load Monitoring Using Prior Models of General Appliance Types. In *AAAI*.
- [Pena-Bello et al., 2017] Pena-Bello, A., Burer, M., Patel, M. K., and Parra, D. (2017). Optimizing PV and grid charging in combined applications to improve the profitability of residential batteries. *Journal of Energy Storage*, 13:58–72.
- [Perraudin et al., 2014] Perraudin, N., Paratte, J., Shuman, D., Martin, L., Kalofolias, V., Vanderghelynst, P., and Hammond, D. K. (2014). GSPBOX: A toolbox for signal processing on graphs. *ArXiv e-prints*.
- [Perret et al., 2019] Perret, L., Chevillat, Y., Wyrsh, N., Bloch, L., Holweger, J., Weber, S., and Péclat, M. (2019). Flexi 2 Déterminer le potentiel de flexibilisation de la demande d’électricité des ménages. Technical report, Federal office for energy.

Bibliography

- [Perret et al., 2015] Perret, L., Fahrni, J., Wyrsh, N., Riesen, Y., Puddu, S., Weber, S., and Pfacheco Barzallo, D. (2015). FLEXI Determining the flexibilization potential of the electricity demand. Technical report, Fedral office for energy.
- [Pina et al., 2012] Pina, A., Silva, C., and Ferrão, P. (2012). The impact of demand side management strategies in the penetration of renewable electricity. *Energy*, 41(1):128 – 137. 23rd International Conference on Efficiency, Cost, Optimization, Simulation and Environmental Impact of Energy Systems, ECOS 2010.
- [Planair et al., 2020] Planair, Sauter, Y., and Jacqmin, F. (2020). Observation du marché photovoltaïque 2019. Technical report, SuisseEnergie.
- [Ponocko and Milanovic, 2018] Ponocko, J. and Milanovic, J. V. (2018). Forecasting Demand Flexibility of Aggregated Residential Load Using Smart Meter Data. *IEEE Transactions on Power Systems*, 8950(c):1–1.
- [Poosri and Charoenlarnnopparut, 2016] Poosri, O. and Charoenlarnnopparut, C. (2016). Harmonics Impact of Rooftop Photovoltaic Penetration Level on Low Voltage Distribution System. *International Journal of Electronics and Electrical Engineering*, pages 221–225.
- [Prionistis et al., 2021] Prionistis, G., Souxes, T., and Vournas, C. (2021). Voltage stability support offered by active distribution networks. *Electric Power Systems Research*, 190.
- [Rabiner, 1989] Rabiner, L. (1989). A tutorial on hidden Markov models and selected applications in speech recognition. *Proceedings of the IEEE*, 77(2):257–286.
- [Rahimpour et al., 2017] Rahimpour, A., Qi, H., Fugate, D., and Kuruganti, T. (2017). Non-Intrusive Energy Disaggregation Using Non-negative Matrix Factorization with Sum-to-k Constraint. *IEEE Transactions on Power Systems*, PP(99):1–1.
- [Rahimpour et al., 2020] Rahimpour, Z., Verbič, G., and Chapman, A. C. (2020). Actor-critic learning for optimal building energy management with phase change materials. *Electric Power Systems Research*, 188:106543.
- [Rai and McAndrews, 2012] Rai, V. and McAndrews, K. (2012). Decision-making and behavior change in residential adopters of solar PV. *World Renewable Energy Forum, WREF 2012, Including World Renewable Energy Congress XII and Colorado Renewable Energy Society (CRES) Annual Conferen*, 4:2875–2880.
- [Reda and Andreas, 2004] Reda, I. and Andreas, A. (2004). Solar position algorithm for solar radiation applications. *Solar Energy*, 76(5):577–589.
- [Remund et al., 2019] Remund, J., Albrecht, S., and Stickelberger, D. (2019). Das Schweizer PV-Potenzial basierend auf jedem Gebäude. Technical report, Meteotest.
- [Ren et al., 2016] Ren, Z., Grozev, G., and Higgins, A. (2016). Modelling impact of PV battery systems on energy consumption and bill savings of Australian houses under alternative tariff structures. *Renewable Energy*, 89:317–330.
- [Renaldi et al., 2017] Renaldi, R., Kiprakis, A., and Friedrich, D. (2017). An optimisation framework for thermal energy storage integration in a residential heat pump heating system. *Applied Energy*, 186:520–529.
- [Riesen et al., 2017] Riesen, Y., Ballif, C., and Wyrsh, N. (2017). Control algorithm for a residential photovoltaic system with storage. *Applied Energy*, 202:78–87.

- [Roje et al., 2017] Roje, T., Marín, L. G., Sáez, D., Orchard, M., and Jiménez-Estévez, G. (2017). Consumption modeling based on Markov chains and Bayesian networks for a demand side management design of isolated microgrids. *International Journal of Energy Research*, 41(3):365–376.
- [Romande Energie, 2019] Romande Energie (2019). Prix.
- [Roux et al., 2018] Roux, M., Apperley, M., and Booysen, M. (2018). Comfort, peak load and energy: Centralised control of water heaters for demand-driven prioritisation. *Energy for Sustainable Development*, 44:78–86.
- [Ruzzelli et al., 2010] Ruzzelli, A. G., Nicolas, C., Schoofs, A., and O’Hare, G. M. P. (2010). Real-Time Recognition and Profiling of Appliances through a Single Electricity Sensor. In *2010 7th Annual IEEE Communications Society Conference on Sensor, Mesh and Ad Hoc Communications and Networks (SECON)*, pages 1–9. IEEE.
- [Saele and Grande, 2011] Saele, H. and Grande, O. S. (2011). Demand response from household customers: Experiences from a pilot study in Norway. *IEEE Transactions on Smart Grid*, 2(1):102–109.
- [Salpakari and Lund, 2016] Salpakari, J. and Lund, P. (2016). Optimal and rule-based control strategies for energy flexibility in buildings with PV. *Applied Energy*, 161:425–436.
- [Sánchez et al., 2019] Sánchez, C., Bloch, L., Holweger, J., Ballif, C., and Wyrsh, N. (2019). Optimised Heat Pump Management for Increasing Photovoltaic Penetration into the Electricity Grid. *Energies*, 12(8):1571.
- [Scheidler et al., 2018] Scheidler, A., Thurner, L., and Braun, M. (2018). Heuristic optimisation for automated distribution system planning in network integration studies. *IET Renewable Power Generation*, 12(5):530–538.
- [Schibuola et al., 2016] Schibuola, L., Scarpa, M., and Tambani, C. (2016). Parametric study on the financial performance of battery-supported photovoltaic systems connected to smart grids in current and future market scenarios. *Science and Technology for the Built Environment*, 22(6):751–765.
- [Schittekatte et al., 2018] Schittekatte, T., Momber, I., and Meeus, L. (2018). Future-proof tariff design: Recovering sunk grid costs in a world where consumers are pushing back. *Energy Economics*, 70:484–498.
- [Schulz, 2015] Schulz, C. (2015). *Course Notes : Graph Partitioning and Graph Clustering in Theory and Practice*. Karlsruhe Institute of Technology (KIT), Karlsruhe.
- [Schulz et al., 2020] Schulz, M., Kemmler, T., Kumm, J., Hufendiek, K., and Thomas, B. (2020). A more realistic heat pump control approach by application of an integrated two-part control. *Energies*, 13(11).
- [Sekitou et al., 2018] Sekitou, M., Tanaka, K., and Managi, S. (2018). Household electricity demand after the introduction of solar photovoltaic systems. *Economic Analysis and Policy*, 57:102 – 110.
- [SFOE, 2018] SFOE (2018). Calculateur solaire.
- [SFOE, 2019a] SFOE (2019a). Schweizerische Gesamtenergiestatistik 2019. Technical report, Swiss Federal office for energy, Bern.
- [SFOE, 2019b] SFOE (2019b). Schweizerische Statistik der erneuerbaren Energien. Ausgabe 2019. Technical report, Swiss Federal Office for Energy, Bern.
- [SFOE, 2021] SFOE (2021). PERSPECTIVES ÉNERGÉTIQUES 2050+ - RÉSUMÉ DES PRINCIPAUX RÉSULTATS. Technical report, Swiss Federal Office for Energy, Bern.

Bibliography

- [Shah, 2020] Shah, A. (2020). *Solar Cells and Modules*, volume 301 of *Springer Series in Materials Science*. Springer International Publishing, Cham, Springer's edition.
- [Shiba et al., 1995] Shiba, T., Yokoyama, R., and Ito, K. (1995). Optimal sizing of a heat pump/thermal storage system based on the linear programming method. *International journal of energy research*, 19(8):665–674.
- [SIA, 2015] SIA (2015). Donnees d'utilisation des locaux pour l'énergie et les installations du bâtiment. Technical report, Swiss society of engineers and architects, Zurich.
- [Simshauser, 2016] Simshauser, P. (2016). Distribution network prices and solar PV: Resolving rate instability and wealth transfers through demand tariffs. *Energy Economics*, 54:108–122.
- [Singh and Majumdar, 2017] Singh, S. and Majumdar, A. (2017). Deep Sparse Coding for Non-Intrusive Load Monitoring. *IEEE Transactions on Smart Grid*, pages 1–1.
- [Soares et al., 2019] Soares, I., Alves, M. J., and Antunes, C. H. (2019). Designing time-of-use tariffs in electricity retail markets using a bi-level model – Estimating bounds when the lower level problem cannot be exactly solved. *Omega*.
- [Sociaal en Cultureel Planbureau, 2005] Sociaal en Cultureel Planbureau (2005). Tijdsbestedingsonderzoek 2005 - TBO 2005. *DANS*.
- [Srivastava et al., 2019] Srivastava, A., Van Passel, S., and Laes, E. (2019). Dissecting demand response: A quantile analysis of flexibility, household attitudes, and demographics. *Energy Research & Social Science*, 52:169–180.
- [Staats et al., 2017] Staats, M. R., de Boer-Meulman, P. D., and van Sark, W. G. (2017). Experimental determination of demand side management potential of wet appliances in the Netherlands. *Sustainable Energy, Grids and Networks*, 9:80–94.
- [Stadler et al., 2016] Stadler, P., Ashouri, A., and Maréchal, F. (2016). Model-based optimization of distributed and renewable energy systems in buildings. *Energy and Buildings*, 120:103–113.
- [Stadler et al., 2018] Stadler, P., Girardin, L., Ashouri, A., and Maréchal, F. (2018). Contribution of model predictive control in the integration of renewable energy sources within the built environment. *Frontiers in Energy Research*, 6:22.
- [Stankovic et al., 2016] Stankovic, L., Stankovic, V., Liao, J., and Wilson, C. (2016). Measuring the energy intensity of domestic activities from smart meter data. *Applied Energy*, 183:1565–1580.
- [Stankovic et al., 2014] Stankovic, V., Liao, J., and Stankovic, L. (2014). A graph-based signal processing approach for low-rate energy disaggregation. In *2014 IEEE Symposium on Computational Intelligence for Engineering Solutions (CIES)*, pages 81–87. IEEE.
- [Stein et al., 2016] Stein, J. S., Holmgren, W. F., Forbess, J., and Hansen, C. W. (2016). PVLIB: Open source photovoltaic performance modeling functions for Matlab and Python. In *2016 IEEE 43rd Photovoltaic Specialists Conference (PVSC)*, pages 3425–3430, Portland, OR, USA. IEEE.
- [Suciu et al., 2018] Suciu, R., Stadler, P., Girardin, L., and Maréchal, F. (2018). Multi-period multi-time optimisation of co2 based district energy systems. In Friedl, A., Klemeš, J. J., Radl, S., Varbanov, P. S., and Wallek, T., editors, *28th European Symposium on Computer Aided Process Engineering*, volume 43 of *Computer Aided Chemical Engineering*, pages 1057–1062. Elsevier.
- [Sugiyama, 2012] Sugiyama, M. (2012). Climate change mitigation and electrification. *Energy Policy*, 44:464–468.

- [Swissgrid, 2021] Swissgrid (2021). Statistique de l'énergie Suisse 2009-2021. Technical report, Swissgrid, Arau.
- [Swissolar, 2019] Swissolar (2019). Guide pratique de la consommation propre. Technical report, Suisse Energie.
- [Swissolar, 2020] Swissolar (2020). Assurer l'alimentation électrique. Technical report, Swissolar.
- [Talent and Du, 2018] Talent, O. and Du, H. (2018). Optimal sizing and energy scheduling of photovoltaic-battery systems under different tariff structures. *Renewable Energy*, 129:513–526.
- [Thunberg, 2019] Thunberg, G. (2019). 'Our house is on fire': Greta Thunberg, 16, urges leaders to act on climate.
- [Tielens and Van Hertem, 2016] Tielens, P. and Van Hertem, D. (2016). The relevance of inertia in power systems. *Renewable and Sustainable Energy Reviews*, 55:999–1009.
- [Torriti, 2012] Torriti, J. (2012). Price-based demand side management: Assessing the impacts of time-of-use tariffs on residential electricity demand and peak shifting in Northern Italy. *Energy*, 44(1):576–583.
- [Tsaousoglou et al., 2019] Tsaousoglou, G., Efthymiopoulos, N., Makris, P., and Varvarigos, E. (2019). Personalized real time pricing for efficient and fair demand response in energy cooperatives and highly competitive flexibility markets. *Journal of Modern Power Systems and Clean Energy*, 7(1):151–162.
- [Verhelst et al., 2010] Verhelst, C., Axehill, D., Jones, C. N., and Helsen, L. (2010). Impact of the cost function in the optimal control formulation for an air-to-water heat pump system. In *8th International Conference on System Simulation in Buildings (SSB), Liege, Belgium*.
- [Verhelst et al., 2012] Verhelst, C., Logist, E., Van Impe, J., and Helsen, L. (2012). Study of the optimal control problem formulation for modulating air-to-water heat pumps connected to a residential floor heating system. *Energy and Buildings*, 45:43–53.
- [Viral and Khatod, 2012] Viral, R. and Khatod, D. K. (2012). Optimal planning of distributed generation systems in distribution system: A review. *Renewable and Sustainable Energy Reviews*, 16:5146–5165.
- [Vrettos et al., 2013] Vrettos, E., Lai, K., Oldewurtel, F., and Andersson, G. (2013). Predictive control of buildings for demand response with dynamic day-ahead and real-time prices. In *European Control Conference (ECC), Zürich, Switzerland*.
- [Vu, 2018] Vu, T. (2018). A stochastic methodology to determine reinforcement cost of power distribution grid for integrating increasing share of renewable energies and electric vehicles. *International Conference on the European Energy Market, EEM*, 2018-June.
- [Wang, 2003] Wang, S.-C. (2003). Artificial Neural Network. In *Interdisciplinary Computing in Java Programming*, pages 81–100. Springer US, Boston, MA.
- [Wang et al., 2018] Wang, Y., Chen, Q., Hong, T., and Kang, C. (2018). Review of Smart Meter Data Analytics: Applications, Methodologies, and Challenges. *IEEE Transactions on Smart Grid*, pages 1–1.
- [Wimmer, 2004] Wimmer, R. W. (2004). Regelung einer Wärmepumpenanlage mit Model Predictive Control. *Eidgenössischen Technischen Hochschule Zürich*, Doctoral thesis 15709:25–30.
- [Wittenberg and Matthies, 2018] Wittenberg, I. and Matthies, E. (2018). How do pv households use their pv system and how is this related to their energy use? *Renewable Energy*, 122:291 – 300.

Bibliography

- [Wu et al., 2017] Wu, X., Hu, X., Yin, X., Zhang, C., and Qian, S. (2017). Optimal battery sizing of smart home via convex programming. *Energy*, 140:444–453.
- [Xu et al., 2018] Xu, B., Oudalov, A., Ulbig, A., Andersson, G., and Kirschen, D. S. (2018). Modeling of Lithium-Ion Battery Degradation for Cell Life Assessment. *IEEE Transactions on Smart Grid*, 9(2):1131–1140.
- [Yan et al., 2020] Yan, B., Di Somma, M., Graditi, G., and Luh, P. B. (2020). Markovian-based stochastic operation optimization of multiple distributed energy systems with renewables in a local energy community. *Electric Power Systems Research*, 186(April):106364.
- [Yang et al., 2015] Yang, Y., Enjeti, P., Blaabjerg, F., and Wang, H. (2015). Wide-scale adoption of photovoltaic energy: Grid code modifications are explored in the distribution grid. *IEEE Industry Applications Magazine*, 21:1–10.
- [Yilmaz et al., 2020] Yilmaz, S., Xu, X., Cabrera, D., Chanez, C., Cuony, P., and Patel, M. K. (2020). Analysis of demand-side response preferences regarding electricity tariffs and direct load control: Key findings from a swiss survey. *Energy*, 212:118712.
- [Yong et al., 2018] Yong, J. H. C., Wong, J., Lim, Y. S., and Tang, J. H. (2018). Assessment on Various Allocations of Energy Storages Systems on Radial Distribution Network for Maximum PV Systems Penetration. In *2018 International Conference on Smart Grid and Clean Energy Technologies (ICSGCE)*, pages 89–94. IEEE.
- [Young et al., 2016] Young, S., Bruce, A., and MacGill, I. (2016). Electricity network revenue under different Australian residential tariff designs and customer interventions. In *2016 IEEE Power and Energy Society General Meeting (PESGM)*, pages 1–5, Boston, MA, USA. IEEE.
- [Young et al., 2019] Young, S., Bruce, A., and MacGill, I. (2019). Potential impacts of residential PV and battery storage on Australia’s electricity networks under different tariffs. *Energy Policy*, 128:616–627.
- [Yu et al., 2016] Yu, C.-N., Mirowski, P., and Ho, T. K. (2016). A Sparse Coding Approach to Household Electricity Demand Forecasting in Smart Grids. *IEEE Transactions on Smart Grid*, pages 1–11.
- [Zhang and Tang, 2019] Zhang, S. and Tang, Y. (2019). Optimal schedule of grid-connected residential PV generation systems with battery storages under time-of-use and step tariffs. *Journal of Energy Storage*, 23:175–182.
- [Zhang et al., 2020] Zhang, W., Roald, L. A., Chien, A. A., Birge, J. R., and Zavala, V. M. (2020). Flexibility from networks of data centers: A market clearing formulation with virtual links. *Electric Power Systems Research*, 189:106723.
- [Zhang et al., 2013] Zhang, Y., Li, F., Hu, Z., and Shaddick, G. (2013). Quantification of low voltage network reinforcement costs: A statistical approach. *IEEE Transactions on Power Systems*, 28(2):810–818.
- [Zhao et al., 2016] Zhao, B., Stankovic, L., and Stankovic, V. (2016). On a Training-Less Solution for Non-Intrusive Appliance Load Monitoring Using Graph Signal Processing. *IEEE Access*, 4:1784–1799.
- [Zhao et al., 2018] Zhao, B., Stankovic, L., and Stankovic, V. (2018). Electricity usage profile disaggregation of hourly smart meter data. In *4th International Workshop on Non-Intrusive Load Monitoring*.
- [Zhao et al., 2015] Zhao, Y., Lu, Y., Yan, C., and Wang, S. (2015). MPC-based optimal scheduling of grid-connected low energy buildings with thermal energy storages. *Energy and Buildings*, 86:415–426.
- [Zoha et al., 2012] Zoha, A., Gluhak, A., Imran, M., and Rajasegarar, S. (2012). Non-Intrusive Load Monitoring Approaches for Disaggregated Energy Sensing: A Survey. *Sensors*, 12(12):16838–16866.

- [Zoha et al., 2013] Zoha, A., Gluhak, A., Nati, M., and Imran, M. A. (2013). Low-power appliance monitoring using Factorial Hidden Markov Models. In *2013 IEEE Eighth International Conference on Intelligent Sensors, Sensor Networks and Information Processing*, pages 527–532. IEEE.

JORDAN HOLWEGER

Energy system engineer

🏠 Rue Soubeyran 3A, 1203 Genève - Switzerland

@ jordan.holweger@gmail.com ☎ +41 76 308 98 07



👤 EXPERIENCE

Ph.D. Student EPFL-photovoltaic laboratory (May 2017- Ongoing)

- Research work on PV system flexibility
- Mathematical modeling and optimization
- Teaching activities

Technology transfer officer – EPFL Transportation center (December 2015 – May 2017)

- Technology transfer activities
- Building partnership between academia and industrial company

Computational fluid dynamic engineer – Hydros Innovation (February – December 2015)

- Computational fluid dynamic (CFD) study
- Ship hydrodynamic performance evaluation
- Open source code: *OpenFOAM*

🎓 EDUCATION

Master -bachelor in mechanical engineering EPFL (2009-2015)

Aerodynamic and structural mechanics, minor in energy

Erasmus at Heriot-Watt University (Edinburgh, UK) (2011-2012)

Mechanical engineering

🎧 INTEREST

- Musician, alt. sax jazz
- Sport sailing

👥 REFERENCE

- Dr. Nicolas Wyrsh: nicolas.wyrsh@epfl.ch
- Prof. Christophe Ballif: christophe.ballif@epfl.ch

🧠 PERSONALITY

Enthusiast



Teamwork



Communication



🛠 SKILL

PV system

Energy system modeling

Optimization

Geographical Information System

Project management

Database

💻 COMPUTER SKILLS

Python



MATLAB



LaTeX



Microsoft Office



🌐 LANGUAGE

French (native speaker)



English



German



301